School of Engineering Systems
Instituite of Health and Biomedical Innovation
Queensland University of Technology

Passive Control of a Bi-Ventricular Assist Device: An Experimental and Numerical Investigation

Nicholas Richard Gaddum
Bachelor of Engineering (Mechanical) (Hons), Canterbury

A thesis submitted for the degree of Doctor of Philosophy in the Faculty of Built Environment and Engineering and Institute of Health and Biomedical Innovation, Queensland University of Techonology according to QUT requirements

2008

Keywords

Passive Control, Bi-Ventricular Assist Device, Baroreceptor Response, Venous Return, Numerical Simulation, Rotary Pump Design

Abstract

For the last two decades heart disease has been the highest single cause of death for the human population. With an alarming number of patients requiring heart transplant, and donations not able to satisfy the demand, treatment looks to mechanical alternatives.

Rotary Ventricular Assist Devices, VADs, are miniature pumps which can be implanted alongside the heart to assist its pumping function. These constant flow devices are smaller, more efficient and promise a longer operational life than more traditional pulsatile VADs. The development of rotary VADs has focused on single pumps assisting the left ventricle only to supply blood for the body. In many patients however, failure of both ventricles demands that an additional pulsatile device be used to support the failing right ventricle. This condition renders them hospital bound while they wait for an unlikely heart donation. Reported attempts to use two rotary pumps to support both ventricles concurrently have warned of inherent haemodynamic instability. Poor balancing of the pumps' flow rates quickly leads to vascular congestion increasing the risk of oedema and ventricular 'suckdown' occluding the inlet to the pump. This thesis introduces a novel Bi-Ventricular Assist Device (BiVAD) configuration where the pump outputs are **passively** balanced by vascular pressure.

The BiVAD consists of two rotary pumps straddling the mechanical passive controller. Fluctuations in vascular pressure induce small deflections within both pumps adjusting their outputs allowing them to maintain arterial pressure. To optimise the passive controller's interaction with the circulation, the controller's dynamic response is optimised with a spring, mass, damper arrangement.

This two part study presents a comprehensive assessment of the prototype's 'viability' as a support device. Its 'viability' was considered based on its sensitivity to pathogenic haemodynamics and the ability of the passive response to maintain healthy circulation.

The first part of the study is an experimental investigation where a prototype device was designed and built, and then tested in a pulsatile mock circulation loop. The BiVAD was subjected to a range of haemodynamic imbalances as well as a dynamic analysis to assess the functionality of the mechanical damper. The second part introduces the development of a numerical program to simulate human circulation supported by the passively controlled BiVAD. Both investigations showed that the prototype was able to mimic the native baroreceptor response. Simulating hypertension, poor flow balancing and subsequent ventricular failure during BiVAD support allowed the passive controller's response to be assessed. Triggered by the resulting pressure imbalance, the controller responded by passively adjusting the VAD outputs in order to maintain healthy arterial pressures. This baroreceptor-like response demonstrated the inherent stability of the auto regulating BiVAD prototype.

Simulating pulmonary hypertension in the more observable numerical model, however, revealed a serious issue with the passive response. The subsequent decrease in venous return into the left heart went unnoticed by the passive controller. Meanwhile the coupled nature of the passive response not only decreased RVAD output to reduce pulmonary arterial pressure, but it also increased LVAD output. Consequently, the LVAD increased fluid evacuation from the left ventricle, LV, and so actually accelerated the onset of LV collapse. It was concluded that despite the inherently stable baroreceptor-like response of the passive controller, its lack of sensitivity to venous return made it unviable in its present configuration.

The study revealed a number of other important findings. Perhaps the most significant was that the reduced pulse experienced during constant flow support unbalanced the ratio of effective resistances of both vascular circuits. Even during steady rotary support therefore, the resulting ventricle volume imbalance increased the likelihood of suckdown. Additionally, mechanical damping of the passive controller's response successfully filtered out pressure fluctuations from residual ventricular function. Finally, the importance of recognising inertial contributions to blood flow in the atria and ventricles in a numerical simulation were highlighted.

This thesis documents the first attempt to create a fully auto regulated rotary cardiac assist device. Initial results encourage development of an inlet configuration sensitive

to low flow such as collapsible inlet cannulae. Combining this with the existing baroreceptor-like response of the passive controller will render a highly stable passively controlled BiVAD configuration. The prototype controller's passive interaction with the vasculature is a significant step towards a highly stable new generation of artificial heart.

Table of Contents

Table of Figures

Nomenclature

$\underline{\mathbf{A}}$	System matrix for the linear CV model
$A_{\#}$	Pump specific constants, (indicated by number #), derived from corresponding experimental pump performance data
ACl	compressed air to the LV
ACr	compressed air to the RV
AR	Amplitude Ratio
Ao	Aorta
AoC	Aortic/Systemic arterial compliance ($L.mmHg^{-1}$)
AoP	Aortic Pressure (mmHg)
A_{LVAD}	Projected area normal to the impeller rotational axis of the LVAD lower shroud (m^2 unless specified)
A_{RVAD}	Projected area normal to the impeller rotational axis of the RVAD lower shroud (m^2 unless specified)
B_1 to B_4	Pump specific constants for pressure vs. clearance relationship
B_5 to B_8	Pump specific constants for flow vs. clearance relationship
BC	Boundary Condition
BS	Bronchial Shunt
BiVAD	Bi-Ventricular Assist Device
BiVAD	Bi-Ventricular Assist Device
BiVF	Bi-Ventricular Failure
BiVS	Bi-Ventricular Support
C	Compliance ($ml.mmHg^{-1}$)
CO	Cardiac Output ($L.min^{-1}$)
CV	Cardiovascular
CVP	Central Venous Pressure (mmHg)
DOM	Dermal/Organ/Muscular
EDV	End Diastolic Volume (ml)
EF	Ejection Fraction
ESV	End Systolic Volume (ml)
F	Force (N)
FBD	Free Body Diagram
H	Pump pressure head (mmHg)
HR	Heart rate (BPM)
Ht	Haematocrit (%)
L	Fluid Inertiance ($mm.Hg.s^2.ml^{-1}$)
LA	left atrium
LH	Left Heart
LU	Lower Upper, (when referring to an LU decomposition)
LV	left ventricle
LVF	Left Ventricular Failure
LVP	Left Ventricular Pressure (mmHg)
LVDT	Linear Variable Displacement transducer
M	Torque (N.mm/1000)
MAP	Mean Arterial Pressure (mmHg)
MAoP	Mean Aortic Pressure (mmHg)
MCL	Mock Circulation Loop
MLVAD P	Mean LVAD Pressure head (mmHg)
MPAP	Mean Pulmonary Artery Pressure (mmHg)
MRVAD P	Mean RVAD Pressure head (mmHg)
N	Pump Speed (RPM)
NIH	Index of Haemolysis ($g.100L^{-1}$)
NR	Normalised Residual
ODE	Ordinary Differential Equation
PA	Pulmonary Artery
PAC	Pulmonary arterial compliance ($L.mmHg^{-1}$)
PAP	Pulmonary Artery Pressure (mmHg)
PHYSBE	Physiological Simulation Benchmark Experiment
PQ	Pulmonary flow ($L.min^{-1}$)
PV	Pressure-volume (in the context of pressure-volume plots, or pressure-volume loops)
PVC	Pulmonary venous compliance ($L.mmHg^{-1}$)
PVR	Pulmonary venous resistance ($mmHg.s.L^{-1}$)
Q	Flow rate ($L.min^{-1}$)
R	Fluid resistance ($mm.Hg.s.ml^{-1}$)
R_G	Gas Constant for air 287 ($J.kg^{-1}.K^{-1}$)
RA	Right atrium
RAP	Right atrial pressure (mmHg)
RH	Right Heart
RV	Right Ventricle
RVF	Right Ventricular Failure
RVP	Right Ventricular Pressure (mmHg)
SQ	Systemic flow ($L.min^{-1}$)
SVR	Systemic venous resistance ($mmHg.s.L^{-1}$)
SVC	Systemic venous compliance ($L.mmHg^{-1}$)
T	Time (seconds)
TAH	Total Artificial Heart
U	Air temperature (K)
V	Volume (ml, unless stated otherwise)
VAD	Ventricular Assist Device
V_i	Initial Volume (ml, unless stated otherwise)
b	Right hand side vector, (of a linear system)
b_2	Outlet impeller blade dimension (mm)
c	Axial distance between the impeller blades and the floating lower shroud (mm)
d	Damping coefficient ($N.s.mm^{-1}$)
d_1	Inlet impeller blade dimension (mm)
e	Absolute fluid velocity ($mm.s^{-1}$)
f_n	Natural frequency (Hz)
g	Product of gravitational constant and unit conversion constant
k	Generalised Spring Constant ($N.mm^{-1}$)
m	Mass (g)
p	Pressure (mmHg)
r	radius (mm)
s	Passive controller hub assembly theoretical degree of freedom, (later replaced with the hub position, *y*)
t	Time (s)
u	Absolute impeller velocity ($mm.s^{-1}$)
w	Relative fluid velocity with respect to the impeller ($mm.s^{-1}$)
x	State vector housing pressures, flow rates and hub clearances for the linear CV model
y	Floating assembly position from its central location toward the RVAD (mm)

$\dot{y}$	Linear velocity of the floating assembly ($mm.s^{-1}$)
$\ddot{y}$	Linear acceleration of the floating assembly ($mm.s^{-2}$)
α	Relative fluid velocity angle
β	Absolute fluid velocity angle
$\Delta freeHb$	Increase in plasma free Haemoglobin ($g.10L^{-1}$)
ξ_H	Pump pressure decrement
ξ_Q	Pump flow decrement
Φ	Local state, (pressure, flow or hub position)

Subscripts:

A	Arterial
AoV	Referring to the Aortic Valve
L	Left
LA	Referring to the Left Atrium
LV	Referring to the Left Ventricle
LVDT	Denotes a property of the LVDT
LVAD P	Referring to the LVAD pressure head
MV	Referring to the Mitral Valve
PC	Denotes the Passive Controller
R	Right
RVAD P	Referring to the RVAD pressure head
V	Venous
air	Denotes a property of the 'air bubble spring'
atm	Denotes atmospheric properties, i.e. p_{atm} = 101.3 kPa
breath	Denotes a respiratory breath
clearance	Denotes a property of the 'clearance spring'
effective	Denotes a property of the combined passive controller spring
ejected	Referring to the ventricular ejection
i	Denotes an initial value
pleural	Denotes pleural pressure
1	Inlet
2	Outlet
?	Outside vascular wall

Superscripts

i	Denotes the present time step
j	Referring to a time step (Δt) of length *j* seconds

Statement of Authorship

The work contained in this thesis has not been previously submitted for a degree or diploma at any other higher education institution. To the best of my knowledge and belief, the thesis contains no material previously published or written by any other person except where due reference is made.

_____

Nick Gaddum
2008

Acknowledgements

I would like to extend my thanks and convey my upmost respect to Dr Daniel Timms. Throughout this research program he has lent me thoughtful and unrestrained inspiration. This was particularly appreciated in the first 18 months where he provided directional advice and technical knowledge in my preliminary investigations. His outstanding works in mock circulation too provided a world class *in vitro* testing facility. Without access to such equipment the significance of this project would have been considerably less.

Professor Mark Pearcy's contribution to this project was consistently encouraging and engaging. I would like to thank him for his listening ear, his constructive wisdom and his continued efforts to create a relaxed environment in which I could work.

Even from abroad, my parents provided substantial input to this project. They cannot have realised how important a sympathetic ear was in a time of need. To Richard and Linda Gaddum; thank you for your continued support and constant enthusiasm. I would also like to acknowledge the work put in by Linda Gaddum in editing this thesis.

This project was part of a linkage project with The Prince Charles Hospital in Brisbane, Australia. Having a clinical partner in the project has given the investigation regular exposure to the clinical requirements of artificial hearts. I would like to thank Dr Keith McNeil in particular for his enthusiasm in the project as well as clinical expertise.

Throughout this PhD program I have been fortunate to have interacted with a number of people who have, in one way or another, provided some input to this work. I would like to extend my thanks to the following individuals:

- Ben Cumming for his mathematical advice and intense efforts trying to create a fully non-linear solution algorithm for the numerical program. Despite our lack of success in this endeavour you instilled a lot of confidence in my ability to apply mathematical techniques in other parts of this project.

- Dr Cameron Brown for his patience and calm. Your friendship and conversation throughout this project has made a job into a pleasure. I enjoyed the reassurance created from the two of us treading the same path.
- Professor Andy Tan for his initial works in this project. As chief investigator of this project I would like to thank you for your coordination and contributions.
- Julie Balen for being there from start to finish. Always interested to listen and provide feedback, I'd like to thank you for sharing in the achievements and failures during my project.
- Wayne Moore for his spectacular workmanship in fabricating and assembling the BiVAD prototype. This research department is privileged to have your experience as well as your technical perspective and capabilities. Yet again, your perfectionism has provided our research group with another functional, high quality prototype.
- Nick Greatrex for his interest in the project and his help in trying to develop a non-linear solution algorithm for the numerical program.
- All the technical staff in the Built Environment and Engineering Department including
    - Mark Hayne for his continued involvement in the project and his persistence in acquiring the 3D prototyping machine.
    - Lincoln Hudson for his patience with a mechanical engineer trying to describe electronic systems needed for the experimental. Your help and advice made the *in vitro* testing a smooth process.
    - Melissa Johnston and Jon James for their help with day to day issues and prototyping.

1 Introduction

Since 1990 an aging population, urbanisation and adjustments in lifestyle have contributed to cardiovascular disease being the world's most prolific killer. In Australia, circulation disease accounts for over 34% of annual deaths (AIHW 2006). The World Health Organization has warned that circulation disease is crippling not only the developed world as more than 60% of the global burden occurs in developing countries (Mackay and Mensah 2004).

Treatment of end stage heart failure requires clinical intervention where the failing heart's pumping function is assisted or replaced. In the United States just over 2000 heart transplants are carried out annually which amounts to 65% of global transplant procedures (UNOS 2005). However, it is estimated that 50,000 Americans currently require a heart donation (Debakey 2000). This extraordinary imbalance has accelerated the development of mechanical alternatives particularly in the form of Ventricular Assist Devices, VADs.

VAD technology has seen a range of fluid pump types miniaturised and modified. The resulting devices are required to be implantable, cause minimal blood damage and provide adequate support for a single failing ventricle. Traditionally, VAD designers focused on diaphragm type pumps as they emulate the natural pulse of the native heart. However, after the establishment of the International Society for Rotary Blood Pumps (ISRBP) in 1993, the development of rotary type blood pumps has gained traction (Takatani 2006). These devices are smaller, more efficient and incorporate fewer moving parts promising higher reliability of the support system.

Circulation of blood through the body demands a high work load from the left ventricle. For this reason much of the heart muscle contributes to left ventricular function. A common cause of heart attack is when a blockage occurs in coronary arteries occluding perfusion to the heart muscle. This condition, infarction, commonly leads to a part of the bulky Left Ventricle (LV) dying. Consequent congestion of the lungs has seen 20% of patients who suffer from a failed left ventricle develop subsequent right ventricular failure (Furukawa, Motomura, and Nose 2005). However, there is no single implantable rotary device to treat these

patients. Furthermore, there are very few reports of rotary Bi-Ventricular Assist Device (BiVAD) development outside our research group. This is likely a reflection of the reported difficulty experienced when trying to balance the VAD flows during preliminary clinical tests of rotary BiVAD support (Timms *et al*. 2006; Nonaka *et al*. 2002).

In order to control the implanted VAD the system controller needs to sense the cardiovascular (CV) system demands as well as quantify the VAD output. This is difficult as blood provides a hostile environment for mechanical sensors, especially pressure sensors. Substantial research has focused on means of actively controlling rotary VADs through observations of motor current, voltage and in some cases the arterial flow rate (Endo *et al*. 2000; Misgeld, Werner, and Hexamer 2005; Olegario *et al*. 2003; Endo *et al*. 2001). This issue is further complicated by the need for VADs to incorporate physiological controllers to account for high variability in patient CV demands (Wu *et al*. 2004). However, in order to create a robust active physiological controller, the circulation needs to be highly observable through accurate pressure and flow sensing.

This study was motivated primarily through the lack of available options for patients with Bi-Ventricular Failure (BiVF). Additionally, complications in haemodynamic sensing and BiVAD flow balancing encourage a fresh approach to the way cardiac support devices are controlled. This thesis documents an investigation into a novel BiVAD design where the pumps' outputs are **passively controlled** by the haemodynamics.

1.1 Significance

In a broad sense, the significance of this study is that it documents the first attempt to provide mechanical cardiac support without active monitoring and active control. The concept of a passively controlled VAD requires the device to sense haemodynamic signals from the vasculature and passively maintain its output to provide autoregulated support.

Research into BiVAD design and passive VAD control has attracted very little attention. Because of this much of the work in this thesis is novel by default. The configuration of the BiVAD, impellers, mechanical controller and the tailored numerical modelling in particular all incorporate novelty. The significance of this work therefore, also extends to the original designs and numerical methods which are being brought into the public domain.

It is clear that the significance of this investigation will only be felt if concepts from this thesis diffuse into the research community. Whether parts of this thesis are used for device development or conversation is encouraged by the ideas discussed then the study will have had significance. Ultimately, the candidate hopes that this study will initiate further investigations into developing inherently stable and self regulating blood pumps.

1.2 Aims and Objectives

1.2.1 Aim

The aim of this study was to assess the viability of a novel BiVAD prototype which is passively controlled by vascular pressure signals.

1.2.2 Objectives

This study is presented as a two part investigation in order to achieve the aim. The first is an experimental study where the design of a passively controlled BiVAD is detailed along with the construction of a prototype. Following this, the *in vitro* testing of the prototype in mock circulation is presented. The second part is an *in silco* study where a numerical program is developed to simulate the novel BiVAD operating in the human circulation. Considering the results from both studies the aim will be revisited in the discussion chapter towards the end of this thesis.

A number of objectives need to be met in order to achieve the aim of this study. These objectives are:

- The design and construction of a functional BiVAD prototype which passively responds to changes in vascular pressure.
- *In vitro* testing of the prototype in light of the project aim. This will be done in a pulsatile Mock Circulation Loop (MCL) which incorporates both systemic and pulmonary circuits.
- Development of a numerical program to simulate the supported circulation. This should be able to simulate the MCL and human circulation. This will require,
    - Numerical characterisation of the MCL and human CV systems
    - Numerical characterisation of the BiVAD prototype, its hydraulic performance and the response of the passive controller itself.
    - Generation of a flexible user-input based program to simulate supported and unsupported circulation. The modelled circulation structure too should be flexible in order to simulate the MCL or a human circulation.
- Carry out numerical simulations of supported circulation with the BiVAD prototype in light of the project aim.

1.3 Thesis Overview

This thesis consists of eight chapters which document the assessment of a novel BiVAD configuration intended to be completely self regulating. The content follows two separate investigations which together form a progressive study into the interaction between the prototype and the CV system. The structure of the thesis is very simple and from a broad perspective can be broken into four parts.

The first part includes **Chapters 1 and 2** which introduce the concept of Bi-Ventricular Support (BiVS) to the reader and provide a detailed review of relevant work to date. In this part the significance of the project aim becomes clear in the context of the demand for BiVS and the associated instability of rotary BiVADs.

Chapters 3 and 4 then form the second part of this thesis where the experimental study is presented. Initially this section provides a detailed account of the conception

of the prototype's configuration as well as the CAD design and construction. The *in vitro* testing is presented where the device is tested in mock human circulation. Experimental testing subjected the device to a range of sudden pathological haemodynamics to examine its passive response and ability to autoregulate. Individual discussions are included in this section to provide an analysis of each chapter's material.

The numerical study is presented in **Chapters 5 and 6** which makes up the third part of this thesis. The development of the numerical model includes a large body of work with a considerable number of appendices. This is representative of the time spent on this particular study. However, the results from the numerical model provide further insight into the BiVS and the prototype's operation than was initially expected. This made the numerical investigation a valuable part of the combined study. Again, individual discussion sections allow continuity by providing comments on each chapter's material.

In light of the aims presented in the first part, the results from the second and third parts of this thesis are drawn together to create the fourth in **Chapters 7 and 8**. These chapters provide a global discussion of the whole study. As well as addressing the aim of this study, a number of additional findings are outlined as well as issues faced in completing the experimental and numerical investigations.

The two part study provided a comprehensive insight into how a rotary BiVAD passively controlled by vascular pressure would interact with the human circulation. In employing an *in vitro* and *in silico* study no clinical testing was necessary. This was useful as tests could be repeated quickly and at little expense and did not challenge any ethical regulations. Furthermore simulations could be pushed passed what was physically or physiologically viable.

Following the main body of the thesis, detailed references are provided as well as minor appendices. In addition to this thesis a compact disk is provided. The compact disk includes the major appendices including MATLAB programming and supplementary documentation of the numerical model development. MATLAB programs to build the rotary pump geometries as well as the numerical model itself

are included as soft copies so that they can be used by others for non-commercial applications. The supplementary documentation for the numerical model details failed solution methods attempted during the construction of the model. These include mathematical functions used to characterise the rotary pump performance which were found to be unrepresentative. A number of methods used to incorporate these functions into the numerical solution algorithm are also described along with their numerical shortcomings. Even though they were not used in the final solution algorithm, they have been included as they document the process of constructing the numerical program. References to both the major and minor appendices are given at appropriate times throughout the thesis.

1.4 Research Output

"A Passively Controlled Bi Ventricular Support Device", (Gaddum, N., Timms, D., Pearcy, M.; *Manuscript submitted to Artificial Organs in Dec. 2008*).

"Optimising the Response from a Passively Controlled Bi Ventricular Assist Device, BiVAD", (Gaddum, N., Timms, D., Pearcy, M.; *Manuscript submitted to Artificial Organs in Dec. 2008*).

"Numerical Simulation of Supported Circulation with a Passively Controlled Bi Ventricular Support Device", (Gaddum, N., Pearcy, M., *full manuscript for journal publication is being prepared*).

"Miniature Pump Performance Manipulation through Changes in Pump Geometry", (Gaddum, N., Timms, D., Pearcy, M., *full manuscript for journal publication is being prepared*).

"Passive Control of a Rotary BiVAD; an Experimental and Numerical Investigation", (Gaddum, N.; Abstract published and Oral Presentation for the International Society for Rotary Blood Pumps, (ISRBP), Huston, U.S.A., October 2008).

“A Passively Controlled BiVAD”, (Gaddum, N., Timms, D., Pearcy, M.; Abstract published and Oral Presentation for the International Society for Rotary Blood Pumps, (ISRBP), Sydney, Australia, November 2007).

“Mixed Flow Impeller Design to Improve RVAD Performance for BiVAD Application”, (Gaddum, N., Timms, D.; Abstract published and Oral Presentation for the International Society for Rotary Blood Pumps, (ISRBP), Leuven, Belgium, September 2006).

2 Literature Review

2.1 Introduction

A review of current literature initially provided a description of the working environment for an artificial heart pump. This environment includes the Cardio Vascular, (CV), system, blood as the working fluid and the fragility of the blood tissues. These are obvious primary requirements for a study into mechanical support of the human circulation.

Further investigation needed a little more insight as a cardiac device that uses the hydraulic signals from the body to allow a passive controller response has never been attempted before. So, an analysis of what signals the native heart receives from the circulation and how it and the circulation respond provided a frame work for useful 'inputs' and 'outputs' for the passive controller.

The following review, therefore, outlines not only the device's environment but a system of hydraulic interactions between the heart and the circulation vessels which allow the cardiovascular system to stabilise itself. Heart disease is also examined along with current means of treatment.

2.2 The Burden of Heart Disease

Over the last century the increase in heart disease related deaths is a widely publicised reminder of a changing human lifestyle. Certainly convenience has changed the way we eat and exercise. However the 754,700 Australians suffering from heart, stroke and vascular disease (ABS 2005) is an indication of the lack of effective treatment available for this condition.

The 50,000 Australian deaths related to cardiovascular disease each year (AIHW 2004) is also a hint at the lack of effective treatments for this condition. With approximately 3000 heart donations made in the entire world annually (UNOS 2006)

and only 202 in Australia in 2006 (*Transplant Australia*) there is very little hope in relying on transplantation alone to ease this burden.

In the most recent national survey, 1.1 million Australians had disabling conditions associated with heart, stroke and vascular diseases (AIHW 2004). In this last decade the prevalence of cardiovascular disease in Australia has increased by 18.2% (AIHW 2004) which has encouraged the development of mechanical alternatives. Figure 2-1 emphasises the dominating portion of deaths attributed to cardiovascular disease in Australia for 2002.

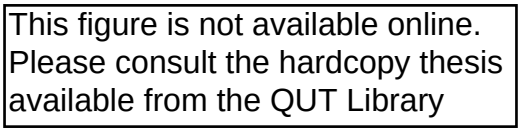

Figure 2-1: Death by disease categories in 2002. Source (AIHW 2004).

Heart disease commonly begins as left ventricular dysfunction caused by heart attack, coronary valvular disease, hypertension, cardiomyopathy, vascular disease, myocarditis and viral infection (Guyton 2005). Left untreated, the dysfunctional ventricle can deteriorate causing congestive heart failure.

A diseased left ventricle strains vital organs by not providing sufficient perfusion. A strain is also experienced by the right ventricle as elevated pulmonary pressure adds extra load to the right ventricles workload. Over 20% of left ventricular failure patients develop subsequent right ventricular failure (Furukawa, Motomura, and Nose 2005).

2.3 The Cardiovascular System

The circulatory system, in its entirety, is a hydraulic series circuit[1]. The schematic in Figure 2-2 depicts this circuit.

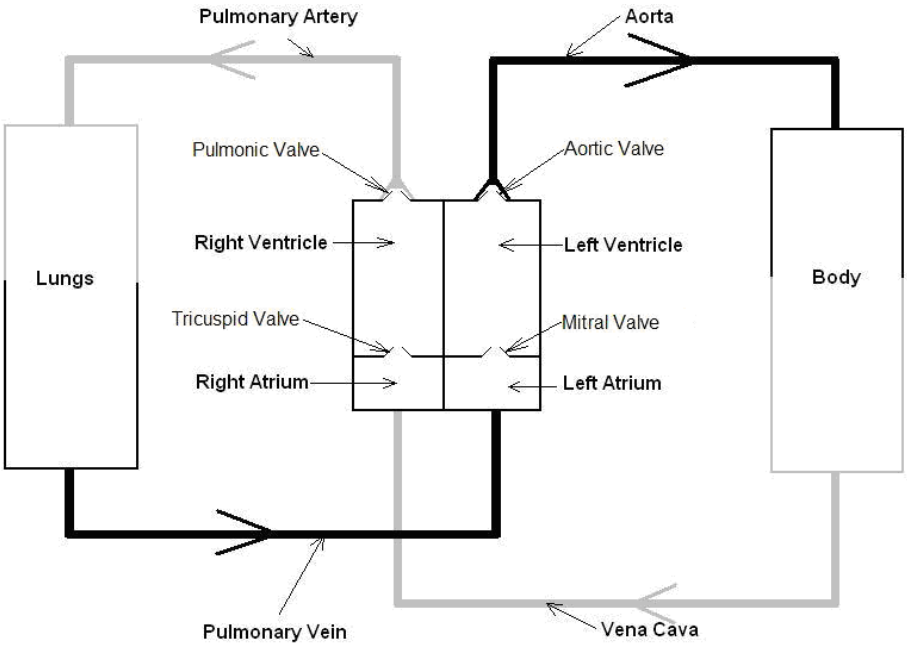

Figure 2-2: Schematic of human circulation.

The two boxes labelled 'body' and 'lungs' are parallel sub-circuits. The dark type lines show the path of the oxygenated blood and the grey type shows the de-oxygenated. The main arteries shown, the Aorta and Pulmonary Arteries; sustain high pressure and pulsatile blood flow. The veins, Pulmonary Vein and Vena Cava carry blood back to the heart and have a relatively constant cross sectional velocity profile over time.

Within each sub-circuit is a network of vessels beginning with arteries which feed the arterioles. From the arterioles the blood is channelled into capillaries which allow gas and nutrient exchange through the tissues to facilitate respiration. The blood then moves through the venules and into the veins to return back to the respective heart chamber.

---

[1] The bronchial shunt creates a parallel circuit from the Aorta to the Pulmonary Vein which is an exception to this generalisation. However, for the explanation of basic cardiovascular principles a series hydraulic circuit will be assumed.

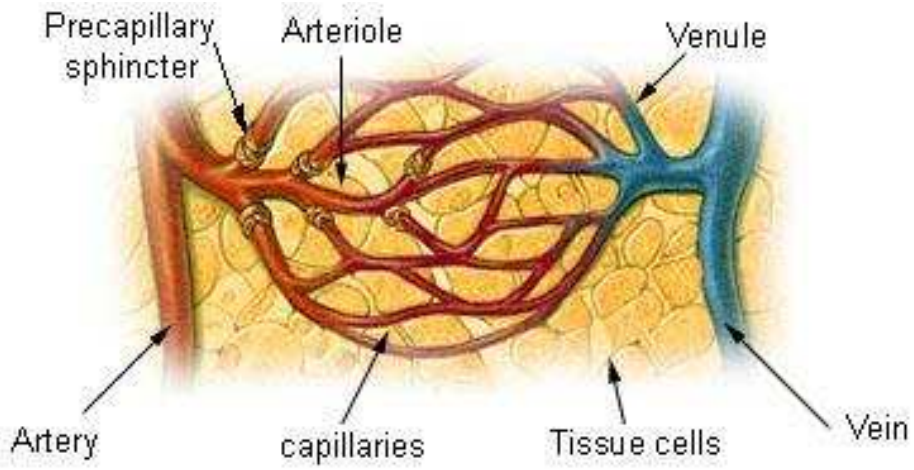

Figure 2-3: Illustration of a arterial to venous vascular network. Modified from source (Guyton 2005).

Resistance to flow is known as the peripheral, or vascular, resistance. This is affect by a number of factors including vessel diameters, blood viscosity, vessel compliance and precapillary sphincters. Precapillary sphincters are positioned at bifurcations within the arteriole network. Swelling of the sphincter causes a stenosis of the arterioles and allows localised perfusion control by restricting flow downstream and increasing upstream pressure.

2.3.1 Healthy Heart Function

Figure 2-4 shows a multiplot for the healthy left heart during one cardiac cycle. The atrial, ventricular and aortic pressures are shown as the top three plots. The native heat beat consists of a blood ejection phase, systole, and a blood filling phase, diastole.

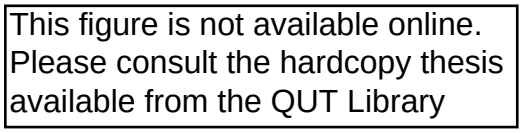

Figure 2-4: Multiplot during the healthy left heart's cardiac cycle. Source (Guyton 2005).

During systole the filled ventricle contracts its muscles increasing the ventricular blood pressure. This elevated pressure causes ejection through the aortic valve into the artery. At the same time, the mitral valve shuts preventing blood flow back into the atrium. The atrium then begins to fill as pulmonary venous blood returns to the heart. Systole, therefore, consists of ventricular contraction causing fluid ejection and atrial filling.

Completion of systole is signalled by the relaxation of the ventricle and the subsequent closure of the aortic valve. The valve's closure is apparent by the characteristic 'dicrotic notch' which sees a second pulse in arterial pressure. As the aortic valve leaflets fill with receding arterial blood following the pressure gradient back toward the ventricle, the backflow is suddenly stopped. The inertia of the suddenly halted blood causes fluid shock inducing a compliant response at the artery sinus increasing pressure.

The diastolic phase then begins as the mitral valve opens to let blood fill the ventricle. Then, just before the ventriclular systolic phase begins again, an atrial systolic contraction increases the kinetic energy of theblood entering the ventricle. This helps to prevent back flow into the atrium as the mitral valve closes.

Textbooks indicate that it is difficult to quantify general healthy haemodynamic parameters. In general this is due to the wide range of body sizes, states of health and ages of people in the general population. For example, the mean aortic pressure for the average human is around 78 mmHg at birth and around 115 mmHg for an 80 year old. However for the purpose of this project, particularly with the experimental and numerical simulation, healthy pressures and flows will be defined based on text data. Healthy aortic pressure pulses between 120 and 80 mmHg with a mean pressure of around 100 mmHg and pulmonary artery pressure pulses from 10-25 mmHg with a mean pressure of around 15 mmHg. The flow rates for both circuits will be considered equivalent unless stated at 5 $L.min^{-1}$, (this assumes a negligible effect from the Bronchial shunt), (Guyton 2005).

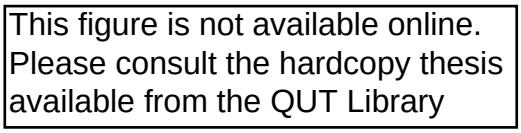

Figure 2-5: Native pulsatile pressure through the human circulatory system whilst lying down. Source (Guyton 2005).

Figure 2-5 shows the pulsatile pressure through different sections of the circulatory system around the schematic diagram given in Figure 2-2. The regions of high pressure oscillations are, as would be expected, in the large blood vessels after the ventricular chambers (Guyton 2005).

2.3.2 Ejection Fraction

The Ejection Fraction, *EF*, of the ventricle, (usually *EF* refers to the left ventricle output), is the ejected volume during systole divided by the end diastolic volume,

$$EF = \frac{V_{ejected}}{V_{\max}}.$$

Equation 2-1

In this equation, $V_{ejected}$ is the volume ejected (ml) from the ventricle during systole and V_{max} is the end diastolic ventricular volume (ml), or maximum ventricle volume. The ejection fraction is a function of the contractility of the heart. The resident blood volume in a healthy left ventricle goes from 150-80 ml from the beginning to the end of systole. This equates to an ejection of 70ml for both the left and right ventricles during each cardiac cycle. According to Equation 2-1, this corresponds to an ejection fraction of approximately 47% for a healthy heart. During heart failure the contractility can decrease causing a lowering of the *EF* (Guyton 2005).

2.3.3 Blood, The Working Fluid

The primary constituents of blood are the platelets, the red and white blood cells and the plasma suspension. Red blood cells, or Erythrocytes, consist primarily of Haemoglobin which provides a media for carbon dioxide and oxygen to diffuse between the lungs and muscle tissue. Between 6-8 μm in diameter, these disk-shaped cells have an average life span of around 120 days. The red blood cells are very sensitive to their surroundings and can rupture when they come in contact with non-endothelial surfaces. The breaking of the cell wall and consequent spilling of the cellular contents into the plasma is called Haemolysis.

Minimising haemolysis is a key issue in blood pump development. Blood cell exposure to prolonged shear stress (Wood et al. 2005; Paul et al. 2003) or heat (Araki and Taenake 1995) are both key issues for pump designers to minimise. A testing standard has been adopted by heart pump developers to quantify haemoysis caused by any particular pump. The Standard Practice for Assessment of Hemolysis in Continuous Flow Blood Pumps (ASTM_F1841-97 1998) requires the determination of the Normalised Index of Haemolysis, NIH ($g.100L^{-1}$),

$$NIH = \Delta freeHb \times \frac{100 - Ht}{100} \times \frac{100V}{QT_{Total}}.$$

Equation 2-2

The *ΔfreeHb* term is the increase in plasma free Haemoglobin (g.10L^{-1}). To account for test specific conditions; the initial Haematocrit, *Ht* (%), the test volume, *V* (ml), the blood flow rate, *Q* (L.min^{-1}), and the total testing time, T_{Total} (mins), are also employed to determine the NIH.

A common unit for the NIH is g.100L^{-1} (Kameneva *et al*. 1992; James *et al*. 2003; Masuzawa *et al*. 1999; Araki and Taenake 1995). Associated with this standard unit a common target threshold *NIH* has evolved. State of the art blood pumps appear to aim to maintain the *NIH* below 0.02 g.100L^{-1} in their pump blood testing. Hematocrit is a volume ratio of red blood cells to gross blood and is normally around 43-49% in males and 37-43% in females.

Paul *et al.* (2003) passed whole blood through a Couette device where the shear stress and time of exposure could be prescribed. Figure 2-6 illustrates the effect on the *NIH* from both shear stress magnitude and exposure time. The test showed that a minimum exposure time of 0.6s per pass is required before red blood cells begin to break down at shear levels of over 420 Pa.

Figure 2-6: Plot of *NIH* as a function of both fluid shear stress and time. Source (Paul *et al.* 2003).

Arguably a more serious issue is thrombus, or clot formation. If blood is left stationary it will stagnate and then coagulate into a jelly-like network that obtains an inherent structural stiffness. Blood pumps are particularly susceptible to thrombus formation if there are areas of recirculation, or areas of stationary flow. Thrombi can grow and dislodge (an embolism) from the pump's surface and travel down the vascular tubes causing a blockage somewhere in the body, e.g. a stroke if the blockage occurs in the brain. It is, therefore, important that the fluid paths within the pump are designed carefully so as to maintain a continuous fluid change in the device.

Further detail of the biochemistry and cascade reactions of blood damage can be found in (Guyton 2005) and a quantitative study in (Leverett *et al*. 1972).

2.4 Cardiovascular Bio-Signalling

The native control system of the heart was investigated so as to provide inspiration for designing the passive controller system of the BiVAD. It was assumed that a device that used similar signal inputs to render similar outputs to the native heart's control system would promote sensitivity and stability in a mechanical BiVAD. CV system control responses can be divided into three categories. These are short, medium and long term regulation.

2.4.1 Short Term Regulation

Short term regulation is largely achieved by the inherent redistribution of blood driven by pressure gradients throughout the arteries and veins. The nature of ventricular interaction, including the Frank-Starling Mechanism, is essentially the dynamic fluid system working to operate at its lowest energy state. However, the circulation is also constantly being affected by nervous stimulation in a closed loop control system.

2.4.1.1 Short Term Regulation: Pressure to Flow Energy Conversion

The schematic in Figure 2-2 incorporates an important structure allowing effective inherent pressure regulation. Due to the compliant nature of vessels, pressure energy can be stored and converted into kinetic energy to redistribute blood around the systemic and pulmonary circuit. Similarly, the two phase action of the pumping ventricles together with the passive filling during diastole allows the heart to redistribute blood between vascular circuits. The latter is, in essence, the Frank-Starling Mechanism.

The Frank-Starling Law

The Frank Starling Law forms part of the body's haemodynamic regulation mechanism. It explains the physiological means through which the pulmonary and systemic circuit fluid volumes are balanced. The law states that increased diastolic filling, caused by elevated atrial pressures, will induce increased fluid ejection and therefore cardiac output (CO [$L.min^{-1}$]). Consequently, if one vascular circuit becomes slightly congested, elevated venous pressures will encourage increased venous return. Increased venous return will ensure a higher end diastolic volume in the downstream ventricle. The ejected volume will increase thus moving congested fluid to the other vascular circuit (Starling and Visscher 1926).

This means of passive flow balancing is something which is enjoyed by pulsatile blood pumps which incorporate a passive filling stroke, such as the native heart. The most important feature of this phenomenon is that the end diastolic volume is dictated by the filling, or atrial, pressure.

Ventricular Interdependence

If the Frank-Starling Mechanism is viewed from the perspective of the whole CV system, this implies an interdependence of both ventricles. Since both ventricles pump in a series circuit, the output of one will affect the End Diastolic, ED, volume of the other.

As would be expected, this interdependence is dynamic as it takes a finite duration for pressure signals to be transmitted through a compliant vascular circuit between ventricles. What is perhaps not so obvious, however, is the effect of CV disease, such as left ventricular dysfunction, on this interdependence. In this case, the resulting dilated left ventricle is operating close to its elastic limit and so is less sensitive to preload changes. A diseased CV system, therefore, looses much of its ventricular interdependence and therefore haemodynamic control (Mandarino *et al*. 1994).

Another form of ventricular interdependence exists due to the proximity of the left and right ventricles. The septum, the tissue within the heart which separates the ventricles can bulge into either ventricular cavity depending on pressure variation. This is called septal shift and occurs when ventricles are dilated. This has a noticeable effect on ED volumes, and therefore cardiac output. An increased RV ED volume will decrease the LV ED volume as the LV becomes less compliant. Surprisingly however, an increased LV ED volume has very little effect on the RV ED volume probably due to the geometric differences between the ventricles. Instead, the End Systolic, ES, volume of the RV will decrease indicating an increased RV output. This is caused by the dilated LV assisting the RV pumping function and therefore contractility (Pinsky *et al*. 1996).

2.4.1.2 **Short Term Regulation through Nervous Response**

Nervous responses control the constriction or dilation of vessels and precapillary sphincters as well as changes in Heart Rate, HR, and contractility of the ventricle. Total blood volume in the body is also regulated by the kidneys to alter the Central Venous Pressure, CVP. These nervous responses are triggered by the sympathetic and parasympathetic nerves reacting to pressure fluctuations and in some cases

changes in chemical concentration. These nervous reactions induce localised hormone secretions which vary the constriction of the smooth muscle surrounding the vessels as well as the contractility of the heart.

The Heart

Since the heart is positioned between the main veins and arteries, (see Figure 2-2), controlling inputs are virtually exclusively vascular pressures. Baroreceptor-like nodes in the arterial system provide signals to the heart muscle to increase contraction power through the Sympathetic Nervous System. Parasympathetic nodes in the atria sense the filling pressure and inhibit the sympathetic stimulation. The sympathetic and parasympathetic nervous systems create a closed loop control system equipped with the ability to elevate and lower vascular pressures. This ability to regulate global pressures is often referred to as the CV system's baroreceptor response.

Figure 2-7 depicts the sympathetic communication lines and the parasympathetic nodes, (the S-A and A-V nodes), and parasympathetic communication lines, (the Vagi), within the heart.

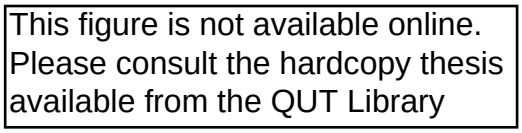

Figure 2-7: Cardiac sympathetic and the parasympathetic vagus nerves. Source (Guyton 2005).

An explanation of the Frank-Starling Mechanism indicated the vital role that the atrial, or diastolic filling pressure, has on affecting CO. CO has maximum sensitivity to atrial pressure between -2 and +2 mmHg as this filling pressure determines the end diastolic volume. Each profile shown in Figure 2-8 shows the impact that atrial pressure has on CO. Furthermore, the figure shows how increased or decreased nervous stimulation can further augment CO.

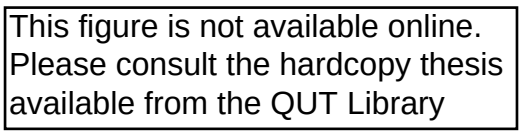

Figure 2-8: Effect on the cardiac output for different degrees of sympathetic or parasympathetic stimulation. Source (Guyton 2005).

According to Equation 2-1, with a maintained EF, the ejected volume per heart beat (which determines the CO) is proportional to the end diastolic volume. The sympathetic and parasympathetic nervous system is employed to regulate the highly sensitive CO by adjusting contractility of the heart. This stimulation allows the heart to maintain adequate flow and peak systolic pressure over a range of vascular demands.

The Vascular System

The sympathetic nervous system has strain activated nodes in the walls of the systemic arteries, particularly the aortic branch and the carotid arteries. A drop in

arterial pressure will decrease the hoop strain in these vessels. Sensed by the sympathetic nervous nodes, the system will act to elevate the arterial pressure. Secretion of hormonal vasoconstrictors into the muscular arterial wall then causes the vessels to constrict to increase the strain energy in the flexible vessel walls. Similarly, vasoconstrictors released into the heart muscle increase the contractility of the ventricles as well as increasing heart rate. One of these hormones is commonly known as Adrenaline, or Epinephrine.

A parasympathetic nervous response works to inhibit the sympathetic nervous action of elevating pressure. These act to decrease elevated vascular pressures through dropping ventricular contractility and dilating blood vessels. An example of a vascular dilator is Histamine which is a hormone released locally into the capillaries to increase flow to damaged tissue which causes localised swelling.

It should be noted the nervous response is not solely pressure sensitive. Within the capillary system there are sympathetic and parasympathetic hormone releases that are actuated by local metabolism. This means that these particular hormones, (Endothelin and Bradykinins respectively), constrict and dilate vessels to regulate flow, and therefore rates of gas and nutrient exchange, (Guyton 2005).

2.4.2 Medium Term Regulation

The Kidneys play a vital role in haemodynamic regulation as they control the total blood volume to regulate the CVP. Renal regulation has been classed as a medium term means of regulation as it requires at least 10-20 minutes to create notable pressure changes.

2.4.2.1 **The Kidneys**

The kidneys control the rate of expulsion of fluid from the body, including the blood. Regulation of the total blood volume is analogous to the regulation of the CVP. Essentially this means that the kidneys have the ability to increase or decrease the CVP which can raise or lower the global vascular pressures respectively.

Heart failure causes decreased arterial pressure and therefore a lowered EF. The renal response is to increase CVP so as to increase the preload on the heart. This increases the End Diastolic Volume, EDV, distending the ventricle walls. The increased strain on the ventricle wall caused the heart muscle to approach its elastic limit essentially increasing the contractility of the ventricle. Thus, the increased fluid volume can increase contractility and therefore Stroke Volume, SV, so lift the diseased EF. It is important to note that this effect can only occur if the contractility of the ventricles is volume dependent.

Figure 2-9 shows the ability of the kidneys to regulate vascular pressure when excess blood is infused into a canine model (Guyton 2005).

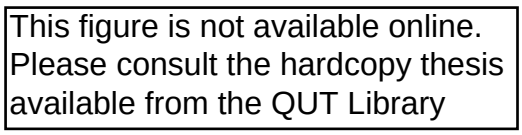

Figure 2-9: Transient multi-plots showing the kidney's ability to drop vascular pressures through fluid expulsion when blood volume is increased. Source (Guyton 2005).

After the infusion, the vascular pressure rapidly increases. The increased atrial pressure causes an increase in cardiac output by approximately 230%. To overcome these elevated pressures and excessive flow, the urinary output increases to try to

expel fluid and drop the vascular pressure and therefore the CO to a more physiologically safe state (Guyton 2005).

2.4.3 Long Term Regulation

When the cardiovascular system is subject to a long term change in haemodynamics, long term regulatory responses initiate vascular or cardiac remodelling. Changes can be as minor as a small cut or abrasion or as major as an infarction. Remodelling includes variation in vessel diameter as well as number of vessels to adjust local blood pressure and flow. The geometry of the myocardium may also change to allow a higher or lower contractility inducing a respective adjustment to the Cardiac Output, CO. Such physical changes to the components of the CV system can occur in days to months depending on the extent of restructuring of the tissue, (Guyton 2005).

2.5 Heart Failure and Therapy

Heart failure, (or congestive heart failure), is a disease that originates from ventricular dysfunction. This can be due to a number of reasons namely heart attack and cardiac valve disease. Left untreated the heart may either recover or degenerate under the strain and develop into Heart Failure (Dargie, McMurray, and McDonagh 1996).

2.5.1 Ventricular Dysfunction to Heart Failure

A heart attack, or myocardial infarction, occurs when there is a blockage in one of the two coronary arteries. All muscle that received blood downstream of the blockage is starved of oxygen and consequently dies. The bulky left ventricle incorporates most of the muscle mass of the heart and requires more blood flow as it does, approximately, five times the work of the right ventricle. Ventricular dysfunction, therefore, is most commonly a failing of the left ventricle. This condition renders the left ventricle unable to circulate sufficient blood for the body. In serious cases this will result in the Ejection Fraction, *EF*, decreasing to a level where there is insufficient output to perfuse the end organs, i.e. kidneys and liver.

As previously discussed, a healthy *EF* is around 47%. During heart failure the ejection fraction can fall to around 20-25%. If the end diastolic volume remained at 150 ml, the left ventricle would eject only 30 ml per cardiac cycle.

To raise the CO from this dangerously low level, the body will increase total blood volume by consuming and retaining water. The increase in total fluid volume increases the Central Venous Pressure. Consequently the elevated atrial pressures will increase ventricular filling allowing an increased end diastolic volume. The now swollen ventricles have volumes ranging from approximately 230 to 180 ml during systole. However, as the *EF* still remains at around 25% the ejected volume has risen to 50 ml. This condition is known as dilated cardio myopathy (Guyton 2005) and is the body's natural reaction to elevate vascular pressure to allow perfusion to all its organs.

Elevated filling pressure and distended muscle tissue means there is heavy loading of the ventricles. Unless treated, the patient risks the condition deteriorating from ventricular dysfunction to congestive heart failure.

Due to the elevated atrial pressures the right heart too is now extended and straining to eject fluid into a congested pulmonary circuit that isn't being evacuated sufficiently by the diseased left heart. This strain on the right heart is a popular diagnosis for the frequent subsequent failure of the right heart after left ventricular failure.

The severity of heart failure is commonly gauged using the New York Heart Association (NYHA) Functional Classification. This measures the burden of the patient's disease upon a scale from Class I to Class IV in increasing severity, (Dolgin 1994). These are,

I. Patients with no limitation of activities; they suffer no symptoms from ordinary activities.
II. Patients with slight, mild limitation of activity; they are comfortable with rest or with mild exertion.
III. Patients with marked limitation of activity; they are comfortable only at rest.
IV. Patients who should be at complete rest, confined to bed or chair; any physical activity brings on discomfort and symptoms occur at rest.

2.5.2 Treatment

Treatment of ventricular dysfunction depends on the severity of the disease. For those with left ventricular dysfunction it is commonplace to maintain a course of drug therapies to reduce congestion of blood in to the pulmonary circuit. BETA-blockers and diuretics or ACE-Inhibitors are often prescribed to reduce CVP by lowering vessel resistance and decreasing blood volume. This attempts to unload the ventricle to promote regeneration, but can cause organ damage as it suppresses the body's sympathetic nervous response to maintain elevated vascular pressure. If the patient progresses to Class IV or end stage heart failure, more invasive treatments are required. These include mechanical assistance, xenoplasty, cardiomyoplasty and organ replacement (Timms 2006).

Early detection of patients with subsequent right ventricular failure (RVF) is vital so that Bi-Ventricular Support (BiVS) can be given to reduce the high rate of mortality of those whose right ventricles fail after left ventricular failure (LVF) (Meyns 2005). It is claimed that the incidence of such a cascade leading to death could be as high as 77% (Furukawa, Motomura, and Nose 2005).

2.6 Mechanical Ventricular Support

Mechaical assistance of ventricular function has been provided using two distinct types of devices; pulsatile devices and continuous flow, (or non-pulsatile), devices.

An important question regarding these two different types of cardiac support is that of the benefit in retaining our natural pulse. This is an issue that has been examined from a physiological standpoint. Chronic testing of pulsatile *vs.* non-pulsatile support seems to indicate that a pulse is not vital (Yozu *et al*. 1994). It is advised that non-pulsatile support should be provided at a higher flow to pulsatile support (Nose and Kawahito 1997). However, concern over the effectiveness of sympathetic nervous constriction without periodic hoop strain of the artery walls is a concern. There exist rotary VADs which have an incorporated pulsatile function by oscillating the pump speed (Chou *et al*. 2001).

2.6.1 Pulsatile Ventricular Support

Pulsatile blood pumps normally involve a reciprocating pressure plate or diaphragm along with inlet and outlet valves to drive fluid through the pump. The reciprocating, or pulsatile, action of these pumps makes their operation a two phase process where fluid is drawn into the pump in the first phase and then ejected in the second. In general, these devices are cheaper than their rotary counterparts and the pulsing operation imitates the native ventricle action. However, one of the most attractive features of many pulsatile pumps is their ability to be operated using an active or passive filling mode.

Active filling is achieved by mechanically inducing a negative pressure in the VAD to suck blood through the inlet cannula. Passive filling mode is where blood is driven into the VAD by venous pressure only. When the passive filling mode is used the VAD can emulate the Frank Starling mechanism and therefore enjoy the flow regulation that is achieved by the native passive filling ventricles, (Mesana 2004). Figure 2-10 shows the EXCOR Berlin pulsatile VAD (Drews et al. 2000) where the inlet and outlet flow conduits are both directed to the left. The drive line protruding from the right allows air to enter the device to drive the diaphragm against the blood creating the systolic function. Air can then be sucked back up the drive line for active filling, or driven back by the passive filling blood pressure.

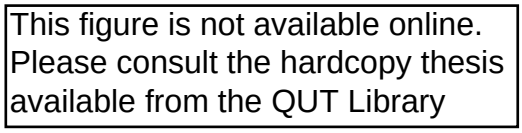

Figure 2-10: The EXCOR Berlin pulsatile VAD.

Pulsatile pumps, (Bhunia and Kung 2004; El-Banayosy *et al*. 2005; Park *et al*. 2003), are commonly large and complex due to the range of motion of reciprocating parts. These moving parts are also subject to periodic stresses and so material susceptibility to fatigue failure is a critical issue (Teixeira *et al*. 2001). Bleeding, thromboembolism, and infection are also regularly attributed to this mode of

operation. This is because these reciprocating pumps invariably incorporate areas of stagnation as well as inducing localised high velocity jets of blood (Wilhelm *et al*. 2005). This is a particular issue for the regions around each of the two valves required for each pump.

2.6.2 Non-Pulsatile Ventricular Support

Rotary type LVADs have been developed to cater for the larger market of patients with LVF such as the Australian developed VentrAssist (Tansley, Vidakovic, and Reizes 2000) shown in Figure 2-11.

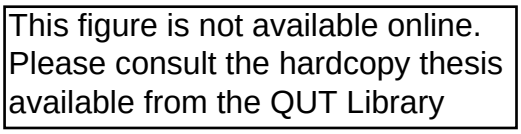

Figure 2-11: The VentrAssist from Ventracor. Clinical device, side view *(left)*. View of rotor through a partially transparent housing *(right)*. Source (Ventracor 2008).

Single ventricle supporting pumps have taken the form of axial flow and radial flow, (centrifugal flow), pumps. These devices have seen a surge in popularity since the late 90s and provide a continuous flow support system. These devices incorporate a pump casing with a fluid inlet, outlet and pressure developing diffuser and a rotating impeller. Kinetic energy is supplied to the fluid by the impeller which is then converted into pressure energy as it moves through the diffuser. Technical detail regarding rotary pumps can be found in the literature, (Timms 2006; Stepanoff 1957; Wood et al. 2005).

Without the need for reciprocating parts, rotary type VADs are smaller and more compact than pulsatile pumps. Reduced size increases the implantability and makes them a less cumbersome treatment for heart failure. A reduced wetted area of these

devices reduces the likelihood of areas of stagnation. The development of these devices has seen a progression from shaft driven impellers with fluid seals through to magnetically levitated and driven impellers. These are carefully discussed in Timms (2006).

Like the pulsatile devices, rotary blood pumps have a number of feasibility issues with their operation which are carefully scrutinised in Mesana (2004). Rotary pumps inherently cause suction at their inlet. This suction makes the ventricle cavity susceptible to collapse if blood is completely evacuated. Additionally rotary pump failure causes a concern as they do not incorporate valves to block backflow should the impeller stop rotating. Haemolysis too is an issue for these devices as the small impellers run at high speeds causing high levels of sheer stress in the blood within the pump. However, continued material developments and computational modelling of the flow field inside these pumps have reduced haemolysis levels considerably.

2.7 Bi-Ventricular Support

For patients with end stage bi-ventricular heart failure, (Class VI of the NYHA Functional Classification), who are no longer improving with drug therapy, mechanical support for both ventricles is often their only option while waiting for a heart donation. Since the demand for right heart support is comparatively low, there are limited options for these patients. Almost invariably, a paracorporeal pulsatile VAD, such as the EXCOR shown in Figure 2-10, is used to support the RH (Furukawa, Motomura, and Nose 2005).

Depending on the severity of the disease and the treatment protocol set out by the patient's cardiologist, the portion of pumping work done by the VADs can vary. This is known as the level of support. For a patient receiving 50% support, half of the flow will pass through the VAD and the other half will be ejected through the arterial valve. Total support from a VAD is when the heart valve remains closed so that all the flow passes through the VAD.

Currently there are no FDA or TGA[2] approved rotary BiVS systems (Timms *et al*. 2006). Until a donor heart is sourced, Australian patients with BVF are supported using two extracorporeal pulsatile pumps, such as those depicted in Figure 2-12, that require them to remain in a hospital bed.

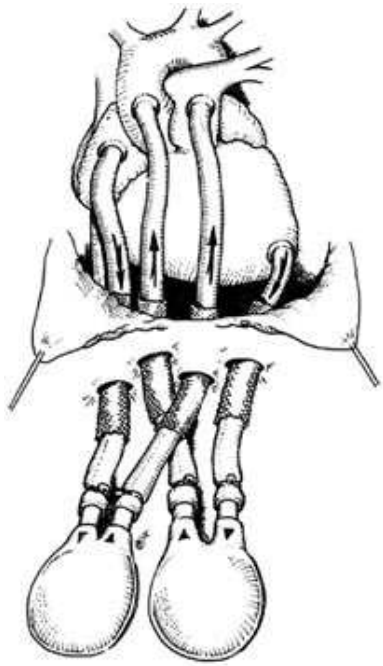

Figure 2-12: Two characteristic pulsatile VADs providing BiVS. The LVAD (on the right) cannulates the apex of the LV and then returns blood to the base of the aortic arch. The RVAD (on the left) takes blood from the RA to the PA.

The LVAD takes blood from the apex of the left ventricle through the inlet cannula. It then pumps the blood up the outlet cannula into the aorta. This essentially forms a parallel circuit with the LV. The RVAD inlet cannula is typically inserted into the RA, although occasionally the RV. Primarily the reason for this is due to the geometry of the RV as the RV wall is reasonably close to the septum. There is therefore the risk that the septum will occlude the RVAD inlet port. The RVAD then pumps blood through the outlet cannula into the PA.

Although no BiVS systems have been approved by national health authorities, some groups have been investigating BiVS using rotary pumps. Dual rotary pumps have been tested with moderate success both as dual extracoperal, such as the Biomedicus

[2] Food and Drug Administration, (FDA), the US clinical health authority. Therapeutic Goods Association , (TGA), the Australian clinical health authority

pumps (Berger *et al*. 1998) and a totally implanted system using Gyro pumps (Nonaka *et al*. 2002; Takami *et al*. 1998; Watanabe *et al*. 2004). Additionally, the CorAide was used in combination with a modified CorAide called the DexAide (Fukamachi *et al*. 2005) to provide BiVS (Fukamachi *et al*. 1999). The main underlying issue with these dual rotary support systems has been flow balancing between the pumps. It seems that with a single VAD, the passive filling of the native right ventricle has a considerable hand in balancing the circuits.

The BiVACOR is a single device incorporating a dual rotary pumping system. Designed for complete implantation, acute extracorporeal *in vivo* tests have shown that the device is potentially a feasible means of BiVS. This device, however, is still in development after recently having completed the first round of acute animal testing (Timms 2007; Timms et al. 2008).

2.8 Non-Pulsatile Blood Pumps

Non-pulsatile support is achieved using two different configurations of rotary pumps. These are radial flow (or centrifugal flow) and axial flow pumps. Both of these configurations include a rotating impeller inside a pump housing, although the generation of pressure head is different. The term radial flow or axial flow indicates the direction of the work done upon the fluid with respect to the rotating axis of the impeller. Figure 2-13 and Figure 2-14 show sectioned depictions of the DeBakey axial VAD (Tayama et al. 1999) and a characteristic radial flow pump respectively, showing the direction of blood flow through the devices.

This figure is not available online.
Please consult the hardcopy thesis
available from the QUT Library

Figure 2-13: Sectioned depiction of the DeBakey axial flow VAD.

The orientation of the blade faces indicate the direction that work is done upon the fluid.

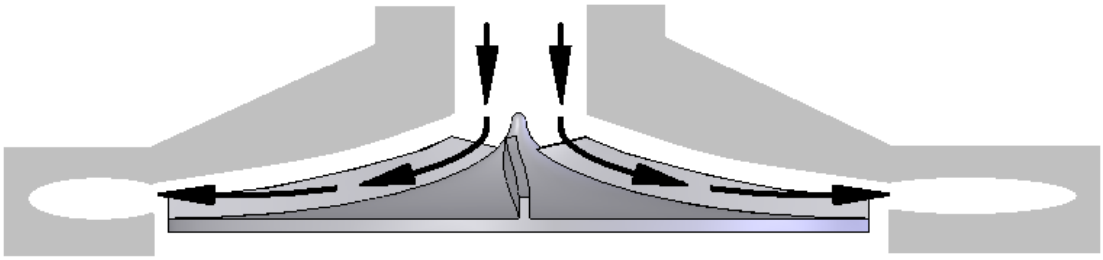

Figure 2-14: Sectioned image of a radial flow pump indicating the direction of blood flow through the device.

The axial and radial flow impeller blade arrangements shown are both supported by a single lower shroud only, these are called ‘semi-open impellers’. Rotary impellers may have numerous types of shroud configurations as shown in Figure 2-15. An upper shroud may also be included connecting the upper tips of the blades to provide fully enclosed flow channels. These are called an ‘enclosed impeller’. An impeller may also incorporate no shrouds at all. Each configuration incorporates differing attributes when used in blood pumps. A review of these can be found in Timms (2006).

This figure is not available online.
Please consult the hardcopy thesis
available from the QUT Library

Figure 2-15: Rotary impeller configurations; open, semi-open and enclosed, source (Tuzson 2000; *Engineers Edge - Pump Impeller Types*).

The job of the impeller is to increase the tangential component of the fluid velocity, (e_u). It will be shown that the increase in e_u is approximately proportional to the developed pressure head.

Rotary pumps are not restricted to completely axial or radial flow modes, in fact many rotary pumps may have a slight mixture of blade orientations. Technically, these are called a mixed flow mode; however, traditionally a mixed flow pump has an obvious axial inlet to the impeller and an equally obvious radial outlet as illustrated in Figure 2-16

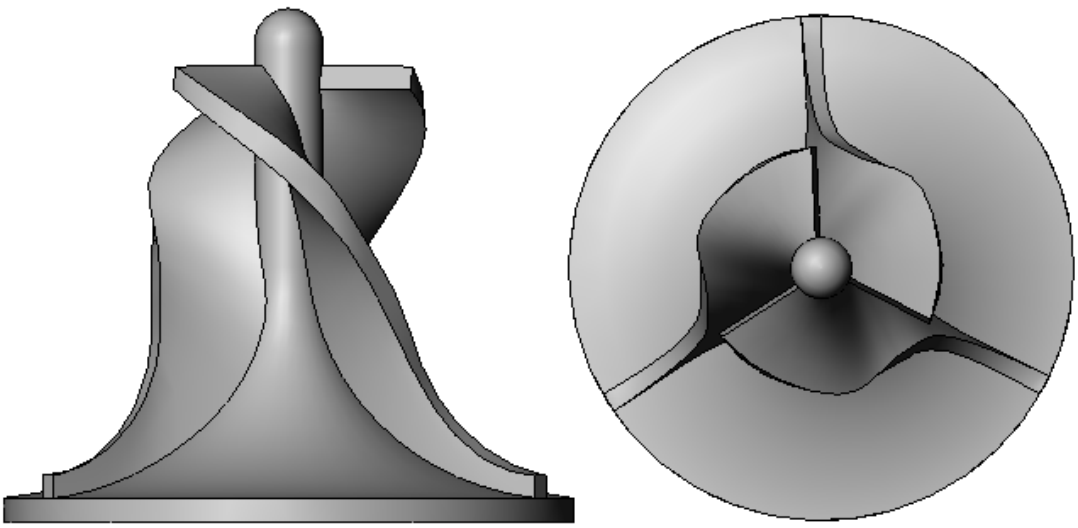

Figure 2-16: Side elevation, left, and plan view of a mixed flow impeller.

At the inlet of the impeller, the blade faces are predominantly in the axial direction. Near the outer, or impeller periphery, the blade faces are predominantly radially

oriented. The mixed flow impeller, therefore, does axially directed work, (in the negative z direction), at the inlet and radially directed work at the outlet.

In the interest of maximising pump efficiency, axial flow pumps are generally employed in 'high' flow – 'low' pressure applications whereas radial flow pumps are used in high pressure – low flow. A measure of what classes as high and low can be found in Stepanoff (1957). A pressure of 100 mmHg and a flow rate of 5 $L.min^{-1}$ would be classed as a low flow – high pressure case making a radial mode of flow a potentially more efficient device.

Typically axial flow blood pumps are smaller incorporating rotors with an outer diameter of Ø4-10 mm as opposed to radial flow blood pumps with a typical outer impeller diameter of approximately Ø40 mm. Consequently, the efficiency is compromised further in axial flow VADs and they operate at a higher speed. However, their smaller size increases device implantability and patient comfort (Song *et al*. 2003). A detailed investigation into the relative merits of rotary VAD flow modes can be found in sources (Timms 2006; Song *et al*. 2003; Wood *et al*. 2005).

2.9 Haemodynamic Complications during BiVS

There are a number of complications that can affect the safety of a BiVAD. Earlier, issues involving blood damage were discussed including thrombus formation and lysis of the red blood cells. However in the context of barometric control, in which this study is primarily concerned, there exist a number of haemodynamic complications. These include, but are not limited to, poor flow balancing, increased circuit pressure due to hypertension and a further failing ventricle.

2.9.1 Flow Balancing and Ventricular 'Suckdown'

The Frank-Starling mechanism is the body's natural flow balancing system. If too much blood is being pumped by the right ventricle into the pulmonary circuit for instance, the filling pressure into the left heart will increase thus increasing the output into the systemic circuit. Since CO is so sensitive to preload, 'flow balancing' is achieved so that blood volume in both circuits is maintained.

To date a dual rotary support system, with its inherent suction inlets, has not been able to auto regulate congested vascular circuits. This is because such a device cannot replicate a Frank-Starling-like communication between the pulmonary and systemic circuits through passive ventricular filling.

Without sufficient flow balancing, tests by Nonaka *et al.* (2002) and Endo *et al.* (2000) have observed a high incidence of ventricular suckdown . To try to ebb the incidence of suckdown in patients supported with an LVAD, numerous active control algorithms have been designed to drop pump speed before suckdown occurs, (Choi, Boston, and Antaki 2007; Oshikawa *et al*. 2000; Endo *et al*. 2001).

Further complications for BiVS are brought about by shunt flow in the cardiovascular system. Although not noted in Figure 2-2, blood flows from the Aorta through the bronchial shunt back into the PA. This means that the LV CO is actually higher than the RV (Guyton 2005). Studies with two gyro pumps discussed the need to maintain the flow of the RVAD lower than the LVAD in a BiVS situation due to the shunt to avoid pulmonary congestion (Nonaka *et al*. 2002).

Complications were also seen using a pump designed for LVAD application as an RVAD at low speeds as the lower rotational flow caused numerous issues with cannula blockage (Watanabe *et al.* 2004). This may have been due to thrombus formation in areas of low flow.

Only one documented study has attempted to flow balance a BiVAS without active closed loop VAD speed control. A common Eccentric Roller Total Artificial Heart, ERTAH, is a pair of positive displacement peristaltic pumps with suction inlets. In an attempt to balance the flows, an inter-atrial shunt connected ERTAH inlets to allow leakage between the pump inlets. Aside from the obvious dilution of oxygenated blood entering the LVAD inlet, the study reported improved operation through increased stability of vascular circuit volumes. It claimed the technique 'may be effective in balancing the left and right sides of the artificial heart' (Wada *et al*. 1999).

2.9.2 Hypertension

Contrary to the name's implication Hypertension is not always caused by hypertensive vessels. Hypertension means elevated pressures in a vascular circuit. Clinicians recognise two mechanisms by which a hypertensive circuit can be facilitated. These are Backward and Forward Hypertension and are usually associated with the pulmonary system.

Backward Hypertension is usually caused by a failing ventricle's decreased output. In the case of left ventricular failure, the decreased LV output causes the pulmonary venous pressure to increase elevating the end diastolic volume to increase LV output. Assuming the pulmonary circuit resistance stays constant, the RV systolic pressure then increases to maintain adequate flow through the lungs. The pulmonary circuit then experiences a global pressure increase. Due to the increased demand in the RV, Backward Hypertension is a common cause of RVF.

The cause of Forward Hypertension is more indicative of its name. It is where the pulmonic capillary vessels reduce flow area thus becoming hypertensive. This reduction in flow area is called stenosis, and is typically caused by cholesterol build up or aneurism. Forward Hypertension is caused by stenosed arterioles causing an elevated Pulmonary Artery pressure and decreased capillary pressure. To maintain adequate vascular pressure in the vascular bed, the vessels constrict. The hypertensive vessels are downstream, or ahead, of the partially blocked vessels, hence the term Forward Hypertension, (McNeil 2008).

Either mechanism causes elevated circuit pressure whether it is from a sympathetic nervous response, (Forward Hypertension), or due to a failing ventricle, (Backward Hypertension).

2.9.3 Further Failing Ventricles

After VAD implantation, the VAD output is set so as to assist the ventricle. However, it should be realised that in some patients, especially after long term support, the ventricle can provide a large amount of the work. This is called the ventricle's residual function. Furthermore, poor management of VAD, or BiVAD, support in

long term clinical trials has seen end organ failure as well as further heart failure from ischemia, or poor circulation (Goldstein and Oz 2000; Christiansen *et al*. 2006).

2.9.4 Complications during Bi-Ventricular Support

From a more general perspective, both the long and short term haemodynamic effects of BiVS are poorly understood. This is particularly the case for non-pulsatile support. This is perhaps because there have been relatively few clinical trails of BiVS but also because these trails have shown little success in sustaining long term and safe BiVS.

As mentioned, poor flow balancing has been identified as an issue that plagues constant flow support, particularly BiVS. This is probably because the Frank Starling balancing mechanism is lost. Nonaka *et al.* concluded from chronic *in vivo* studies of rotary BiVS that subsequent pulmonary congestion is a major problem (Nonaka *et al*. 2002). This was further backed up in a review article or cardiac support, (Mesana 2004). Because the blood volume in the pulmonary circuit is low, (around 15% of total blood mass (Milnor 1982)), a congested pulmonary circuit can significantly reduce venous return to the left heart. This further elevates the danger of left ventricular suckdown.

2.10 Current Rotary Devices and Their Means of Control

Control of rotary VADs, particularly rotary BiVS systems, is an issue fraught with complications. This is not surprising considering the complexity and interdependence involved in CV bio-signalling. Choi *et. al.* 2007 commented that "hemodynamic control of left ventricular assist devices (LVADs) is generally a complicated problem due to diverse operating environments and the variability of the patients" (Choi, Boston, and Antaki 2007).

2.10.1 Steady State Haemodynamic Control

Artificial hearts include a controller within the support system that takes signals from the pumping system and adjusts the power to the pump to maintain safe support. A schematic sketch of the Heartmate III support system is depicted in Figure 2-17. The

figure shows the external batteries and controller, the Transcutaneous Electro Transmission (TET) for transmitting power through the skin, the internal battery and the pump and cannulae arrangement.

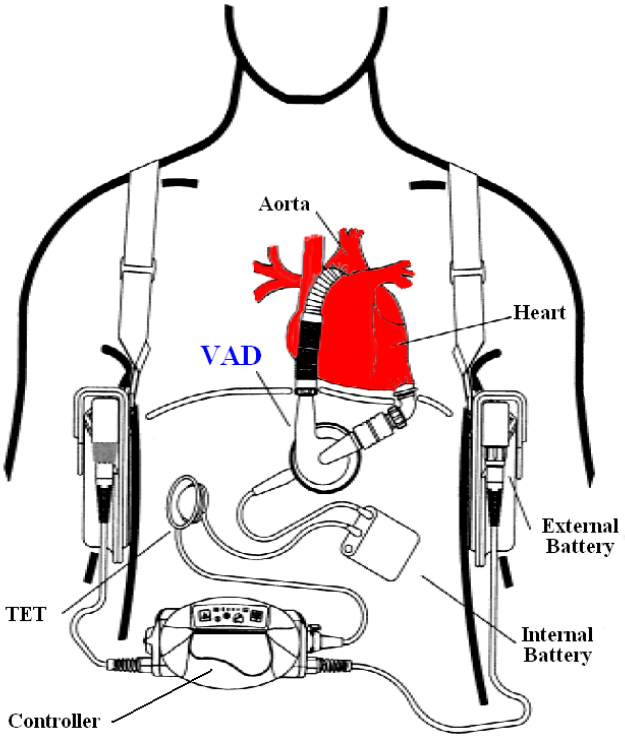

Figure 2-17: System sketch of the Heartmate III including pump and cannulae, power supply and transmission and controller. Modified from source (Bourque *et al.* 2001).

The means of system state sensing for rotary pumps varies from device to device. Many devices make use of the current and voltage signals to the pump to indicate the pump torque and speed respectively. Then, referring to pump performance curves and pump efficiency data the controller can make approximation regarding the pressure head and the flow rate (Ayre *et al.* 2000). However, since pump pressure head is a floating potential, (the difference between outlet and inlet pressure), neither inlet or outlet pressure is known. Additionally, power sensing errors on top of discrepancies between experimental performance data and *in vivo* operational performance decrease system control.

Incorporating invasive pressure sensors bring about reliability issues in that they are commonly blood contacting. This can encourage thrombus formation around the

sensor which can disturb readings. Furthermore, sensor failure could be fatal requiring back up control systems.

Some devices incorporate flow meters such as the DeBakey Axial VAD which has a dopler flow sensor around the outlet cannula (Mesana 2004). The Magnevad is an axial VAD that senses the rotor displacement caused by the developed pressure head and quantifies the pressure head by referencing the displacement to a known axial stiffness (Goldowsky, Lafaro, and Reed 2005; Goldowsky 2004).

2.10.2 Suckdown Sensing and Control

A recurrent issue for rotary type devices is the incidence of the 'sucking' inlet causing negative pressures at the inlet cannula causing ventricular collapse. In essence, suckdown occurs when venous return is insufficient to supply the required flow at the VAD's operating point. At that point the ventricle cavity will collapse on itself much like the effect of sucking all the air from a balloon. Assuming that the VAD is properly managed and the operation speed isn't too high, this is caused by a number of conditions where venous return becomes too low. Hypertension is the primary cause of decreased venous return to the heart. Pulmonary hypertension is particularly common in patients who receive mechanical support (Nonaka et al. 2002).

Post-operative Pulmonary Embolism is a common condition for hospitalised patients. It is where a lack of physical movement sees thrombus formation in the systemic venous system, (such as Deep Vein Thrombosis, DVT). Eventually, the thrombus can dislodge and then move up through the Vena Cava, through the right heart and then lodge itself in the narrow arterioles or capillaries in the lungs. This problem is also a serious issue for VAD patients as it decreases venous return to the left heart and therefore increases the risk of LV suckdown.

Similarly, as found by Nonaka, Linneweber *et al*. (2002), pulmonary hypertension during BiVS sees an increased pulmonary vascular resistance obstructing flow. Consequently, the decreased venous return decreases left ventricular volume. This is further affected by the low fluid volume reserve in the pulmonary circuit. Rotary

BiVS with their inherent sucking inlets are therefore particularly susceptible to inducing LV suckdown.

When the ventricle collapses, flow into the cannula is blocked allowing flow from the venous system to fill the ventricle again. Provided the VAD does not attempt to move its steady state operating point to a lower flow, the ventricle can repeatedly suckdown or remain collapsed. The collapsing motion is damaging to the heart muscle and can cause bleeding at the cannulation site. Furthermore, it can encourage thrombus formation in regions of flow within the ventricle.

As discussed, the issues discouraging the use of pressure sensors make it difficult to know when the ventricular pressure starts to drop dangerously low. So, many devices use the transient current signal to the pump to try to predict ventricle collapse without a direct inlet pressure sensor, (Yuhki *et al*. 1999; Endo *et al*. 2001; Oshikawa *et al*. 2000). Since the current is a good indication of the applied impeller torque, the torque therefore can be indirectly monitored. Observed oscillations in the drawn current amplitude would indicate that the flow into the VAD is becoming unsteady.

2.11 Conclusion

Considering heart transplantation as a treatment for congestive heart failure supplies less than 0.5% of the demand in Australia, safe mechanical alternatives are a sought after treatment option. However, devices to support patients with bi-ventricular failure are few and early in their development. Thus, these patients are forced to remain on a hospital bed receiving cardiac support while they await a donation. Currently there are no implantable BiVADs with FDA or TGA approval. The premature nature of the artificial heart market is indicated by serious safety issues with both pulsatile and non-pulsatile artificial hearts.

Conclusive evidence outlining the superiority of non-pulsatile support devices does not exist. However, a brief review of the issues surrounding both modes of operation of artificial hearts was presented. Better biocompatibility and implantability encourages continuous flow VAD research due to smaller device size, less moving parts and the decreased likelihood of thromboembolism.

The relative merits of axial and radial modes of flow, (and a mixed flow mode), were discussed in brief outlining the efficiency benefits in supporting a left ventricle, at least, using a radial flow pump. However, this project was restricted by the geometry of the prototype to select mixed flow modes for both the LVAD and RVAD.

Flow balancing rotary bi-ventricular support systems and associated pulmonary hypertension have proven to be typical complications during *in vivo* experimentation. Such support is compounded with the additional issues that single VAD patients face including high dependence on the device reliability and induced blood and tissue damage. A means of stabilising and controlling a dual rotary pump is an area of research that has been given little attention. This thesis documents the development of such a system which incorporates a passive mechanical controller to takes pressure signals from the CV system to passively control the BiVAD output.

3 Device Design and Development

3.1 Introduction

The literature review discussed the artificial heart as a support device needing to be implantable, biocompatible, reliable and minimally invasive for the patient. While single ventricle support using a VAD is now quite common, support for bi-ventricular failure, BiVF, using appropriate rotary pump technology has proved difficult to achieve due to flow balancing issues. To this end, parallel investigations using numerical simulation and experimentation were used to develop a passively flow balancing support system using dual rotary VADs in a single device; a passively controlled BiVAD.

This chapter details the design process for the experimental prototype BiVAD and the considerations taken for its configuration. A design process is explored where the device was developed around a theoretical controller system; from conceptual designs to the final prototype. The incorporation of a floating impeller shroud assembly and the associated dynamic components are the key functional designs to provide the passive controller.

The physical design of the pump components have been influenced by text book design procedures, previous experimental designs and the physical geometry limitations of the device and passive controller.

3.2 Passive Response from a Cardiac Device

Before the passively controlled BiVAD could be designed, the device's environment was examined including the controller input and output signals as well as the controller system itself.

As mentioned earlier, pressure signals provide much of the bio-signalling sensed by the cardiovascular system. Pathological haemodynamics will often cause rises or falls in vascular pressure making this the ideal signal for the passive system. Another

attractive attribute of a pressure signalled system is that pressure changes can be sensed mechanically using pitot tubes, deformable membranes and pressure plates. Ideally we would like to sense the flow also; however, this is difficult to do mechanically without paddle meters which are susceptable to thrombus formation.

The output from the system was selected to be the output fluid power of the pump, the pressure head (*H*) and flow (*Q*). Due to the compliant nature of the vascular beds, vascular pressure can be increased or decreased depending on the resident fluid volume within the compliant vessels.

The human cardiovascular system is a dynamic system with fluid resistance, compliant or elastic vessels and fluid inertia. This creates a dynamic environment for the device where pressures and flows within the circulation are subject to delayed and periodic responses to inputs. The VAD's responses therefore need to be dynamic and for the purpose of experimental testing need to be variable. A desirable dynamic controller within the BiVAD, therefore, would incorporate some sort of mass, damper and spring response.

Figure 3-1 gathers the selected pressure inputs, the VAD's pressure and flow outputs and the dynamics system into a schematic of the open loop controller model. This controller model gives the basis from which the passive controller BiVAD was designed.

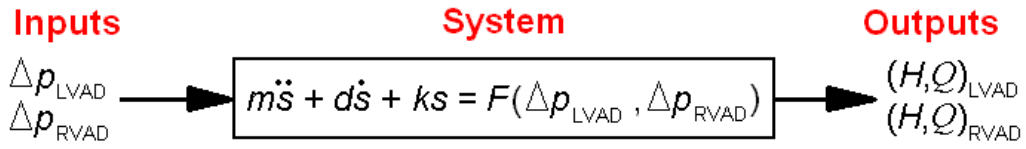

Figure 3-1: Passive Controller theoretical control model.

The input parameters refer to the changes in the absolute pressure of the resident fluid within the LVAD and RVAD, *Δp*. Terms used in the system model are an inertial coefficient, *m*, a damping coefficient, *d*, a spring coefficient, *k*, some degree of freedom of the controller, *s*, and the external forces upon the system *F*. The outputs of the open loop controller are then the affected pressure head and flow rates of the VADs.

The system model incorporates a single degree of freedom, s, which is sensitive to the output, H and Q, of both VADs. This degree of freedom is acted upon by a resultant force, F which is proportional to changes in pressure.

3.3 Impeller and Casing Design: Theory and Considerations

A comprehensive rotary pump design review primarily sourced text book empirical procedures. However, the empirical data were exclusively based from experimentation of industrial sized pumps. So, text book design procedures were combined with documented miniature blood pump design studies to design the pump geometries. Additionally, numerous tests have been carried out by the candidate and colleagues to test the pump's performance sensitivity to a number of geometric parameters.

3.3.1 Basic Theoretical Rotary Pump Design Procedure

Axial, mixed and radial flow pump texts normally initiate the design procedure with a basic theoretical equation for a 100% hydraulically efficient pump. Then empirical data from industrial pumps are used to predict hydraulic losses. To allow a range of pumps to be designed from these data, non-dimensional parameters are employed to normalise the design steps. Empirical detail has been omitted from this document as maximising the VAD hydraulic efficiencies was not the aim of the study. Text book design procedures were taken from multiple sources (Japikse, Marscher, and Furst 1997; Stepanoff 1957).

Before the design process was started, the desired pressure head *H*, flow rate *Q*, the running speed *N* and the impeller outer diameter were nominated.

3.3.1.1 **Theoretical Impeller Design**

Initial theoretical calculations for axial, mixed and radial flow impellers are essentially identical. Determining global geometry and blade angles can be approximated regardless of flow mode. However, different modes of flow affects the direction of the meridional vectors, e_{m1} and e_{m2} where both have units ($mm.s^{-1}$).

Figure 3-2 provides a plan view of a radial flow impeller with the absolute fluid velocities at the impeller inlet and outlet, e_1 and e_2 respectively with units ($mm.s^{-1}$). Relevant vector components of the fluid velocity have also been included as these are used in the impeller design process.

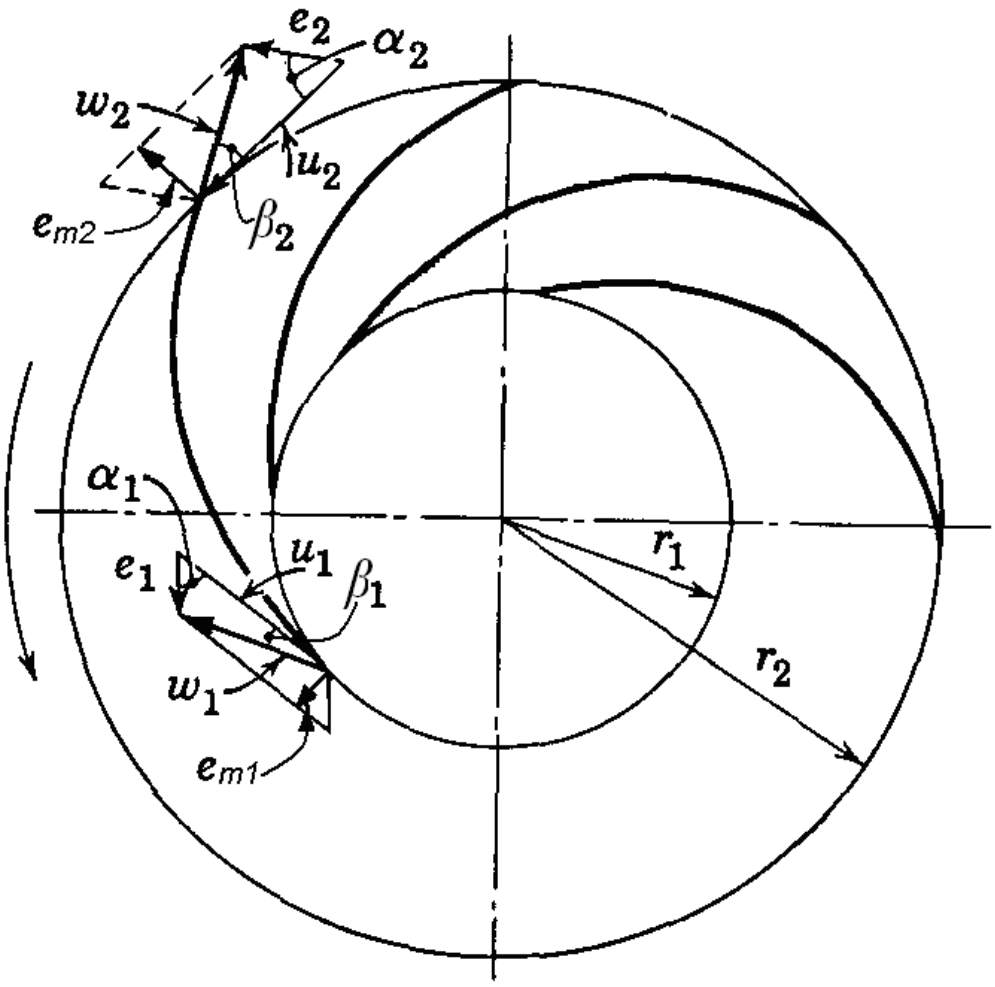

Figure 3-2: Plan view of a radial flow impeller depicting inlet and outlet velocity triangles. Modified from (Stepanoff 1957).

Where u is the absolute linear impeller velocity, w is the relative fluid velocity with respect to the impeller, α is the absolute fluid velocity angle to the tangent of the impeller's rotation and β is the fluid velocity angle to the rotational tangent from the rotating impeller's frame of reference. Notice that the subscripts ($_1$) and ($_2$) refer to the inlet and outlet, (eye and periphery), of the impeller.

The theoretical head of a radial and axial pump is evaluated by ensuring that the angular momentum of a quantity of fluid mass is conserved from the inlet of the

impeller through to the outlet. This simply means that the work done by the torque from the impeller is converted into an increase in fluid kinetic energy as it passes over the profile of the impeller from inlet to exit.

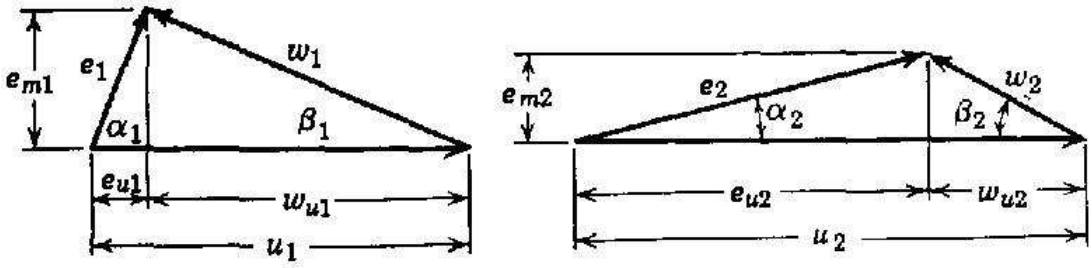

Figure 3-3: Velocity triangles at the inlet, (left), and outlet, (right), of the impeller. Modified from Source (Stepanoff 1957).

Beginning with Newton's 2nd law in polar coordinates; the torque applied to the fluid by the impeller can be equated to the rate of change of the fluid's tangential momentum,

$$M = \frac{dn}{dt}(r_2 e_2 \cos\alpha_2 - r_1 e_1 \cos\alpha_1),$$

Equation 3-1

where M is the applied torque, $\frac{dn}{dt}$ is the rate of change of fluid mass in time and r is the impeller radius. From this starting point, the Euler's equation for theoretical pumping head can be derived, (detailed in (Stepanoff 1957)) as given in Equation 3-2 to

$$H_i = \frac{u_2 e_{u_2} - u_1 e_{u_1}}{g},$$

Equation 3-2

where H_i is the theoretical developed pressure head, g is the product of gravitational acceleration and a dimensionless constant to account for unit difference. The subscripts '$_{u1}$' and '$_{u2}$' indicate the magnitude of e in the direction of u_1 or u_2. The derivation of Equation 3-1 and Equation 3-2 can be found in Stepanoff (1957).

Since the operation of a pump is within a highly pulsatile environment, the inlet conditions won't be constant, but more importantly, they won't be steady. This is an important issue in the design of inlets without some sort of flow straightening precursor to the eye of the impeller.

An identity for the actual head is given in Equation 3-3 where the Euler head, H_i, is multiplied by the hydraulic efficiency,

$$H = \eta \frac{u_2 e_{u_2} - u_1 e_{u_1}}{g}.$$

Equation 3-3

The hydraulic efficieny of the pump η, is used to determine the actual developed pressure head H.

The blade heights at the inlet and outlet can now be determined through text book calculation; however, experimental studies found that the suggested blade heights from texts are too small. It was found that exit blade heights lower than 1 mm caused serious throttling which made a maximum pump flow rate of around 3 L.min^{-1} for speeds less than 3000 RPM. The dimensions of concern are shown in Figure 3-4.

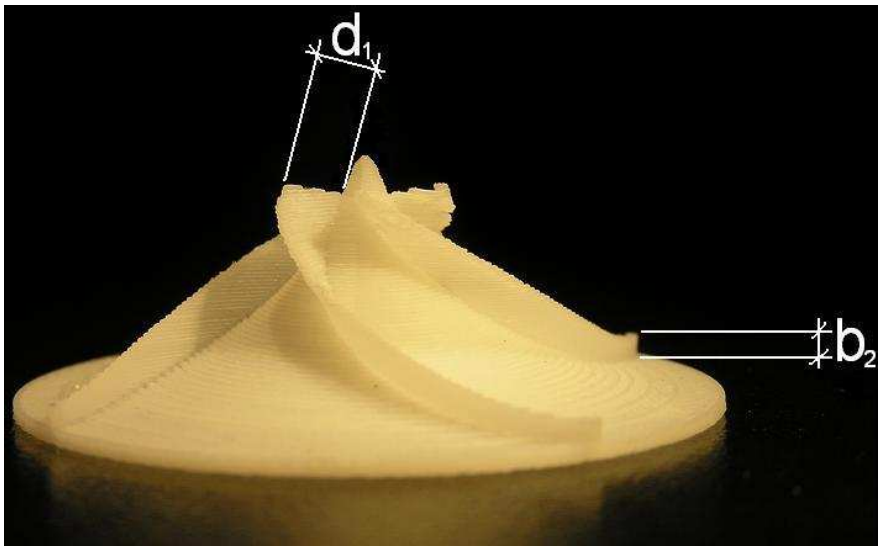

Figure 3-4: Side elevation of an experimental mixed flow impeller with labelled blade height dimensions.

Now, sufficient tools are available to determine the basic impeller geometry. However, a number of assumptions need to be made, beginning with the tangential fluid velocity at the inlet, e_{u1}. Then, provided a running speed (N), pressure head (H), and flow rate (Q) have been nominated, the tangential component of the fluid at the impeller outlet, e_{u2}, can be evaluated using Equation 3-3. Following this, the velocity triangles in Figure 3-3 can be drawn up, and considering impeller losses, the blade angles can be found. Further detail into text book design procedure of radial flow impellers can be found in (Timms 2006).

3.3.1.2 **Theoretical Volute and Diffuser Design**

The volute collects the fluid coming off the periphery of the impeller and guides it to the throat, and then the outlet. Energy is converted from the tangential component of the kinetic energy of the rotating fluid to pressure energy throughout the volute and in the diffuser itself. It is in this collection channel that most of the pump losses occur (Tuzson 2000). Figure 3-5 highlights many of the important geometric parameters of the volute and diffuser.

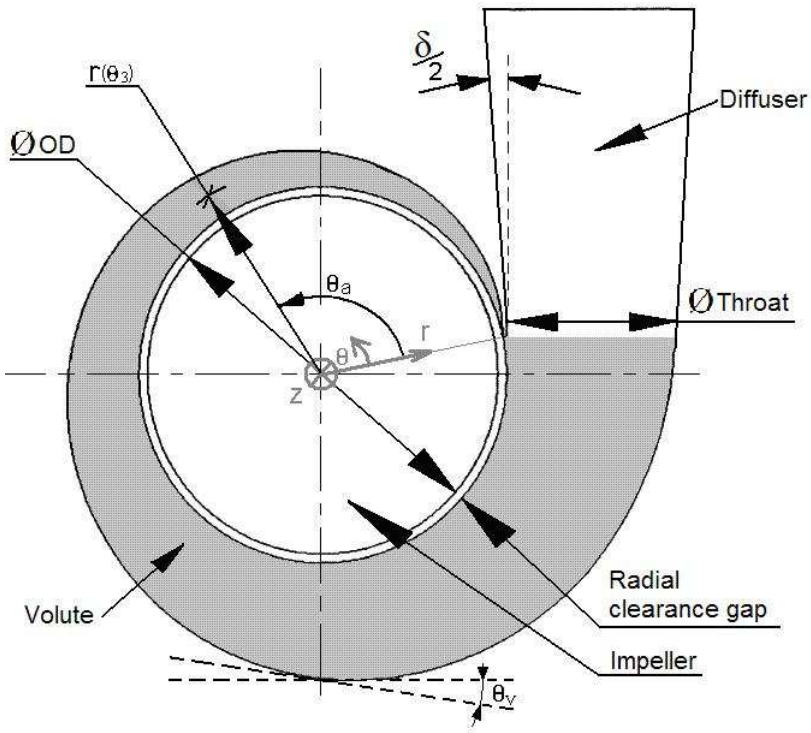

Figure 3-5: Plan view of a sectioned pump casing detailing the volute, diffuser and key geometric parameters.

Where δ is the volute throat angle, θ_v is the volute angle, (to the tangent), and the subscript, ($_3$), denotes a mean volute fluid parameter.

First, the volute angle is calculated so as to minimise fluid shock coming from the impeller. To do this it is advised to make the volute angle equivalent to the absolute velocity angle of the incoming fluid, α_2, calculated from the velocity triangles in Figure 3-3. Following this, empirical data are referenced to determine the required tangential fluid velocity in the volute, e_3, to provide the necessary pressure development,

$$e_3 = K_3\sqrt{2gH}\ .$$

Equation 3-4

The employed empiracle data lends the losses coefficient, *K*, which increases with an increasing pressure to flow ratio, (Stepanoff 1957). As mentioned, however, the use of industrial pump design texts provides poorly representative empirical coefficients for miniature pumps.

The other important geometric parameter is the throat area, A_{Throat}, at the end of the volute and the start of the diffuser. This is calculated simply by dividing the nominated flow rate by the velocity found in Equation 3-4,

$$A_{Throat} = \frac{Q}{e_3}.$$

Equation 3-5

Texts suggest maintaining an approximately consistent flow area from impeller inlet, to impeller outlet to volute throat. The volute throat area found in Equation 3-5 is then compared to the impeller inlet and outlet areas to assess the continuity of the flow channel area. The design process therefore, is an iterative task to maintain flow area continuity, while minimising inefficiencies. This introduces a problem at the impeller periphery since miniature impellers incorporate high boundary layer interaction. The final VAD designs, therefore, see little continuity between the impeller inlet and outlet areas and the throat area.

Further detail into text book design procedure radial flow volutes and diffusers can be found in (Timms 2006).

3.3.2 Effect of Axial Clearance Adjustment on Performance

An important feature of the device's passive controller is adjustment of the clearance above the impeller blades. This clearance is shown for a radial flow pump in Figure 3-6.

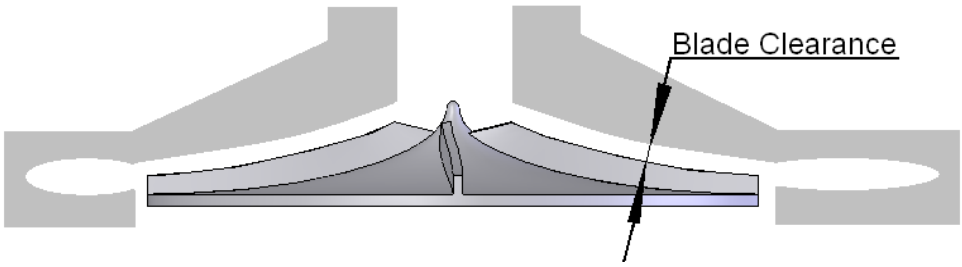

Figure 3-6: Section of a radial flow pump indicating the blade clearance length, c, between the impeller blade and the pump casing.

Timms *et al.* (2006) discussed this as an effective way to vary a rotary pump's output during operation without adjusting the pump speed. Timms increased the clearance between the pump casing and the impeller blades of the Ø50 mm semi open impeller. The result was a drop in performance as the adjustment allowed fluid leakage over the blade tips dropping the efficiency and therefore, output. Another feature of this means of performance adjustment is that most of the performance drop occurred between c = 0 and 0.3 mm. This suggests a non-linearity in the relationship between H and c and Q and c, (Timms 2006; Timms *et al*. 2006).

As mentioned earlier in this chapter pressure was to be used as the passive controller input signal because it is able to mechanically affect a device using deformable membranes or pressure plates. It was thought that Timms' result could be applied to a pressure plate configuration so that the pressure in either VAD could affect the blade clearance. This will be explained later. Initially, the candidate needed to replicate this effect to ensure that it could be used effectively to adjust the pressure and flow rate from a radial flow pump. Figure 3-7 shows one of the mixed flow impellers used by the candidate to replicate Timms' reported results.

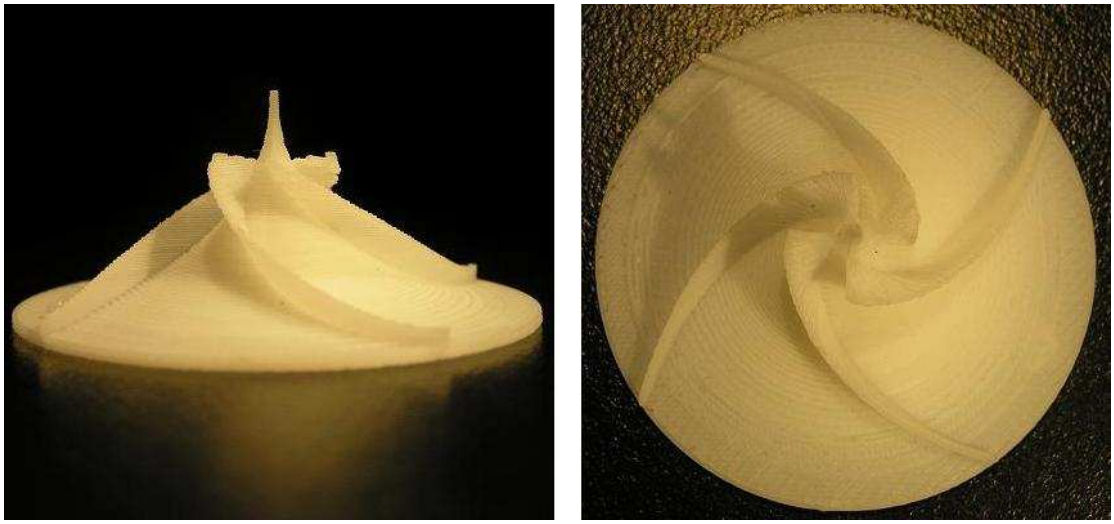

Figure 3-7 a and b: Example impeller from axial clearance repeat test; Side elevation (left), planar view (right).

A range of mixed flow and radial flow pumps were tested in a hydraulic loop to derive the performance curves at varying blade clearances. Pressure sensors upstream and downstream of the pumps indicated the pressure head while a flow meter

measured the flow rate. A micrometer was used to axially locate the impeller inside the pump casing. The pumps were then run at a range of pump speeds from 1400 to 2400 RPM and the caircuit resistance was gradually changed throught the test using a pinch valve.

Figure 3-8 is the corresponding experimental *H* vs. *Q* curve for a mixed flow pump using the impellers shown in Figure 3-7 with an axial clearance as close to zero as possible, i.e. $c \approx 0.0$ mm.

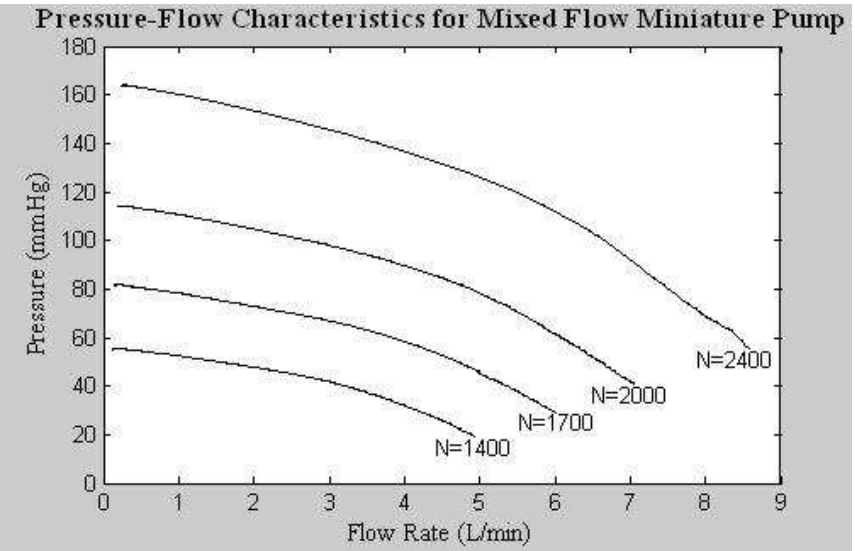

Figure 3-8: Pump performance characteristic *H*(*Q*) for different speeds, *N*.

The plot shown in Figure 3-9 shows the change in pump performance when the impeller clearance is increased from $c \approx 0.0$ mm (solid black), to $c = 1.0$ mm, (dashed).

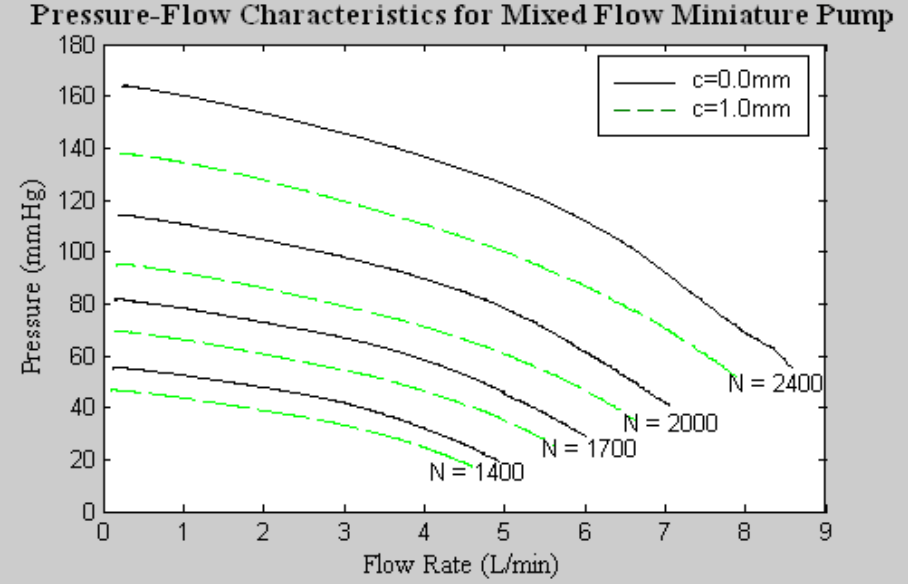

Figure 3-9: Pump performance characteristic for two different clearances.

It can be seen that the pressure drop due to increasing the blade clearance is similar in effect to decreasing the pump speed. Increasing the clearance from 0 to 1.0 mm is approximately proportional to decreasing the pump speed by 100 to 200 RPM. This is a rough approximation but will be used in the numerical model and in post processing experimental data.

From these results it can be seen that both axial adjustment and speed control are effective means of performance adjustment during the operation of a mixed flow pump.

3.4 Passively Controlled BiVAD Configuration

The controller design in Figure 3-1 sets out a framework with which to design the physical controller. Considerations were taken so as to actuate the controller with the selected inputs, incorporate dynamic controller response and create a causal controller to provide the desired outputs. Similar to most design processes, the device developed through a number of concepts. The concepts followed by the impeller and casing design for both VADs are described in this section.

3.4.1 Preliminary Concepts

The interaction between the heart and the pressure signals used to control arterial pressures needed to be replicated as closely as possible in a passively controlled BiVAD. Furthermore, it was envisioned that some sort of VAD output interdependence could be created between LVAD and RVAD similar to the ventricles' interaction. A CAD model of the initial concept model for the device is shown in Figure 3-10.

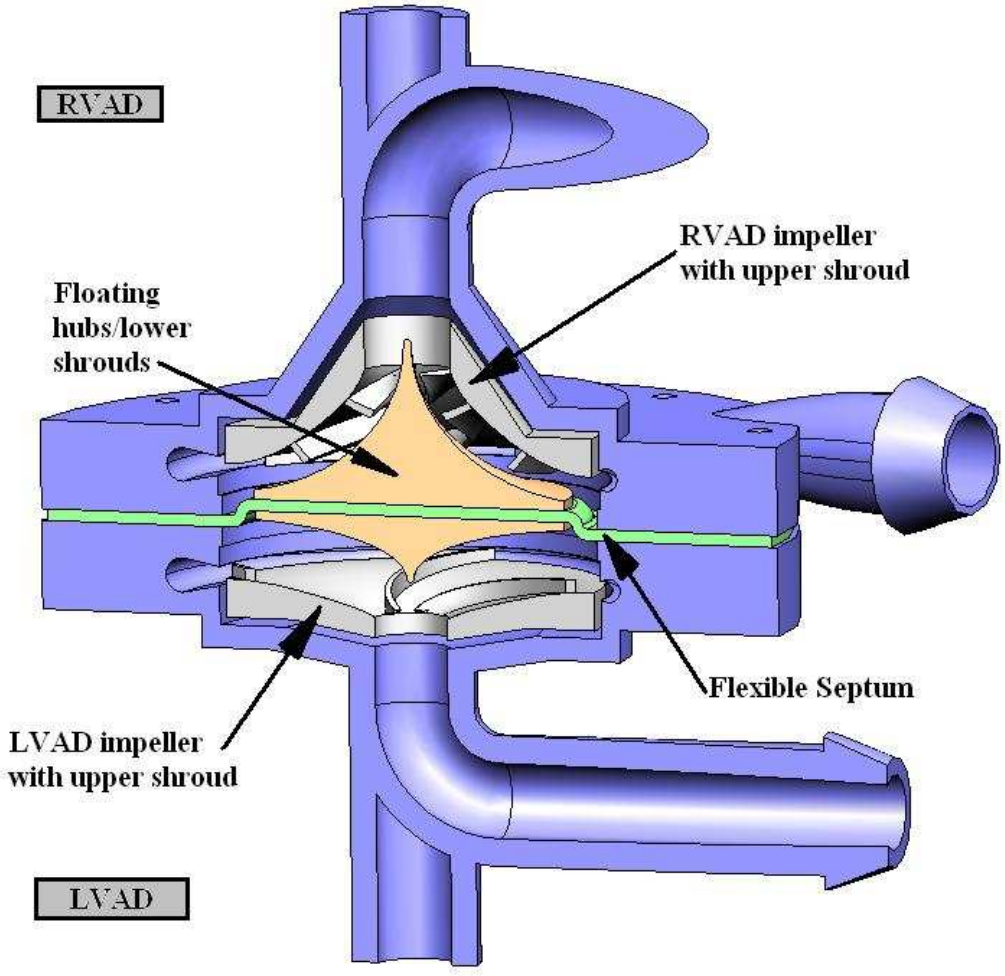

Figure 3-10: Passive Controller BiVAD Concept 1. Annotated CAD model.

This concept includes two semi-open impellers each incorporating an upper shroud. Between them is a non-rotating assembly which essentially consists of the lower shroud forms for each impeller. This assembly is mounted on a flexible 'septum' that can deflect between each VAD depending on pressure variations. A deflection

upward would increase the output of the RVAD and decrease the LVAD performance, and visa versa, to provide an interdependent septum action.

It was recognised that this is not exactly the same interdependence caused by the septum shift in the heart. However, it was postulated that this might aid in the device's ability to flow balance. A congested pulmonary circuit would elevate resident fluid pressure in the RVAD causing a deflection towards the LVAD thus lowering RVAD output and increasing LVAD output. This would then pump less fluid into the pulmonary circuit as well as evacuate more fluid from the congested circuit through the LVAD. The design was miniaturised and prototyped as shown in Figure 3-11.

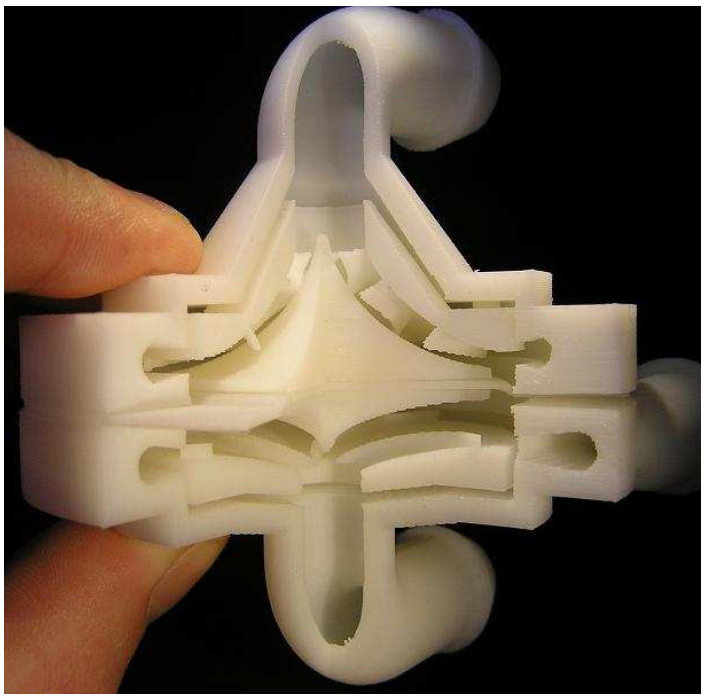

Figure 3-11: Passive Controller BiVAD Concept 2. Prototyped ABS plastic model.

3.4.2 Design Considerations for the Final Prototype

There were two important concerns with the functionality of the described concepts. The first was that, for a total support scenario, the LVAD operates at five times the mean pressure of the RVAD. This means that during steady state operation the lower shroud assembly would be heavily deflected. Close examination of Figure 3-10 reveals that the candidate constructed it in the deflected position to show this effect.

Where the device is providing total support, the mean arterial pressures in the Ao and PA will be around 100 and 20 mmHg respectively, or 100 and 25 mmHg if the pulmonary circuit is hypertensive. The latter is a pressure ratio of 4:1 between the LVAD and RVAD respectively. A cardiac support device, whose operation is intended to be as self regulating as possible, needs to be as inherently stable in its operation as possible. To allow the hub to be centrally located at steady state support, the forces from these two pressures upon the either side of the lower shroud assembly needs to be balanced. The area ratio of the lower shrouds therefore, should be around 1:4 respectively.

The second issue was that there was no control of the lower shroud assembly motion. Figure 3-10 depicts the assembly located by a flexible membrane support which would permit oscillation. A particular concern was that when the device was providing partial support it would reciprocate under a pulsatile inlet condition therefore rending the passive response ineffective. The lower shroud assembly, therefore, needed some dynamic restraint to optimise its motion. It was foreseen that a spring, mass, damper type configuration would be essential in adjusting the response of the device. With the inclusion of the damper, any oscillations could to be mechanically damped in order to filter out pressure signals from the contracting ventricles.

A means of providing these dynamic parameters so that they were reliable, repeatable and able to be varied during operation was a difficult design problem. The implementation of the dynamic components will be explained in the next section.

Further considerations were needed to create a prototype which could be physically assembled and run with relatively high tolerances maintained between the impellers and non-rotating lower shrouds. Another difficult issue was the impeller drive. Each impeller was to be driven individually which meant penetrating the VAD inlets with the drive shaft. Furthermore, radial and axial stability of the impellers needed to be ensured so that all the passive response was provided by the lower shroud assembly.

The device components, assembly and machine-shop drawings were designed and drafted in SolidWorks. CAD software was particularly helpful in designing what eventuated into a complex device with many components.

3.4.3 Final BiVAD Concept with Passive Controller

There are numerous distinguishing features in the final concept, when compared to earlier concepts. In terms of the device's functionality, the important features are the increased RVAD impeller diameter, incorporated mechanical dynamics to the lower shroud assembly and dual flexible diaphragms. These features, along with the intended response of the device are discussed in this section.

It should be noted that the final concept figures in this section were sourced from CAD models after the completion of the design. However, specific impeller and casing geometry detail will be given later.

3.4.3.1 **The Prototype at a Glance**

A sectioned elevation of the prototype is shown in Figure 3-12. The section has had much of the physical detail removed for clarity, (e.g. seal grooves and some physical part lines). The sectioned figure shows the orientation of the RVAD and LVAD as well as the central Passive Controller Body. The positon of the inlet and outlet volute of each VAD is shown as well as the impellers. The VADs physically oppose each other and between them, they straddle the Passive Controller which locates a non-rotating floating hub incorporating lower shrouds (hatched).

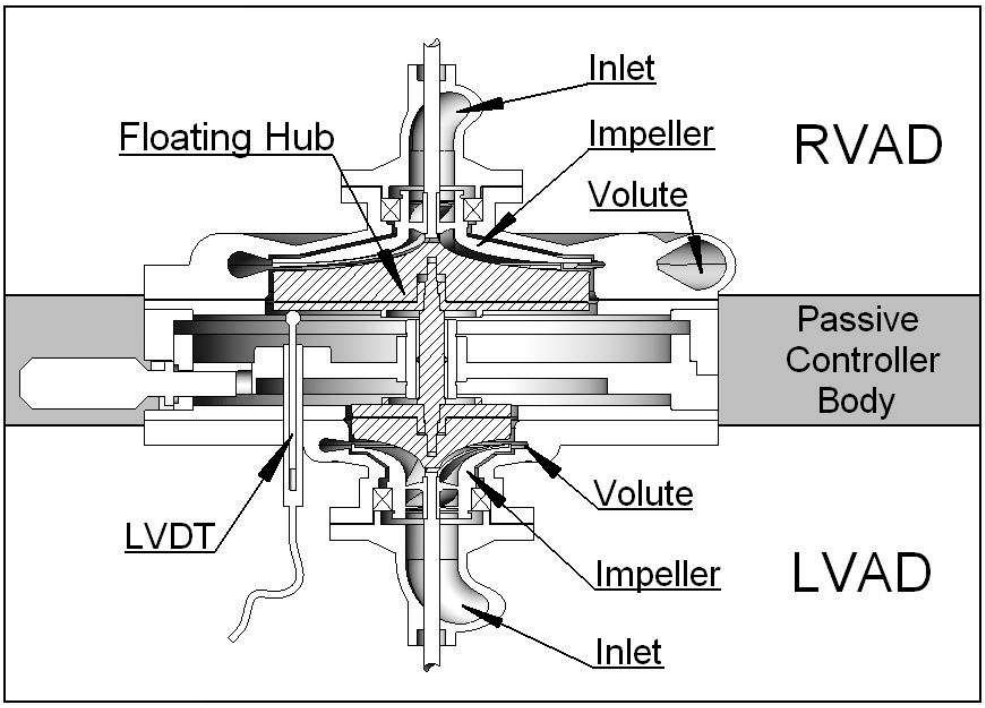

Figure 3-12: Sectioned elevation of prototype for construction with sensors and dynamic components included.

A position sensor enters the Passive Controller body from the LVAD side to monitor the position of the floating assembly within the pump. The sensor is a LVDT with ±2.5 mm range, (Solartron, 922939 DG5.0, RC Components Australia), which maintains contact with the floating assembly using a spring loaded, spherical tip sensor rod.

The lower shroud diameters are no longer the same; in fact the RVAD impeller and lower shroud diamters are twice those of the LVADs, (Ø100 mm and Ø50 mm respectively). This LVAD to RVAD lower shroud diameter ratio of 1:2 creates an area ratio of 1:4. This was intended to approximately balance AoP:PAP ratios between 4:1 and 5:1, (depending on the simulated pulmonary hypertension).

3.4.3.2 **Detailed Assembly Drawing**

A detailed numbered assembly drawing of the prototype is given in Figure 3-13 and following this the numbered parts are identified in Figure 3-14. Please note that the sectioned drawing is orientated at 90° about the verticle axis with respect to Figure 3-12.

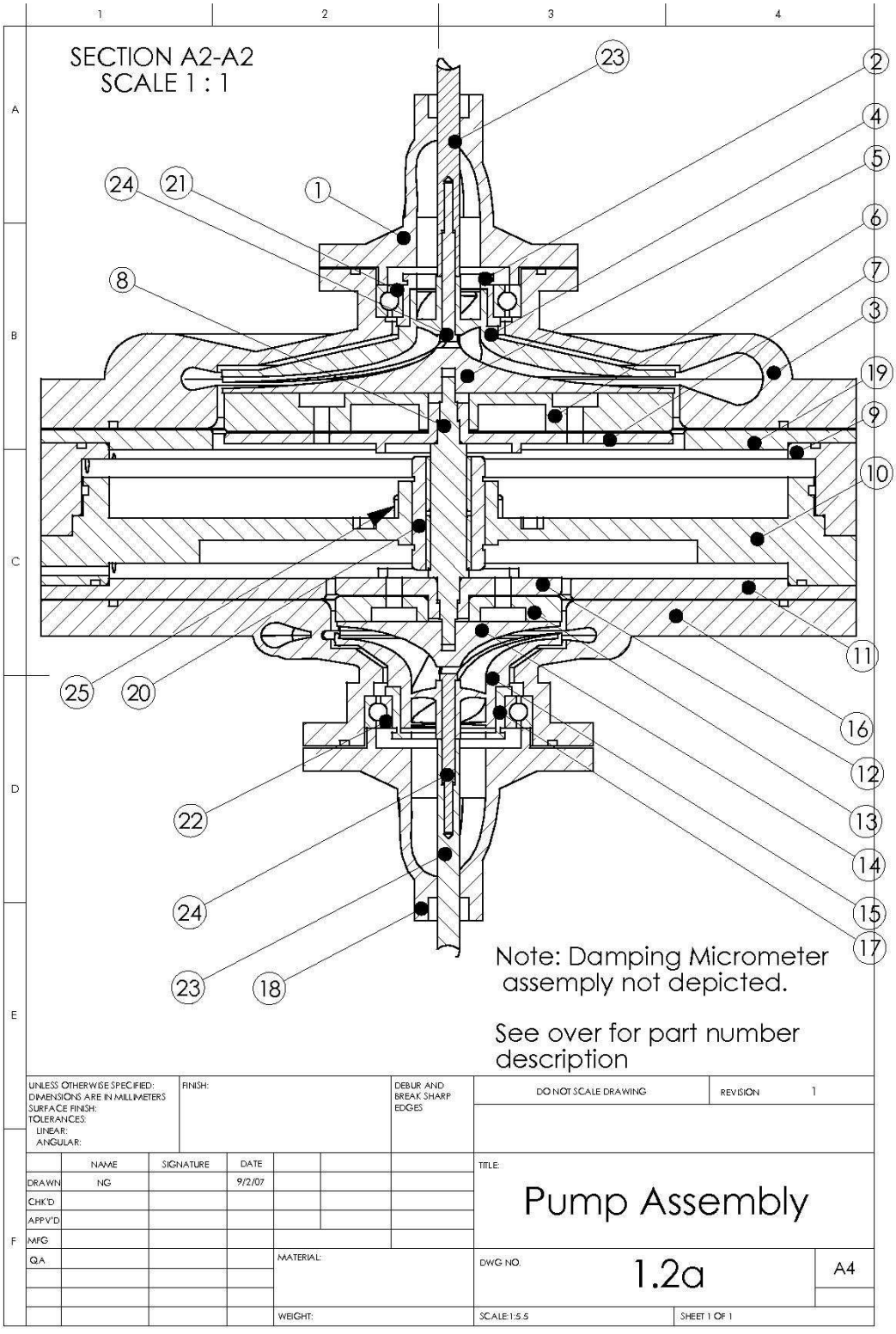

Figure 3-13: Sectioned numbered assembly drawing of the prototype.

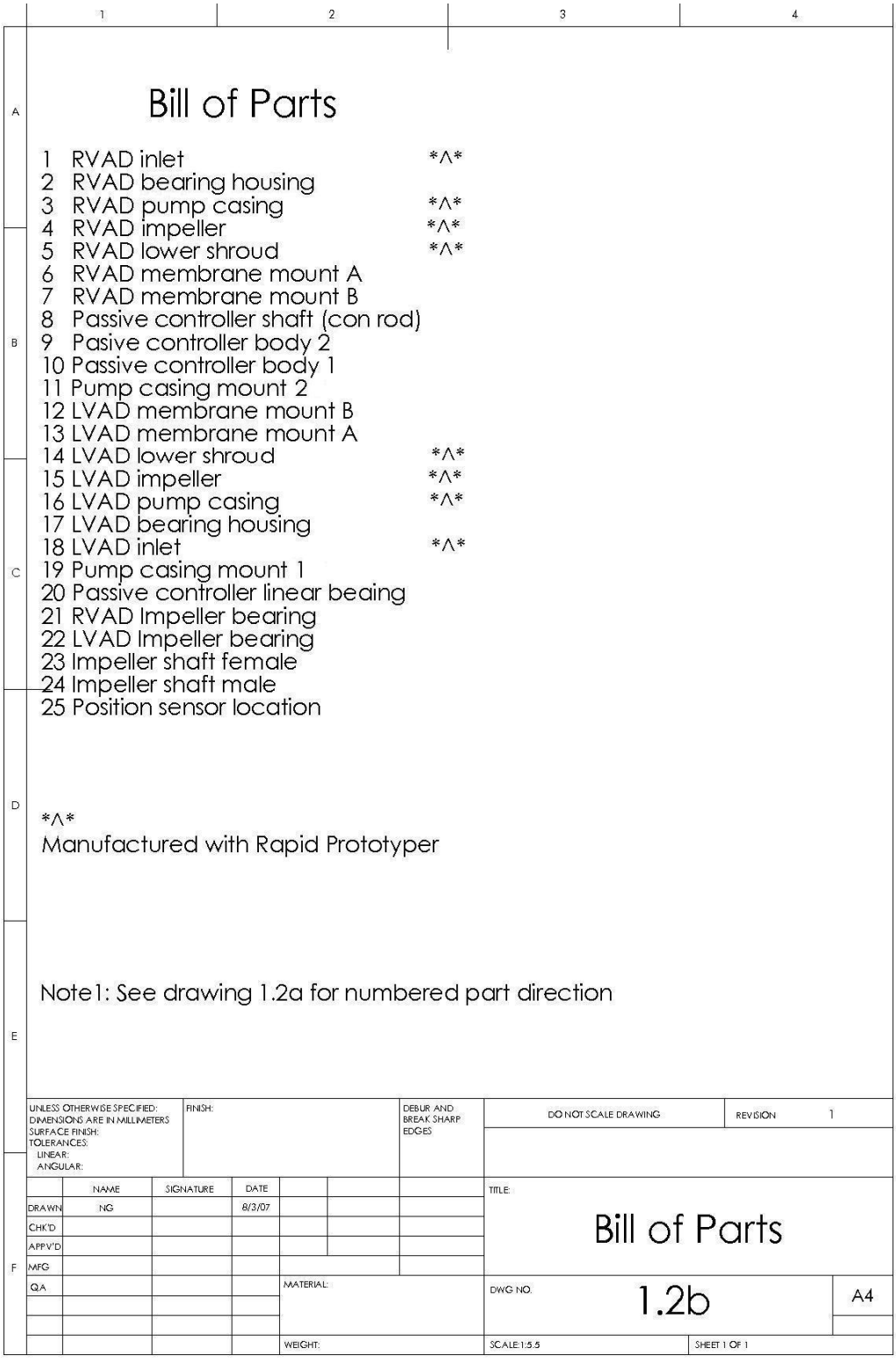

Figure 3-14: Numbered Parts from sectioned assembly drawing.

3.4.3.3 **The Impellers, Non-Rotating Hub and Blade Clearance**

Fundamental to the understanding of the passive action is the location of the impellers, non-rotating lower shrouds and therefore where the blade clearance, c, lies. Figure 3-15 shows a window on the right with a zoomed in image of the LVAD. For ease of reference, parts of interest have been numbered according to those provided in Figure 3-13.

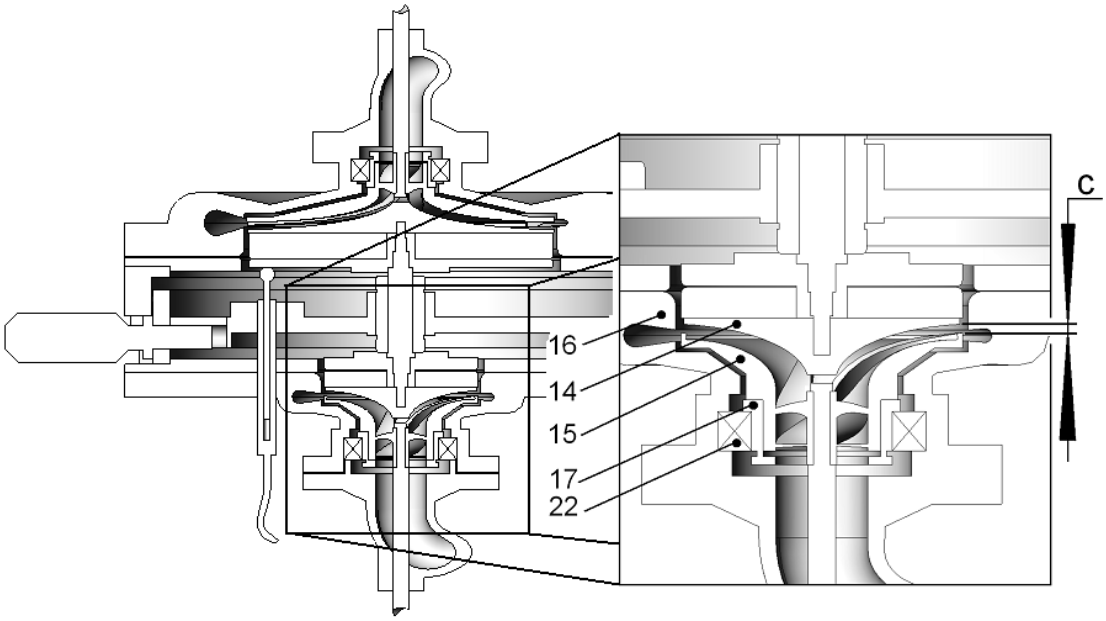

Figure 3-15: Zoomed image of the LVAD impeller and impeller location, non-rotating lower shroud and physical blade clearance (c).

Note the semi-open LVAD impeller with an upper shroud (part 15). The blades are located on the concave side of this shroud and their inner edge profile matches the profile of the non-rotating lower shroud (part 14). The detailed drawing in Figure 3-13 shows that there is also a clearance between the RVAD impeller and its corresponding non-rotating lower shroud.

Highlighted using mono-directional hatching, the floating hub assembly is shown in Figure 3-12 and includes parts 5-8 and 12-14 in Figure 3-13. This floating hub assembly was a feature developed from the lower shroud assembly detailed in the concept shown in Figure 3-10. The floating assembly is made up of two assemblies called lower shroud assemblies and connected by a con rod. The two lower shroud

assemblies straddle a cavity divided in two. The divided cavity creates the Passive Controller Body.

3.4.3.4 **The Passive Controller Body – A Double Fluid Chamber**

The Passive Controller Body was constructed out of four components which stack together to form two chambers. These are parts 9, 10, 11 and 19 shown in Figure 3-13. The Controller Body provides a structure with which to provide dynamic restraints to the floating assembly as well a base to attach the VADs. The dynamic restraints are a spring, mass, damper arrangement that axially locate the floating hub to the Controller Body. Figure 3-16 below highlights in white the Passive Controller Body, and the wetted components of the passive controller's fluid cavity.

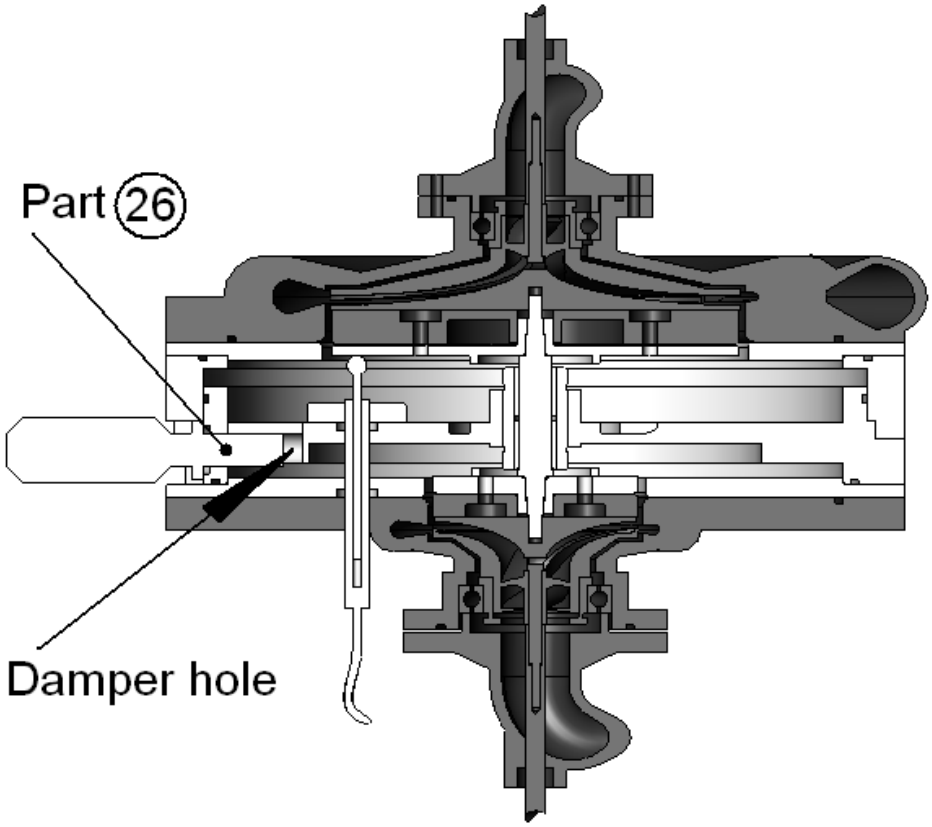

Figure 3-16: Sectioned elevation of prototype with highlighted wetted components of the Passive Controller fluid cavity.

An Ø8 mm hole enters part 10 from the side creating what is labelled the damper hole in Figure 3-16. This hole bores through a triangular slot which connects the two Controller Body chambers. Providing adjustable occlusion of the triangular slot is a

micrometer spindle, (part 26), which can be extended or withdrawn through the damper hole. More detail on this mechanism is given later in this chapter.

Preparation of the device for use begins by completely filling one of the Controller Body chambers with water. The other is filled with both water and a small, measured volume of air. Water can move from one compartment to the other through the damper hole. This provides the damping function for the floating hub's motion. Depending on the adjustable area of the damper hole, the level of damping can be adjusted. During operation the device is orientated with the impellers' rotating axes parallel to the ground. The device was then rotated so that the damper hole is at least 90° from the top of the device preventing the air bubble from travelling between chambers.

The fluid within the divided passive controller cavities was sealed from the fluid within each pump by means of flexible membranes. These membranes lie between parts 6 and 7, and 13 and 19 on the RVAD side and between parts 12 and 13, and 11 and 16 on the LVAD side, see Figure 3-13. The membranes were thin sheets of latex; a product used by dentists called Dental Dam. The membranes divide the cavities within the device into three; the RVAD pump fluid cavity, the Passive Controller fluid cavity and the LVAD fluid cavity.

3.4.3.5 **The Passive Response**

The essence of the passively actuated controller is the floating hub which responds to changes in vascular pressure through axial translation to adjust both the differential flow and pressure between the LVAD and RVAD. Figure 3-17 shows the hub position when the AoP is raised (left) and the PAP is raised (right). Consequently, the figure contains sketches of the resulting pressure head and flow rate from both VADs.

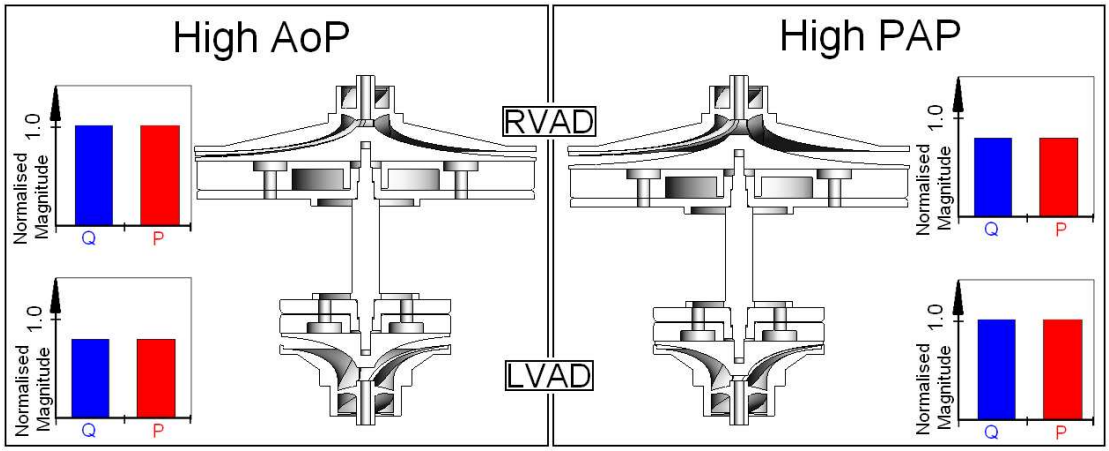

Figure 3-17: Sketch of the normalised pressure head, H, and flow, Q, from the LVAD and RVAD as well as hub position during an elevated AoP senario (left) and an elevated PAP senario (right).

As an example of how the passive response works in a clinical application; a congested, or oedematous, systemic circuit will cause elevated pressure in the aorta, (see Figure 3-17 (left)). The pressure change due to the hypertensive circuit is transmitted back to the LVAD driving the hub away from the LVAD impeller. This translation increases the LVAD clearance decreasing the LVAD hydraulic output. The AoP is then reduced, as is the flow into the congested vasculature. Additionally the decrease in the RVAD clearance increases fluid removal from the systemic venous system. This passive action encourages stability in arterial pressures imitating the native baroreceptor response. The total axial length available for hub translation will be referred to as the Total Clearance.

3.4.3.6 **Controller Dynamic Components; Spring, Mass and Damper**

In order to achieve a viable passive control system it was assumed that the dynamics of the floating hub's response would need to be optimised. To do so a spring, mass, damper configuration was used to affects the hub's motion. These three components were designed to be adjustable.

The mass component is the mass of the floating hub assembly, approximately 160g, plus any added weight placed in a cavity between parts 6 and 7 under the RVAD lower shroud. Damping of the hub's motion, as mentioned already, was achieved by variable restriction on water flow from one Controller Body cavity to the other.

An added spring response was initially planned to be achieved by way of a mechanical spring attached to a recess in part 10 and a spigot on part 7, see Figure 3-13. A number of springs were manufactured having a range of spring constants. However, it was found that the small air bubble in one of the chambers could be harnessed to be a very effective spring. Consider the difference in lower shroud areas of the two VADs. An axial translation of the hub will cause an overall change in the total volume of both chambers. This caused the air bubble to expand or contract providing a spring-like response. This will be explained and analysed in more detail in the next chapter.

The aforementioned components allowed the dynamic response to a differential pressure in the form of the floating assembly's velocity, acceleration and displacement respectively, within the device to be optimised. An example scenario and response of the floating assembly's dynamics is as follows:

The heart beats at approximately one beat per second and each ventricle is located approximately 100mm upstream of each VAD's inlet. The left heart's peak pressure is higher than that of the right heart inducing a high pressure differential approximately every second. The BiVAD's function will not benefit from the floating assembly hitting against the RVAD's physical axial stopper every second. To prevent this happening the adjustable fluid restriction, or damper, (proportional to velocity dynamic component) will be set such that the velocity of the fluid passing through the hole will be restricted. This will limit the flow rate and hence the volume of fluid required for a response to such a high frequency pressure differential.

3.5 BiVAD Pump Geometry

As mentioned, a number of resources were used for the design of the LVAD and RVAD geometry. Textbook pump design procedure was used as a basis for design geometry but deviations were taken where needed. Since the functionality of the passive controller is the focus of the study, as opposed to pump efficiency, this was not detrimental to the aims of the project.

Both VADs incorporate a mixed flow pump with semi open shroud configurations and a single spiral volute. The geometries of the LVAD and RVAD are given in Table 3-1.

Table 3-1: LVAD and RVAD Design and Geometric Parameters.

Nominated LVAD Operation Parameters	
H (mmHg)	100
Q (L/min)	5
N (RPM)	2400
$\emptyset OD$ (mm)	50

	LVAD Geometry	
Blade Angles	β_1 (°)	45
	β_2 (°)	80
Blade Heights	inlet	5.7
	outlet	1.2
Channel Areas	A_1 (mm^2)	130
	A_2 (mm^2)	188
	A_{throat} (mm^2)	33
Inlet	$\emptyset OD$ (mm)	16.4
	$\emptyset ID$ (mm)	5
Volute	θ_{volute} (°)	2.5

Nominated RVAD Operation Parameters	
H (mmHg)	20
Q (L/min)	5
N (RPM)	1200
$\emptyset OD$ (mm)	100

	RVAD Geometry	
Blade Angles	β_1 (°)	65
	β_2 (°)	80
Blade Heights	inlet	4.5
	outlet	1.2
Channel Areas	A_1 (mm^2)	80
	A_2 (mm^2)	377
	A_{throat} (mm^2)	186
Inlet	$\emptyset OD$ (mm)	14
	$\emptyset ID$ (mm)	5
Volute	θ_{volute} (°)	3

Firstly, the inlet blade lengths, *d1*, were chosen for both VADs so that the shaft and bearing arrangement, (see Figure 3-12), could be fitted inside the inlet housing. This was a problem for the RVAD as the impeller periphery area A_2 was so much larger than the impeller inlet area A_1 at the eye. This decreases the impeller efficiency as the meridional component of the fluid velocity would undergo a negative acceleration over the impeller face. However, this was sacrificed for ease of device manufacture.

A pre-swirl assumption was made for both inlets that the tangential velocity component, e_{u1}, was 10% of the mean inlet blade velocity. As mentioned earlier, inlet angle design is difficult for a pump in a highly pulsatile and unsteady flow environment.

During operation of the VADs the passive response will induce high clearances under the blades. In early tests it was expected that the overall clearance would be around 2 mm and in final tests this would be reduced to 1 mm. This implies that centrally

located, both impellers would have a clearance around 1 mm and then 0.5 mm respectively. It was assumed that this would induce a high level of fluid leakage over the impeller blades during operation. The outlet blade angles, β_2, were therefore designed to be higher than the calculated angles from the velocity triangles to maintain the designed delivery pressure with a high clearance. These angles were made 80° for both VADs; more than double that calculated from empirical theory.

The outlet blade height of both impellers, b_2, were kept to a minimum of 1.2 mm for both pumps due to earlier experiments indicating that blade heights less than 1mm caused too much throttling at the entrance to the volute. It was assumed that this was because; miniature pumps with an outer diameter of <Ø50 mm experience affected performance from high boundary layer activity. The 1.2 mm blade height, b_2, resulted in high impeller peripheral areas which could further increase, due to the floating assembly increasing the blade clearance.

The volute angles of both pumps were reduced from the resulting calculations of the outlet fluid velocity angles, α_2. This was to reduce device size for practicality of testing at the further expense of hydraulic efficiency of the pumps.

Resulting from the LVAD and RVAD design process were two pumps that could deliver acceptable hydraulic outputs. Additionally, the designs accommodated for the floating assembly of the passive controller to allow the proof of concept prototype to simulate a passive response. Furthermore, adequate impeller and shaft location could be incorporated to ensure true running of the impellers and reliable torque transmission.

3.6 Pump Generation

A computer program was written in MATLAB by the candidate which takes user supplied geometric parameters to provide output files consisting of coordinate arrays. This software can be found in the CD accompanying this thesis. These arrays describe 3D geometric profiles of the pumps which are imported by a CAD program called SolidWorks. The output files prescribe curves by linking the coordinates in Cartesian space to define the geometric form of the impeller and casing. When these

curves are imported by SolidWorks into an existing impeller or casing files, blade, shroud or volute profiles are updated to create a new pump part. From here the new impeller and casing part files are formatted for exporting to a rapid prototyping 3D printer. The formatted part files are then uploaded into the 3D printer where the components are formed from ABS plastic. Figure 3-18 shows numerous rotary pump configurations that were created in earlier studies using the program.

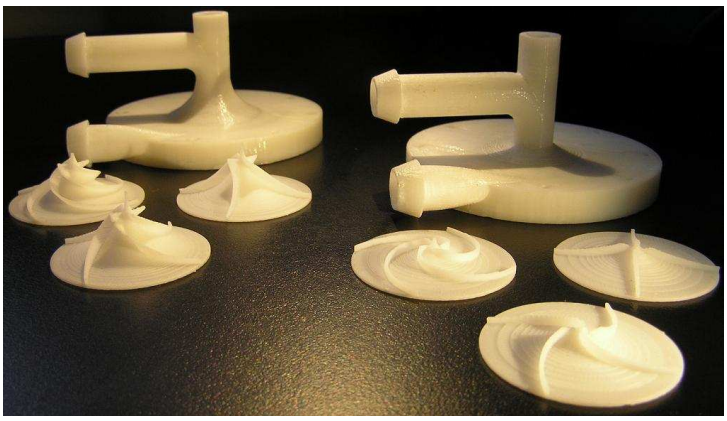

Figure 3-18: Impellers and their respective casings for an early set of miniature pump tests.

The software was developed to enable the rapid creation of numerous impeller and pump casings for VAD prototypes. It provides a non-commercial means of developing rotary pump geometries. The program has so far been used for manufacture of experimental test pumps and creating geometries for numerical fluid simulation. The order of operations within the program sees the generation of the impeller profiles first followed by the casing profiles.

3.6.1.1 **Impeller Generation**

The program consists of two parts. Impeller generation in the first half, and casing in the second. Figure 3-19 indicates some of the important geometric parameters specified by the program to construct the impellers for the testing within the first section of the program. The figure shows a semi-open mixed flow impeller with an upper shroud. The blade heights d_1 and b_2 have not been included in the figure as they were specified in Figure 3-4.

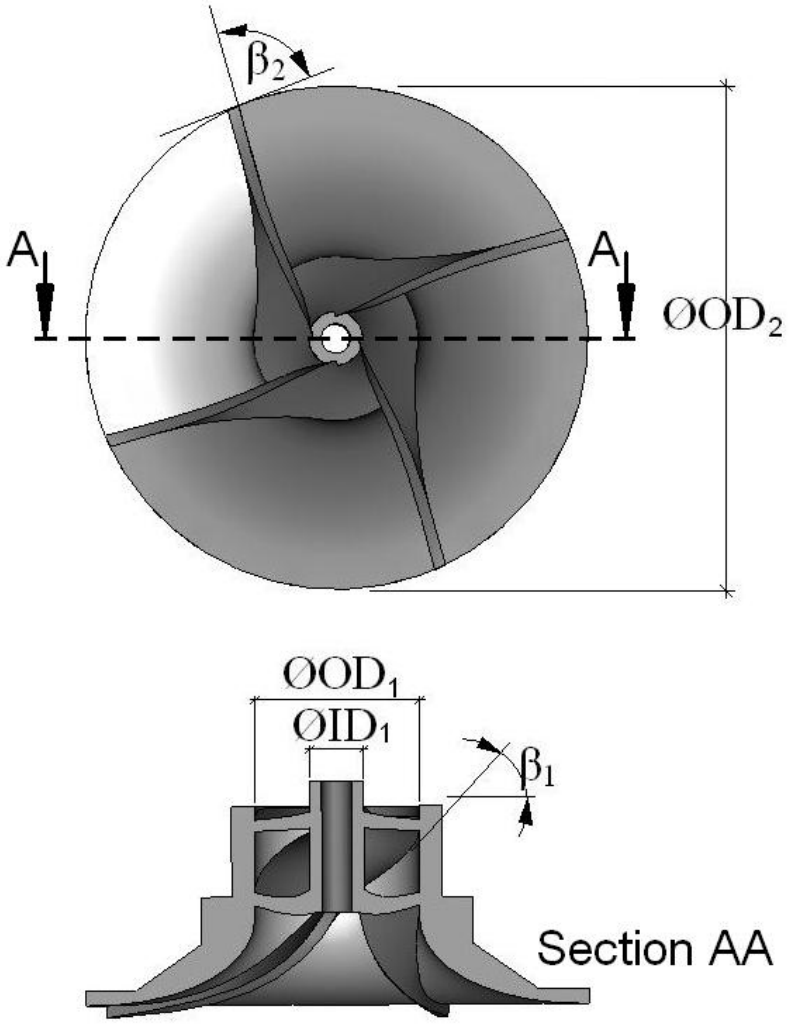

Figure 3-19: Bottom view and paln section of a completed CAD model of a dimensioned impeller that was used for testing.

When the input parameters have been entered into the code, the program is run to generate the profiles needed to create the CAD models like those shown in Figure 3-19. The image in Figure 3-20 shows three views of the prescribing curves of an impeller generated by the program.

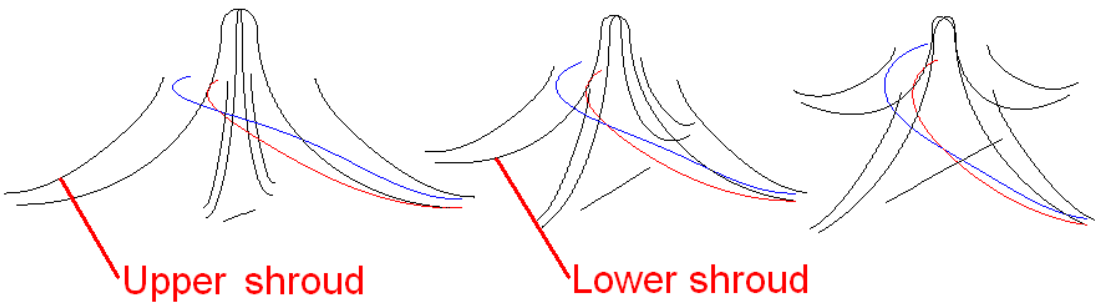

Figure 3-20: Impeller prescribing curves in 3D space rotated through three views.

The lower shroud of the impeller as well as a reference line which indicates the underside of the lower shroud is located first. Following this, the blade profile is generated. The MATLAB program creates a blade geometry which is later repeated around the rotating axis depending on the number of desired blades. The red and blue lines shown in Figure 3-20 prescribe the outer and inner edge of a single blade. SolidWorks recognises these two lines and then connects them with an extruded feature to form the blade. The blade feature is then rotated about the vertical axis to create additional blades. Once the outer edges of the blades have been located, the upper shrouds can be defined.

The output profiles from the program in MATLAB are exported into SolidWorks for the embodiment of the components like those shown in Figure 3-19. Here the user updates the shroud and blade profiles to obtain new CAD components. Depending on the desired impeller the user can use either, or both shroud profiles to generate a semi open or closed impeller respectively.

3.6.1.2 **Casing generation**

In the second part of the Matlab program the profiles used to generate the pump casings are created. The embodiment in SolidWorks and the rapid prototyping follows the same procedure as that of the impeller generation. Figure 3-21 provides sectioned side and plan views of a pump casing which show some of the important geometric parameters specified within the program. Note that the casing shown in the figure is not from the passive controller, however, it was a pump used for preliminary experiments. A casing for a semi-open impeller with a lower shroud from a previous test has been selected to illustrate the geometries due to its simplicity. However, the indicated geometries are representative of the passive controller VAD casing geometries.

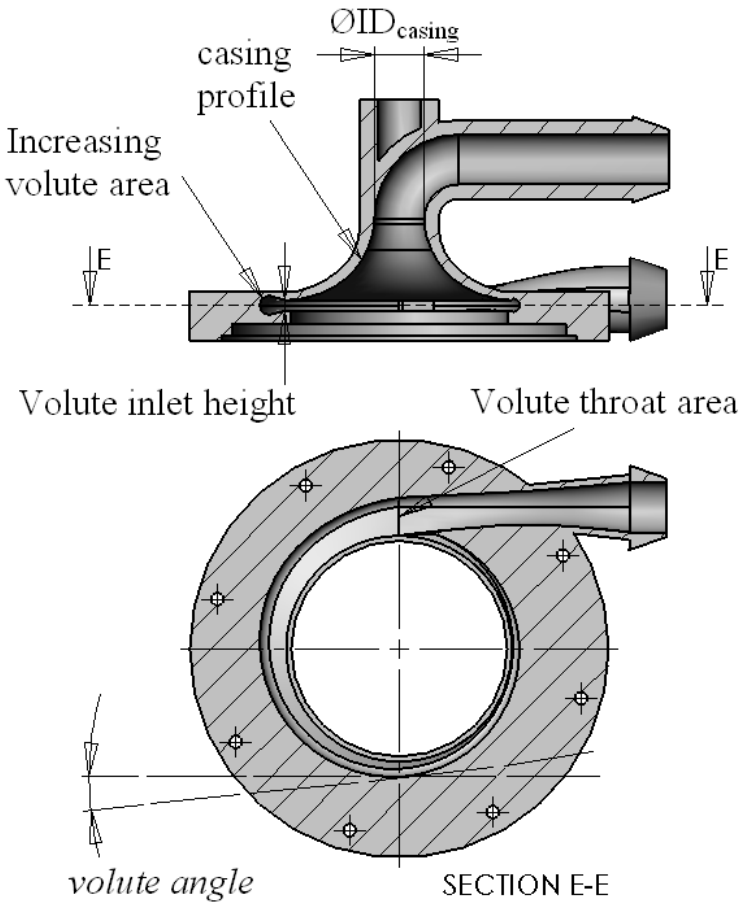

Figure 3-21: Sectioned side and plan views of a completed CAD model of a dimensioned casing that was used for testing.

Figure 3-22 shows three views of the casing prescribing curves that are created by the program. These consist of the outer edge of the single volute or fluid collection profile (the large spiral), the small quarter circle volute sections profiles, four inner edges of casing that double as the upper shroud profile, and the base of the casing for special referencing within SolidWorks.

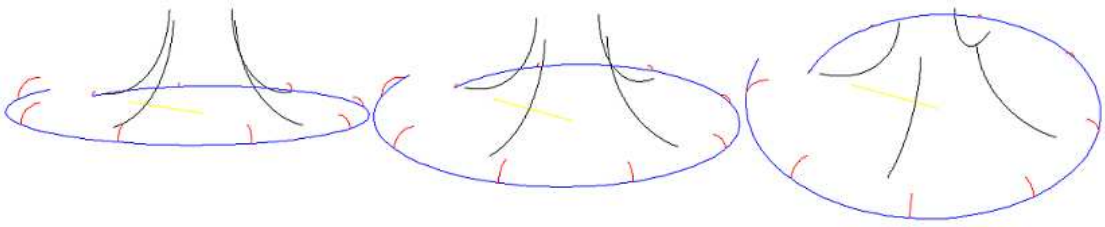

Figure 3-22 Casing prescribing curves in 3D space rotated through three views.

3.7 The BiVAD Prototype

The completed prototype is shown in a side elevation photo in Figure 3-23. Note, device has been rotated 180° about its vertical axis to that shown in Figure 3-12.

Figure 3-23: Side elevation of Passive Controller BiVAD prototype.

The prototype was constructed from numerous materials to permit ease of manufacture, high geometric tolerances and resistance to corrosion. The VAD casings and impellers were created using the rapid prototype 3D printer from white ABS plastic. The passive controller body was fabricated using Perspex and Polycarbonate, (Lexan). All additional components were stainless steel or Polycarbonate, (Lexan).

3.7.1 The Mechanical Layout of the Prototype

The basic components of the device are laid out in Figure 3-24. They do not include the linear displacement transducer (LVDT, Solartron DG5.0, (range ±2.5 mm)), flexible membranes, motors and coupling, device mounting rig and cannulae.

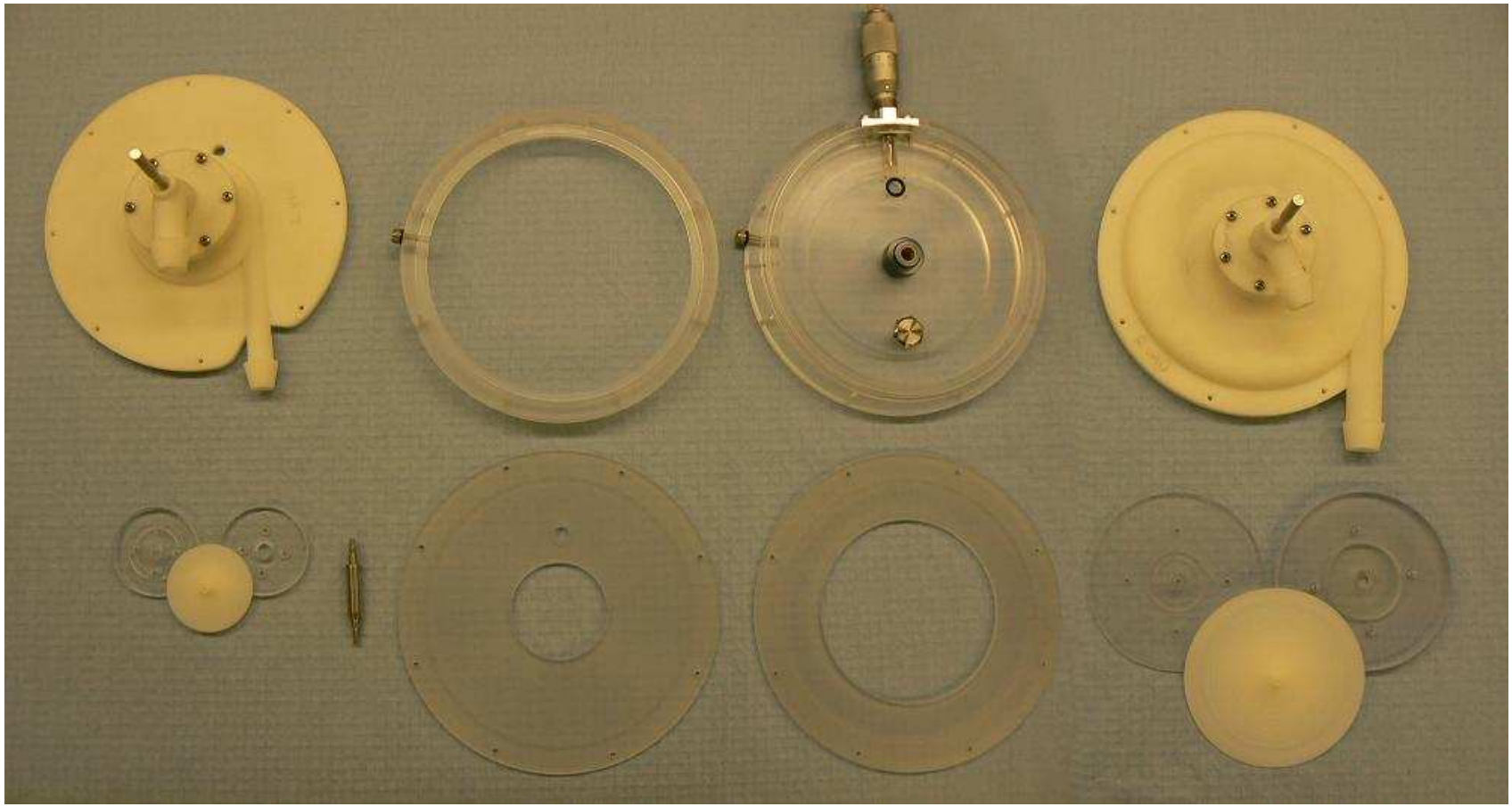

Figure 3-24: Passive Controller BiVAD components after manufacture, (landscape view). Clockwise from top left; Assembled LVAD with drive, Passive Controller Body upper, Passive Controller Body lower, assembled RVAD with drive, RVAD lower shroud assembly[#], RVAD to Controller Body mounting plate, LVAD to Controller Body mounting plate, floating assembly shaft[#], LVAD lower shroud assembly[#]. ([#] A component of the complete floating assembly).

The assembly of components are drawn together with threaded rods, locknuts and wing nuts through eight holes evenly distributed around the circumference of the device as can be seen in Figure 3-23.

Large scale assembly drawings that were used for manufacture are shown in Appendix 10.1. These should be compared to the exploded view figures for assembly visualisation. The assembly drawings included in Appendix 10.1 are as follows:

- Drawing 1.1: Section of the device with isometric views
- Drawing 1.2a: Section of the device with numbered parts
- Drawing 1.2b: Bill of parts as described in Drawing 1.2a
- Drawing 1.3: Viscous Damper configuration detail
- Drawing 1.4: Isolated floating assembly detail with axial and radial location
- Drawing 1.5: Layout of impeller and floating assembly clearance
- Drawing 1.6: Layout of impeller and casing clearance, (radial bearing detail)
- Drawing 1.7: Layout of complete device assembly, critical dimensions

(Note, the intended use of the drawings in Appendix 10.1 were for manufacture. For this reason, notes are instruction for the fitter and turner. However, the detail is useful for explanation of the device configuration)

Three exploded view figures have been assembled for ease of assembly visualisation. These are detailed in Figure 3-25 to Figure 3-27.

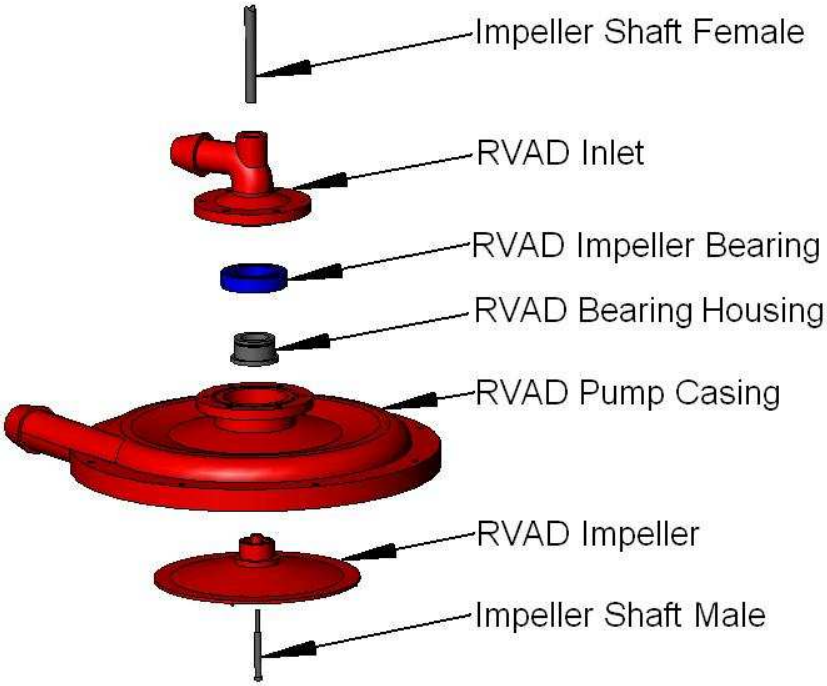

Figure 3-25: Exploded view of RVAD Components, a sub assembly of the complete device.

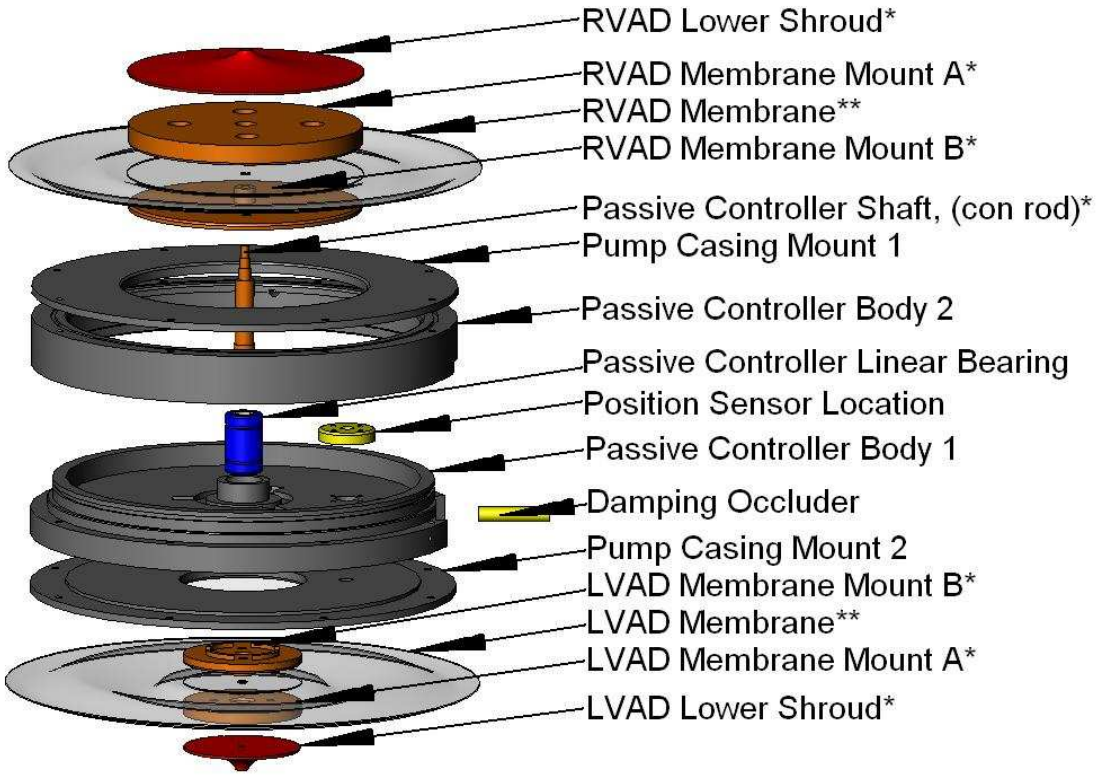

Figure 3-26: Exploded view of Passive controller and floating assembly, a sub assembly of the complete device.

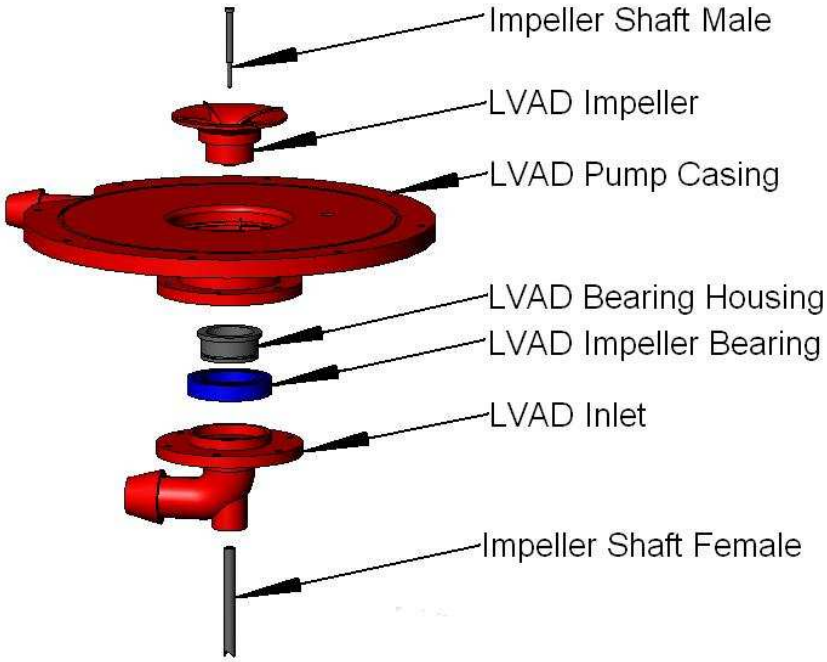

Figure 3-27: Exploded view of LVAD Components, a sub assembly of the complete device.

(*Component is part of the floating assembly. **Component is not shown in the Appendix 10.1 drawings. Note the LVDT position sensor has not been included in any of the exploded views. Note also, that the Damping Occluder in Figure 3-26 is indicated with a cylinder – in the prototype, the occluder is a micrometer spindle)

3.7.2 Subassemblies and Test Rig

The following are specific notes on some of the components that are not self explanatory from the previous discussions.

3.7.2.1 **Impellers and Impeller Location**

The impellers were radially located using deep groove ball bearings locating the eye of the impeller with the inlet of the pump casing. To ensure that the 3D prototyped impellers ran truly within the pump casing, stainless bearing housings were fitted between the bearings and the impeller. The LVAD impeller, stainless bearing housing and impeller shaft male, are shown in Figure 3-28.

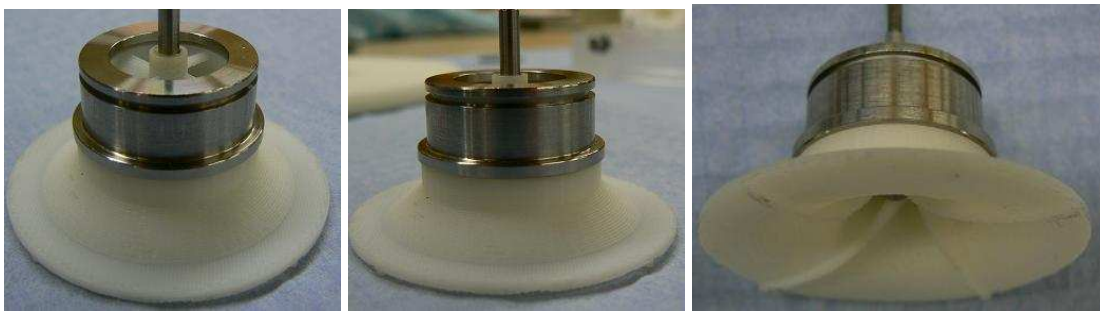

Figure 3-28: Rotated views of LVAD impeller with the stainless impeller housing for radial bearing location.

The figure offers a close inspection of the semi-open impeller configuration with an upper shroud. The impeller inlet is shown in the left hand image and the impeller blades running down the inside of the shroud are shown in the right hand image.

3.7.2.2 **Adjustable Damping**

As mentioned earlier there is an occluded hole between the divided cavities. This hole is occluded by a micrometer spindle, (referred to as the Damper Occluder in Figure 3-26). Figure 3-29 shows a planar view of the Passive Controller Body with the occluding micrometer labelled. The figure also provides a detail of the micrometer and 'tear shaped' occluded hole, (previouslty referred to as the triangular slot). The micrometer spindle can be withdrawn from the tear shaped hole to provide restricted fluid flow between the Passive Controller cavities. The result is a damping effect upon the floating assembly's axial translation. A tear shape was used for the hole so that fine damping adjustment could be provided during high damping operation.

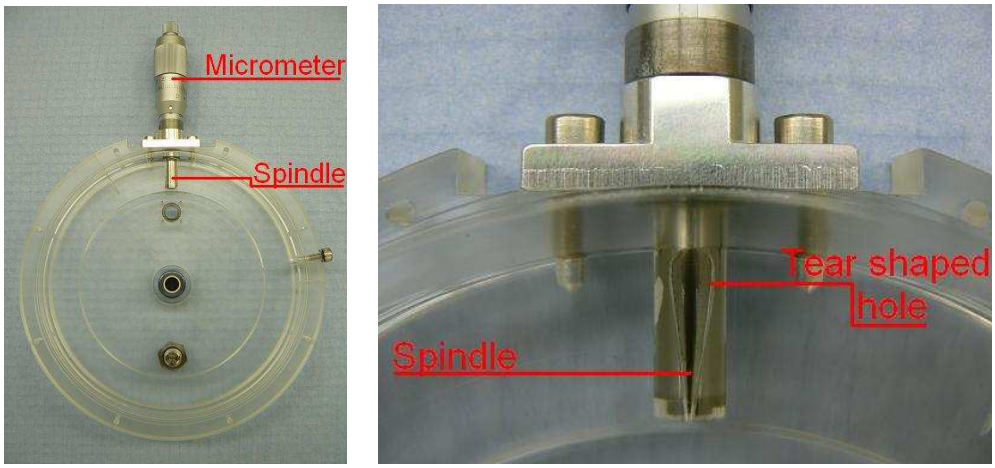

Figure 3-29: Passive Controller Body 1 planar view, (left), detail of micormeter occluder, (right).

3.7.2.3 **Membrane Configuration**

Membranes cover the pump casing mounts to seal the fluid between the Controller cavities and the VADs. Thin latex rubber sheets, used by dentists, called Dental Dam were used as membranes. Dental Dam is less than 100 μm thick and can comfortably cope with a strain of up to 400%, with a maximum tensile capacity of 14.5 MPa (Ahlers, Abdullah, and Platzer 2003). The membranes were clamped between the VAD membrane mounts using screws, see Figure 3-30. Butyl rubber gaskets and silicon sealant were used to seal between the membrane mounts.

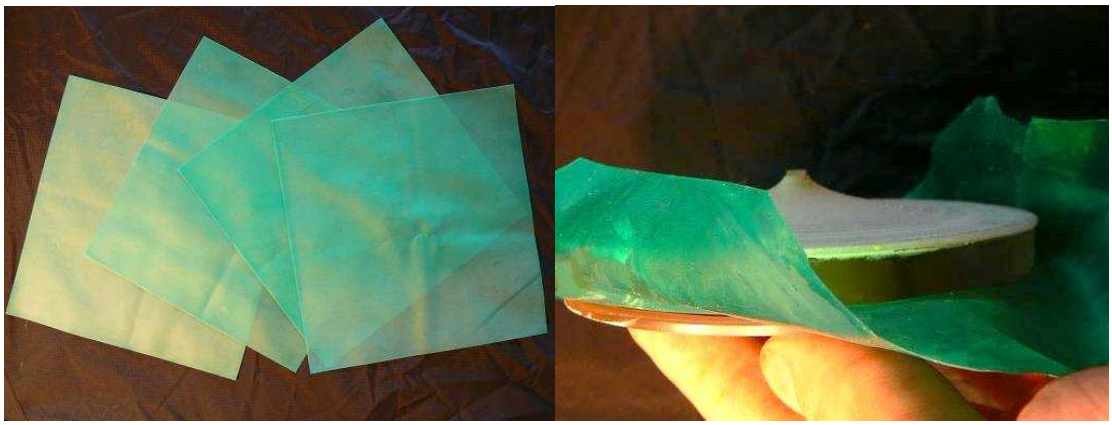

Figure 3-30: Dental Dam sheets, (left), Membrane clamped between the floating assembly membrane mounts, (right).

The protruding Dental Dam sheets were then pressed between their respective pump casings and pump casing mounts. Additionally 800 μm butyl rubber gaskets and silicon sealant was used to stop leakage and were applied as shown in Figure 3-31.

Figure 3-31: Silicon application to the pump mounting plate, (left), the butyl rubber gasket, (right). (Note, the small hole at the top of the mounting plate and gasket allow the LVDT position transducer to protrude through).

The completed controller body with gaskets and membranes sealing the Controller Body is shown in Figure 3-32.

Figure 3-32: Plan view of the Controller body with attached RVAD membrane, (without the butyl rubber gasket). The view is from above the RVAD lower shroud.

3.7.2.4 **Floating Assembly; Axial Translation Limits**

At the eye of the lower shrouds, (at either end of the floating assembly), a polycarbonate button was manufactured and glued in place, as shown in Figure 3-33.

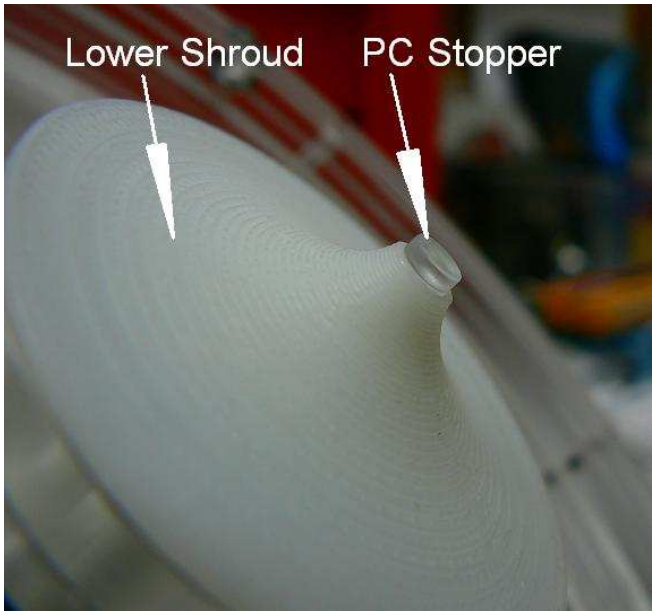

Figure 3-33: Lower shroud with polycarbonate, (Lexan), axial translation stopper.

At either translational axial limit, the Poly Carbonate, PC, (Lexan), stopper meets the bottom of the impeller shaft. The PC stoppers and the shafts, therefore, create the physical stopper for the floating assembly.

3.7.2.5 **Setting the Total Axial Clearance**

Early in the design process it was foreseen that the total axial clearance may need to be adjusted during testing. The distance between the LVAD and RVAD impeller shafts dictates the total translational range for the floating assembly. It was predicted that the accumulated tolerance error from the six stacked components, including the VAD casings, (see Appendix B, drawing 1.1), could render a range of axial clearances. In an attempt to minimise this error, one of the Passive Controller Body part geometries was machined after partial assembly to ensure the correct clearance, (see Appendix B, drawing 1.7). However, 0.5 mm and 1.0 mm shims were employed between the Passive Controller Body parts which were used to increase the total clearance.

Figure 3-34: Placing the 1.0 mm shims on the Passive Controller Body part 1, (left), plan view of the shims in place before replacing the Passive Controller Body part 2, (right).

Figure 3-34 shows the placing of the 1.0 mm shims around the coincident face of the Passive Controller Body parts, (left), as well as a plan view of all the shims in place, (right). The male-to-female location of the Controller Body parts allows them to slide axially depending on the thickness of the shims. An O-ring around passive Controller Body part 1 prevents any leakage between the two components. The shim and the O-ring configuration allow the total axial clearance between the VAD shafts to be manipulated. The total axial translation range for the floating assembly, therefore, is adjustable, and can be measured with the LVDT.

It should be noted that there are two variables that will be referred to which relate to the clearance between the impeller blades and the lower shroud. These are the clearance, *c*, and the floating assembly position, *y*. The clearance, *c*, specifically refers to the distance between the blades and the lower shroud of one particular pump, see Figure 3-15. The floating assembly position, y, on the other hand, is the translated distance of the floating assembly from the central position, see Figure 4-18. The sign convention for the floating assembly position is positive towards the RVAD impeller. The difference between these two parameters should be kept in mind as they are both used for explanation and discussion in the coming chapters.

3.7.2.6 **Testing Rig**

A test rig was constructed to house the device lying on its side. The rig also housed the LVAD and RVAD brushless motors (Amax32, Maxon Motors, Switzerland).

These 20W motors were mounted on either side of the device along its rotating axis. The rig was made of aluminium and Perspex. Two views of the device in the rig with the mounted motors are shown in Figure 3-35 and Figure 3-36.

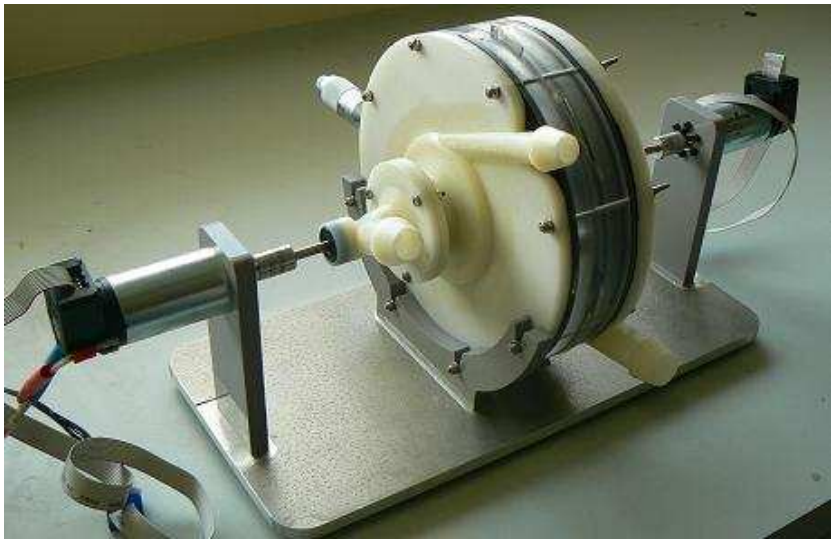

Figure 3-35: Angled view of the prototype housed in the test rig with the twin 20W motors.

Fixed to the end of the DC motors are encoders to record the impeller rotational speed.

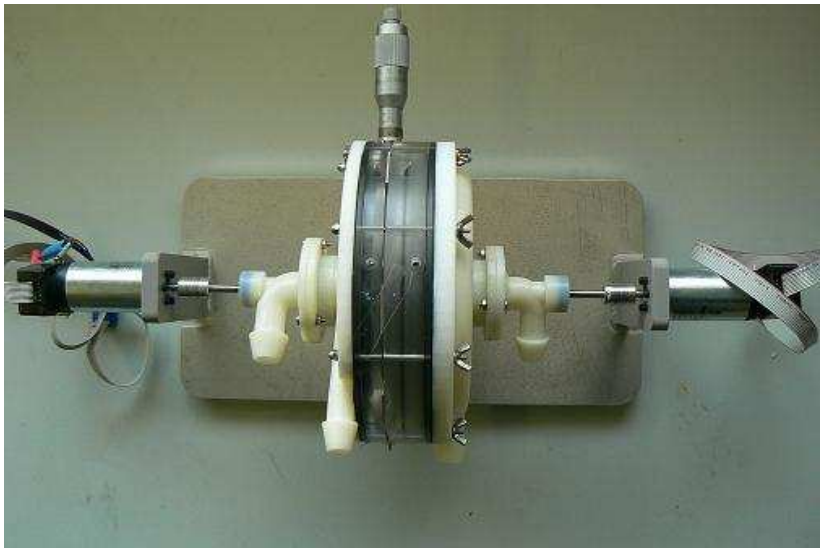

Figure 3-36: Plan view of the prototype housed in the test rig with the twin 20W motors.

3.7.2.7 **Shaft Sealing and Drive Coupling**

An enlarged section of Figure 3-36 is shown in Figure 3-37 with the BiVAD inlet seals arrangements and the shaft coupling. A lip seal was pressed into a plastic sleeve and that then fitted over the shaft inlet into the pump inlet bend. The coupling used was a flexible spiral coupling to account for any axial or angular mismatch in the coupling shafts.

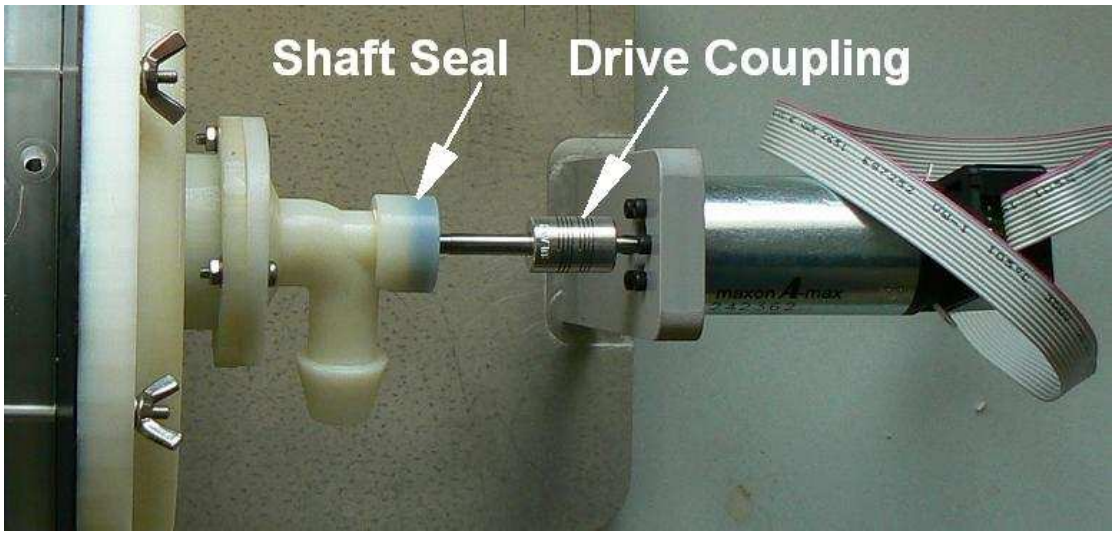

Figure 3-37: Shaft sealing and coupling detail, plan view of the shaft configuration within the test rig.

3.8 Conclusion

Dual rotary pumps were incorporated into a BiVAD with the aim of assessing the device's ability to passively control acute CV events. A relatively complex device design eventuated into a functional prototype that could provide a passive response to vascular pressure fluctuations. Opposed semi open impellers with an upper shroud, together with a floating assembly incorporating lower shrouds, implemented the passive response. Actuated by the pressure fluctuations, the floating assembly translates axially to increase or decrease the clearance over the impeller blades to affect the pump output.

The dynamics of the floating assembly's axial motion is optimised by a mechanical mass, spring and damper configuration. The magnitude of these dynamic components can be varied to optimise performance.

A test rig was built to allow the device to be held and easily cannulated to the Mock Circulation Loop (Timms *et al*. 2005). Incorporated into the rig were the 20W DC motors to provide individual drive to the LVAD and RVAD impellers through a coupling and shaft configuration.

Construction of the device, together with the rig, has rendered a means of testing the feasibility of a passively controlled cardiac support system as well as assessing the prototype design as a mechanical configuration for a passively controlled BiVAD.

4 *In Vitro* Testing and Device Evaluation

4.1 Introduction

The primary goal of the experimental testing was to address the aim of assessing the viability of the device and control strategy. Therefore, the *in vitro* tests focused as a whole on assessing the viability of the prototype to provide BiVS. However, the experiments also provided data with which to verify the numerical model. This will be described in Chapter 6. Provided good agreement is achieved between the two simulations the numerical model will be used to extend the experimental results observed in this chapter.

Commonly, steady state performance curves accompany haemolysis results to introduce a cardiac assist device's hydraulic functionality. However, these have limited value in this study as the functional feature of interest is the control strategy and configuration. To test the viability of the mechanical passive controller the device needed to be tested in a:

- pulsatile environment
- dual circuit rig to simulate the interaction between the systemic and pulmonary systems
- dynamic hydraulic rig that simulates the resistance, compliance and inertiance of the cardiovascular system

The prototype configuration and its means of control would be considered viable if:

- acute or chronic cardiovascular incidences, (such as Pulmonary hypertension or suddenly lying down), could be controlled and partially or completely corrected
- the passive controller only responded to pressure signals caused by flow imbalance or disease, (as opposed to pulses from residual ventricular function).
- it could support the cardiovascular system, if needed, as a total support device

The passively controlled BiVAD was tested in a dual circuit Mock Circulation Loop, MCL, (Timms *et al*. 2005). This method of *in vitro* testing allowed an initial

understanding of the interaction between the dynamic controller and the dynamic vascular circuit.

Recall that this thesis presents an experiemtnal and a numerical study to assess the viability of the prototype as a cardiac support device. In order to prevent confusion between results from each investigation a general colour scheme has been used to quickly tell them apart. Any plotted experimental result, (predominantly in this chapter only), will be set on a white background. Any plotted numerical simulation result will be set onto a grey background. A reminder of this colour scheme will appear later before the numerical results are presented.

4.2 The Mock Circulation Loop, MCL

The MCL is a physical hydraulic model of the human cardiovascular system. It includes both systemic and pulmonary circuits connected in series to simulate vascular system interdependence and interaction during normal, diseased and assisted cardiac function.

4.2.1 Mock Circulation Structure

The rig consists of systemic and pulmonary circuits with vascular compliance and resistance, atria and ventricles as well as isolated arterial and venous chambers. Both the atrial and ventricular chambers along with the vascular chambers are upright cylinders with both the inlet and outlet at the cylinder base. There are a series of pressure tapings and two flow meters measure the flow rate on either side of the circulatory system. A schematic of the MCL is depicted in Figure 4-1.

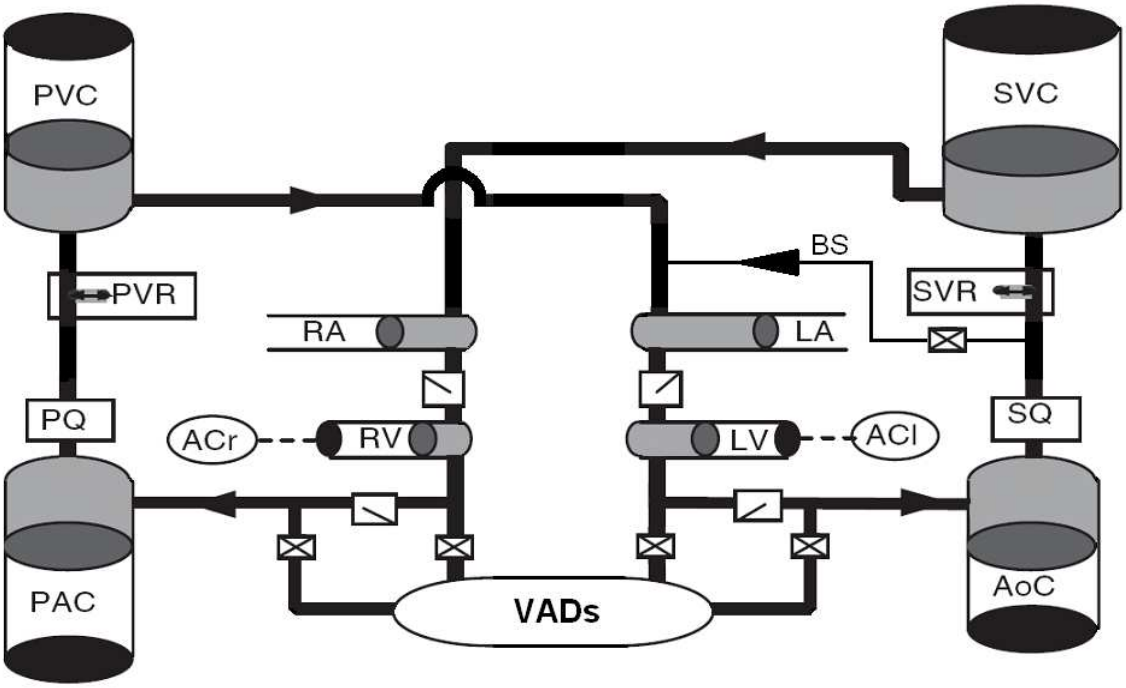

Figure 4-1: Schematic of the dual circuit Mock Circulation Loop; LA, left atrium; LV, left ventricle; ACl, compressed air to the LV; AoC, systemic arterial compliance; SQ, systemic flow meter; BS, bronchial shunt; SVR, systemic venous resistance; SVC, systemic venous compliance; RA, right atrium; RV, right ventricle; ACr, compressed air to the RV; PAC, pulmonary arterial compliance; PQ, pulmonary flow meter; PVR, pulmonary venous resistance; PVC pulmonary venous compliance; VADs position of ventricular assist device(s).

A photo of the MCL supported with an RVAD is shown in Figure 4-2. Included in this photo are the flow paths around the loop. The oxygenated and deoxygenated blood flows are represented in red and blue respectively. The purple line indicates flow from the cannulated right ventricle, through the RVAD and out into the pulmonary artery.

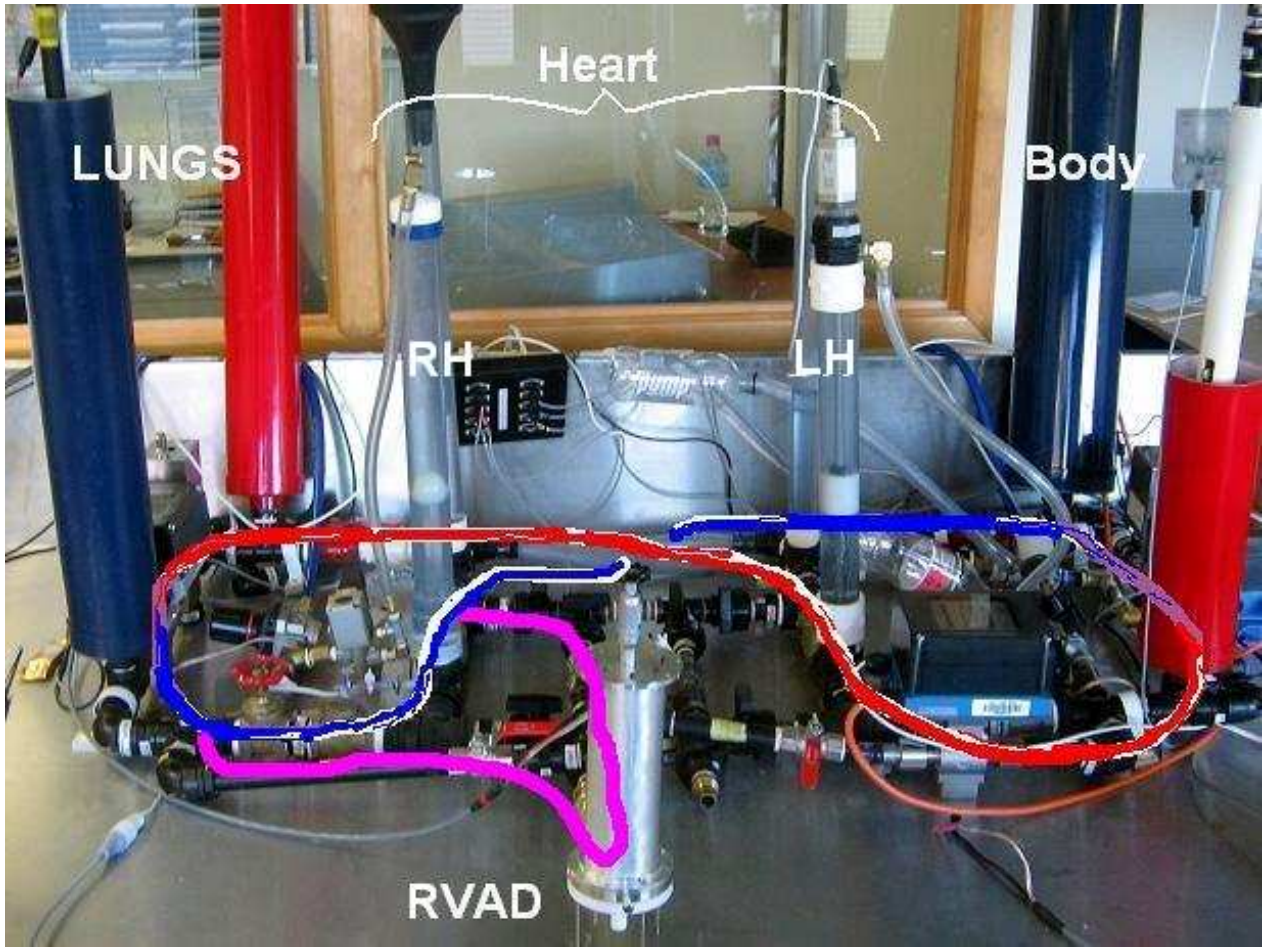

Figure 4-2: Mock Loop supported by an RVAD. Flow paths of oxygenated and de-oxygenated blood are shown in red and blue respectively. The purple line indicates the flow through the RVAD.

The MCL is controlled using a desktop computer running CONTROLDESK software. The software provides the interface for the dSPACE controller board, (DS1104, Novi, MI, U.S.A.). The controller board incorporates eight analogues to digital inputs and eight digital to analogue outputs. These can sample or signal at up to 1 kHz. This limits the data acquisition to eight real time signals, (unless signal splitting is employed which was not available in the MCL during the Passive Controller BiVAD testing). MATLAB Simulink is used to process the raw sensor signals.

Only eight data signals for the dual circuit MCL meant that the experimental testing system was limited in its observability. Regardless of this the eight data signals were sufficient for a comprehensive study. However, the limited observability encouraged the development of a highly observable numerical model as a parallel investigation tool to the experimental testing. The development of the numerical model and the resulting simulations will be covered in the latter half of this thesis.

Ventricular systole is emulated by channelling compressed air into the top of the ventricular cylinder forcing the column of residing fluid out into the main artery. The diastolic period is achieved through passive filling of the ventricles from the diastolic atrial to ventricular pressure gradient. The bronchial shunt is also included in the mock loop to simulate the shunt from the systemic arterial system, through the lung tissue and then into the pulmonary vein. The MCL can simulate both normal heart function and heart disease. Different forms of achievable heart disease simulation include hyper and hypo contractility as well as irregular heart beat frequency and systolic period. Additionally vascular disease can be induced such as increased or decreased vascular compliance and resistance.

4.2.2 General MCL Operation Procedure

All experimental testing for this study was carried out using the MCL. Three types of tests were run, each of these are presented in this chapter. These were pump performance tests, haemodynamic simulations and dynamic vibrational testing.

4.2.2.1 **Performance Testing**

Basic pump performance tests required either the systemic or pulmonary circuits to be isolated. A pump was then tested by measuring the gauge pressure at the pump's inlet and outlet as well as the circuit flow rate. The circuit resistance was then gradually decreased using an active proportional pinch valve, (HASS Manufacturing, New York, NY, U.S.A.). Performance data could then be derived for different pump speeds and impeller clearances.

4.2.2.2 **Haemodynamic Simulation**

The second test type was the haemodynamic simulations. This type of testing is the MCL's primary function. First, the MCL is set up to imitate the human circulation by calibrating the pressure sensors and filling the circuits to provide a physiological Central Venous Pressure, CVP.

Fluid filling and pressure calibration of the MCL was carried out in two stages. The first saw the filling of all the horizontal plumbing of the fluid circuit with the arterial and venous compliance chambers open to air. This used approximately four litres. At this point, the pressure sensors were calibrated and set to 0 mmHg and the compliance chambers were sealed. Finally, a further 1-2 litres of fluid was added creating positive pressure in the sealed compliance chambers and increasing the fluid volume in the upright atrial and ventricular cylinders which were open to atmosphere. The volume of added fluid was such that the pressure sensors read 8-10 mmHg. By definition, this was the CVP. It is important to note that even though the MCL held around 5-6 litres, (similar to an adult human), the collective displacement of compliant vessels was only 1-2 litres. For this reason, the circuit volume in the numerical model too was made 1-2 litres.

From this point, CONTROLDESK is used to actuate and adjust ventricular action and circuit resistance to simulate healthy or diseased circulation. Compliance changes are done manually before the simulation starts by positioning, and then sealing, a plunger down the length of the compliance chamber to adjust its internal air volume.

The pneumatic ventricular action in the MCL was not quantified. Active control over each ventricle's contractility, heart rate and systolic time period was controlled using an active proportional solenoid valve, (SMC-317, Inianapolis, IN, U.S.A.) and a throttling valve. It also depended on the laboratory mains air pressure which fluctuated slightly.

CONTROLDESK is also used to operate the VADs and maintain their speed for supported simulations. However, dSPACE can only provide a maximum voltage output of 10 V. This was not sufficient to overcome the required torque to drive the Passive Controller LVAD for some of the simulations so a separate power source was used.

4.2.2.3 **Dynamic Vibrational Testing**

Dynamic testing of the Passive Controller provided an experimental vibrational analysis of the dynamic floating assembly. This was used to test the passive controller damper to assess its performance in filtering residual periodic translation caused by residual ventricular pulses.

Again, the pulmonary and systemic circuits were isolated and a single ventricle was made to pulse at a range of frequencies. Pressures inside both VADs were measured along with the LVDT displacement data. This allowed periodic force vs. displacement data to be derived to achieve the dynamic analysis of the passive controller.

4.2.3 Haemodynamic Characteristics of the MCL

Testing the passive controller action of the device required an *in vitro* testing rig that would simulate the bio-signalling features of the native heart. Most importantly was that the MCL incorporated dual circuits and passive filling ventricles to simulate the Frank Starling Mechanism.

The MCL is a world class human circulation simulator and has been extensively tested to assess its ability to simulate human haemodynamics (Timms *et al*. 2005).

The Frank Starling mechanism has been simulated as has the Vasalva Technique; a voluntary hyper tensing of the pulmonary circuit done by a patient for a clinician to evaluate the condition of the heart.

Since the loop is a mechanical circuit there are, of course, short comings in its ability to recreate human circulation. These are mainly due to the following:

- The loop operates with water as its primary working fluid as opposed to blood.
- The acquisition of no more than eight real time data signals meant that the MCL had limited observability.
- Non-flexible mechanical components such as heart valves and ventricle contractions[3].
- The inability to simulate exercise due to the minimum pulmonary circuit diameter restricting high flow simulation.
- Feedback control of aortic pressure (baroreceptor)

However, the versatile functionality of the MCL has allowed the prototype to be tested in pulsatile, non-pulsatile, heart failure and supporting conditions. It also allowed simple dynamic testing of the floating assembly as well as performance testing of the pumps.

4.3 Pump Performance Testing

In order to characterise the VADs' hydraulic performance, tests were carried out to get pressure flow relationships over a range of pump speeds. These tests were also important to realise the effect on the VADs' outputs through adjustment of the clearance, *c*.

4.3.1 Method

Performance testing of the VADs was difficult due to the nature of the controller. Its passive response meant that, unrestrained, the floating assembly could translate from

[3] To reduce this, the compressed air actuated ventricular contractions have associated compliance chambers to simulate a more 'sinusoidal' ventricular pressure profile.

one side to the other as the resultant force across the hub changed throughout each test. As previously discussed, (and will be shown), the pump performance is very sensitive to this clearance. To ensure that the floating hub was stationary throughout each VAD performance test, the other VAD was removed in order to physically restrain the hub.

The systemic loop was isolated and used for the tests. In turn each VAD was plumbed in and run at constant speed and clearance over a range of circuit resistances. This test was repeated for a number of speeds and clearances for each VAD. The LVDT was used to measure the central hub's position to ensure that it was restrained.

Additional tests were carried out where each VAD was run in the loop at a constant speed and constant fluid resistance. The clearance was then increased from $c \approx 0.0$ to 2.5 mm to observe the consequential drop in performance. This was useful as it indicated the relationship between H and c as well as Q and c in a continuous data set.

4.3.2 Results

The raw performance curves for the LVAD are shown in Figure 4-3 . The pump was tested over a range of pump speeds from N = 2200 to 4200 RPM. The presented data represents the LVAD's performance with a clearance of $c \approx 0.0$ mm.

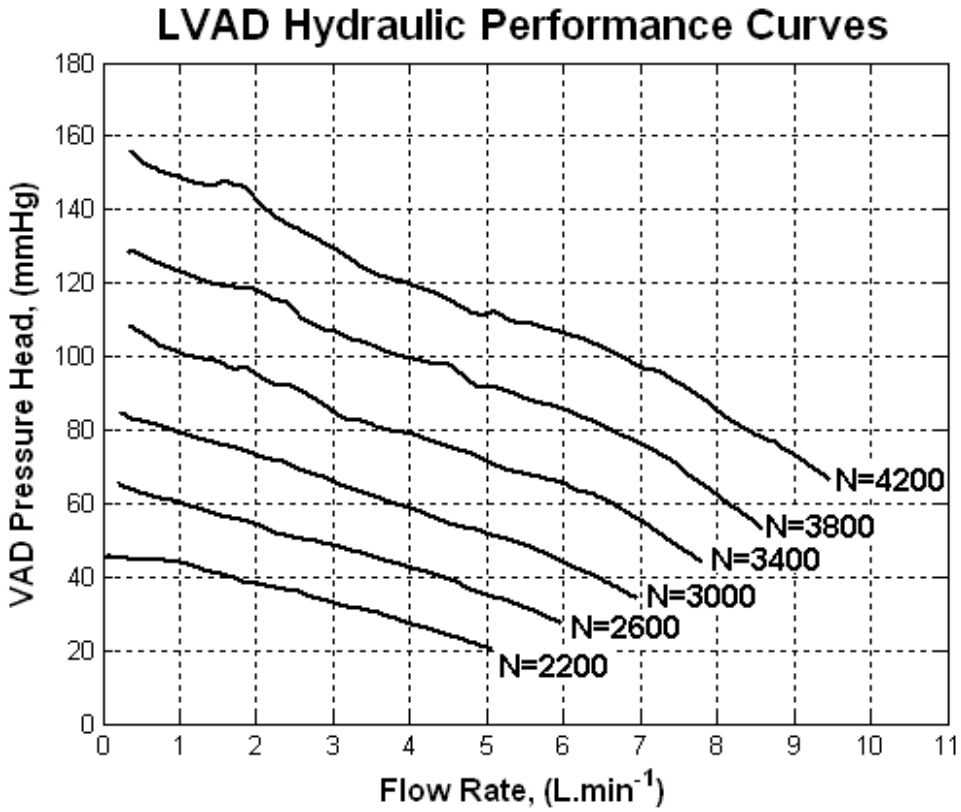

Figure 4-3: LVAD characteristic performance curve for speeds between *N* = 2200 and 4200 RPM with a minimal clearance.

A set of performance curves for the LVAD is shown in Figure 4-4 for a running speed of N = 3400 RPM at clearances of $c \approx 0.0$, 0.5 and 1.0 mm. The figure indicates the non-linear relationship between H and c.

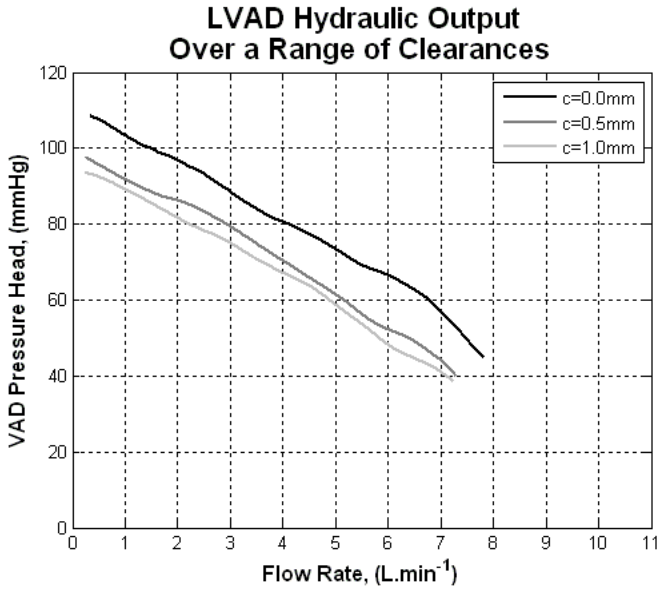

Figure 4-4: LVAD performance at 3400 RPM over three discrete clearances.

Pressure and flow versus clearance plots are shown in Figure 4-5, again running at N = 3400 RPM, where the variation in clearance is continuous from $c \approx 0.0$ to 3.1 mm. The figure indicates the apparent exponential decay of both pressure and flow with clearance. It is apparent that clearance adjustment affects the output fluid power of the pump.

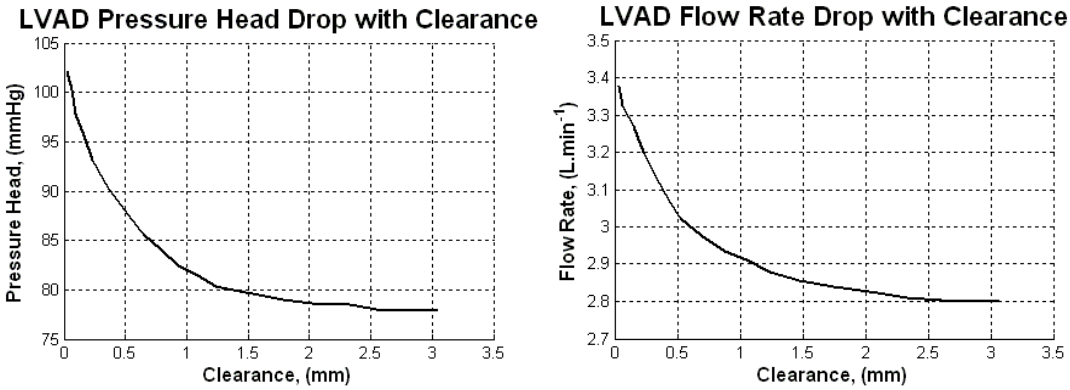

Figure 4-5: Degraded pressure, (left) and flow (right) of the LVAD as the clearance is increased N = 3400 RPM.

RVAD performance tests were carried out over seven pump speeds from N = 600 to 1200 RPM as shown in Figure 4-6. Again, the clearance for the presented performance tests is $c \approx 0.0$ mm.

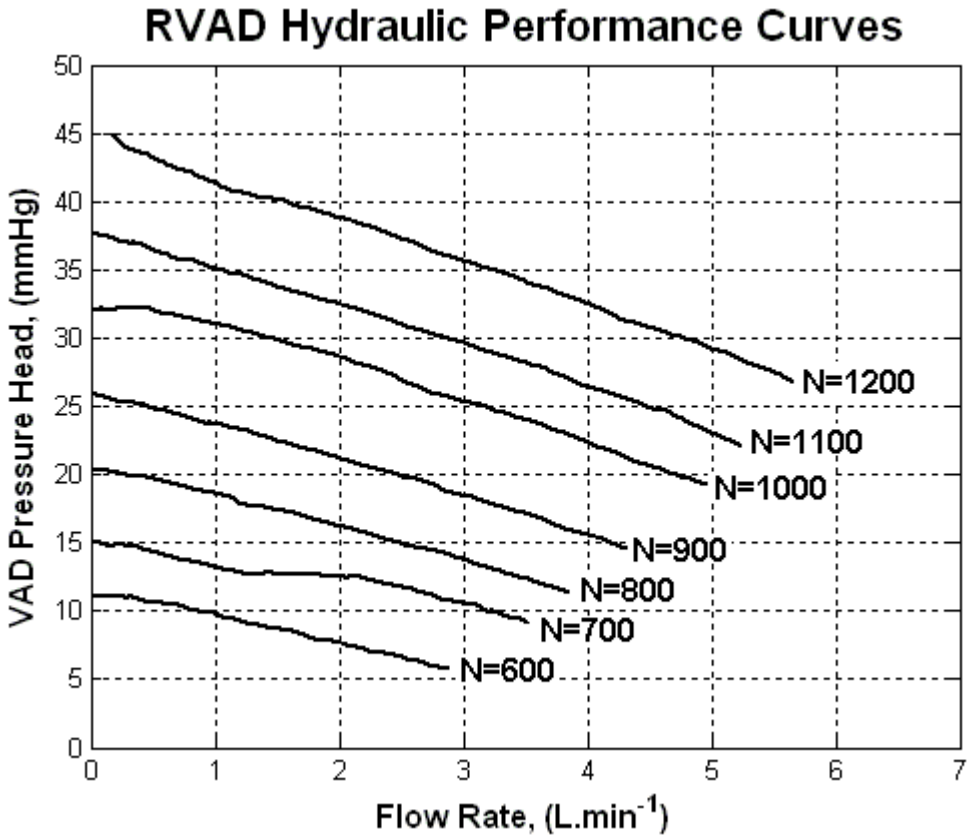

Figure 4-6: RVAD characteristic performance curve for speeds between *N* = 600 and 1200 RPM with a minimal clearance.

An interesting result was seen in the RVAD pressure and flow head drop due to an increasing clearance as shown in Figure 4-7. The initial gradient appeared to be approximately $-\infty$ mmHg.mm^{-1}. For certainty, this test was repeated rendering a similar trend.

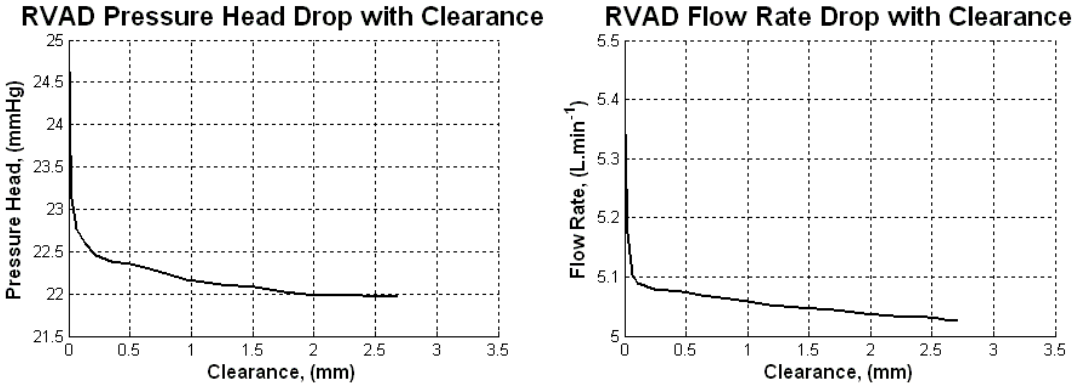

Figure 4-7: Degraded pressure, (left) and flow (right) of the RVAD as the clearance is increased *N* = 1100 RPM.

4.3.3 Discussion

The LVAD performance testing showed that total LV support could be provided by this pump at $N \approx 4000$ RPM. This is a very high running speed for an impeller of diameter 50 mm. It was assumed that the semi-open impeller with an upper shroud incorporated unforseen losses. Further work will be needed in order to understand this deviation from the designed operating speed. However, the running speeds and efficiencies were not major concerns for this study so no further pump design iterations were done.

There were two issues with the basic performance testing which made it hard to get accurate and smooth performance profiles. The first was the hub position. In order to maintain the hub position during each test the fluid inside the Passive Controller Body needed to be pressurised to counter the pressure inside the pump. However, over each test, the pressure inside the pump varied from the shut off pressure (low flow) to the pressure at high flow.

Another issue was that the tests were carried out in one of the vascular circuits of the MCL. Unfortunately, this included a compliance chamber at the pump outlet. The effect of this was that every discrete change in resistance was met with a small settling time for the pressure and flow. To minimise this settling time, the compliance was set to a minimum by removing as much air as possible from the compliance chamber.

The degradation of LVAD pressure head and output flow with clearance appears to decay exponentially. This result is in keeping with Timms *et al.*'s report that increasing the clearance decreases the output hydraulic power as mentioned in the previous chapter, (Timms *et al*. 2006).

It appears, over the clearance range tested, that the developed pressure and flow decay exponentially at first and then decrease at some linear rate. An explanation for this has been formulated but not tested beyond the presented results above. It was assumed that the dynamic fluid structure within the rotary pump goes through two phases. The first, at very small clearances, is a forced vortex between the two shrouds where the angular velocity of the fluid, e_u/r, is constant. The second is where the

blades loose their ‘grip’ on the rotating fluid and the fluid structure takes on a free vortex fluid structure. The continuing linear degradation could be attributed to increasing ‘slip’ of the fluid over the blades as the clearance increases.

Total RV support could be provided by the RVAD at $N \approx 1000$ RPM which is a lower speed than the nominated operation speed of 1200 RPM.

When the clearance was increased from $c \approx 0.0$ to 0.1 mm there was a very large decrease in RVAD pressure head. In fact, this clearance change saw over 85% of the pressure drop observed over the total testing range, $c = 0$ to 2.7 mm. This is an unusual result although may be due to the larger diameter impeller’s inability to maintain the forced vortex structure where the rotational fluid inertia is higher, i.e. at the impeller periphery.

4.4 Physiological Testing with Discussions

The following results and discussion examine the passive controller prototype’s response to a number of acute circulation events. Most of these events incorporate pathological haemodynamics although the effect of physical movement of the patient is also studied. The results demonstrate the passive action of the device and the success of its implementation as a treatment to these complications.

Initially, healthy circulation and chronic supported simulations were carried out in order to characterise the MCL simulation. Then the passive response to acute CV conditions tested the primary thesis aim followed by frequency testing of the device’s floating assembly. All the supported simulations were carried out with the BiVAD operating in a constant speed mode.

4.4.1 Generalised Method

The MCL data acquisition hardware allowed eight real time data sets to be recorded per test. Seven of these were used. These were the two ventricular pressures, the aortic and pulmonary artery pressures, the systemic and pulmonary flow rates and the LVDT displacement data.

The procedure for this testing was to initially set the Central Venous Pressure, CVP ≈ 5 mmHg, by adding fluid to the testing rig. Following this, the mock loop was run at healthy haemodynamics with flow rates of 5 $L.min^{-1}$. The Aortic pressures were maintained at 120/80 mmHg and the Pulmonary Artery at 25/10 mmHg. This provided the healthy, (and therefore unsupported), data.

To simulate acute heart failure, the contractility of the left and right ventricles was decreased so as to drop the pulse pressures to approximately 60/40 mmHg and 15/10 mmHg respectively. This was done by clamping the compressed air line into the ventricles with solenoid pinch valves, (ACl and ACr, see Figure 4-1). Consequently the circulation flow rates were reduced to between 3 and 4 $L.min^{-1}$.

To simulate chronic supported heart failure, the device was plumbed into the MCL and both DC motors run until the VADs restored healthy haemodynamics. As would be predicted, the pulsatility of the flow was reduced with the constant flow pumps. In order to provide sufficient support to both vascular circuits the VADs were run at N_{LVAD} = 3370 RPM and N_{RVAD} =600 RPM. These speeds provided global flow rates of 5 $L.min^{-1}$ and arterial pressures, MAoP and MPAP, or 100 and 22 mmHg respectively.

Total support simulations were carried out by ceasing any ventricular contractions. Due to the absence of work contributed by the ventricles, the VAD speeds were increased to provide the total support. The required speeds were N_{LVAD} = 3870 RPM and N_{RVAD} = 920 RPM. This provided global flow rates of 5 $L.min^{-1}$ with AoP and PAP of approximately 100 and 22 mmHg respectively. These running speeds were approximately consistent with all the presented tests.

The total axial clearance for all the presented tests, (unless stated), was set at y = ±0.17 mm, (i.e. total translational range of 0.34 mm). Earlier tests were carried out with a higher total clearance and the device was less sensitive to pressure fluctuations.

4.4.2 Healthy and Heart Failure Testing, (Acute, and Chronic Supported)

MCL tests initially involved tests of the healthy haemodynamics and subsequent bi-ventricular heart failure. This allowed a means of comparison for the following supported chronic heart failure simulations. From this data the device's operation during chronic support could be observed.

4.4.2.1 **Results**

Steady, healthy haemodynamics were simulated by the MCL in Figure 4-8. The pulsatile ventricular pressures in light grey are indicative of the cardiac cycle. The mean Aortic and Pulmonary Artery pressures are shown in black as are the mean flow rates at the bottom of the figure. The data presents mean parameters for clarity when comparing to later data.

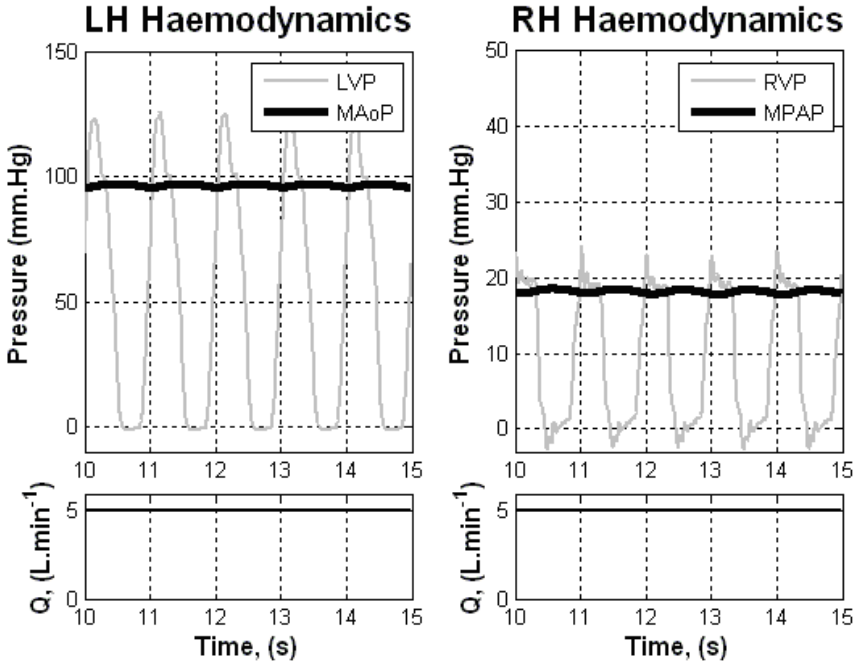

Figure 4-8: Simulation of healthy haemodynamics.

A number of haemodynamic nomenclature are introduced in this figure including the Left and Right Ventricle Pressures, LVP and RVP respectively, the Mean Aortic Pressure, MAoP, and the Mean Pulmonary Arterial Pressure, MPAP. Reference to

the absolute aortic and pulmonary artery pressures will also be employed using the acrynoms AoP and PAP.

A decrease in the pneumatically activated contractions simulates acute heart failure, (Figure 4-9). The vascular pressures, as well as the mean flows, are dropped to the target levels described in the method section as well as the mean flows.

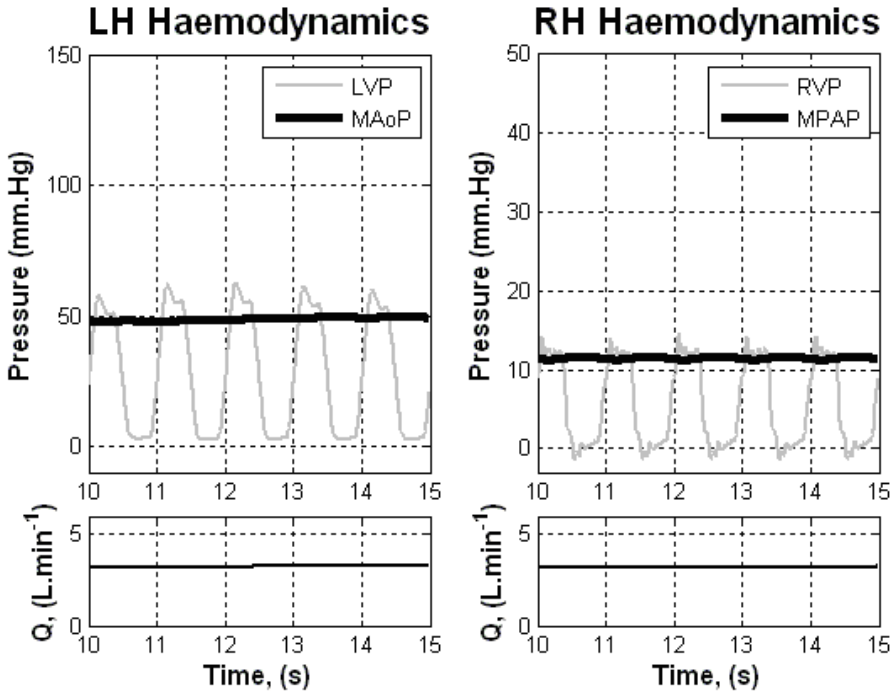

Figure 4-9: Simulation of acute Bi-Ventricular Failure, BVF.

The simulated heart failure was given bi-ventricular support using the BiVAD prototype as shown in Figure 4-10. The additional bold dark grey lines indicate the mean VAD pressure heads. By definition, the mean VAD head profiles, in grey, are the mean differences between the black arterial pressures and the light grey ventricle pressures. The mean VAD pressure head profiles are included as MLVAD P and MRVAD P. Again, mean VAD pressures are shown for clarity.

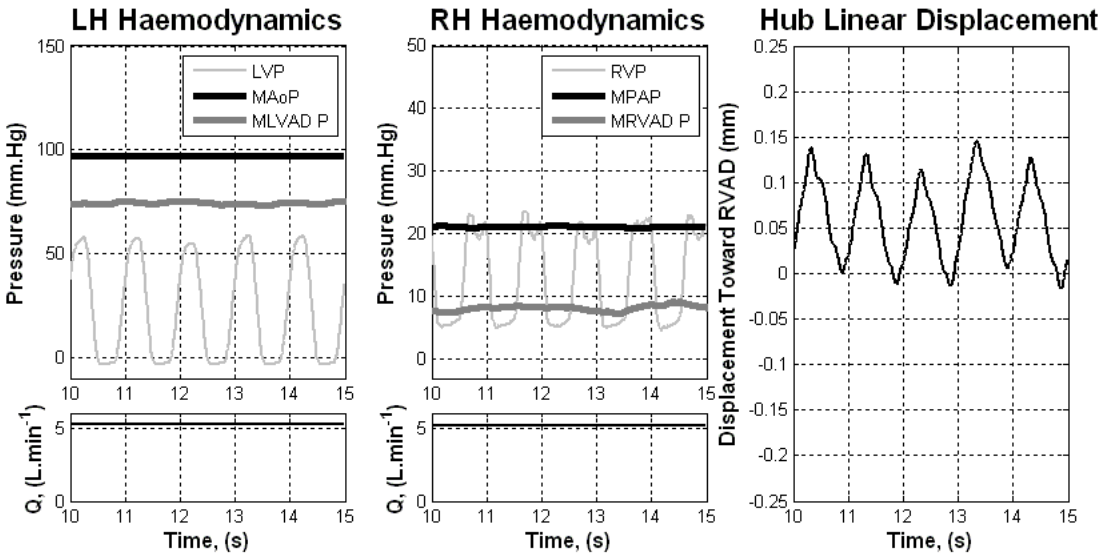

Figure 4-10: Simulation of a patient's haemodynamics once supported and stable with the prototype BiVAD.

The plot on the right hand side is the transient floating assembly (hub) position from its zero point where positive is toward the RVAD impeller. It is clear that the pulsatile pressure profile is causing the floating assembly to oscillate. As would be expected, the systolic phase is received with a translation toward the RVAD due to the dominating LV systolic pressure. Note that the hub is oscillating about $y \approx +0.08$ mm for a mean arterial pressure ratio of around 4:1.

The prototype was tested in total support mode as shown in Figure 4-11. Without pulsatile ventricular pressures, the floating assembly position remains steady.

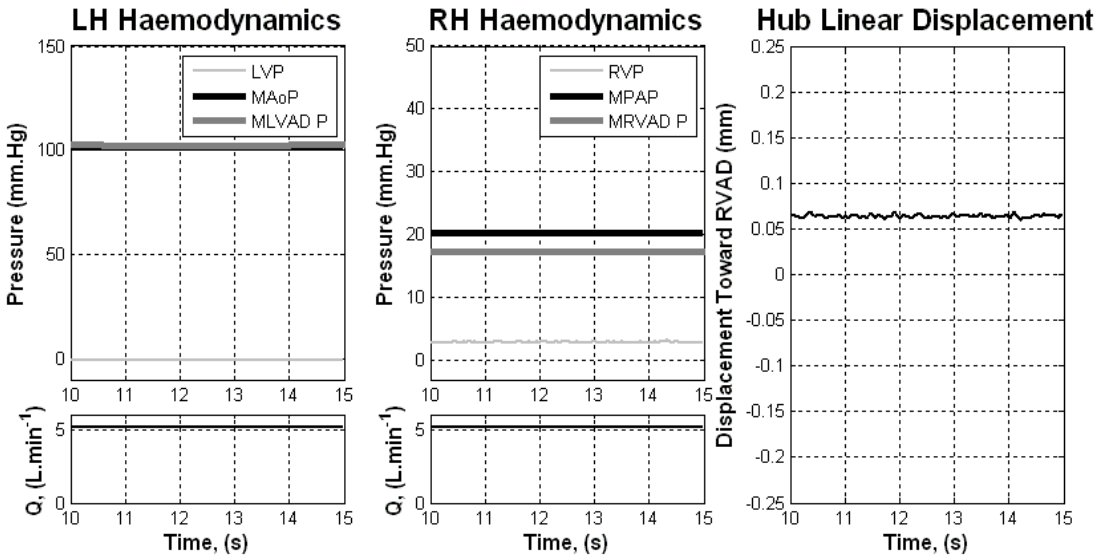

Figure 4-11: Simulation of a patient's haemodynamics once supported with the prototype BiVAD in total support mode.

4.4.2.2 **Discussion**

The MCL allowed representative simulation of healthy and heart failure circulation. Additionally the LDVT provided the ability to record the precise location of the floating assembly's axial position.

The assisting VADs elevate the diseased circulation flow rates back to 5 L.min^{-1} in Figure 4-10. The artery pressures were also restored to 100 mmHg and 22 mmHg. Although not shown in the results, low diastolic ventricular pressure gives an indication of suckdown. This occurs with pressures around -4 mmHg.

The prototype showed its versatility as a partial and total support device. The data were presented as mean profiles, (except the ventricular pressures and the hub position), to allow clear indications of trends. These plots should be referred to in the following results sections as stable comparisons.

It can be seen from Figure 4-11 that the steady state position for the floating assembly when supporting the CV system is approximately 0.08 mm. This indicates that there is a resultant force toward the RVAD. The deflection is dependent on the employed spring stiffness, *k*. It is reasonable that the steady state position would be higher than

zero as the LVAD to RVAD lower shroud area ratios is 1:4 and the AoP to PAP ratio is just under 5:1.

4.4.3 Acute Supported Cardiovascular Event Simulation

Many haemodynamic events which could compromise the safety of mechanical support systems involve gradual changes in pressure either side of the device. However, gradual changes in haemodynamics and the resulting gradual response from the device are hard to observe. So, sudden CV events were carried out to imitate the symptoms of these events. Consequently the sudden device response was very obvious emphasizing the nature of the response.

Four acute tests were carried out in the MCL. The tests all began simulatin total BiVS and then were suddenly destabilised through manually varying systemic and pulmonary resistance, ventricular contractility and circuit volumes. These provided supported simulations of acute systemic and pulmonary hypertension, infarction and physical movement/poor flow balancing respectively

4.4.3.1 **Systemic Hypertension Simulation**

The first physiological test was a systemic hypertension simulation conducted primarily to compare the haemodynamics of dual rotary support with and without a passive response.

Method

To initialise the test the Central Venous Pressure (CVP) was set to 8 mmHg by adding fluid to the MCL. Since the primary objective of this test was to observe the effect of the passive response, a larger total clearance of 0.5 mm, (y = ±0.25 mm), was used. For clarity of the result a reduced pressure ratio of 3.5:1, (using a PAP of 29 mmHg), was used so as to position the hub near the LVAD impeller before the simulated hypertension. This was done by increasing the RVAD speed as well as pulmonary circuit resistance. Note that this non realistic pressure ratio and high total clearance was used for this test only for purposes of comparison. Acute systemic hypertension

was then simulated by suddenly increasing the systemic resistance by way of actuating the systemic pinch valve.

Two tests were carried out to observe the difference in resulting haemodynamics after suddenly induced hypertension with and without a passive response. The first test, with the passive response, needed no preparation beyond what has been described. To prevent the passive response in the second test, the damper hole was completely occluded with the micrometer spindle. This prevented fluid from moving between the Controller Body chambers through the triangular slot, therefore prevented the hub from moving.

The primary function of this systemic hypertension test was to illustrate the effect of the passive response on suddenly increased aortic pressure. For clarity, only the aortic pressure, systemic flow and hub position data will be presented. Later, a pulmonary hypertension simulation will present more extensive haemodynamic data.

Results

The simulations, shown in Figure 4-12, saw one test with the passive response, and the other without it. The results were then overlayed to demonstrate the change in performance attributed to the passive adjustment in clearance over the impeller blades.

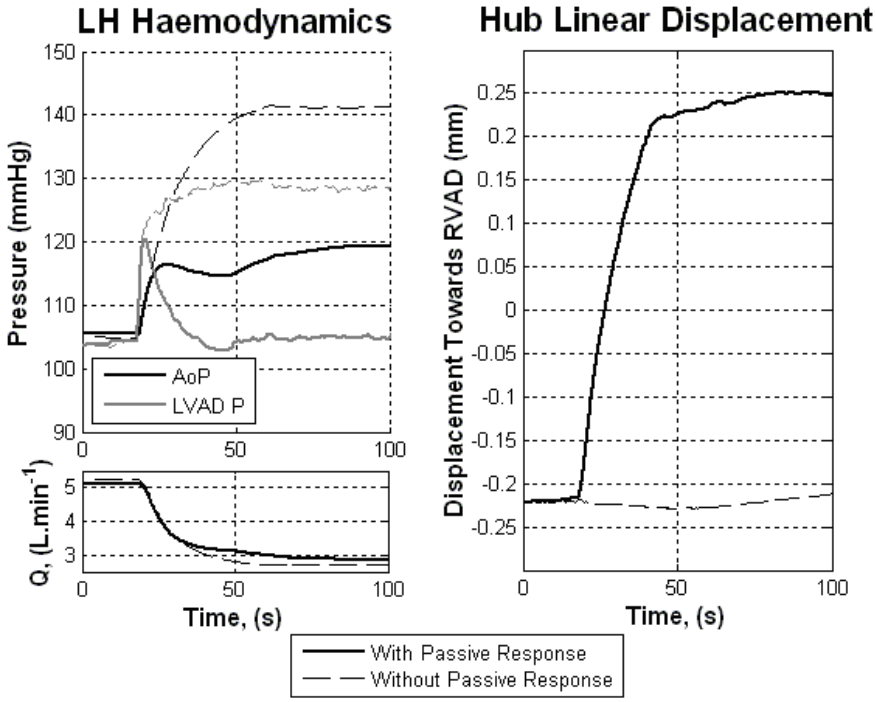

Figure 4-12: Comparison of prototype response to sudden Systemic Hypertension with and without the passive response, (Note, the solid, bold lines represent the response with a passive response and the dashed lines represent without).

The solid profiles represent the haemodynamics resulting from the passive response and the dashed lines show the devices operation without. This is shown in the two hub axial position profiles on the right of Figure 4-12. The difference between the dashed and solid profiles gives a clear indication of the magnitude of the passive controller's effect.

Discussion

Without passive controller intervention the sudden hypertension elevated the aortic pressure to 140 mmHg. Met by the increased resistance, the LVAD operating point moves to the left of the performance curve increasing pressure and dropping flow. Furthermore, there was a slightly larger drop in flow through the LVAD without the passive response

.

When the passive response is employed, the rising aortic pressure causes the hub to translate away from the LVAD. The slightly delayed hub response to the increasing aortic pressure allows for an apparent pressure spike in the LVAD head. The passive

controller then drops the LVAD head maintaining the aortic pressure below 120 mmHg as indicated by the solid black line. Thus, the aortic pressure increase is halved by the passive response. This test illustrates the auto-regulating baroreceptor-like response of the passive controller. The hub position is sympathetic to arterial pressure changes. This effect will be shown in three other tests in this section although more detail in the global haemodynamics will be included in the results.

Arterial pressures are well treated through the passive response. However, the flow rate is reduced drastically. The flow drops to around 3 $L.min^{-1}$ indicating that perfusion requirements will no longer be met. This is not a particular flaw in the passive control scheme, or rotary VADs in general. It is a simple hydraulic consequence that if circuit resistance in increased and the pressure head is maintained, the flow will decrease. Such issues will, and do, require clinical intervention to reduce vascular resistance.

4.4.3.2 **Pulmonary Hypertension Simulation**

Method

This simulation was actuated by a sudden increase in pulmonary circuit resistance. The resistance is increased by actuating the pulmonary circuit pinch valve. It simulates a condition that is the product of many different CV conditions. Perhaps one of the most common is left heart failure, where it fails to redistribute fluid from the Pulmonary Vein to the Aorta. The VAD pumps were operated, as with all the testing, in a constant speed mode. The device was operated as a total support device for these results to allow further clarity in the pressure profiles.

The hub clearances were reduced to y = ±0.17 mm, (i.e. a total clearance of 0.34 mm) and global flow rates were initialised at 5 $L.min^{-1}$. An initial AoP to PAP ratio of just under 5:1 was used for all the remaining tests with arterial pressures at around 100 and 22 mmHg respectively.

Results

Pulmonary Hypertension was then simulated in the data shown in Figure 4-13. The sudden increase in Pulmonary Artery pressure causes the hub to translate away from the RVAD.

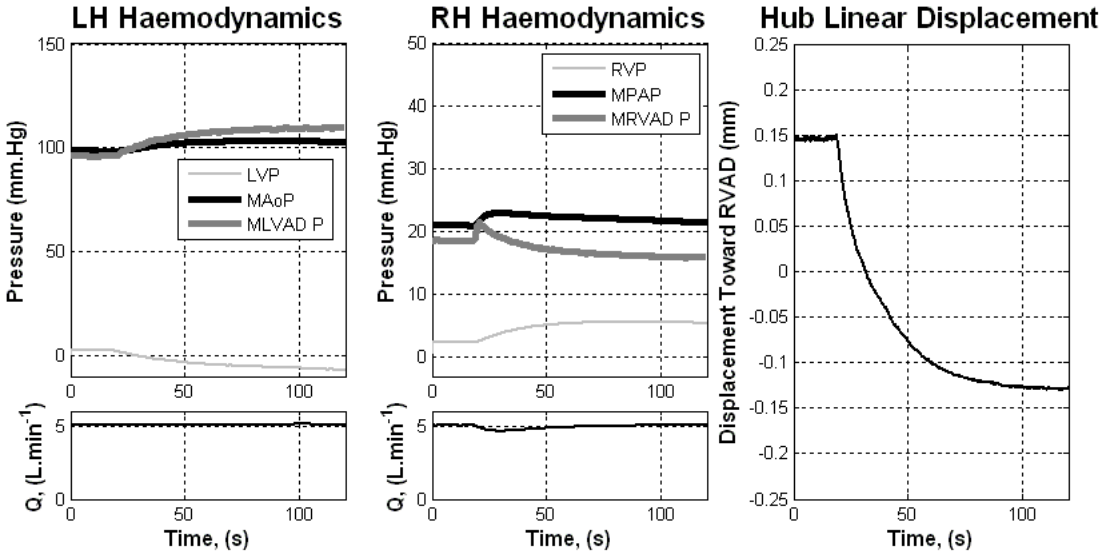

Figure 4-13: Simulation of BiVAD prototype response to sudden Pulmonary Hypertension.

Discussion

The sudden increase in pulmonary resistance caused a sharp increase in Pulmonary Artery pressure and consequently a lower flow. The consequential translation of the floating assembly away from the RVAD impeller causes a sudden drop in RVAD pressure head. Consequently, the Pulmonary Artery pressure is maintained near 20 mmHg decreasing the adverse effects of pulmonary hypertension. The result shows that the passive controller acts to alleviate hypertensive circuit pressures regardless of the affected circuit.

The prototype was able to passively reduce hypertensive circuit pressures through translation of the floating assembly. The effect of the passive response was quantified where the controller was able to halve the pressure increase of a hypertensive systemic circuit providing a baroreceptor-like effect. The results are encouraging although left ventricular suckdown was occasionally observed during Pulmonary Hypertension simulations and the consequential drop in pulmonary venous return.

4.4.3.3 **Acute Myocardial Infarction**

Method

An infarction was simulated by a sudden decrease in left ventricular contractility. This was actuated by increasing resistance to the compressed air inflow tube. The result is a degradation of the left heart contractility and therefore arterial pressure.

Results

A further failing left ventricle simulation is shown in Figure 4-14. The results are from a simulation that began with BiVS of a patient with BiVF. At time t = 7s the diseased left ventricle suffers further degeneration, (e.g. infarction), and so the LV output drops. Green boxes show the time scale for the bottom set of plots allowing a closer inspection of the acute infarction response.

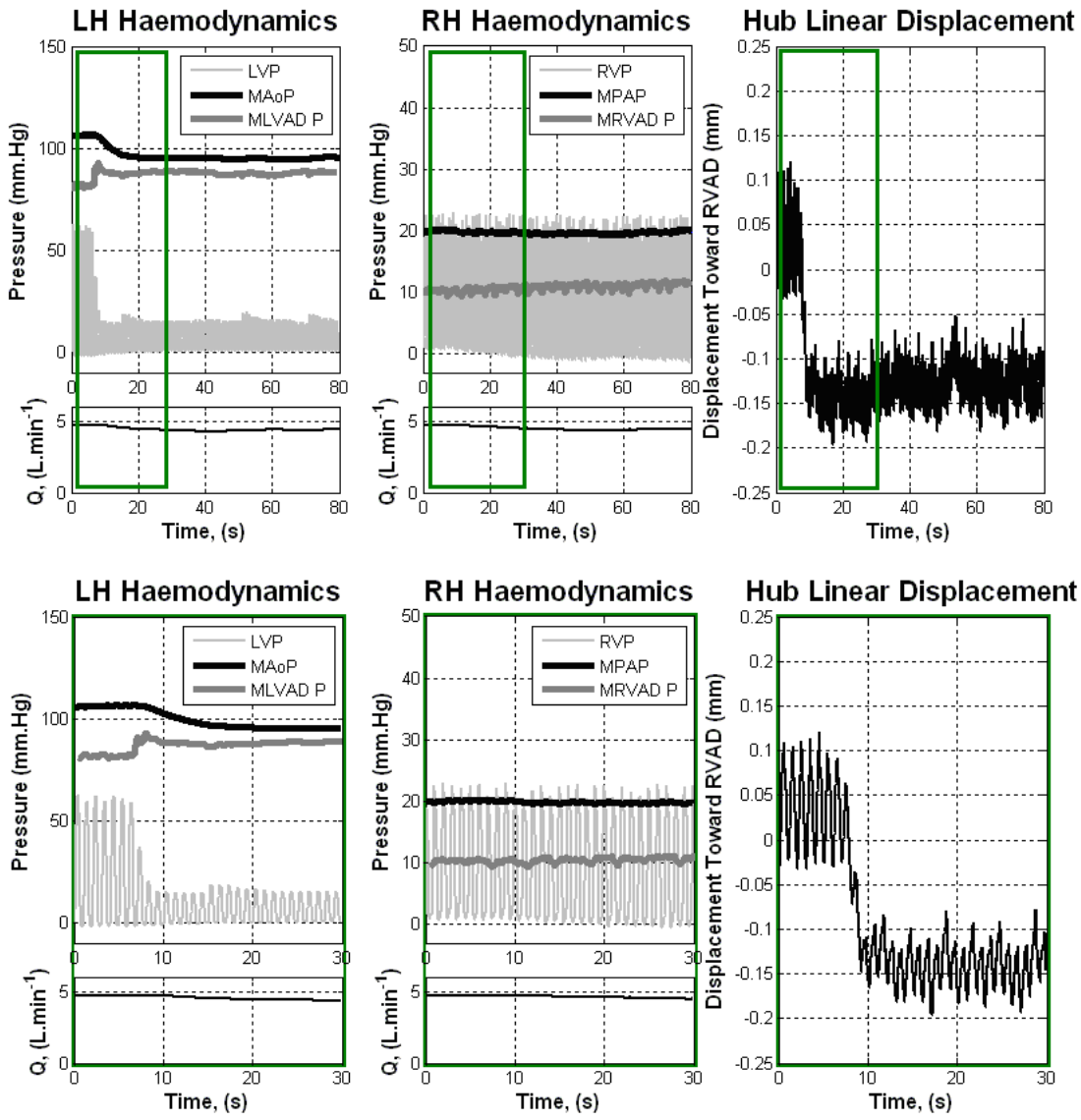

Figure 4-14: Simulation of BiVAD prototype response to sudden further left heart failure, (top), over a shorter time scale for clarity (bottom).

The drop in LV systolic pressure caused the hub to translate toward the LVAD thus increasing its pressure head. Consequently, the LVAD pressure head goes up in an attempt to maintain aortic pressures.

The drop in systemic flow can also be observed and a subsequent drop in pulmonic flow. At the same time a very slight increase in RVAD pressure head is observed.

Discussion

The passive adjustment allowed the LVAD output to increase which in turn decreased the impact on the Aortic pressure. With the Aortic pressure not dropping below 90mmHg, the simulated patient will be ensured adequate perfusion of end organs.

LVAD flow drops slightly decreasing venous return back to the RA, (note the decreasing diastolic RV pressure), and causing slight pulmonary congestion, (note the increasing diastolic LV pressure).

It is also apparent that there is a very slight increase in RVAD pressure head despite the fact that the hub moves towards the LVAD impeller. A review of Figure 4-7 will show that the pressure and flow at a hub position oscillating around y = +0.05mm, (c_{RVAD} = 0.17 – 0.05 = 0.12 mm), has seen the majority of its decay. Further clearance then has little effect on the RVAD pressure and flow. So, the slight increase in RAVD pressure head is likely to be simply a response to the slight decrease in flow along with congestion of blood in the pulmonary circuit.

Hub oscillations existed with amplitude of approximately 0.052 mm. These are small oscillations made so by viscous damping of the hub motion.

4.4.3.4 **Physical Movement**

Method

This test simulated a supported patient with sudden systemic venous congestion. This is a similar haemodynamic response to a patient standing then going into a lying position quickly. This was simulated experimentally by adding fluid, (approximately 600 ml), into the right atrium. The congested systemic venous vessels then cause an increased diastolic filling pressure into the ventricles.

Results

Figure 4-15 indicates an increased RVP caused by pooling of blood in the systemic venous system. This induced a translation of the hub away from the RVAD impeller

dropping the RVAD pressure head. Removal of this fluid dropped the RVP back and the hub position was restored. The times when the fluid addition and removal were carried out are indicated with an asterisk, and a dashed vertical line.

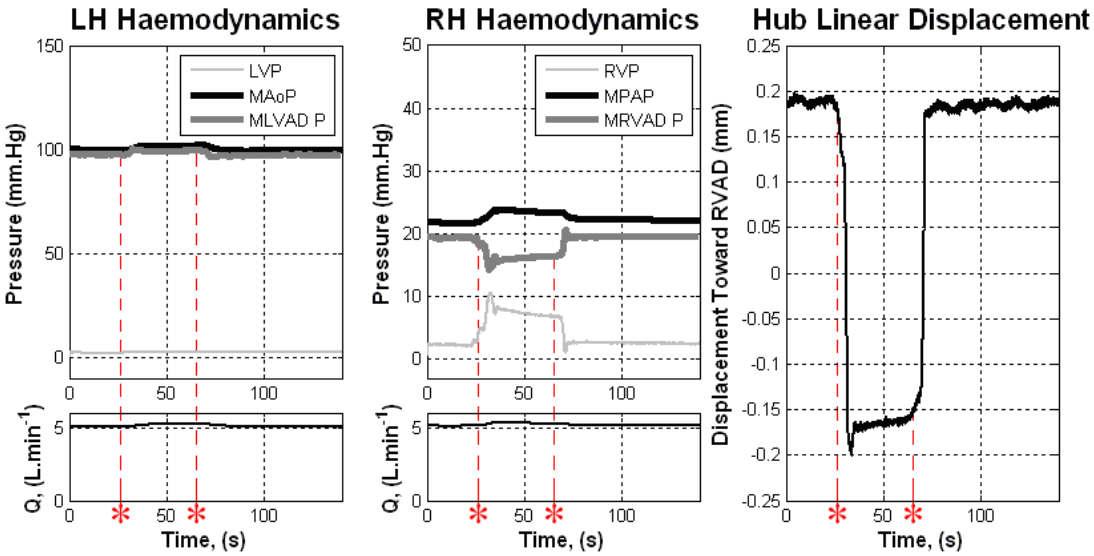

Figure 4-15: Simulation of BiVAD prototype response to patient suddenly lying down, and then suddenly standing up.

The PAP was maintained throughout the simulation between 20 and 25 mmHg by an accommodating RVAD pressure head.

Discussion

Simulated physical movements of a patient such as that shown in Figure 4-15 is more generally an indication of the device's ability to balance arterial pressures. The patient lying down at T = 25s caused a ventricular pressure disturbance due to systemic venous pooling. But it also simulated a situation where the circuits are suddenly poorly balanced. The hub's translation away from the RVAD decreased the developed pressure head which, when added to the raised ventricular pressure maintained the PAP below 25 mmHg.

A change in flow rate after each sudden movement was also observed. When considering the first sudden movement the flow increase is first seen in the pulmonary circuit and then later the systemic circuit. Regardless of the hub translation

decreasing RVAD ouput, the elevated PAP increased the pressure gradient across the pulmonary circuit driving more flow.

Similarly, when the patient suddenly stood back up, the RVP dropped caused by a decrease in systemic venous blood volume. Consequently, the hub moved back toward the RVAD impeller, increasing the pump output and regulating the PAP.

This overall response is similar to a baroreceptor response upon the heart muscle. Initially, the controller simulates the parasympathetic stimulation that would be provided to the RH to reduce the PAP. Then, once the fluid is removed, simulating a sympathetic nervous response to increase the PAP.

4.5 Testing of Passive Controller Dynamics with Discussion

As the vascular system incorporates dynamic resistance, compliance and inertiance, the controller's passive response too is optimised by a mechanical spring mass damper configuration. Quantifying these mechanical parameters was a difficult exercise but necessary to further optimise the passive system. Furthermore, quantifying, or at least characterising, these mechanical parameters may be useful for other devices with alternative control strategies. It is feasible that an actively controlled system could actively adjust blade clearance as a means of control, and in fact will be the case for the BiVACOR device (Timms et al. 2008). In such cases, proportional, derivative and integral control of the blade clearance response will need to be incorporated into the active control system.

The dynamic floating assembly is subject to two sources of vascular pressure fluctuation. The first are the acute cardiovascular events already discussed. It is important that the device responds passively to these fluctuations and so the Passive Controller will need to be sensitive to this source. The second source is the pressure fluctuations induced by residual ventricular function. Every cardiac cycle observes the pressure ratio between the ventricles fluctuating from up to 5:1 during systole to approximately 1:1 in diastole. It is not desirable to have the floating assembly of the Passive Controller forced up against the RVAD PC stop every cycle due to this fluctuating pressure ratio. This further advocated the mechanical spring, mass,

damper configuration to filter out the high frequency pressure signals from residual ventricular function. Figure 4-16 shows a Free Body Diagram, FBD, of the floating assembly due to a deflection y.

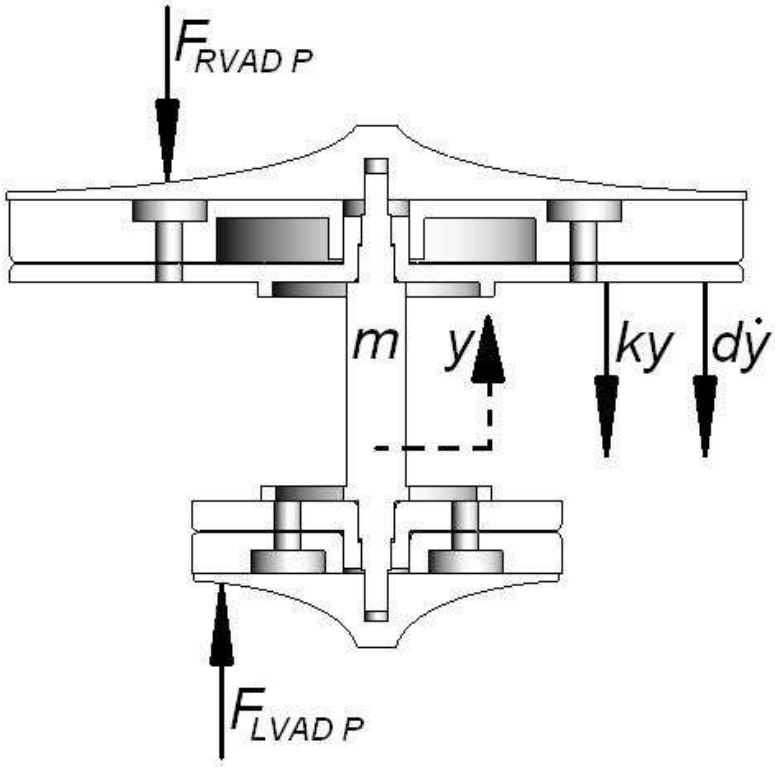

Figure 4-16: Free Body Diagram of the floating assembly during operation due to a deflection *y*.

In the figure, $F_{LVAD\ P}$ and $F_{RVAD\ P}$ are the pressure forces upon the LVAD and RVAD lower shrouds respectively. The spring, mass and damping coefficients, *m*, *k* and *d*, respectively, are also included along with the single degree of freedom *y*.

Note the difference between the hub position, *y*, and the impeller blade clearance discussed earlier, *c*. The clearance, *c*, is the absolute clearance between the shroud and the impeller blades of any given rotary pump. The distance y is the hub, or floating assembly, position with respect to its central position. The physiological testing discussed employed an overall hub translational range of 0.34 mm, or $y = \pm 0.17$ mm.

An analysis of the prototype's ratio of hub translation to resultant pulsing force was carried out over a range of pulse frequencies. This analysis gave natural frequency, f_n,

as well as Amplitude Ratio, *AR*, data to examine the performance of the spring and damper to optimise the floating assembly's motion.

The prototype was subjected to a range of pulse frequencies indicating resonant frequencies of the passive system. The frequency of the ventricular contractions were varied and applied through the left ventricle only. This magnified the pressure fluctuations for high observability. These data could then be normalised providing Amplitude Ratios and allowed comparisons independent of the magnitude of the pulse pressures.

The dynamic system of the floating assembly can be simply modelled as a single mass with a single degree of freedom, *y*. This system has dynamic components and parameters; the mass, *m*, damper, *d*, and spring, $k_{effective}$ as shown in Figure 4-17. The spring constant has been referred to as $k_{effective}$ as later it will be shown that there are a number of components that attribute to the spring constant.

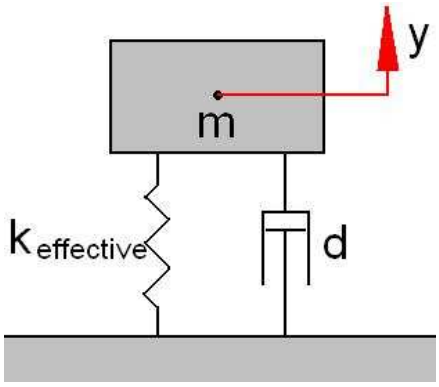

Figure 4-17: Spring, mass, damper configuration of the passive controller floating assembly.

The natural frequency, f_n, of the system is,

$$f_n = \frac{1}{2\pi}\sqrt{\frac{k_{effective}}{m}}\,.$$

Equation 4-1

In this study the natural frequencies will be determined experimentally, however, it is important to note that the natural frequency is a function of the spring constant, $k_{effective}$.

Evaluating the *AR* of a forced oscillation is useful when comparing forced oscillation with varying frequency or damping. The *AR* provides a normalised ratio of the magnitude of the hub oscillation to the magnitude of the applied oscillatory force. It is evaluated using

$$AR = \frac{C}{\left(\frac{F_1}{k_{effective}} \right)},$$

Equation 4-2

where C is the amplitude of floating assembly oscillation and F_1 is the amplitude of oscillatory force. As shown in Equation 4-2, normalisation required the controller spring constant. The non-dimensional *AR* allows comparison between tests independent of oscillation and force amplitude as well as spring constant.

As will be discussed, the spring constant of the passive controller was a difficult parameter to quantify due to the proportional response resulting from three parallel 'springs'. This will be referred to as the Effective or Compound Spring. Furthermore, some of these compound spring components displayed a non-linear elastic relationship with hub deflection, *y*. For this reason, care was taken to maintain constant compound spring parameters during dynamic tests to allow comparison of *AR* data at differing levels of damping.

That said, the primary objective of the dynamic study was to assess the performance of the viscous damper in filtering out ventricular contraction signals. An investigation of the compound spring constant was carried out to ensure comparative ARs were evaluated.

4.5.1 The Mechanical Spring Constant, *k*

Initial testing of the prototype suggested that there was no need to use cumbersome helical steel springs to provide flexible coupling of the floating assembly to the Controller Body. Instead the air bubble spring, described in the previous chapter, was easy to implement and appeared to provide a wide range of spring rates, *k*. The air

bubble spring was also useful in that the position of the hub during stable support could be shifted by adding or removing air during operation.

Further investigation in to the spring response of the passive controller revealed that the air bubble was not solely responsible for the proportional response to hub translation. In fact, there are three identified spring-like contributions. These are the air bubble spring force, F_{air}, the clearance dependent VAD performance, $F_{\Delta y}$ and the spring loaded LVDT force, F_{LVDT}. The three components of this compound spring were analysed allowing an effective spring constant, $k_{effective}$, to be quantified.

The springs act in parallel to form a compound spring affecting the controller's response. As a comparison to Figure 4-16, a FBD of the floating assembly now with the parallel fractional forces is shown in Figure 4-18.

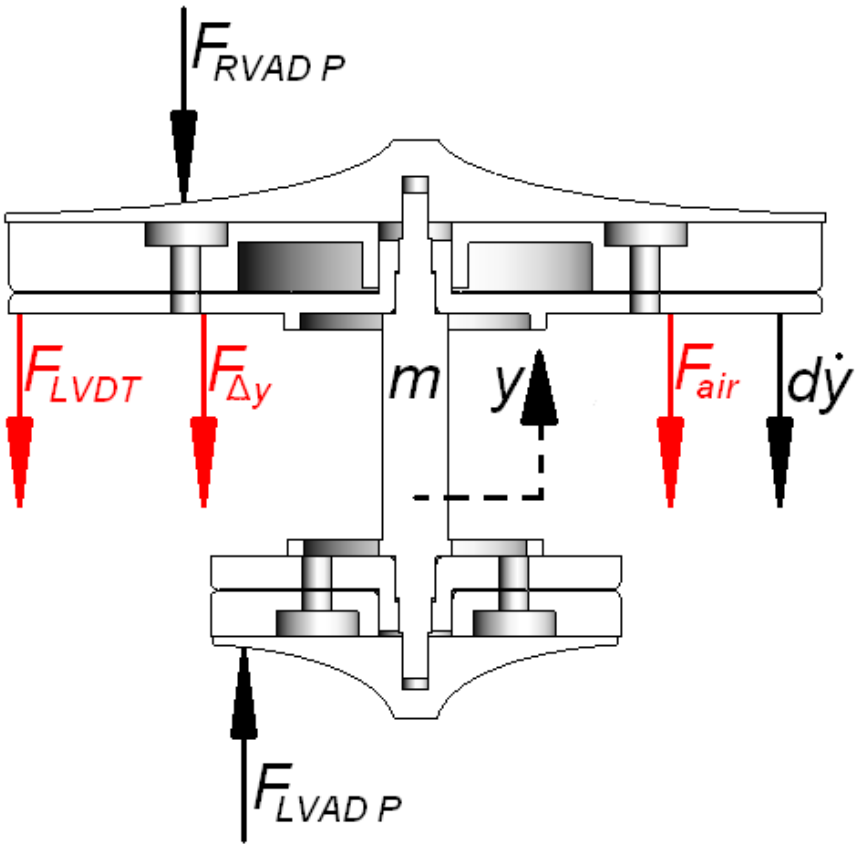

Figure 4-18: Sectioned side elevation of the floating assembly with the proportional forces shown in red.

The clearance dependant performance spring, or 'clearance spring', is in fact a product of the passive controller action itself. For example, translation toward the RVAD will increase the RVAD pressure and decrease the LVAD pressure which acts to restore the hub position. Therefore, since the clearance spring takes into account the pressure response from the pumps, $F_{LVAD\ P}$ and $F_{RVAD\ P}$ can be assumed to be constant as the force applied by either pump at y = 0mm.

The dynamic proportional response to the hub translation therefore can be modelled as three springs in parallel. Parallel springs respond like a single spring whose spring constant is the sum of the parallel spring constants, $k_{effective}$, where,

$$k_{effective} = k_{air} + k_{\Delta y} + k_{LVDT} .$$

Equation 4-3

Similarly, forces in parallel acting on a rigid body can be simply added together to provide a combined, or 'effective' force, $F_{effective}$, where,

$$F_{effective} = F_{air} + F_{\Delta y} + F_{LVDT} .$$

Equation 4-4

Figure 4-19 shows a sketch of what the force vs. hub displacement plot could look like when subjected to a ramp function of amplitude F_1, (without mass or damping). The purpose of this figure is to indicate the fraction work done against each of the spring components. Assuming linear spring stiffnesses, the effective spring stiffness ($k_{effective}$) could be found either by measurement of the compound response, or by adding individual spring responses according to Equation 4-3.

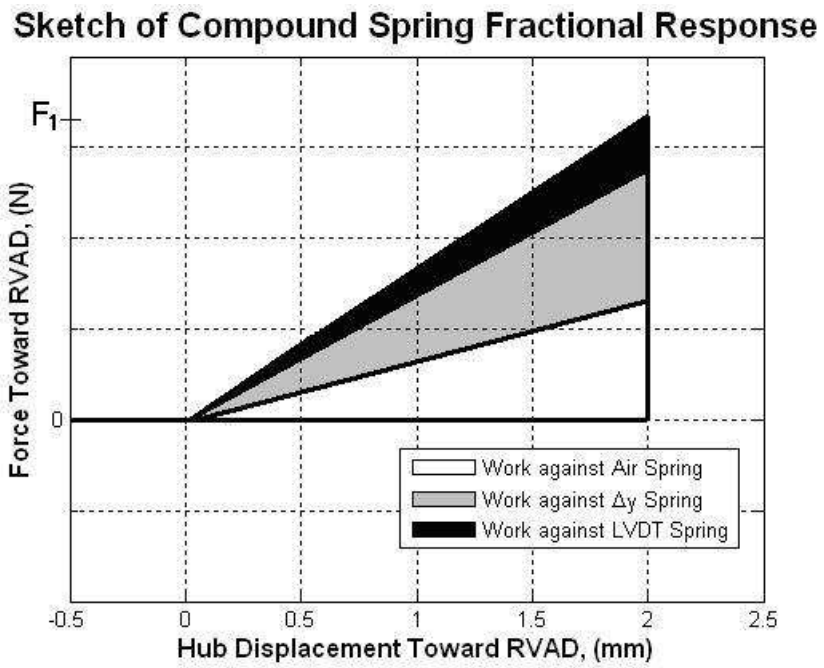

Figure 4-19: Example sketch of the theoretical force vs. hub displacement relationship of the compounding spring.

Because the figure is an example sketch of the relationship between the effective spring responses, the vertical force axis is unquantified. Please note that the relative spring strengths are not representative – the figure is for concept illustration only.

To provide reasonable approximation of the *AR* the spring constant of the compound spring, $k_{effective}$, needed to be evaluated. It was difficult to physically measure $k_{effective}$ so theoretical and experimental analysis was used to quantify the individual spring components. Calculation by these means, as will be shown, provided satisfactory approximations of the components of the compound spring.

4.5.1.1 The Air Spring, k_{air}

The spring response from the air bubble inside the Passive Controller Body was approximated theoretically. It was assumed that the expansion or compression of the air bubble was isothermal and that the air would act like a perfect gas. The Perfect Gas Law was used to relate the pressure to the varying volume;

$$p_{PC} = \frac{mR_G U}{V},$$

Equation 4-5

where p_{PC} is the static pressure in the Passive Controller, m is the mass of the air bubble, R_G is the gas constant for air 287 J.kg^{-1}.K^{-1}, U is the air bubble temperature and V is the air bubble volume.

Provided the initial bubble volume is known, the bubble volume can be found at any hub position. Figure 4-20 shows a simplified schematic of the Passive Controller Body. The division between the two cavities have been left out for clarity. The top image shows the labelled components including the membranes which prevent fluid movement between the VADs and the Passive Controller.

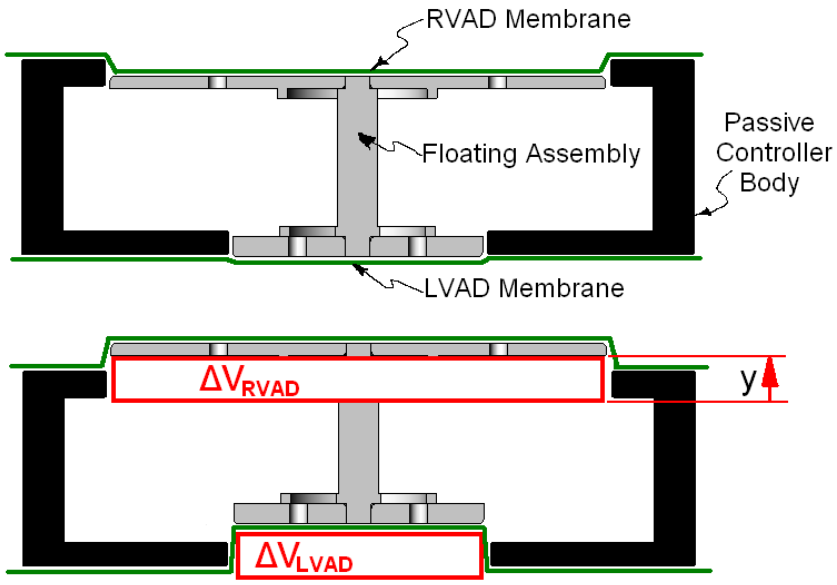

Figure 4-20: Passive Controller schematic showing the initial hub position, (above), and the resulting volume changes due to a hub deflection (below).

When the hub translates distance y, the volume increase on the RVAD side, ΔV_{RVAD}, and the volume decrease on the LVAD side, ΔV_{LVAD}, contribute to a total volume change. This volume change is accounted for by the air bubble's expansion. Thus, the volume of the air bubble, V, is a function of the initial air volume, V_i, the VAD shroud areas, A, and the hub position, y.

With this in mind and a small amount of derivation, the relationship

$$F_{air} = \left[\frac{mR_G U}{V_i + y\left(A_{RVAD} - A_{LVAD}\right)} - p_{atm} \right] \times \left(A_{RVAD} - A_{LVAD}\right)$$

Equation 4-6

was obtained to relate the pressure force inside the controller cavities F_{air} to the hub position y. Also included in this relationship is the initial injected volume of air at atm. pressure V_i, the area under the LVAD and RVAD lower shrouds A_{LVAD} and A_{LVAD} respectively. Atmospheric pressure, p_{atm}, is subtracted from the right hand side of Equation 4-5 as gauge pressures were measured in the experimental loop.

Figure 4-21 shows the theoretical relationships between an applied force to the hub and the resulting translation of the hub with a range of initial injected air volumes. These are derived from the static air pressure and the air density respectively. Equation 4-5 shows that the pressure is inversely related to the air volume, and therefore the applied force is inversely related to the hub movement. This produces the characteristic decaying function as shown in the top plot in the figure.

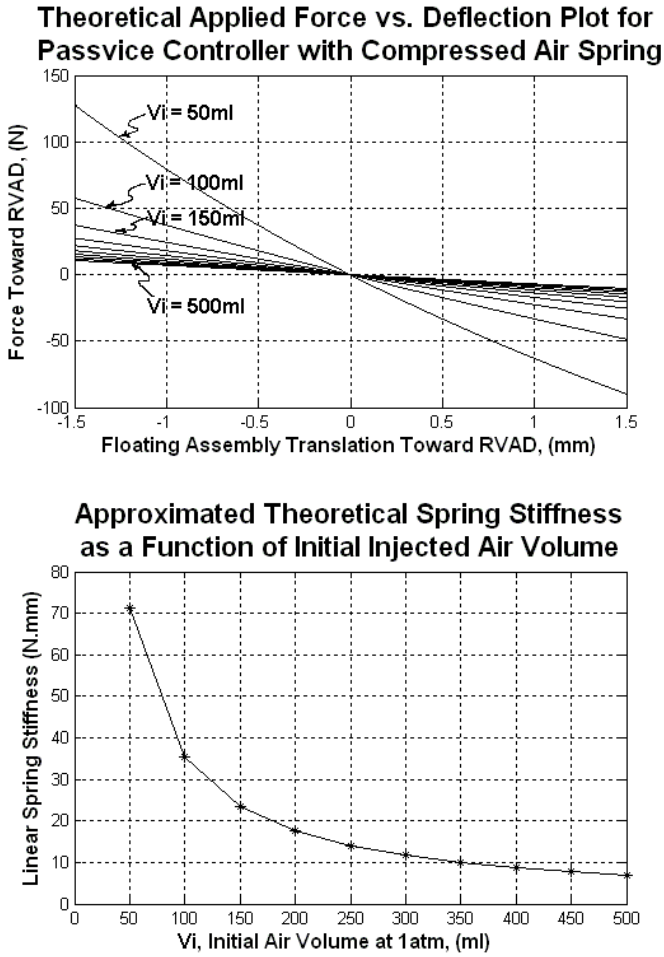

Figure 4-21: Theoretical proportional response, (spring response), due to air bubble of varying initial volumes, V_i, (top), approximated linear spring stiffness as a function of initial injected air volume, V_i, (bottom).

The gradient of the theoretical force vs. deflection plots are, by definition, the theoretical spring constants, k_{air}. For simplicity, the gradient was assumed to be linear over the operating hub range. So, the gradient evaluated at y = -1 to 1 mm. The initial volume dependent gradients, or air spring stiffnesses k_{air}, were then plotted in the bottom plot in Figure 4-21. As would be expected, the air spring constant, k_{air}, is high when the initial air volume is small. Similarly, if there was an infinite initial fluid volume, (i.e. one side of the Controller Body open to air), then the spring constant will be effectively zero.

A curve was fitted to the lower plot in Figure 4-21 using a Hyperbolic, or inverse power, function using Excel. The evaluated power function is

$$k_{air} = \frac{3648}{Vi^{1.0066}},$$

Equation 4-7

the fit having an R^2 value of 1. Later results will be presented with initial air spring volume approximated at Vi = 300 ml. These correspond to theoretical air spring constants of k_{air} = 11.7 N.mm^{-1}.

4.5.1.2 The LVDT Spring, k_{LVDT}

Information provided by the manufacturer prescribed the spring constant of the LVDT sensor tip to be k_{LVDT} = 100 μN.mm^{-1}. This spring force is comparatively small enough to be ignored over the entire operating range of the LVDT.

4.5.1.3 The Clearance Dependent VAD Performance Spring, $k_{\Delta y}$

The resulting performance variations due to clearance changes from the central position act to restore the un-deflected hub position. This spring like response is the essence of the Passive Controller action as the applied force that acts to restore the hub position is due to the change in pressure head from either pump. Experimental data were used to quantify this spring like response.

Method

Results from a number of hypertension simulations were used as data sets to analyse this spring like response. These were used as the pressure and deflection profiles and were reasonably constant before and after the sudden resistance change. The resultant force and the hub position before and after the hypertension simulation were taken and the spring force was evaluated from these data according to

$$k_{\Delta y} = \frac{F - F_i}{y - y_i},$$

Equation 4-8

where F_i is the initial Resultant force across floating assembly and y_i is initial floating assembly position. This was then approximated as the clearance spring rate at the mean clearance covered during the translation. The mean clearance was considered representative since the spring rate was not constant with respect to clearance. For this reason it would have been inappropriate to use the beginning or ending clearances.

It should be noted that the tests were run at pump speeds of N_{LVAD} = 3870 RPM and N_{RVAD} = 920 RPM, (the total support testing speeds). It is reasonable to assume that $k_{\Delta y}$ will change if the pressure ratio between the VADs varies due to speed changes. However, the majority of tests presented incorporated LVAD to RVAD pressure ratios of just under 5:1. This spring constant will, therefore, be treated as a constant.

The simulations used all had a weak air spring with $Vi \approx$ 300ml corresponding to an air spring constant of $k_{air} \approx 11.7$ N.mm^{-1}. As already discussed, the nature of the parallel springs allows them to be added or subtracted to isolate individual spring components. A translational range of $y = \pm 0.17$ mm was used as this was the range used for the dynamic tests to be discussed later.

Evaluation of the spring response due to the clearance of the hub rendered a range of spring rates. This indicated that the response of the clearance spring was not constant. This was discussed by Timms *et al.*, when it was suggested that most of the performance drop occurred between 0 and 0.3mm from the blade tips, (Timms *et al.* 2006).

The spring rate was then evaluated at a number of different hub positions. To do this, the starting position of the hub was prescribed by adjusting the arterial pressures before the sudden hypertension. As would be expected, $k_{\Delta y}$ was very high near the physical stoppers. Experimentally, when the hub hits a physical stopper on either side, (at $y = \pm 0.17$ mm), any further increase in force toward that stopper will result a nil change in position. This means that at either stopper the stiffness is effectively infinite.

Results

Figure 4-22 presents results from seven acute pulmonary hypertension tests. The hub position has been assigned to the y-axis for consistency with the physiological testing results presented earlier with the positive direction towards the RVAD impeller. The x-axis indicates the spring rate, $k_{\Delta y}$, and it is clear from first glance that $k_{\Delta y}$ is not constant.

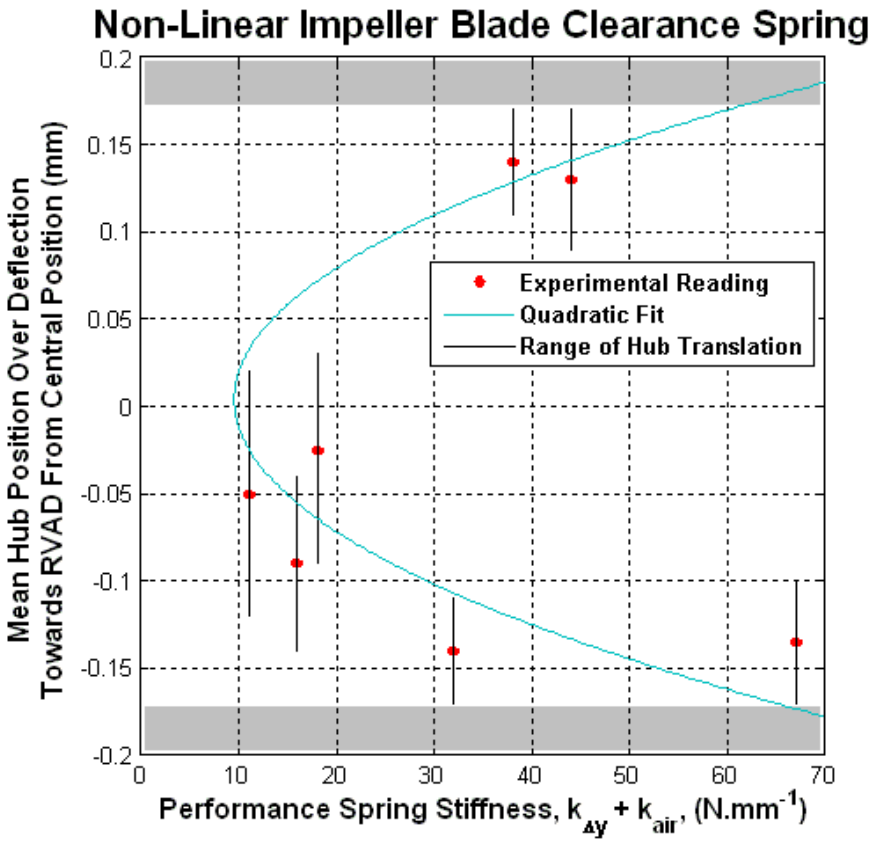

Figure 4-22: Calculated spring stiffness, $k_{\Delta y} + k_{air}$, (where $k_{air} \approx 12$ N.mm^{-1}), vs. hub position during entire translation.

The grey shaded region indicates the physical PC stoppers described in the previous chapter. Since the translational range is $y = \pm 0.17$ mm the hub cannot enter this region.

The black profiles show the translation of the hub during the test. Since all the tests were acute Pulmonary Hypertension, the hub started at the upper most extremity of the black lines and then translated down to the bottom as a response to the increased PAP, (see Figure 4-13). The red dot indicates the average position during the hub

translation. The red dots, therefore, reside half way down the black profiles. The blue profile is a quadratic fit of the data calculated using MATLAB. It was evaluated as,

$$k_{\Delta y} + k_{air} = 1832.7y^2 - 14.3y + 9.5 .$$

Equation 4-9

The fit was quite poor with a normalised residual, *NR*, of *NR* = 30.7, the normalised residual was calculated as the square root of the sum of the clearance spring rates, $k_{\Delta y}$, squared

$$NR \equiv \sqrt{\sum_{i=1}^{n} \left(k_{\Delta y} + k_{air}\right)_i^2} .$$

Equation 4-10

Discussion

Observe that there is a minimum spring rate near the central position. According to experiemtnal result from Equation 4-9 the spring rate at this minimum is $k_{\Delta y} + k_{air(\text{Vi = 300 ml})} = 9.5$ N.mm^{-1}. When taking into account the fact that a weak air spring was also incorporated with a linear spring rate of $k_{air} \approx 12$ N.mm^{-1}, the data suggests that at the central position the clearance spring rate is approximately nil. As the hub moves toward either PC stopper the spring rate, $k_{\Delta y}$, increases until, theoretically, it will be infinite.

It was realised that the poorly fitting polynomial was partially due to the relationship not being quadratic. The relationship cannot truly be quadratic because of the asymptotic clearance spring rate near the PC stoppers where the limit of a quadratic can never be asymptotic. This, in addition to data being taken from tests from numerous different testing days, attributed to a high normalised residual. However, the data indicate that there is most definitely a minimum spring response near the central position along with an increasing spring rate toward the PC stoppers. A modified relationship for the clearance spring alone was generated subtracting the constant air spring. Since the initial volume of the air spring, $V_i \approx 300$ ml, was approximate k_{air} was assumed to be 9.5 N.mm^{-1}. This relationship, as given in

Equation 4-11, will be used to quantify the *AR* provided that the deflections are between y = -0.15 and 0.15 mm;

$$k_{\Delta y} = 1832.7y^2 - 14.3y\,.$$

Equation 4-11

The clearance spring function itself is only indicative of the inherent proportional response caused by clearance changes. It need not be directly employed in the numerical model, which will be explained later, as this inherent response is a result of the effect of clearance changes in both VAD's pressure head. However, it does indicate the magnitude of this proportional response.

4.5.2 Evaluation of the Mechanical Damping, d

The viscous damper created by a tear drop slot and the micrometer spindle configuration was primarily used to filter out the residual heart beat pressure fluctuations. More generally, the damper affected the floating assembly's motion to allow manipulation of the dynamic interaction between the CV system and the prototype. Varying the damping coefficient was achieved by adjusting the occluding micrometer's spindle length. This occluded flow between the Passive Controller cavities and provided a viscous damper.

Quantifying the damping constant, d, was out of the scope of this project. To quantify this parameter a new test rig would need to be built to allow acquisition of empirical viscous loss data. So, for the purpose of this study, the functionality of the damper was tested with the spindle fully retracted and extended over half way. These were labelled medium and high damping respectively. (Low damping could not be achieved as even with the spindle fully retracted, flow between the Passive Controller Cavities was still restricted). This was considered reasonable as the evaluation of the damper aims solely to determine whether or not cardiac pulses can be filtered out.

This study employed the determined spring constants to process oscillatory test data to determine the Amplitude Ratio, *AR*. Resonant frequencies, $f_{n,}$ of the floating assembly were also observed as was the performance of the viscous damping.

4.5.2.1 **Method**

With the VADs operating, the prototype was cannulated into the MCL and subjected to a pulsing left ventricle. This, in combination with a non-active right ventricle, magnified the resultant force across the floating assembly for high observablity. The frequencies were varied from 15 BMP to 90 BPM, (0.25 to 1.5 Hz), at intervals of 15 BMP to determine if the operating range was near the resonant frequency, f_n. The level of damping was then varied to observe the performance of the viscous damper as it attempted to reduce oscillation amplitude.

A Fourier Transform of the hub's transient position data isolated the frequency and amplitude of the major oscillation. The same procedure using the transient force data provided the force amplitudes at the same major oscillation frequencies. This agreement in major oscillation frequencies was not surprising as the pulse drives the hub and therefore dictates the oscillation frequency.

The dynamic tests were run without an air spring leaving only the clearance spring and the negligible LVDT spring. Thus, the spring rate, $k_{effective}$ (= $k_{\Delta y}$), was a function of clearance as given in Equation 4-11. The *AR* was calculated at the major oscillation frequency, (which is analogous to the pulse frequency). Calculation of the *AR* used the amplitude of the force (F_1) and position (C) as well as the spring rate ($k_{effective}$) at the average position according to Equation 4-2.

Two different levels of damping were used; medium and high. These were applied by having the spindle fully retracted and extended over half way. The *AR*s of all the tested frequencies were compared at the two levels of damping to quantify the performance of the damper.

4.5.2.2 **Results**

One of the dynamic oscillatory tests is shown in Figure 4-23 as an example of the collected oscillatory test data at a constant pulse frequency. This particular test was operating at 30 BMP, (0.5 Hz), with medium level damping. The transient force

profile at the top of the figure indicates the systolic and diastolic phases while the bottom shows the oscillating hub position.

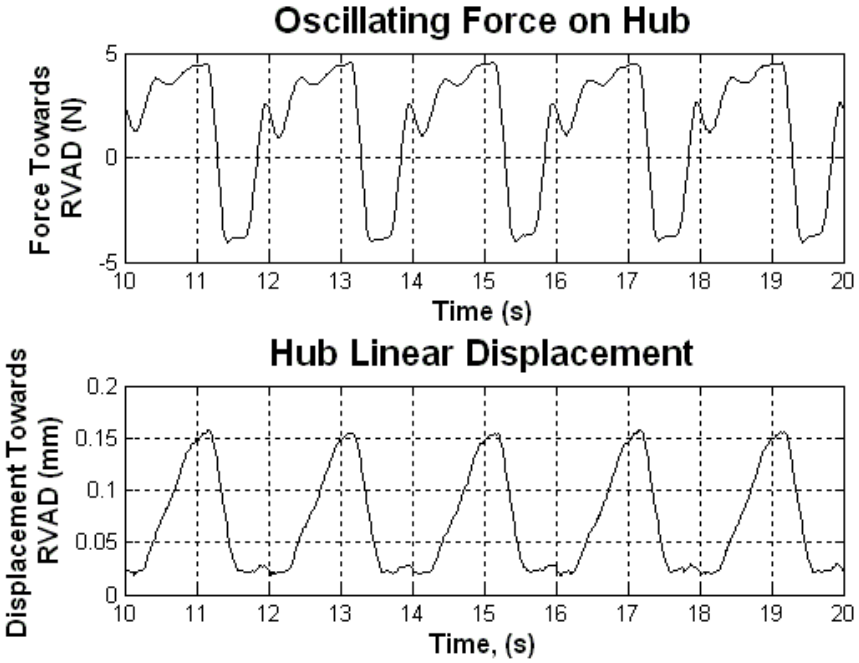

Figure 4-23: Example dynamic test using LV contractions only at 30 BMP.

Note that the oscillating hub position is centred on $y \approx 0.07$ mm. This mean position value was important to interpolate the effective spring constant using Equation 4-11. Figure 4-24 indicates the interpolated effective spring constant based on the mean oscillatory clearance. The background plot incorporates the same scale as that shown in Figure 4-22, the foreground plot has reduced scales for clarity.

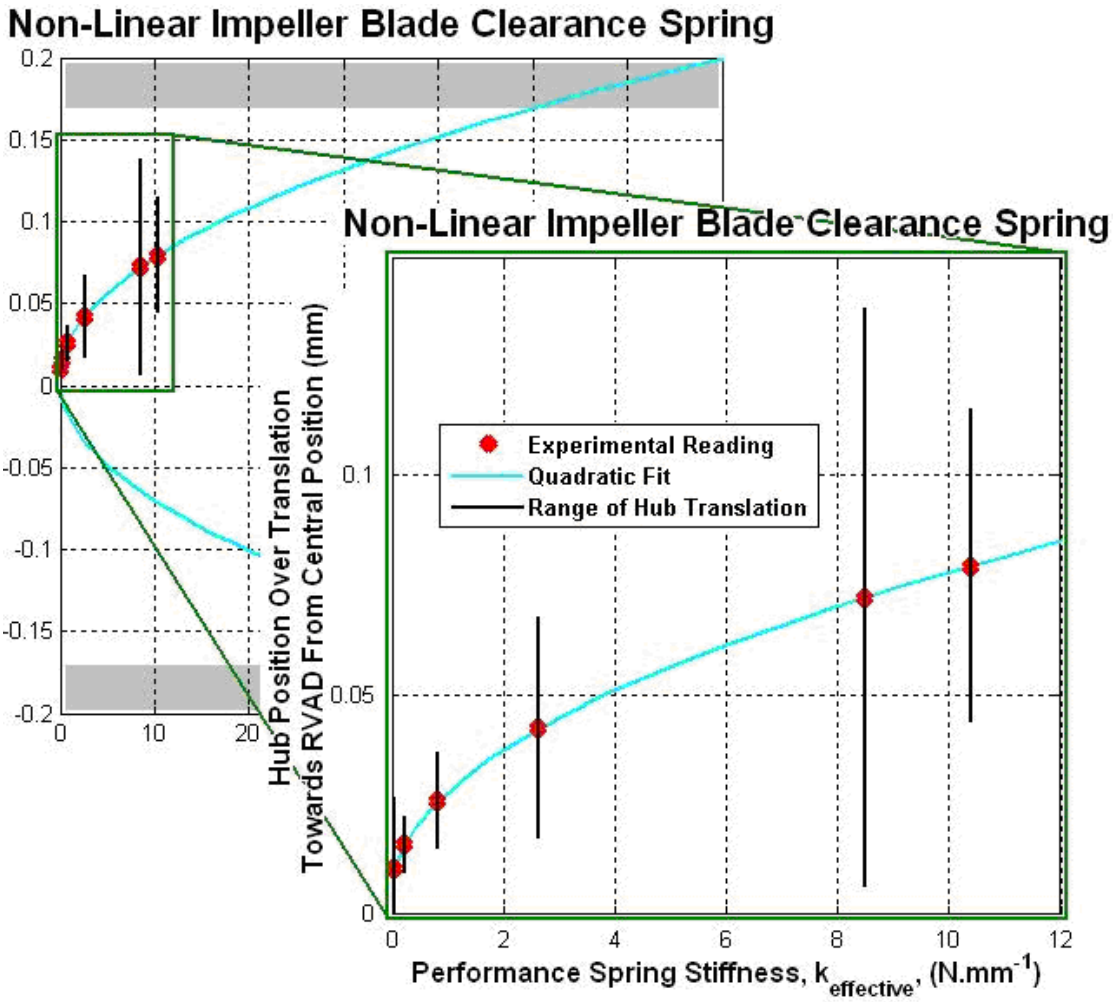

Figure 4-24: Effective spring constant, $k_{effective}$, interpolation based on mean clearance during oscillatory test for a medium level of damping.

The plot at the top of both Figure 4-25 and Figure 4-26 show amplitude and frequency data for each simulated heart rate from a Fourier transform of the oscillatory hub position data. The bottom plots show the amplitude ratio for each of the tests at their respective pulse frequencies. The resonant frequency is that with the largest *AR*. The two figures show the amplitude and *AR* data for low and high damping respectively. Resonance occurs close to 30 BPM, (0.5 Hz), for both tests.

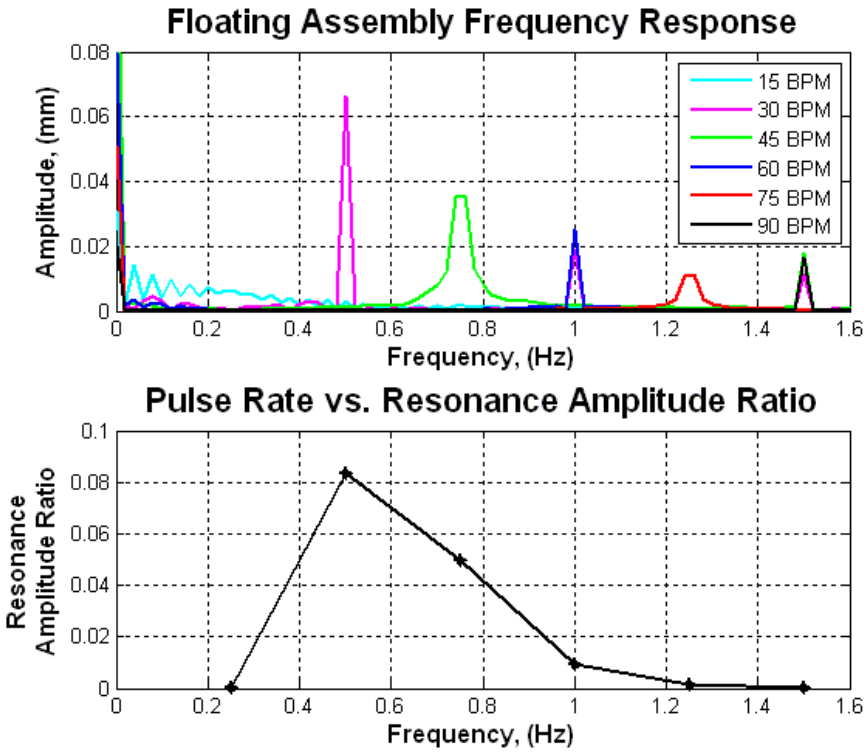

Figure 4-25: Frequency breakdown of hub oscillation with low damping for a range of heart rates, (above), Amplitude ratio of resonance oscillation, (below).

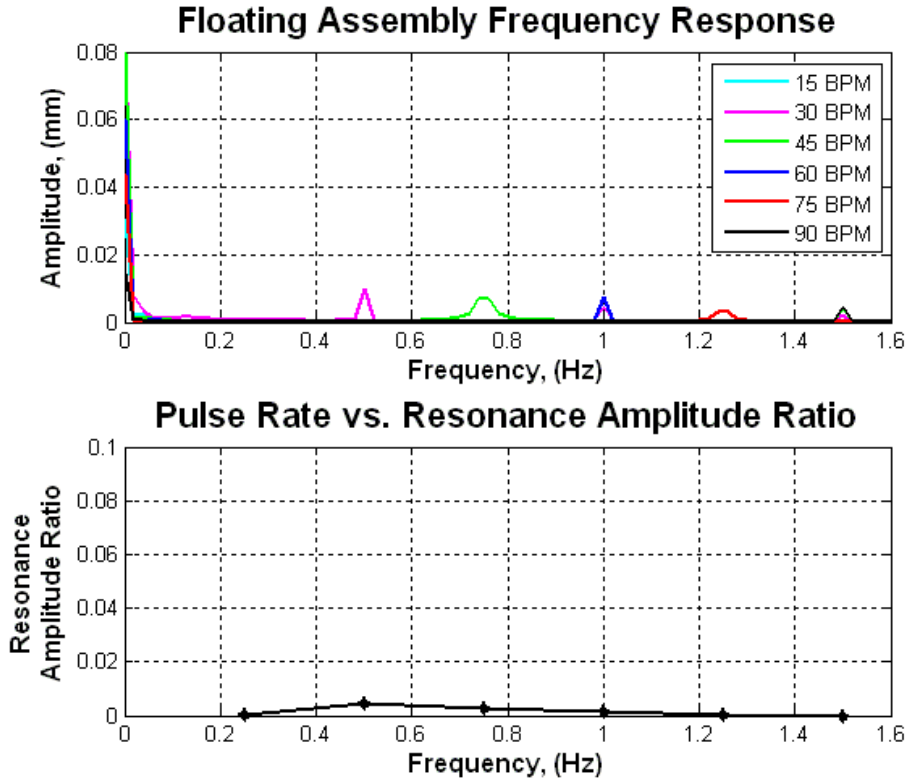

Figure 4-26: Frequency breakdown of hub oscillation with high damping for a range of heart rates, (above), Amplitude ratio of resonance oscillation, (below).

4.5.2.3 **Discussion**

The resultant force plot in Figure 4-23 consists of a very jagged pulse. Systole is indicated by the transient force profile rising up around 1N toward the RVAD. At that time, a retarded hub translation toward the RVAD impeller was observed due to the viscous damper. The oscillations at the beginning of systole are due to the mechanical mitral valve hammering in the valve housing.

Regardless of the irregular 30BPM pulse in Figure 4-23, the floating assembly oscillations are smooth and have high amplitudes. In fact the Peak to Peak Translation, (PPT), is over 40% of the total clearance between the PC stoppers. With such oscillations there is a danger that the flow field inside the VADs cannot develop potentially reducing device efficiency and increasing blood damage.

Figure 4-24 indicated high interpolated variance in spring constants between the medium level damping tests. This was expected because the quadratic function in Equation 4-11 sees a rise in spring constant of 50 $N.mm^{-1}$ between $y = 0$ and $y = 0.17$ mm. If the spring response of the floating assembly is to be properly analysed, further testing should be carried out and a more suitable interpolating function should be determined.

A comparison of Figure 4-25 and Figure 4-26 shows that the viscous damper was very successful in reducing hub oscillations during operation. The *AR* at a pulse rate of 30 BPM was reduced by 94% to 0.005 by increasing the damping. This demonstrated that the damper was very effective in reducing oscillation amplitude.

It appears that the resonant frequency was $f_n \approx 0.5$ Hz, (30 BMP). As shown in Equation 4-1, the natural frequency is a function of the spring constant which is variable. Potentially this means that with different spring constants the natural frequency could fall to 60 BPM, at the normal native heart rate. However, with the dramatic AR decrease witnessed in Figure 4-26 it is presumed that high amplitude resulting from operation near resonance will not occur.

4.6 Experimental Discussion

The desired outcome of the experimental tests was to examine whether the Passive Controller configuration would counteract pathological vascular pressures. The physiological testing showed that the floating assembly moved to constructively address these cardiovascular incidences. Hypertension, poor flow balancing and further failing left ventricle simulations saw the hub being driven away from the high pressure circuit. This created a decreased output to the high pressure circuit and an increased output to the other. In most cases this response restored the arterial pressures. However, suck down of the left ventricle was an issue when simulating Pulmonary Hypertension due to the resulting decreased venous return into the LV. The effect of the floating assembly was to create a baroreceptor like response promoting high stability and a passively controlling operation.

Functionality of the Passive Controller was tested in a systemic hypertension scenario with and without the passive response. The resulting haemodynamics with the passive response saw the mean aortic pressure reduced from 140 mmHg down to 110 mmHg. The comparative result highlighted the substantial increase in stability of the supported arterial pressures when a passively controlled support device is used.

The spring response of the Passive Controller was much more complex than first assumed. Three parallel spring components formed a compound spring including an air bubble spring, clearance spring and LVDT spring. The latter was found to be negligible. An initial air volume dependent spring response from the air bubble spring was determined theoretically. Linear approximations were justified and the linear air spring rate was approximated using Equation 4-7. The clearance spring response was found to be highly non-linear and, due to the geometry, effectively infinite at either translational extremity. Between the PC stoppers, a clearance dependent parabolic relationship between spring rate and clearance was found as given in Equation 4-11.

Amplitude Ratios of oscillatory tests were calculated for medium and high level damping over a number of pulse frequencies. For each level of damping, the *AR*s for all the pulse frequencies were gathered and then compared. This allowed a qualified

analysis of the performance of the viscous damper to filter out pressure pulses caused by residual ventricular contractions. Increasing the damping from 'medium level' to 'high level' reduced the *AR* by up to 95%. The resonant frequency of the system was observed at f_n = 0.5 Hz or 30 BPM, although it was realised that the resonant frequency depends on the employed spring constant. However, it was assumed that since the damping reduced the *AR* by such a substantial amount, that these large amplitudes, caused by resonance, would not eventuate.

4.7 Conclusion

The Passive Controller BiVAD prototype was tested *in vitro* to assess its response to complications caused by a range of cardiovascular incidences. In every simulation, the device's floating assembly responded to partially or completely alleviate pathological vascular pressure. This was encouraging as the Frank-Starling-like response provided by the native heart was imitated by this dual rotary pump support device. A Frank-Starling mechanism was not witnessed however when VAD inlet pressures dropped. The incidence of left ventricular suck-down during Pulmonary Hypertension simulations was increased with an increasing severity of PVR. This will be investigated further in the numerical investigation.

A dynamic analysis of the Passive Controller showed that the applied damping of the floating assembly's motion was very successful in filtering residual ventricular pulses. Increasing the damping from 'medium level' to 'high level' virtually removed any oscillatory motion of the hub. This provides an opportunity for the flow field through the VADs to become as developed as possible while at the same time increasing the effectiveness of the passive response.

Experimental testing of the prototype has presented an encouraging introduction to the passive control of artificial hearts. Where the state of the art VADs and BiVADs see continuous flow pumps as a trade off from stability, this study observed a contrary result. The geometric nature of the rotary flow pumps and the effect of leakage over impeller blades have provided opportunity for a BiVAD with a passive controller design.

5 Numerical Program and its Development

5.1 Introduction

A numerical simulation has been constructed in MATLAB® to simulate the haemodynamics of the CV system with variable magnitudes of heart and vascular disease. Incorporated into the numerical model are two VADs whose performance can be described by multi-variable functions built using experimental performance data. The primary intended use of the numerical simulation was as a design tool for a passively controlled BiVAD prototype, but was also useful as a means of simulating the device's performance *in vivo*.

To assess the ability of the passive BiVAD controller to safely control a diseased human circulatory system, the prototype has been built and *in vitro* testing carried out in a hydraulic Mock Circulation Rig. The passive controller mechanism within the prototype has dynamic components to provide stiffness, damping and inertia. Initially the numerical simulation allowed quantified approximations of these dynamic parameters to provide optimal performance in the pulsatile, dynamic CV system. Then, after *in vitro* testing of the passive controller, the numerical model will test the concept in a circulation model more representative of a human's to provide a better simulation of passive control in a clinical situation.

This chapter documents the design of a flexible numerical program that can simulate the *in vitro* testing rig as well as a supported human circulation system. The program is novel in its comprehensive modelled vascular structure, the inclusion of global fluid inertial parameters, the implementation of experimental pump data to model the supporting BiVAD and the developed solution algorithm. Each of these are reviewed in detail including failed attempts during the program's development.

Validation of the model as well as simulated *in vitro* and *in vivo* results will be presented in the following chapter. As mentioned earlier in this thesis, a general figure colour scheme has been used to prevent confusion between experimental and numerical simulation results. Any plotted experimental result, (predominantly in the

previous chapter only), will be set on a white background. Any plotted numerical simulation result will be set onto a grey background.

All MATLAB® program code is included on a CD submitted with this thesis. Brief documentation of the programs can be found as comments within the code script and in the included pdf on the CD.

5.2 Background

It was apparent that numerical modelling of the cardiovascular system is not a new science. The earliest works date back to the 1960s where the Physiological Simulation Benchmark Experiment, PHYSBE, was created to model fluid and heat transport around the human cardiovascular system (McLeod 1966). Since then, many models have been created with further additions to apply models to different situations and pathologic conditions. Since the late 1990s, numerical models have been created to simulate the assisted circulation with single VADs (Mitsui *et al*. 1998; Vollkron *et al*. 2002) or chest compression devices (Hanson *et al*. 2005). There does not appear to be standard vascular models, standard vascular parameters or common solution algorithms. This is probably due to the broad range of model applications creating the need for specific detail of different parts of the human circulation or algorithm.

5.2.1 Modelling of Vascular Components

A review of present literature documenting studies involving a computational simulation of circulation revealed a number of differing model structures. Many of these approximated entire vascular circuits using dual resistive and compliant combinations in series (Vollkron et al. 2002; McLeod 1966; Mitsui et al. 1998). Figure 5-1 depicts this dynamic structure using an electrical symbol analogue, however the parameters are reqresentative of fluid properties. The symbols p and Q represent the fluid properties pressure and flow respectively in the main artery and vein feeding and draining the vascular circuit. The resistive and complaint components of blood vessel are denoted in the model as R and C and the subscripts $_A$ and $_V$ indicate an arterial or vascular parameter. The '$p_?$' indicates that the models

provided a common pressure across the compliant chambers, (indicating the pressure inside a body pushing against vessel walls, e.g. dermal compliance), but most of the models used a floating pressure or earth, (i.e. 0 mmHg).

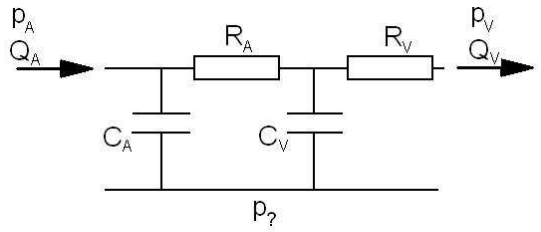

Figure 5-1: Basic vascular model with arterial and venous resistance and compliance.

Some models observed the importance of including fluid inertiance. Some were satisfied to only include fluid inertia within the aortic branch, (Vollkron *et al*. 2002; Mitsui *et al*. 1998), others also included the inertial contribution from the pulmonary artery (Larnard 1986). The fluid inertiance was commonly implemented into the models as a precursor to the arterial compliance and resistance as depicted with the symbol *L* in Figure 5-2.

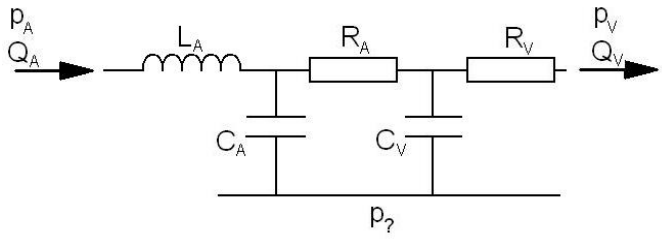

Figure 5-2: Basic vascular circuit model with arterial fluid inertiance included.

One more recent model was published including fluid inertiance in the main arteries as well as in each of the four heart chambers (Hanson *et al*. 2005). However, no information was given regarding quantification of the vessel inertiance. This is unfortunate as it will be shown that the incorporation of inertial parameters in a numerical circulation model is imperative, particularly in the heart chambers. However, its inclusion can induce high instability in the solution algorithm and so caution needs to be exercised when implementing the solution algorithm.

5.2.2 Modelling of the Native Heart

The reviewed numerical simulations modelled the ventricles and atria very similarly to that shown in Figure 5-1. Atria and ventricles are, after all, vascular chambers with associated resistance and compliance. The circuit in Figure 5-3 shows the most common model, (in this case modelling the left heart), employing variable compliance chambers and the one way resistors/diodes which simulate valves.

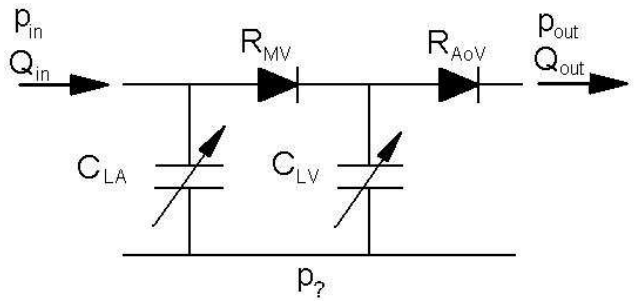

Figure 5-3: Basic atrial and ventricular circuit model with arterial and venous resistance and compliance.

The subscripts in the figure refer to the cardiovascular locations; $_{LA}$, the Left Atrium, $_{LV}$, the Left Ventricle, $_{MV}$, the Mitral Valve and $_{AoV}$, the Aortic Valve. Variable compliance components allow the ventricles and atria to contract. Most of the reviewed articles used a transient ventricular compliance that was updated every time step to provide a fluid driving input to the system, (Vollkron et al. 2002; Mitsui et al. 1998; Hanson et al. 2005; McLeod 1966; McLeod 1968). The changing compliance provided the forcing input which provided energy to the system, (much like the contracting ventricles provide the forcing input to drive blood around the circulatory system). The form of the time dependant ventricular compliance data were sourced from the PHYSBE model (Kohrt 1999; McLeod 1966) and then scaled during the validation process. Atrial compliance functions were found in Guyton (2005) and were subsequently employed in the numerical program.

Cardiac valves were exclusively modelled as diodes or two-state resistors controlled by an ‘if’ statement. A popular means of valve state determination was to compare the upstream and downstream pressures (McLeod 1968). For example, the mitral valve’s ‘if’ statement would compare the left atrial and left ventricular pressure. If the atrial pressure is higher, (diastole), the resistance would be low to simulate the

pressure drop required to get through the open valve. If the ventricular pressure is higher, (systole), the resistance would take on an essentially infinite value to simulate a closed valve. Another means of determination within the 'if' statement was to assess the flow (Hanson *et al*. 2005). This would stipulate the valve state as 'open' if the flow was positive from atrium to ventricle and ventricle to artery. A flow based determination is perhaps more representative of heart valves as pressure alone won't deflect the valves, but rather the fluid-structure interaction from moving blood is required.

For comparison with the *in vitro* tests done with the mock circulation loop, the time dependant ventricular data was approximated using experimental pressure-volume plots. The atrial compliance was assumed constant for comparisons with the mock circulation loop as the atrial reservoirs were open to atmosphere.

5.2.3 Vascular Parameters

Recent studies have chosen to represent vascular segments in a variety of ways; for example the dynamic structures shown in Figure 5-1 and Figure 5-2. In some studies only one of these basic vascular models is used to represent the whole of the pulmonary or systemic circuits. In this case, the vascular parameters of the arterial and venous vessel of that circuit are combined together. The choice of the vascular parameters therefore, depends largely on the chosen structure of the circulation model. For example, the recent models employing the circuit structure shown in Figure 5-2 concentrate the inertial contributions from the whole circuit into one component. Additionally, the arterial, arteriole compliances and resistances are combined and then isolated from the combined capillary, venules and vein compliances and resistances. Considering the variations in vascular models, there was very little agreement between vascular parameters.

Three tables were drawn documenting the employed resistances, compliances and inertiances in a number of vascular models used in recent studies. These are shown in Table 5-1 to Table 5-3.

Table 5-1: Vascular Parameters from the PHYSBE Model.

This table is not available online.
Please consult the hardcopy thesis
available from the QUT Library

(McLeod 1966)

Table 5-2: Vascular Parameters from the Hiroshima School of Medicine Model.

This table is not available online.
Please consult the hardcopy thesis
available from the QUT Library

(Mitsui *et al*. 1996)

Table 5-3: Vascular Parameters from the University of Vienna Model.

This table is not available online.
Please consult the hardcopy thesis
available from the QUT Library

(Vollkron *et al*. 2002)

A large variation is seen between not only the vascular data used but also the recognised vascular parameters used. The lack of agreement between the model parameters provided room for 'educated guesses' for the numerical model within the author's project. Clearly, dynamic vessel data changes from patient to patient, especially patients with differing types and severities of cardiovascular diseases. One modeller commented that the employed vascular data were "in some cases compromises between values from various sources and in others (were) outright guesses" (McLeod 1966).

It should be noted that inertia contributions to the haemodynamics were often ignored in recent studies. It will be shown that fluid inertiance has a high influence on pressure drop across a vessel where there is a high rate of change of flow, dQ/dt. For this reason aortic and pulmonary artery inertiances have been included by Vollkron *et al*. (2002) and Mitsui *et al*. (1996). However, the highest rates of change of flow are in and around the cardiac valves, (atria, ventricles and arteries). Kiorakiantis and Shi (2006) saw the importance of including fluid inertiance in a numerical model to some extent, and so included inertial parameters throughout the systemic and pulmonary vasculature. However, their study did not employ inertiance for the aria and ventricles.

The importance of inertiance in the heart chambers was recognised by Hanson and Levesley *et al*. (2005) who included inertial parameters in every vascular section except venous vessels. Unfortunately no detail was given into quantifying the inertial parameters. An investigation into the effect of global inertiance parameters which are vessel volume dependent will be examined in this chapter.

The parameters for numerical simulation of the circulation have been guessed, transferred from textbook data, e.g. (Milnor 1982; Guyton 2005), or else determined from animal experiment.

5.3 Employed Cardiovascular Model

5.3.1 The Human, or *In Vivo* Circuit

A schematic is provided in Figure 5-4 to show the modelled sections of the employed cardiovascular structure. Each subsection of the model, (e.g. head, arms, lungs), includes fluid resistance, compliance and inertiance for both arterial and venous vasculature. The inclusion of extra systemic branches as well as the incorporation of second order dynamic parameters in both veins and arteries allows for a very flexible model. This will be demonstrated later when the program is used to model the *in vitro* test rig as well as *in vivo* simulations. The schematic also depicts two VADs cannulated from the ventricles into the main arteries.

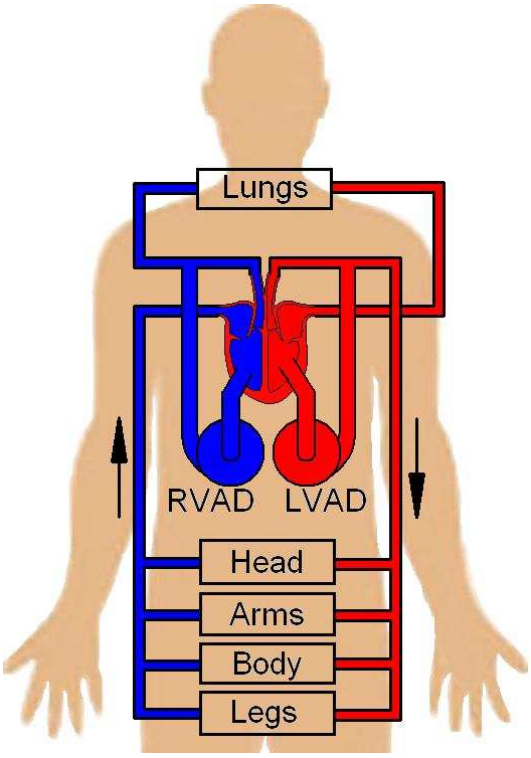

Figure 5-4: Schematic of the modelled sections of the cardiovascular system in the numerical program.

The model, depicted in Figure 5-5 is an electrical circuit analogue of Figure 5-4 which includes arterial and venous sections for each vascular section. The systemic sections are similar to those used in the initial PHYSBE model (McLeod 1966) and employ four fluid branches, (head, arms, legs and body), in parallel between aortic and vena cava branches. The pulmonary system includes a series circuit comprising the Pulmonary Artery, arterial and venous vasculature of the lungs and the Pulmonary Vein. The circuit comprises a repeating vascular model which features in every vascular section. This vascular sub-unit will be described later.

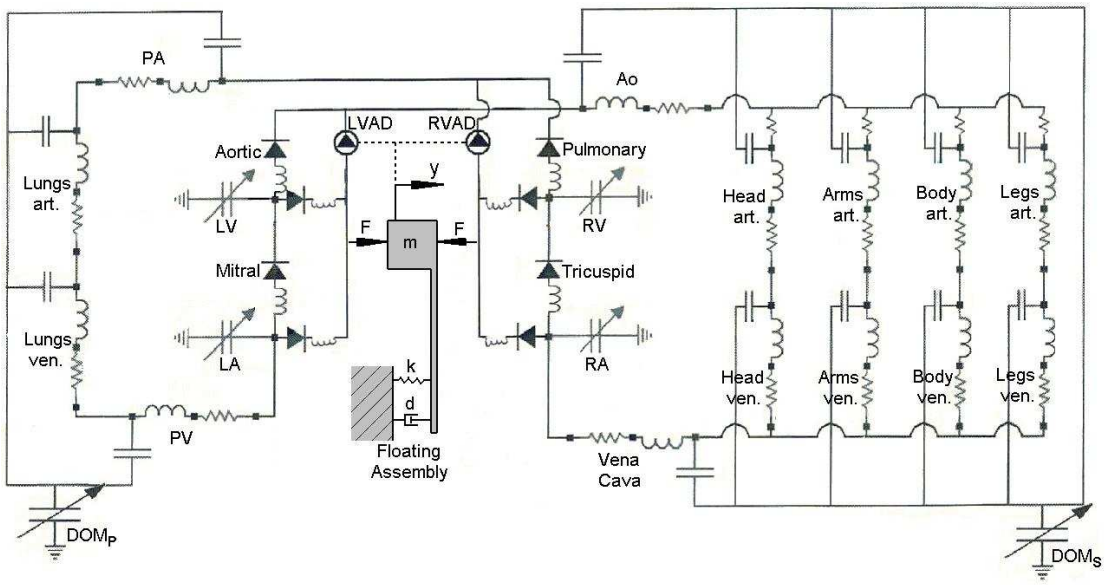

Figure 5-5: Numerical model schematic as an electrical circuit analogue with two assisting pumps. The nomenclature used are, LA, Left Atrium; LV, Left Ventricle; Ao, Aorta; art., arterial vasculature; ven., venous vascularture; RA, Right Atrium; RV, Right Ventricle; PA, Pulmonary Artery; PV, Pulmonary Vien; DOM_S, pressure outside vessels in systemic circuit; DOM_P, pressure outside vessels in pulmonary circuit; *y*, the floating assembly position with respect to its central location; *F*, the pressure force from the VAD upon the floating assembly; *m*, the mass of the floating assembly; *k*, the effective spring striffness; *d*, the damping coefficient.

There are two pumps shown which form parallel circuits with the left and right sides of the heart. These are the LVAD and RVAD respectively. The pumps are fed from either the respective atrium or ventricle depending on the selected cannulation site in the simulation setup. This is done by setting the undesired inlet cannulation resistance very high. The outlets of the VADs are plumbed into their corresponding main artery. Included in the model is the free body diagram of the floating assembly and its associated spring, mass, damper arrangement. The axial position of the floating assembly, y, is also included and the dotted line indicates that this parameter affects the VAD performance.

Inertial components have been included in each vascular section too. This is novel as state of the art computational simulations of the human circulation have generally excluded this parameter from their models. It will be shown that simulation of the hydraulic states in and around the heart valves was very sensitive to their nominated inertiance. So, perhaps due to lack of computational power in the past these parameters have generally been excluded from numerical models of the CV system.

The four resistors upstream, (above), of the head, arms, body and legs branches were a late edition to the circuit structure as non-physiological blood flow was occurring in the arterial vascular sections. Without these resistors the four compliance chambers would resonate as there was no resistive damping while subject to the pulsing AoP. During simulation these resistances were all prescribed as 150 $mmHg.s.ml^{-1}$ and were successful in reducing this vibrational effect.

Including these fluid resistances is reasonable when considered from a physiological perspective. The model provides lumped parameter models of every vascular subsection. The inclusion of these additional resistors only splits the aortic resistance into a resistor followed by four branches each with a resistor at its base. When considering the continuous nature of a vascular resistance this makes the model more realistic. In the vascular system there are resistive contributions in a vessel before all the compliant contributions have been experienced by flowing blood.

Each of the vascular compliance chambers provides an integral flow response between the vascular fluid pressure and the common surrounding compliance, (the outer loop). This outer pressure is defined by the 'Dermal/Organ/Muscular pressure', (DOM pressure), which can be time dependant or constant. This allows for simulation of exercise (providing periodic muscular contraction in the form of time dependant DOM pressure).

5.3.2 The MCL, or *In Vitro* Circuit

The relatively complex model of the human circuit in Figure 5-5 permits dynamic parameters and/or entire vascular branches to be removed to simulate more simplified fluid circuits. This is required for comparison of the experimental testing of the BiVAD prototype *in vitro* within the Mock Circulation Loop, (MCL). The MCL is a simplified circuit of that shown in Figure 5-4 and Figure 5-5 as three of the systemic branches are not included, (see Figure 5-6 and Figure 5-7).

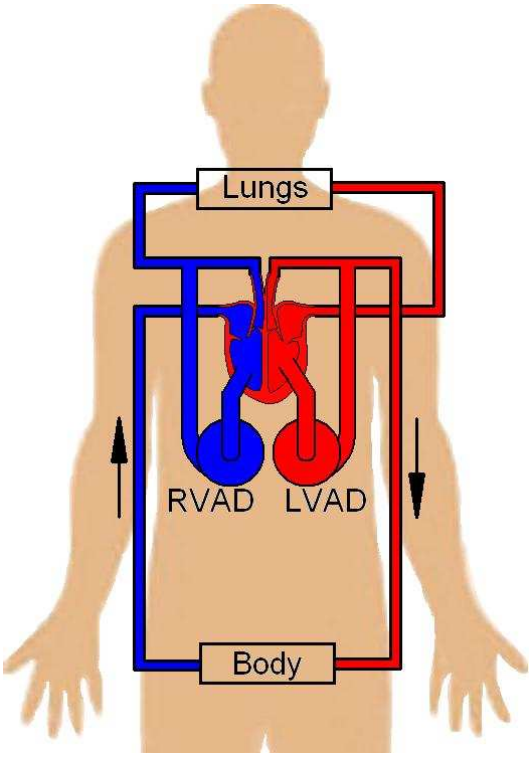

Figure 5-6: Schematic of the modelled sections of the cardiovascular system in the Mock Circulation Loop MCL.

Given that the numerical model is flexible in its simulation model structure, the relatively complex structure shown in Figure 5-5 could be reduced to model the MCL. The reduced electrical circuit analogue is shown in Figure 5-7.

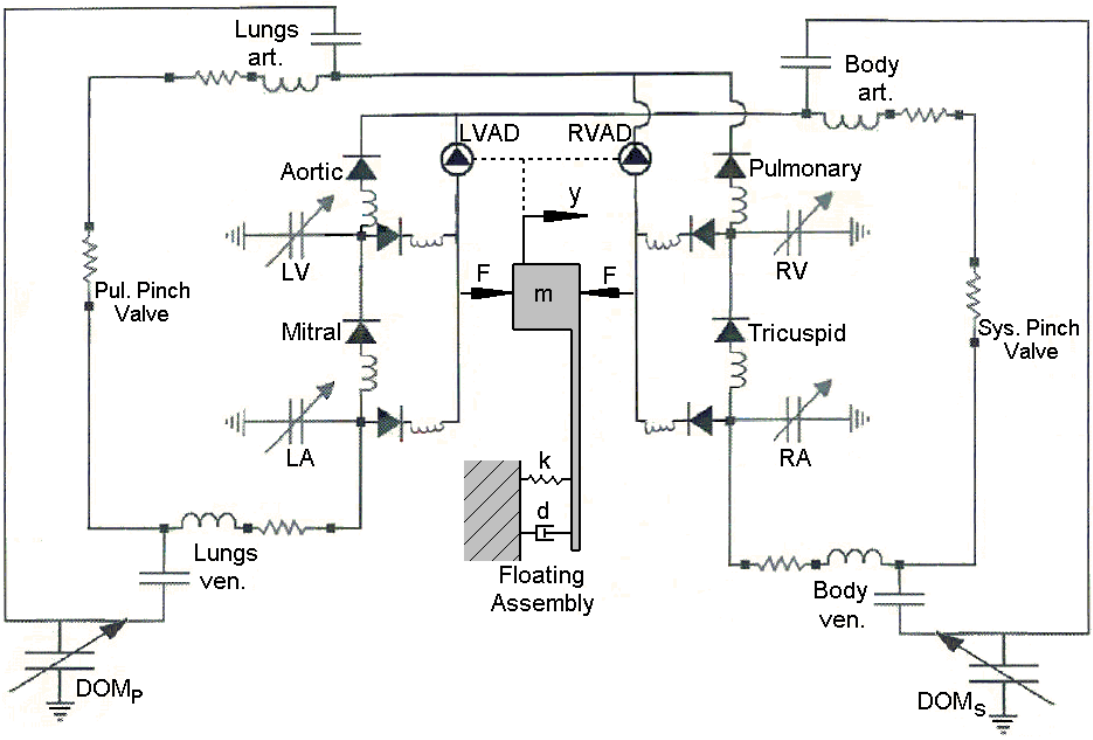

Figure 5-7: Electrical circuit analogue for the modelled Mock Circulation Loop.

The fluid resistance in the pulmonary and systemic circuits are simulated with a single pinch valve between the arterial and venous compliance chambers. Due to the MCL using water as the working fluid, non-discrete fluid inertiance is inherently incorporated into the model. It is important to note that the plumbing within the MCL consists of pipes with an internal diameter of approximately Ø20 mm. There is therefore, significant inertiance within the loop.

Arterial and venous vessels are again modelled using the repeating vascular sub-unit. The associated resistance is an approximation of the pressure drop due to the resistance of the plumbing. Further resistance is applied to each of the vascular circuits between the arteries and veins. This models the pinch valve used by the MCL to regulate pressure.

The Pulmonary and Systemic DOM pressure, (DOM_P and DOMs respectively), were prescribed as zero. This is analogous to the vessel compliance chambers and the ventricles and atria of the MCL having been opened to atmosphere when the pressure sensors were zeroed before each test.

5.3.3 Overview of Simulation Formulations

The numerical program was composed of seven equations to model the fluid within the vascular circuits and the BiVAD. The first three equations relate to the fluid flow around the circuit and provide the relationships between the pressure and flow rate and the user defined vascular parameters such as resistance, compliance etc. One of these equations, as will be explained, will be used to calculate the updated vessel volume dependent inertiance parameter for each sub-unit of the vascular system.

The remaining four equations are used to model the VADs. Two of them are used to formulate the hydraulic performance of the each VAD. These are the Performance Functions and the Clearance Decrement Functions. The final two are used to characterise the motion of the floating assembly and include an Ordinary Differential Equation (ODE) and the clearance spring equation. The ODE characterises the dynamics of the floating assembly with the incorporated spring, mass, damper configuration. The form and empirical derivation of the clearance spring equation was discussed in the previous chapter.

Some of these equations have been decoupled from the linear solution scheme. This was done in order to formulate linear approximations of the BiVAD hydraulic performance as well as allowing for the calculation of the vessel volume dependant inertiance. The equations and their formulations along with the implementation of the decoupled equations are explained in detail in this chapter.

5.3.4 The Vascular Sub-Unit

Each arterial or venous sub-unit within the employed model has an identical model structure as depicted in Figure 5-8. These sub-units will be referred to as vascular sub-units from here on in. The model is the same as that used by Vollkron *et al.* (Vollkron *et al*. 2002) to model the systemic arteries. The compliant component provides an integral flow response to pressure differences between that provided by the DOM and the fluid pressure within the vessel. The inertiance and the resistance then provide a derivative and proportional response to the flow to simulate the dynamic response from blood inertia and viscous drag against the vessel walls.

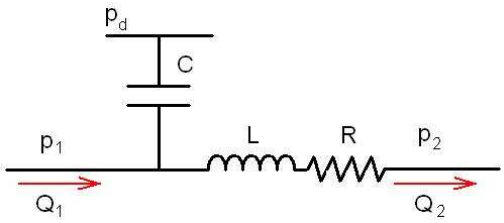

Figure 5-8: Repeating vascular model of dynamic arterial or venous vessels.

The subscripts ($_1$) and ($_2$) indicate properties at the inlet and outlet of the vessel respectively and ($_d$) refers to a property outside the vessel. The compliance, C (with units, (with units [ml.mmHg-1]), and resistance, R (with units [mmHg.s.ml-1]), parameters are specified by the program user for each vascular sub-unit. The inertiance, L (with unit [mmHg.s.ml^{-1}]), by definition, is the mass of the fluid in each vascular sub-unit divided by the vessel cross-sectional area squared,

$$L = A_L \frac{\rho l}{A} = A_L \frac{\rho l}{\left(\frac{\pi \phi^2}{4}\right)}.$$

Equation 5-1

The vessel's cross sectional area A, the blood density ρ, the vessel length l and the vessel diameter ϕ, are used to quantify the inertiance along with a constant, A_L, used to convert the unit to (mmHg.s.ml^{-1}).

However, because the vessels are flexible, the resident fluid mass is a function of resident fluid volume. So, this equation can be modified in two ways, either modelled as a flexible vessel of constant diameter with a varying length, or with a constant length and a varying diameter, (therefore varying area A). Because an updated volume dependent inertiance has never been employed in such a model, both modifications will be tried and each result will be discussed later.

The two forms of the volume dependent inertiance assume a constant diameter and a constant length respectively. These are,

$$L = A_L \frac{\rho l}{\left(\frac{\pi\phi^2}{4}\right)} = A_L \frac{\rho l^2}{V^i},$$

Equation 5-2

and,

$$L = A_L \frac{\rho l}{\left(\frac{\pi\phi^2}{4}\right)} = A_L \frac{\rho V^i}{\left(\frac{\pi\phi^2}{4}\right)^2},$$

Equation 5-3

where the superscript (^{i}) indicates the present time step and V^i is the vessel's resident volume at time step i.

With all the vascular parameters now prescribed, the pressure and flow relationships for the generalised vascular sub-unit can be analysed. To model the transient fluid response through the vascular sub-unit, discrete linear approximations were made. The inertiance and resistance are linked in series and so their fluid impedance is summed as,

$$p_1 - p_2 = RQ_2 + L\frac{dQ_2}{dt}.$$

Equation 5-4

Then, assuming a small time step, Δt, between iterations Equation 5-4 can be linearised to give,

$$p_1 - p_2 = RQ_2^i + L\left(\frac{Q_2^i - Q_2^{i-1}}{\Delta t}\right),$$

Equation 5-5

where the superscript ($^{i-1}$) indicates one time step ago.

The pressure difference across the compliant component provides a response inversely proportional to the vessel compliance as given in,

$$p_1 - p_d = \frac{V}{C} = \frac{V_0 + \int_{t_0}^{t^i} Q(t)dt}{C},$$

Equation 5-6

where t_0 is the time at simulation start and V_0 is the initial volume at t_0. This can then be approximated by,

$$p_1 - p_d = \frac{V_0 + \sum_{t=t_0}^{t=t^i} \left(Q_1^i - Q_2^i\right)\Delta t}{C}.$$

Equation 5-7

Equation 5-5 and Equation 5-7 form the basis of the linear program. With these relationships the CV system was simulated as will be discussed. Additional equations were added to the linear system, such as the non-linear pump performance interpolation functions, as the program was developed.

5.4 Manipulation of Experimental VAD Data in Program

It was considered important that the VAD response within the program was representative of the prototype's actual performance. Experimental data was therefore used to construct interpolating functions for both VADs to be incorporated into the simulation.

Initially, this required identifying all the contributing variables to the pump's pressure head *H*, and the flow, *Q*. These were the pump speed, *N*, and the clearance over the impeller blades, *c*. Characteristic interpolating performance functions were then arranged using these four variables and assessed by inspection of the resulting interpolation function. If the resulting curve was a poor representation of a rotary pump response, the form of the interpolating performance curve was changed and then reassessed.

The basic form of all the tested performance functions was a product and/or summation of Q, N and c polynomials with the pressure head, H, as the subject. The order of each polynomial was altered as the function form was refined in order to make it representative of a rotary pump's hydraulic response. The evolution of this function will be documented in this section.

Incorporated into each polynomial was a series of coefficients. The order of the polynomial indicated the number of coefficients. In order to characterise a particular rotary pump's performance, these constants could be evaluated using that pump's experimental performance data. This meant that a set of calculated coefficients was specific to that pump's geometry.

Software written by the candidate in MATLAB used operating points (Φ) from the prototype VAD performance testing (see Figure 4-3 and Figure 4-6) with which to evaluate these constants. The operating points, or VAD states, were used as boundary conditions (BCs) in the program to create an interpolating function. After evaluating the function constants, the function is plotted and the candidate was able to adjust the fit by changing the defining BCs. This step will be graphically documented in this chapter.

It appeared through early miniature pump testing that pressure, H, varied linearly with clearance, c, and held a parabolic relationship with impeller rotational speed, N. The relationship between pressure and flow, Q, was considered carefully as this relationship would coordinate the actuation of the passive controller. Earlier works investigated geometric parameters to affect the gradient and rate of change of the gradient of the H-Q performance relationship. The profiles took a small range of forms from inverted parabolic forms to flat profiles that steepened suddenly at high flows. The latter appeared to have a varying second derivative with respect to flow, ($\partial^2 H/\partial Q^2$), which indicated a cubic relationship (Gaddum, Timms, and Tann 2006).

Four performance function forms were trialled in an attempt to characterise the hydraulic performance of the VADs. The development and testing of each of the trialled performance functions was a time consuming exercise. The three discarded

performance functions, as well as their ability to model the physical pumps, are documented in the Appendix C provided on the accompanying compact disk.

The first trial function found that a cubic relationship between H and Q induced high instability in the function form over the expected VAD operation region. It was decided to reduce the order of the H vs. Q relationship to a parabola.

The second and the third trial functions varied the inclusion of the clearance term c. The clearance term was multiplied to a product of the pump speed and flow rate parabola functions. However, this created high variation in the effect of clearance over the expected operating region. The clearance term was then added to the product of pump speed and flow rate parabola functions; however, this could not replicate the exponential decay relationship that clearance had with pressure and flow.

The employed function for the numerical model is documented in this section. It has the form $H(Q,N,c)$.

5.4.1 The Ideal Performance Function: $H(Q,N,c)$

Once the device was built the hydraulic response specific to the LVAD and RVAD detailed in Chapter 4 could be closely analysed. This was needed to ensure that the assumed relationship between the hydraulic parameters of the pumps was representative of the VADs' performances.

In Section 4.3 it was observed that the clearance affected both the developed pressure head and the output flow rate. Furthermore, an increase in clearance saw an exponential decay in both pressure and flow which approximately tended to some lower limit. This effect will be illustrated in this section. Ideally, a fully coupled equation would be used such as,

$$H(Q,N,c) = \left(A_1 Q^2 + A_2 Q + A_3\right)\left(A_4 N^2 + A_5 N + A_6\right)\left(A_7 e^{A_8 c} + A_9\right),$$

Equation 5-8

where A_1 to A_9 are pump specific constants.

However, the function given above would have $Q^2 \times \exp(c)$ terms, $Q \times \exp(c)$ terms and Q^2 terms which could not be integrated into the linear system. So, it was decided to decouple the clearance completely from the pump equation so that the performance equation within the linear solution step was of the form $H(Q,N)$. In order to incorporate the effect of clearance however, the performance functions themselves were modified at every time step according to the hub position. For example, if it was expected that the hub was to be positioned at $y = y^i$ after the solution step, the performance equations for that time step would be redefined for each VAD. This would be done according to their respective expected clearances. In order to redefine the VAD performance functions according to the expected clearance, the Clearance Decrement Functions were generated.

The means through which the Performance Functions are redefined by the Clearance Decrement Functions will be explained later. At this stage, it is important to understand their forms, their representation of experimental data and that they are used in conjunction to provide a linear approximation of the ideal performance function given in Equation 5-8. An explanation of their form and representation of experimental data will be covered in this section.

5.4.2 The Clearance Decrement Functions

To include the effect of clearance on the pressure and flow outside of the solultion step, the decoupled clearance term was used to degrade the pump performance equation. The way that this parameter was used to degrade the performance and how this was implemented will be explained later. This section discusses the construction of the decaying, or Decrement Functions in order to include the effect of clearance adjustment on the pump's hydraulics.

The pressure decay, ξ_H, and flow decay, ξ_Q, were each modelled as the sum of two clearance dependent exponential functions as given in Equation 5-9 and Equation 5-10. The reason for using the sum of two exponential functions will be explained. The pressure decrement,

$$\xi_H = \frac{H}{H_{c=0}} = B_1 e^{B_2 c} + B_3 e^{B_4 c},$$

Equation 5-9

where B_1 to B_4 are pump specific pressure vs. clearance constants and $H_{c=0}$ is the developed pressure head at a clearance of zero. The flow decrement,

$$\xi_Q = \frac{Q}{Q_{c=0}} = B_5 e^{B_6 c} + B_7 e^{B_8 c},$$

Equation 5-10

where B_5 to B_8 are the pump specific flow vs. clearance constants and $Q_{c=0}$ is the developed flow at a clearance of zero.

In order to determine the decrement function constants, B_1 to B_8, the experimental data presented in Section 4.3.2 was used. The data were gathered at speed N_{LVAD} = 3400 RPM and N_{RVAD} = 1100 RPM and over a clearance range of c = 0.0 to 3.0mm. It was then down-sampled from 12000 data points to 20. This was done to allow smoothing so that the exponential functions would be representative of the whole testing range.

It was assumed that the form of the decaying function wouldn't vary excessively with pump speed, so the H vs. c and Q vs. c data was normalised for each VAD by dividing the hydraulic parameter by its maximum.

MATLAB was then used to evaluate the clearance decay function constants using a least squares approximation subroutine of the exponential function given in Equation 5-9 and Equation 5-10. The evaluated constants are given in Table 5-4.

Table 5-4: Clearance Decay Function Constants for the prototype LVAD and RVAD.

	Clearance Decay Constants	
	LVAD	RVAD
B_1	0.2283	0.166
B_2	-1.978	-135.1
B_3	0.7719	0.819
B_4	-0.003606	-0.01179
B_5	0.1632	0.06448
B_6	-2.069	-53.11
B_7	0.8469	0.934
B_8	-0.007145	-0.00532

Figure 5-9 and Figure 5-10 show the exponential functions laid over down-sampled experimental data from the tests detailed in Section 4.3.2. The LVAD and RVAD pressure decay is shown in the first figure followed by the flow decay in the second figure. Note that the output decay is plotted against clearance, *c*, which is the absolute distance between the impeller blades and the lower shroud, (as opposed to hub position, *y*, which is the hub position with respect to its central location in the BiVAD).

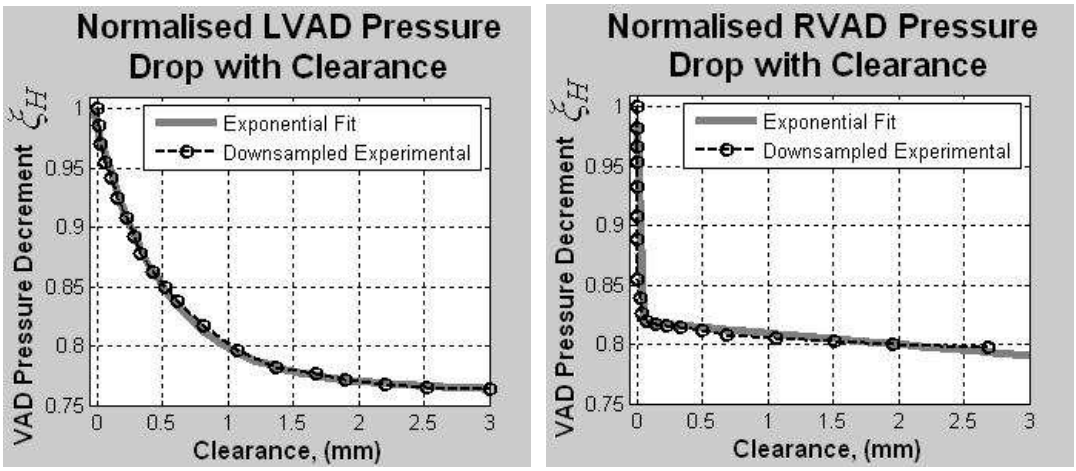

Figure 5-9: Exponential fit and down-sampled experimental data detailing the normalised pressure vs. clearance relationship for the LVAD (left), and RVAD (right).

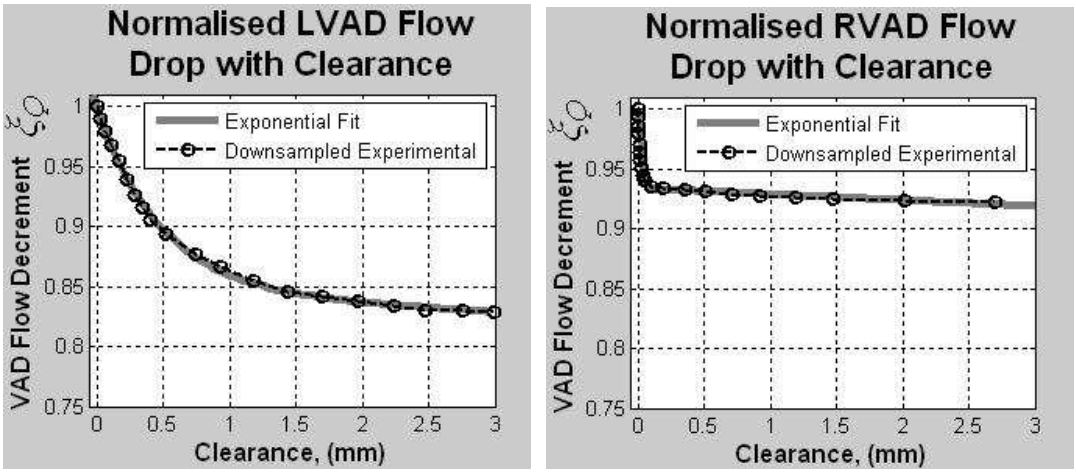

Figure 5-10: Exponential fit and down-sampled experimental data detailing the normalised flow vs. clearance relationship for the LVAD (left), and RVAD (right).

The values of B_4 and B_8, from Table 5-4, are very close to zero. If they were zero the second exponential function in Equation 5-9 and Equation 5-10 would be equivalent to $B_3 \times (1)$ and $B_7 \times (1)$. However, the decaying functions do not appear to display a gradient of zero at maximum clearance, ($y_{max} = \pm 0.17$ mm), and hence B_4 and B_8 are not quite zero. This is the justification for using the sum of two exponential functions.

The operating translational range used in the experiments was $y = \pm 0.17$ mm, (therefore each VAD could have a maximum clearance of $c_{max} = 0.34$ mm). This range, therefore, will employ only the far left section of the plots in Figure 5-9 and Figure 5-10.

Plotted against the employed translational range of $y = \pm 0.17$ mm, the pressure decrements for both VADs are shown in Figure 5-11. Note that if a total translation range of 0.34 mm is employed in the BiVAD, then a clearance of $c = 0$ mm corresponds to a hub position of $y = +0.17$ mm for the RVAD and $y = -0.17$ mm for the LVAD. For this reason, the hub can only reside in the region of the figure with a white background. The shaded regions show hub positions that are beyond the physical PC stoppers attached to the VAD impellers as mentioned at the end of Chapter 3.

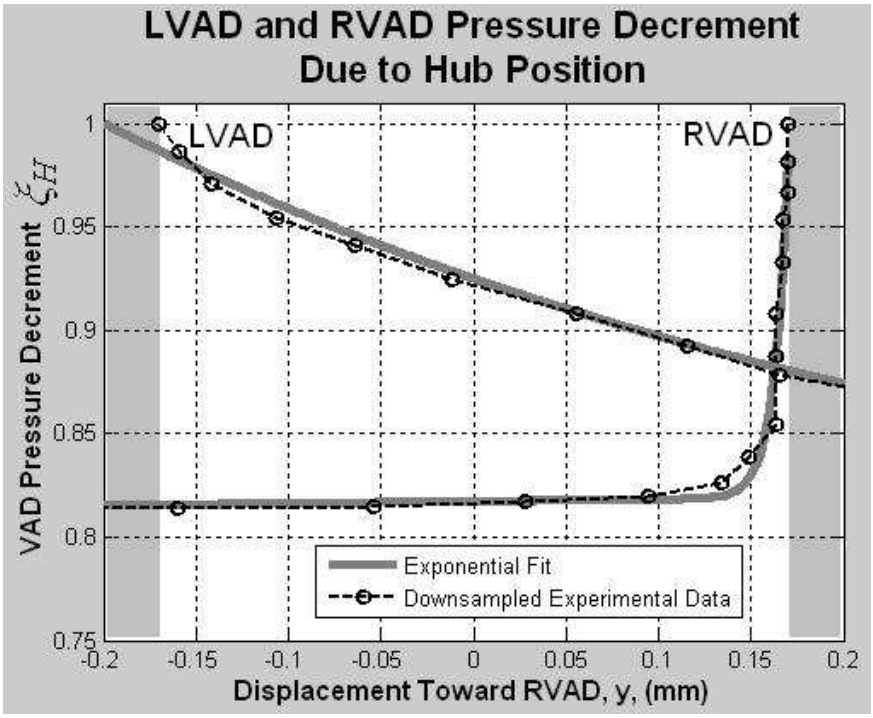

Figure 5-11: Pressure decrements for both VADs as a function of hub position with a total translational range of y = ±0.17 mm.

Similarly, the flow decrements are given over the employed translational range for the LVAD and RVAD in Figure 5-12.

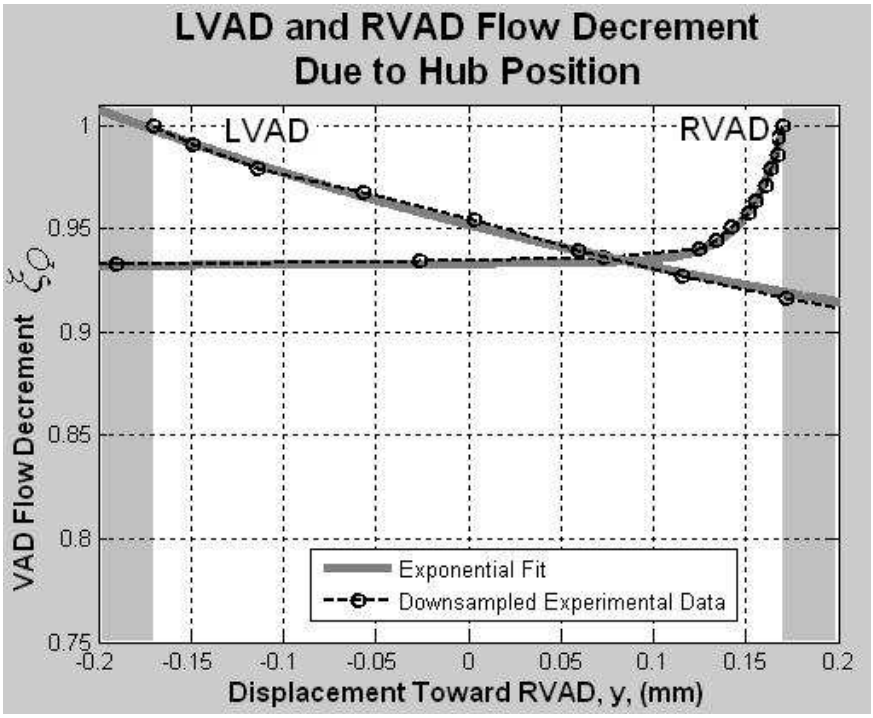

Figure 5-12: Flow rate decrements for both VADs as a function of hub position with a total translational range of y= ±0.17 mm.

Note the magnitude of the RVAD pressure and flow loss from c = 0 to 0.02 mm, (y = +0.17 to +0.15 mm). They were 83% and 79% of the total head and flow loss over the device operating range respectively. This essentially desensitises the RVAD output to clearance unless the floating assembly is very close to the RVAD impeller blades. Later, the form of the decrement functions will be varied to observe their effect in the BiVAD's ability to passively control the CV system.

5.4.3 Construction of the Interpolation Functions

Now that the clearance term is decoupled from the pump performance equations, the remaining H, Q and N terms provide the relationship,

$$H(Q,N)=\left(A_1Q^2+A_2Q+A_3\right)\left(A_4N^2+A_5N+A_6\right).$$

Equation 5-11

The constant, A_1 to A_6, are pump specific constants derived from corresponding experimental pump performance data.

Software was written to take the experimental data from the BiVAD prototype pump performance tests and use it as boundary conditions, BCs, to solve for the pump specific constants. This process will be discussed and illustrated in this section.

The resulting function for the RVAD, however, needed the inclusion of forced, or prescribed, BCs in order to encourage the representative quality of the function. Generation of the RVAD interpolating function will also be demonstrated in this section.

5.4.3.1 **Data Sorting**

Initially the program sorts through the VADs' experimental performance pump data. This data holds H vs. Q curves over a range of pump speeds and impeller clearances. Sorting was useful in order to locate evenly staggered states with which to fit the interpolating function. Staggered BCs over the testing range made the performance curve 'more representative'. 'More representative' is intended to mean that the partial

second derivatives over the operating range of the function weren't too high as to cause sharp peaks or saddles in function form. Additionally the function is 'more representative' if the BCs are taken at the maximum or minimum tested pressures, flow and pump speeds. These states are, after all, the boundaries of the interpolative region. The BCs are then arranged for the modelling of the interpolating function.

The experimental BCs could be point location states, $\Phi = (H, Q, N)$, as well as partial first and second derivatives in time, (Type 1, 2 and 3 BCs respectively). For the generation of either, 6 staggered (H, Q) data points, for 6-7 pump speeds (N) were taken from the experimental set. This provides 36 or 42 data points. When expanded out, Equation 5-11 has 9, (3×3), constants to be evaluated. An equal number of BCs were needed in the linear system of equations to solve for these constants. The vast selection of available data points allowed, if needed, many possibilities for alteration of the chosen BCs.

Equation 5-11 is expanded in Equation 5-12 identifying the nomenclature for the nine pump specific performance constants.

$$H(Q,N) = Q^2\left(D_1N^2 + D_2N + D_3\right) + Q\left(D_4N^2 + D_5N + D_6\right) + \left(D_7N^2 + D_8N + D_9\right),$$

Equation 5-12

where D_1 to D_9 are products of pump specific constants A_1 to A_6.

5.4.3.2 **Fitting the LVAD Performance Function**

The construction of the LVAD pump curve was a relatively problem-free process. Type 1 BCs only, were employed and a representative performance curve was generated as shown in Figure 5-13.

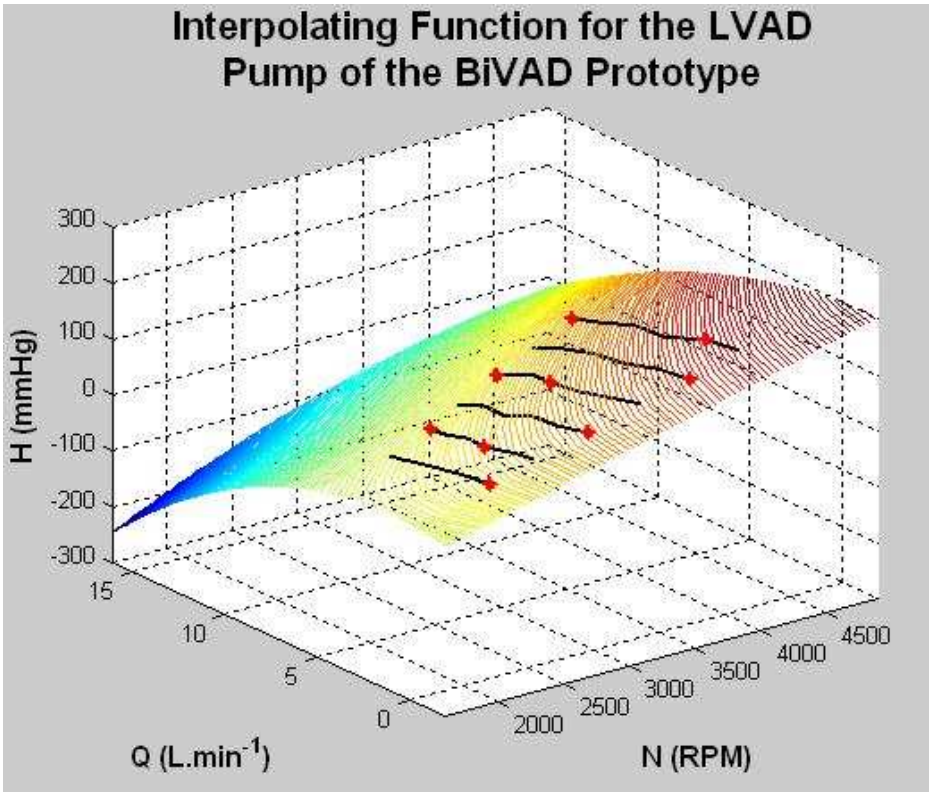

Figure 5-13: The resulting LVAD Interpolating Performance Function.

The employed performance curve, as given in Equation 5-11, finds the pressure head H, in terms of flow Q and pump speed N. Upon the surface of the performance function shown in Figure 5-13 there are six plotted black profiles and nine red crosses. The black profiles are the experimental performance curves at pump speeds N = 2200 to 4200 RPM. The red crosses are the Type 1 BCs used to generate the nine pump specific constants. (Since clearance is decoupled within the decrement functions, the figure is plotted at c = 0 mm, or (y = -0.17 mm) within the BiVAD).

A few simple selection criteria were established to ensure that the function was 'representative':

1. The distribution of BC locations occupies some peripheral hydraulic states as well as max and min pump speeds. Thus expanding the available region that the function will be, by definition, interpolating.
2. There are no uncharacteristic peaks, troughs or saddles in the plotted function profile.

3. The partial second derivatives of H with both Q and N, ($\partial^2 H/\partial Q^2$ and $\partial^2 H/\partial N^2$), were to be negative.

The LVAD performance function plotted in Figure 5-13 fit these criteria well.

5.4.3.3 **Manual BC Adjustments and Fitting of the RVAD Function**

Figure 5-14 shows the pump performance curve from the RVAD over a wide range of Q and N. (The figure is plotted at c = 0 mm, or (y = +0.17 mm) within the BiVAD). Selection criteria 1 is satisfied as the Type 1 BCs are evenly spread and occupy sufficient experimental test range periphery. It also appears as though criteria 3 is satisfied as H vs. Q and H vs. N are approximately parabolic over the whole function. However, it is clearly not representative as H along Q = 15 L.min^{-1} gets as low as -1350 mmHg.

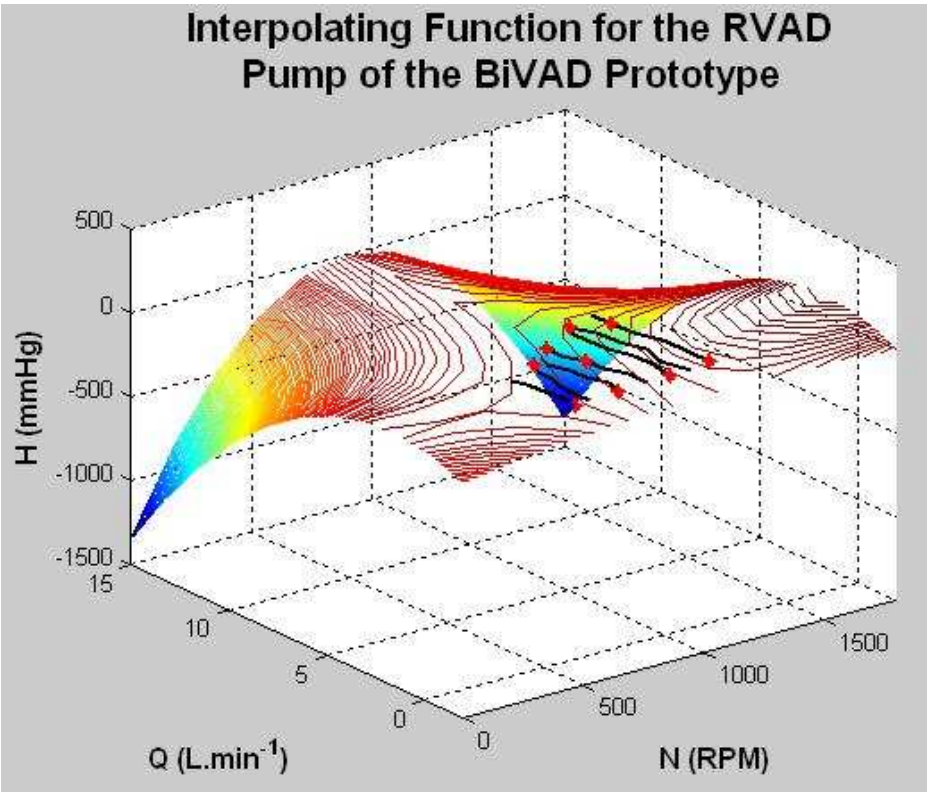

Figure 5-14: Performance function evaluated over a wide range of speeds and flows with a constant clearance.

Different combinations of Type 1 BCs provided similar inadequate function forms. So, a small number of the experimental data point locations were sacrificed for forced point location BCs outside the experimental range. This technique used extrapolated user defined states to tame the performance profiles. Figure 5-15 shows successive 'taming' of the performance functions using one, and then two, forced point location BCs. The forced point locations are indicated with large 6-point stars.

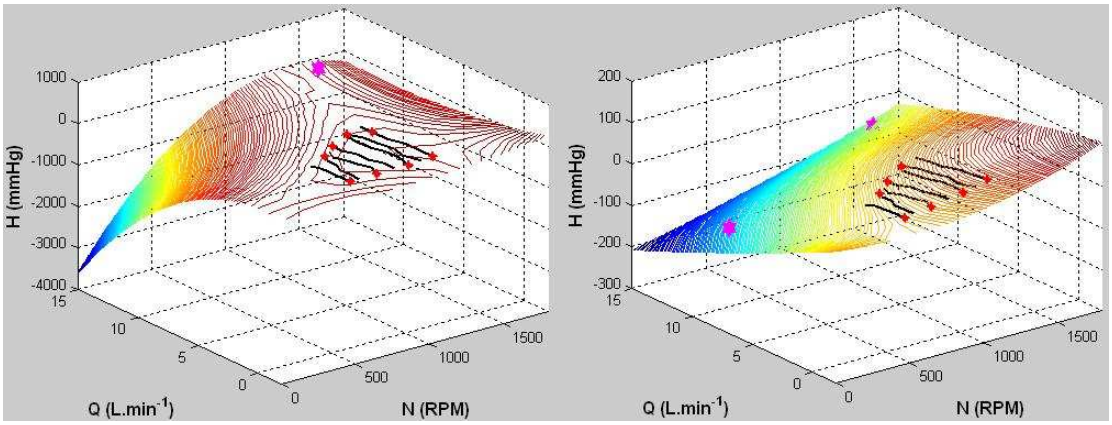

Figure 5-15: Performance function, ine1 forced BC assigned, (left), two BCs assigned, (right).

Observe the decrease in the range of the pressure axes between the two plots. The two extrapolated forced BCs squeeze the function out to a more 'representative' profile.

Figure 5-16 shows the final function form for the RVAD performance function using three forced BCs. The three criteria are satisfied.

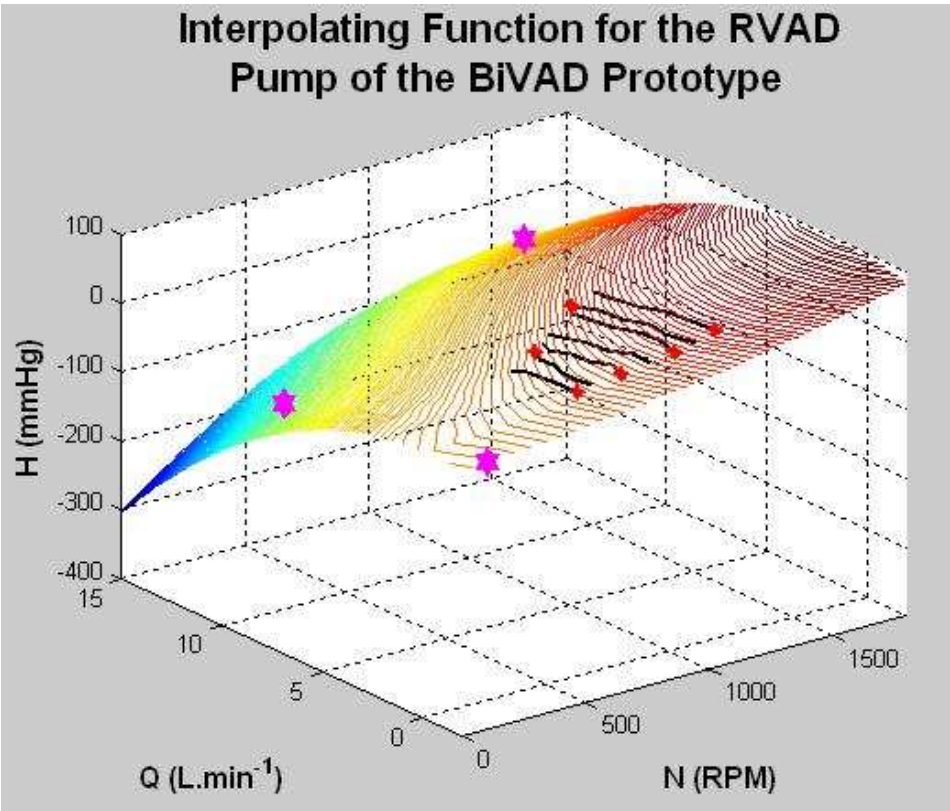

Figure 5-16: Performance function, 3 non-experimental point locations BC specified.

We can now assess the success of using the forced point locations by comparing the interpolating functions before and after the three forced BCs were put in place. Figure 5-17 shows the interpolating function without any point locations (left) and with the three selected point locations (right) on reduced axes.

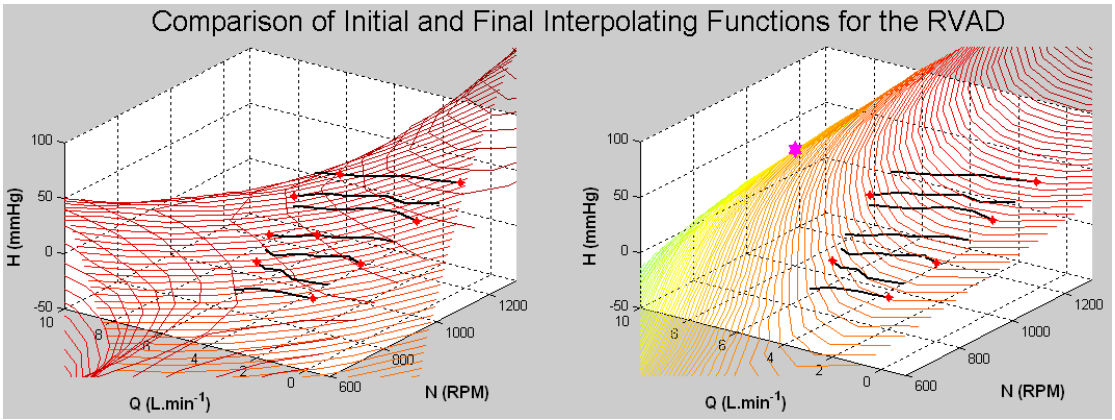

Figure 5-17: Comparison of the initial and final interpolating functions on reduced scale axis. No forced point locations, (left), final interpolating function with three forced point locations (right).

It is clear that the final interpolating function has higher continuity around the regions where the RVAD was operating in the *in vitro* testing. The use of the forced point locations worked well in prescribing an effective pump performance model. The HQ profiles at any reasonable support simulation speed provide the characteristic inverted half parabola performance profile.

5.4.3.4 **Performance Constants**

The nine Performance Function Constants are given below in Table 5-5. These are the pump geometry specific constants for the VADs. It should be noted that these are hydraulic parameters for pumping of water or fluids of similar density and viscosity.

Table 5-5: BiVAD Performance Function Constants.

	Pump Performance Function Constants	
	LVAD	RVAD
D_1	-5.04760E-10	-1.77650E-09
D_2	3.85350E-06	3.66000E-06
D_3	-9.00000E-03	-4.30000E-03
D_4	6.97050E-08	1.95400E-08
D_5	-5.62860E-04	1.42210E-04
D_6	8.62900E-01	8.60000E-02
D_7	3.16670E-06	2.11910E-05
D_8	3.53000E-02	2.02000E-02
D_9	-4.91603E+01	-1.01905E+01

A comparison of the order of magnitude of these constants will indicate that many of them are very small. However, Equation 5-12 indicates that the when D_1, (for example), is multiplied by Q^2N then the order of this contribution will become significant.

5.4.4 'One pressure one flow' – Stability of the Performance Function in the negative flow region

When implementing Equation 5-12 as the performance function for the VAD into the numerical program one major flaw was observed in the function's ability to imitate

rotary pump performance. This was in the regions where the rate of change of pressure *H*, with respect to flow *Q*, was positive, (i.e. normally in the negative flow region). The performance function suggests that there can be more than one stable flow rate for any achievable pressure head. Although no literature could be found on performance profiles in the negative flow region – it was assumed that the performance gradient could not possibly become positive. This was a problem for numerical simulation.

Issues were observed at simulation start up and when simulating ventricular support at low flow rates, (i.e. near to $Q = 0$ L.min^{-1}). At these low flow rates the operating point can slide down the left hand side of the performance profile causing incorrect simulations.

This effect can be observed from the results of a simulation shown in Figure 5-18. The result came from a simulation when the solution method was nearing completion. Since the solution method is yet to be explained, the simulation result is intended for explanation purposes only.

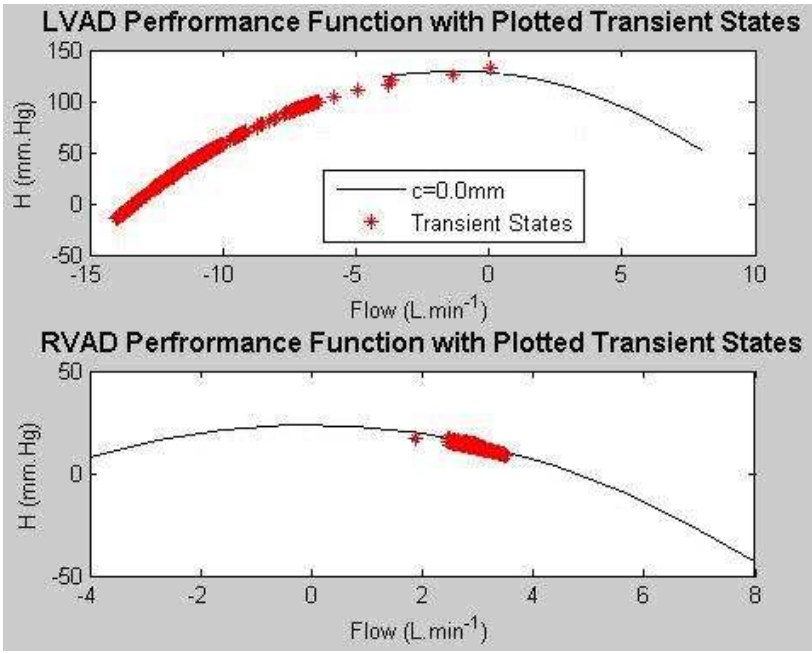

Figure 5-18: Performance functions of the LVAD, (top), and RVAD including the plotted transient states during a simulation.

The figure shows that the operating point of the LVAD started at around 0 $L.min^{-1}$ and then moved further down into the negative flow region. To help protect the simulation from entering into regions of the performance curve where the gradient is positive, the performance function itself became a piecewise function. The non-linear performance function is used when the VAD flow rate is higher than the function maximum, Q^*, and a linear function with a high negative gradient, (-33 $mmHg(L.min^{-1})^{-1}$), is used when the flow rates become lower. The piecewise performance functions are shown in Figure 5-19. The solid lines represent the regions where each function is employed.

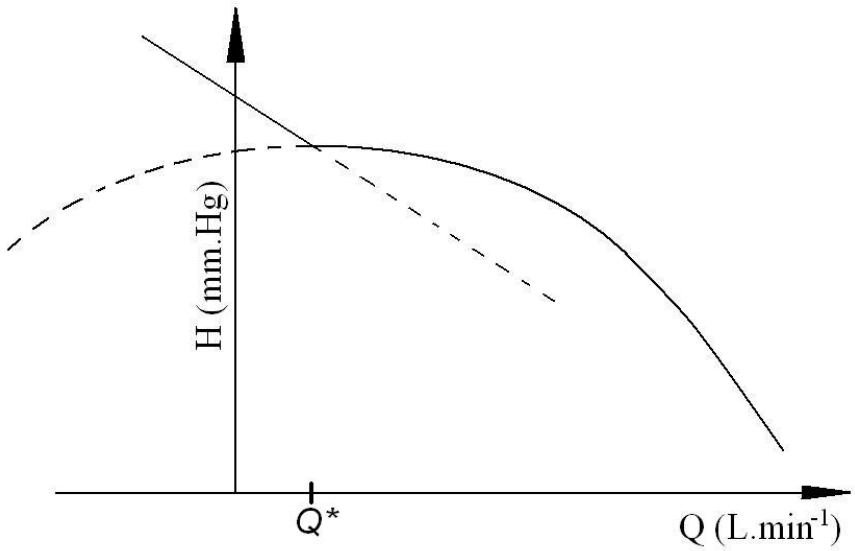

Figure 5-19: Form of the piecewise performance function, (solid lines indicate the regions of each function that was used in the simulation).

The piecewise functions intersect at the parabolic maximum of the performance function Equation 5-11 at $Q = Q^*$. Before a solution is run, this equation is differentiated by the program and the flow rate at this maximum is evaluated by solving for a gradient of zero. Then during the solution the VAD flow rates from previous two time steps are used to make a linear prediction of the present time step flow. The predicted flow rate is then compared to the non-linear performance maximum flow rate to decide which piecewise function to use. This is, therefore, a decoupled function selection. This is not really an issue of how representative the pump functions are as the linear portion of the piecewise function is user defined rather than derived from experimentation.

This feature prevented the transient VAD flow becoming destabilised through the existence of two stable flow rates for every achievable pressure head. Figure 5-20 shows the transient performance states of the two earlier VADs during an identical simulation to that shown in Figure 5-18. The VAD states with a flow rate less than Q^* follow the profile of a linear performance curve that intersects the non-linear performance function at the function maximum.

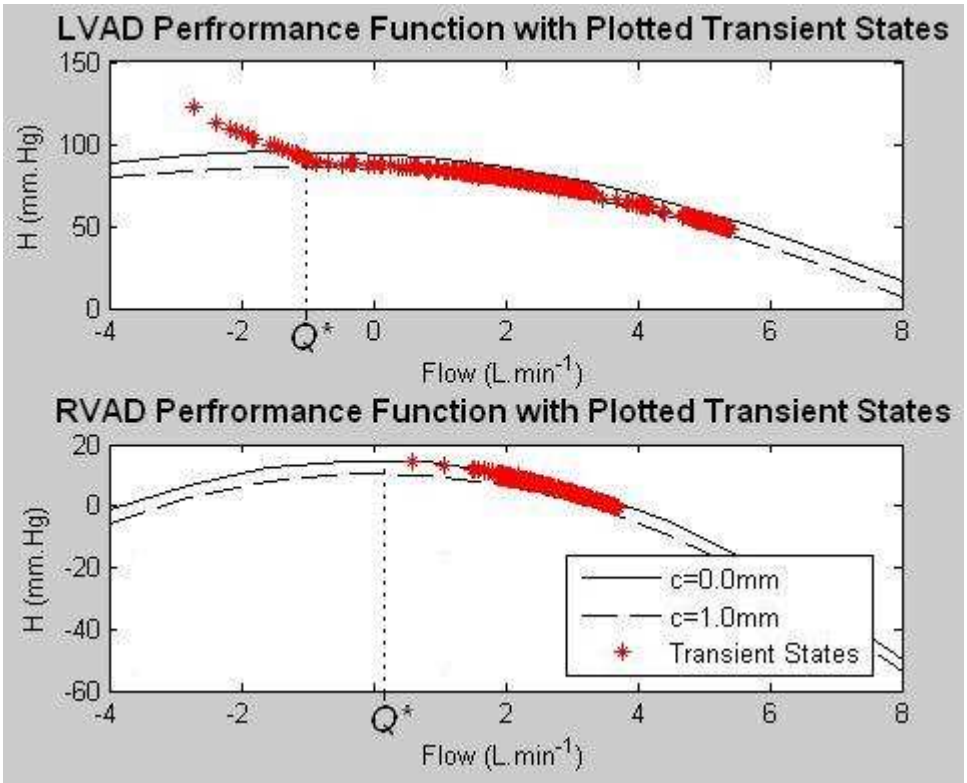

Figure 5-20: Plotted transient VAD states using piecewise performance functions.

As explained, the form of the linear part of the piecewise function is user defined. However, although the hydraulic states occupying the linear function may not be as representative as the non-linear functions, it is important to encourage the VADs not to enter the positive gradient performance region. Since rotary pumps are not designed to enter negative flow regions it is assumed that steady performance cannot be achieved with back-flow. Additionally since the model will only be used to model physiologically viable haemodynamics, accurate simulation in this region of performance is not important. It should be noted, however, that if the simulated VAD operating point resides frequently in the linear performance region this will be taken as an indication that ventricular suckdown has occurred.

5.5 Evolution of the Linear Time Stepped Solution

Figure 5-5 shows an electrical analogue model simulating the human circulation. The model incorporates dynamic fluid components in all the sections of the circulation arteries and veins as well as the heart chambers. The dynamic fluid components are arranged in multiple sub circuits like that shown in Figure 5-8.

This design was implemented in all of the initial program versions. The modelling of the assisting pumps, however, developed once the vascular model was operational. The VAD modelling was easily the most time consuming process from this study and evolved through a number of versions. However, it was a useful progression because as the VAD models became more representative the candidate was able to use the program as an investigation tool. This will be demonstrated in Chapter 6 the program was used to model the interaction between the CV system and the passively controlled BiVAD beyond the experimental work.

A detailed circuit model of the human vasculature is shown in Figure 5-21. It comprises 22 vascular sub-units. Each vascular sub unit has a name and associated number, e.g. RV and 18 respectively. Within each vascular sub-unit there are, usually, two hydraulic states; a pressure and a flow rate. The hydraulic states are comprised of pressures p_1-p_{15}, p_{37}-p_{38} and p_{44}-p_{47} and flow rates Q_{16}-Q_{36} and Q_{39}-Q_{42}. The remaining state, (state 43 or y_{43}), is the floating assembly position. This makes a total of 47 states.

In early versions of the numerical simulation only States 1-36 were used to allow the construction of the CV model without the VADs. Later versions included the other state to incorporate the VADs and cannulation sites. In the final version of the program, the passive controller was introduced bringing with it the floating hub position c as an extra state. The final version also included the resistances above the systemic arteries used to impede numerical resonance in this region and hence more pressure terms were added. For this reason, the indices of the pressure and flow states are strangely ordered.

Additional ‘dummy’ states were added to implement the non-linear performance functions into the linear solution. However, these were decoupled from the solution step. These will be explained in detail later in this chapter.

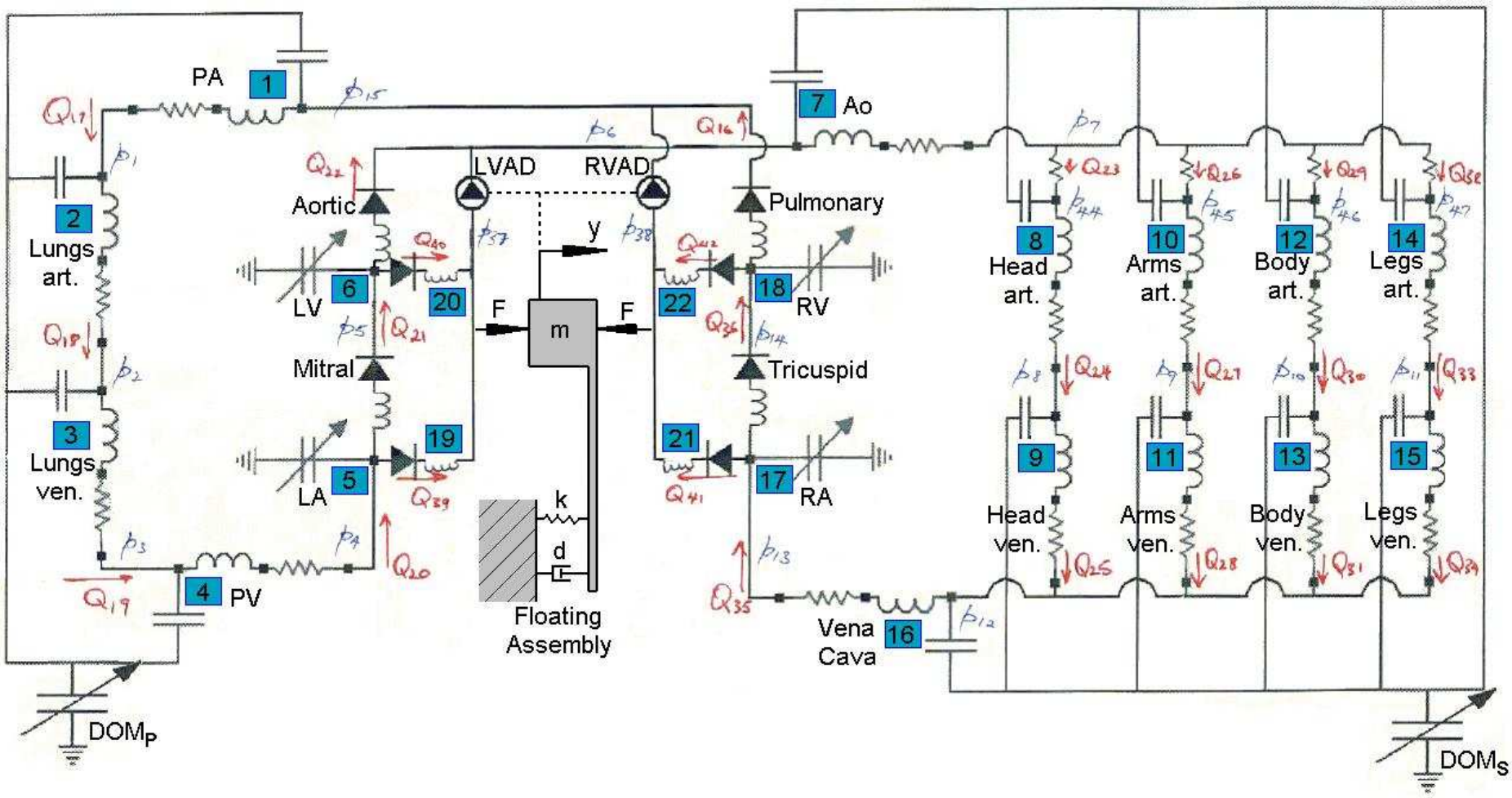

Figure 5-21: Electrical circuit analogue with two assisting pumps with the pressure and flow states labelled as well as numbered circuit blocks.

5.5.1 Version 1: The General Circulation Model

The general circulation simulation saw the modelling of the circuit in Figure 5-21 without the VADs and Cannula, (vascular sub units 19-22), into a system of 36 equations. The 36 equations were used to solve for the pressures 1-15 and flow rates 16-36 at each time step. The pressure drop due to the fluid resistors and inductors as well as the fluid accumulation due to pressure drops across the compliant vessels were modelled using the linear approximation given in Equation 5-5 and Equation 5-7 respectively. The energy inputs to the system were the time varying compliance profiles for both the atria and the ventricles, (circuit blocks 5, 6, 17 and 18, see Figure 5-21). A time varying compliance profile simulated the heart's pumping function.

5.5.1.1 Linear Solution Method and Initial Results

The program arranges the system parameters into a system matrix, $\underline{\mathbf{A}}$. The state vector, **x**, holds 36 state variables including 15 static pressures and 21 flow rates around the system model. The **b** vector holds information about the state variables one time step ago and the time step length. These are then arranged into an $\underline{\mathbf{A}} \times \mathbf{x} = \mathbf{b}$ type solution. The solution vector **x** therefore, is the product of the inverted $\underline{\mathbf{A}}$ matrix and **b**. To save computational time, the **A** matrix is decomposed into two Lower and Upper triangular matrices whose product is **A**. This is called an LU Decomposition. These matrices are then each inverted and multiplied by the **b** vector. The products are then multiplied together to give the new state variable **x**.

Physically running the simulation began with running the Simulation Construction program. This program built the simulation by taking a large amount of user defined parameters. The parameters include:

- Time parameters:
    - A maximum simulation time (T)
    - The time step (Δt)
- Initial states, (pressures 1-15 and flow rates 16-36 and initial vascular sub-unit volumes 1-18 at $t = 0$)
- Vascular fluid resistances for each circuit block
- Vascular compliances for each circuit block

- Vascular geometries with which to calculate the vascular fluid inertiance
- Native heart beat data:
    - Time period
    - Time in systole
    - Maximum and minimum ventricular and atrial compliances, (diastolic and peak systolic compliances respectively)
    - Level of LVF and RVF, (linear scale, 1 ≡ healthy, 10 ≡ no pulse. These are used as weighting constants to augment the specified minimum and maximum cardiac compliances)
- Working fluid density

Additionally the transient ventricular and atrial compliance profiles are constructed using user supplied time and heart beat data. The form of the ventricular systolic compliance profiles was approximated from textbook data (Guyton 2005). This data was then normalised by dividing the transient compliance data by the maximum in the profile. This normalised profile could then be multiplied by the user specified peak systolic compliance. The diastolic compliance specified by the user was then incorporated into the transient profile to complete the cardiac cycle. The atrial contractions were assumed to be sinusoidal during the atrial systolic phase.

Like the PHYSBE model, the parameters were chosen by making educated guesses using previous publications (McLeod 1966; McLeod 1968; Mitsui *et al*. 1996; Vollkron *et al*. 2002), textbook data (Neil 1979; Guyton 2005), and trial and error by running the program. A summary of the parameters used for healthy simulation is given in Appendix 10.2, Table 10-1. This table of parameters will be updated during the validation process in the next chapter; however, it provides an indication of the parameters used for explanation purposes in this chapter.

The valve action was achieved using an ‘if’ statement which observed an approximated value for the flow rate through the valve as described earlier. This was chosen over the pressure comparison as it was believed that the direction of the flow would be the driving factor for opening or closing of the valves.

A steady simulation result is shown in Figure 5-22 where the pressure profiles of the atria, ventricles and main arteries are plotted above and the inverse compliance below. The time period for each cardiac cycle is 1 second and the systolic phase occupies 40% of this.

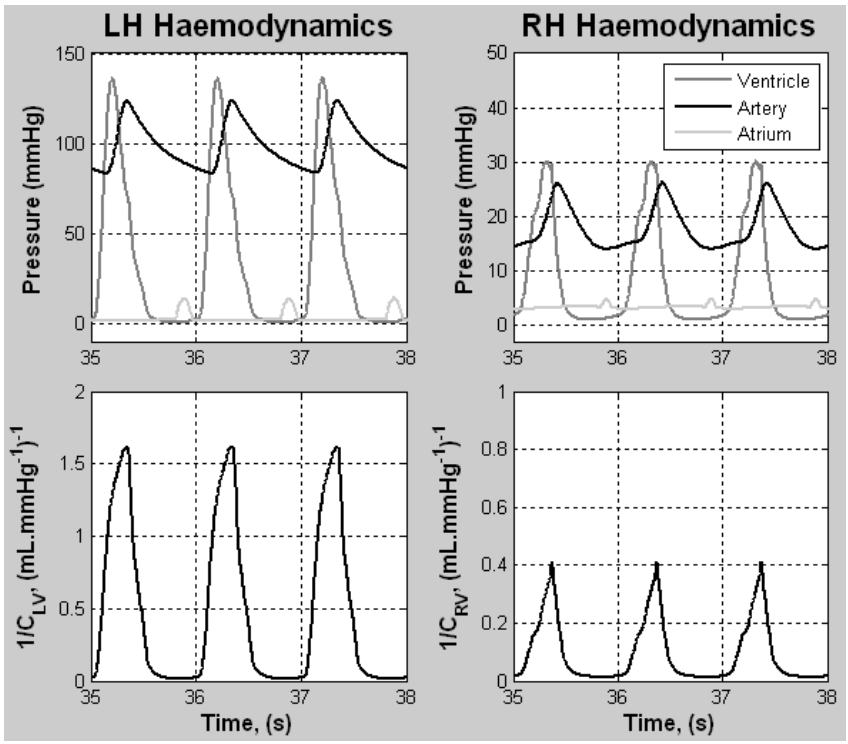

Figure 5-22: Steady heart and arterial pressure profile (above), and inverse compliance profiles (bottom) for the LV and RV.

Note the phase difference between the peak systolic ventricular and arterial pressures. This is due to the modelled inductance in the atria, ventricles and arteries. This will be examined closely later.

When a simulation was initiated it took some time for 'state settling' to occur. This was due to the 'disturbance' caused by the, essentially arbitrary, initial states values given for time $t = 0$. Once settled, the program provided a typical physiological waveform like that shown in Figure 5-22. Figure 5-23 shows a healthy simulation during $t = 0$ to 40 seconds. The 'state settling' see high fluctuations in vessel pressures and flow rates over the first 20 seconds. This outlines the need for a robust solution algorithm to cope with these fluctuations.

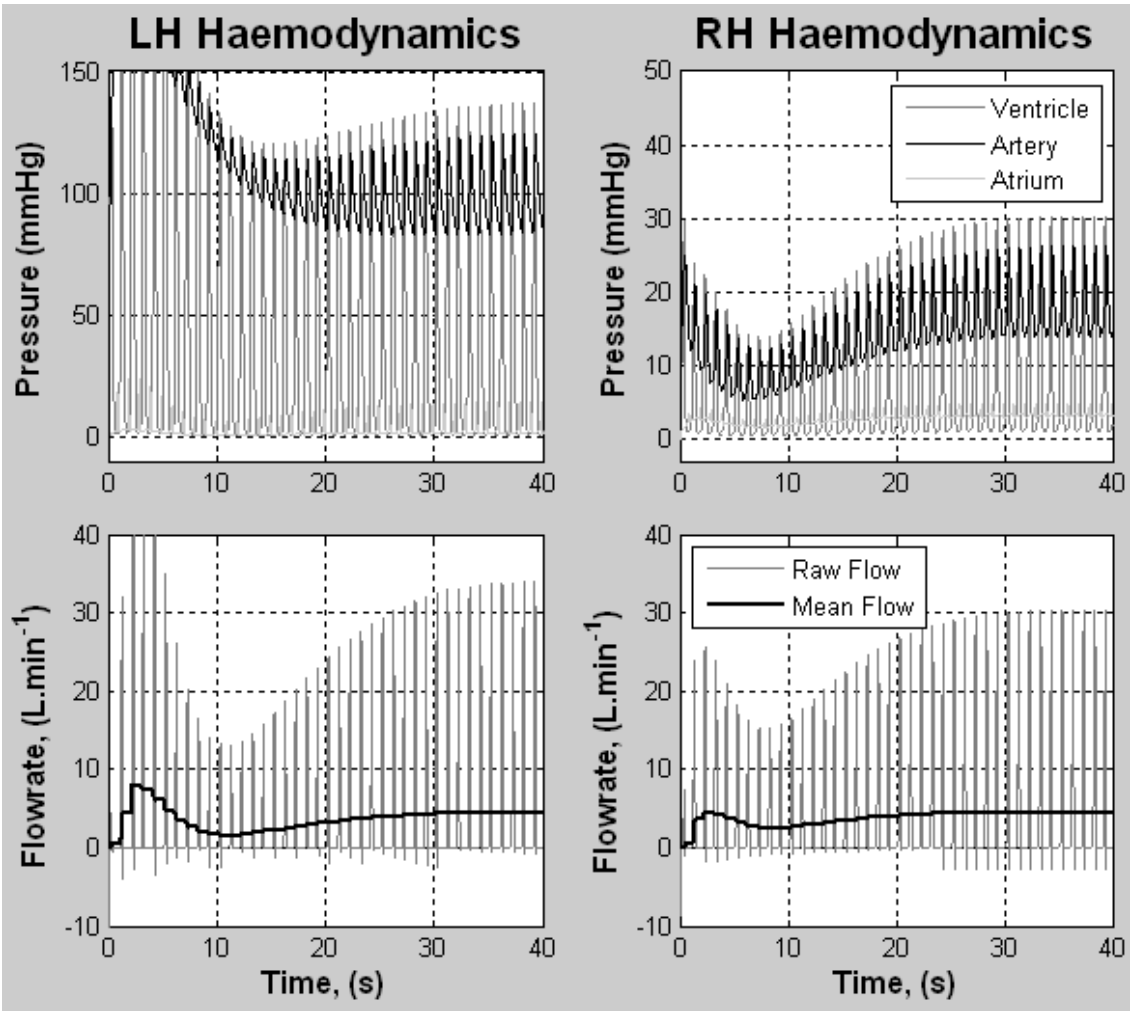

Figure 5-23: Pressure (above) and flow through the arterial valve (below) through a healthy simulation start up.

The linear $\underline{\mathbf{A}} \times \mathbf{x} = \mathbf{b}$ type solution worked very well for the CV system simulation. Parametric adjustment was carried out until pressure, flow and inverse compliance plots were comparable to textbook data. Verification will wait until a comparison with the MCL.

5.5.1.2 Atrial Kick and the Volume Dependant Inertiance

Novel features within this first version are the existence of the 'atrial kick' or atrial contraction as well as the inclusion of global fluid inertiance. A brief examination into these two features is presented in this section. Unfortunately the MCL does not yet incorporate atrial systolic phases. The MCL vessels are also rigid, so the two forms of inertiance calculation cannot be compared. This means that neither of these

features will be validated against *in vitro* simulation. However, a discussion will be included at the end of this chapter.

An atrial systolic period is observed in the native circulation Figure 2-4 beginning at around 80% of the cardiac cycle and ending at approximately 10%. Atrial systole was implemented in much the same way as ventricular systole; using a transient compliance profile. A sinusoidal atrial compliance profile was used for the systolic period and atrial diastole was modelled as a constant high compliance.

As would be expected, the effect of increasing the atrial contractility was a rise in peak systolic ventricular pressure. This is because the end diastolic volume in the ventricle is sensitive to the atrial kick.

As mentioned earlier, in order to implement a novel updated inertiance, either the vessel diameter or vessel length must be assumed constant according to Equation 5-2 and Equation 5-3 respectively. Both methods were tested and it was found that the linear system quickly became unstable when assuming a constant length using Equation 5-2. It was assumed that since the updated volume was on the denominator the $L \propto 1/V$ function would quickly destabilise the $\underline{\mathbf{A}}$ matrix when volumes became very small. So, a constant diameter assumption using Equation 5-3 was employed to update the vessel fluid inertiance.

A study was then carried out into the use of the fluid inertiance parameter as a global variable in the circuit model. It was found that the allocated ventricular and atrial diameters had a very strong bearing on global haemodynamics. Variations in aorta and pulmonary artery diameters held minor influence and variations in central systemic and pulmonary diameters were unfelt. The sensitivity of the left ventricle, LV, haemodynamics to local inertial parameters is graphically shown in Figure 5-24. The figure shows results from simulations where the diameter of the LA ranges from Ø45-Ø65 mm and the diameter of the LV ranges from Ø30-Ø46 mm.

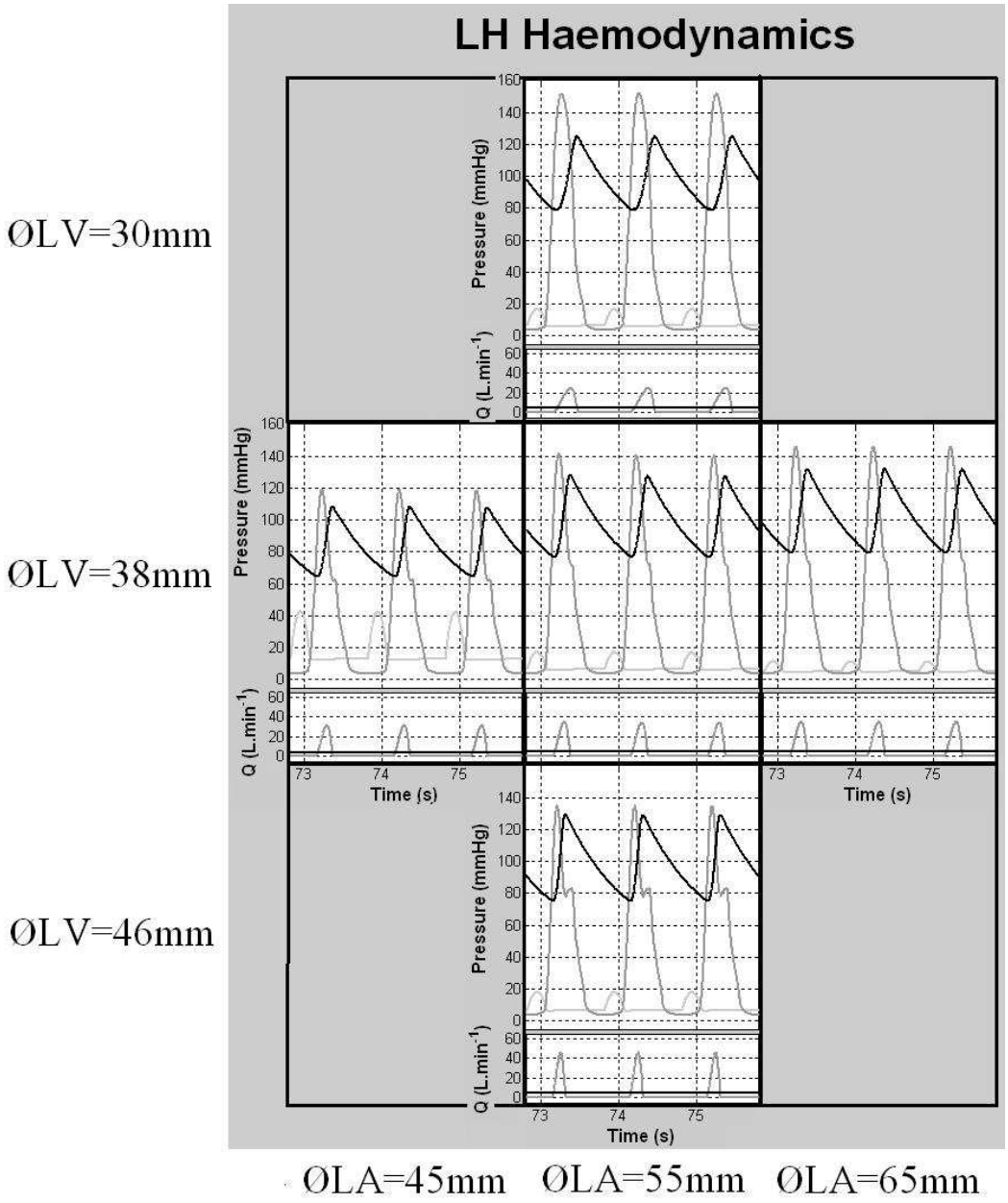

Figure 5-24: Array of settle LV haemodynamics with a varying LA and LV diameters.

Equation 5-4 shows that the pressure drop due to the fluid inertiance *L* is proportional to the rate of change of local flow rate *Q*. It is therefore not surprising that the ventricular and atrial inertiance carry such influence over the circuit haemodynamics as they experience the highest rates of change of flow rate.

Due to the variation in both ventricular geometry and contractility between human individuals, selection of the diameter of the ventricles and atria was difficult. So, these parameters were chosen through comparison of the resulting haemodynamics to pressure profiles, like those in Figure 2-4, to text (Neil 1979; Guyton 2005).

5.5.2 Version 2: Circulation Model with Linear VAD Performance Curves

Upon completion of the first version the second version was started to add the VADs into the numerical model. As an intermediate step, this version used linear VAD performance curves. Once the linear performance profiles were running smoothly within the solution algorithm, characteristick non-linear performance profiles would be used. To further simplify this version, the floating assembly was restricted to remain centrally located. Just like the experiemtnal setup however, a total translational range of 0.34 mm was included. This meant that the clearance was maintained as a constant c = 0.17 mm, (i.e. y = 0.0 mm) for each pump.

Cannulation sites were added at the atria, ventricles, aorta and pulmonary artery as well as the VADs themselves. This added state parameters to the **x** vector as the system required the determination of two more pressures, (the inlet pressures of the VADs), and four flow rates, (the atrial and ventricular inlet cannula flow rates). The system model was therefore the same as that shown in Figure 5-21 except without the passive interaction due to clearance changes.

As the speed or the clearance above the impeller blades were changed the linear plots were scaled as translations of the plot in Figure 5-25 up or down the Head (H), or vertical axis. The generalised equation for the linear pump curves is,

$$H = A_1 Q + A_2 N + A_3 c + A_4 ,$$

Equation 5-13

where A_1 to A_4 are the linear performance function constants. These constants were not intended to be representative of the BiVAD pumps. They were selected by the candidate to be approximately representative of pumps of similar size. This was sufficient to ensure that the solution step had no problems incorporation these extra state variables.

Each VAD was assigned a linear performance function in the form of Equation 5-13. The LVAD performance curve was,

$$H_L = A_1 Q_L + A_2 N_L + A_3 c_{CL} + A_4,$$

Equation 5-14

and the RVAD performance curve was,

$$H_R = B_1 Q_R + B_2 N_R + B_3 c_{CL} + B_4,$$

Equation 5-15

where c_{CL} is the constant central hub position, (at centrally located position, $c = c_{CL}$ = 0.17 mm).

The constants were engineered to provide approximate performance curves for rotary pumps with a Ø50 mm LVAD impeller and a Ø100 mm RVAD impeller rotating at about 2300 RPM and 1200 RPM respectively. The employed coefficients along with their respective units are provided in Table 5-6.

Table 5-6: Linear Coefficients for the Version 2 Linear Pump Curve Simulation.

LVAD		RVAD	
A_1 (mmHg(L.min^{-1})$^{-1}$)	-0.2	B_1 (mmHg(L.min^{-1})$^{-1}$)	-0.2
A_2 (mmHg.RPM^{-1})	0.1	B_2 (mmHg.RPM^{-1})	0.02
A_3 (mmHg.mm^{-1})	-5	B_3 (mmHg.mm^{-1})	-3
A_4 (mmHg)	-85	B_4 (mmHg)	17

The values of A_3 and B_3 were negative as an increasing clearance would induce a drop in performance. Similarly, an increasing flow rate, (indicating a drop in vascular resistance), will correspond with a decreased pressure.

The approximated linear performance functions are shown in Figure 5-25. The figure shows a range of simulated pump speeds where the speeds, *N*, are given in RPM. A red dot on each plot indicates the operation point when the VADs are providing total support.

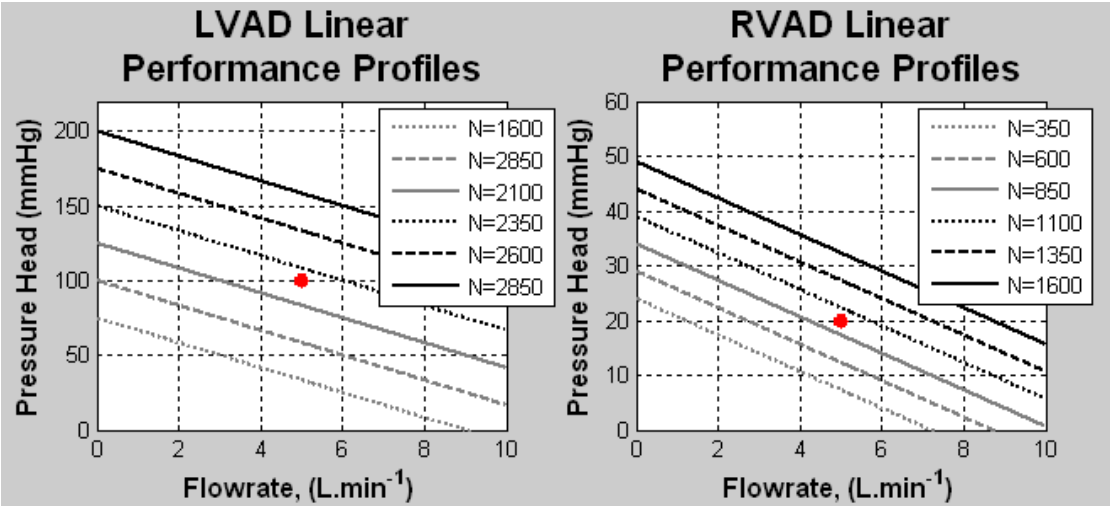

Figure 5-25: Linear approximations of the VAD's performance for Version 2 of the program. The plot shows a constant pump speed and impeller clearances.

Using this linear approximation the same $\underline{\mathbf{A}} \times \mathbf{x} = \mathbf{b}$ type solution could be used. The six added state parameters to the **x** vector required the addition of six new linear equations. Four of these were of the Equation 5-5 type determining the pressure drop due to the fluid resistance and inertiance within the inlet cannula. The final two were of the form given in Equation 5-13 to relate the pressure increase across each VAD to the flow rate. Note that there are no compliant components to the cannulae and VADs. It is assumed that these were all rigid.

A five second trace from a 160s simulation of a supported patient with Bi-Ventricular Failure, BiVF, is shown in Figure 5-26. The simulation was built by specifying a 90% decrease in ventricular contractility and the pump speeds were 2300 RPM and 1100 RPM for the LVAD and RVAD respectively.

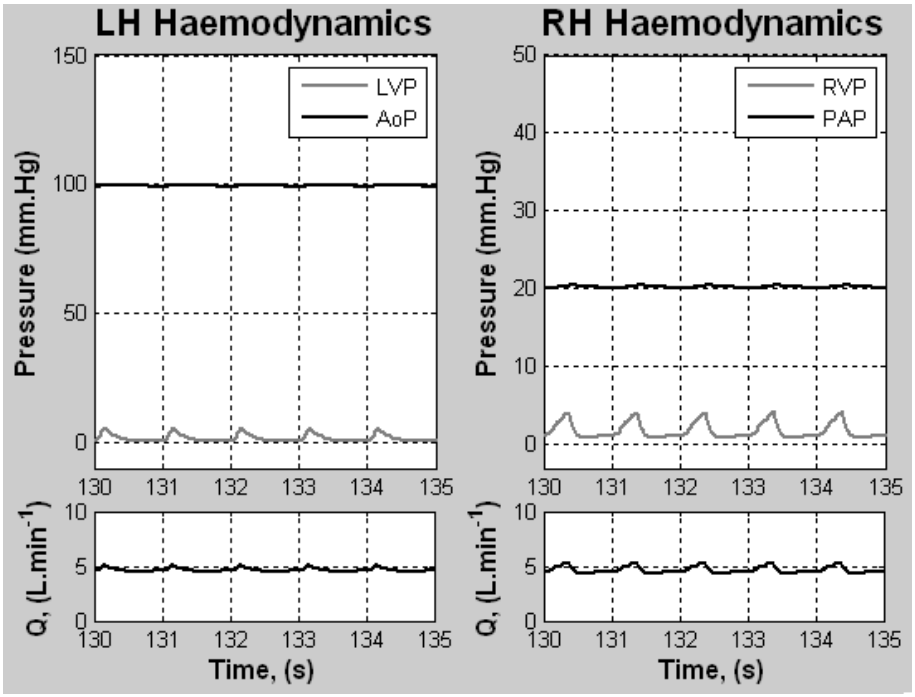

Figure 5-26: Simulation of supported patient with BiVF using the linear performance VADs.

Since the clearance and pump speeds were constant throughout the simulation shown in Figure 5-26, the transient pump operating points all lie on the linear performance profiles as shown in Figure 5-27. The red dots indicate discrete transient states down-sampled from the last 40s of the time-stepped solution. The range of flow rates that the transient states cover is an indication of the residual pulsatility provided by the ventricles.

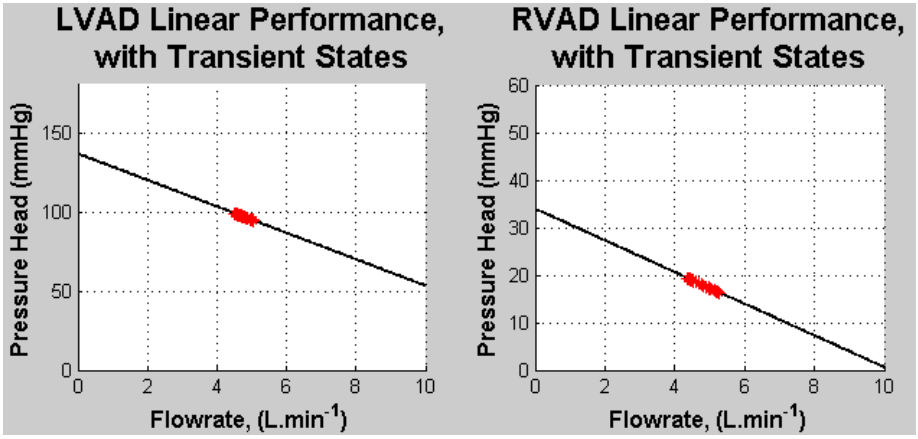

Figure 5-27: Transient VAD states, $\Phi_n = (H, Q)_n$, where the pump speeds were 2300 RPM and 1100 RPM for the LVAD and RVAD respectively and the clearances maintained at 0.17 mm.

Version 2 successfully saw the implementation of the pumps and cannulation sites into the original CV simulation. Simulated Bi-Ventricular Support, BiVS, was achieved with the flexibility to nominate *N*, *c* and level of heart failure, (hf). The next step will be to implement the passively responding floating assembly.

5.5.3 Version 3: Implementing the Dynamic Passive Controller

The third version was developed to incorporate the dynamic pusher plate action: the essence of the passively controlled BiVAD. This new version had a new state variable; *y*, the hub position. To prevent confusion it is worth reiterating that *c*, coupled clearance above the impeller blades, is the clearance between the impeller blades and the lower shroud. The variables *y* and *c* therefore, are closely related as *y* is the floating assembly, or hub, position. For any given *y* therefore, there will be corresponding *c* values for both the LVAD and the RVAD.

To include the hub position, *y*, the linear system needed to incorperate another equation. This equation is the dynamic equation which related the floating assembly's position, velocity and acceleration to the resultant force upon the assembly from the VAD pressures as well as the forces associated with the Passive Controller's dynamic components. The free body diagram of the floating hub, as seen in the previous chapter, is reiterated in Figure 5-28.

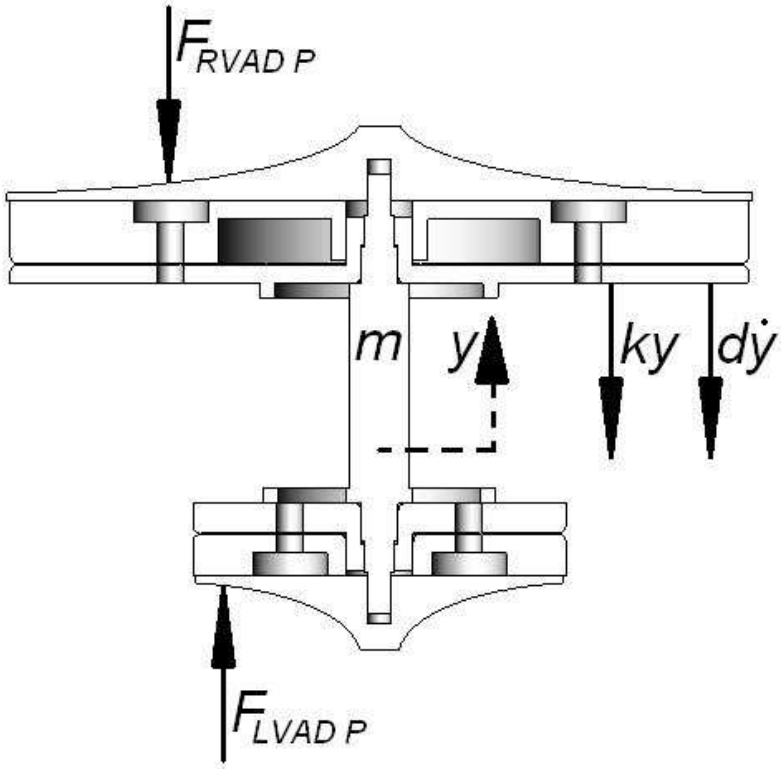

Figure 5-28: Free body diagram of the floating assembly with the Passive Controller, where $F_{LVAD\ P}$ and $F_{RVAD\ P}$ are the pressure forces from each VAD, *y* is the displacement of the hub from its central position, *m* is the mass of the floating assembly, *k* is the effective spring stiffness and *d* is the damping coefficient.

This single Degree Of Freedom, DOF, system's equation of motion is an Odinary Differential Equation, (ODE), where,

$$-d\dot{y}-ky-F_{RVAD\_P}+F_{LVAD\_P}=m\ddot{y}.$$

Equation 5-16

This was linearised in time by assuming that between each time step the rate of change of displacement was constant to give,

$$-d\left(\frac{y^{i}-y^{i-1}}{\Delta t}\right)-ky^{i}-F_{RVAD\_P}+F_{LVAD\_P}=m\left(\frac{y^{i}-2y^{i-1}+y^{i-2}}{\Delta t^{2}}\right).$$

Equation 5-17

In the physical prototype the forces $F_{RVAD\ P}$ and $F_{LVAD\ P}$ are, by definition, a representative pressure function, *p(r)*, integrated across the surface of the lower shroud. As an example the LVAD pressure force, $F_{LVAD\ P}$, is given in its general form,

$$F_{LVAD\_P} = \int_{r_{inlet,mean}}^{r_{outer}} p_{LVAD}(r) \times 2\pi r dr \ .$$

Equation 5-18

Since the pump is by nature a pressure source within the system there is a non constant pressure distribution within the pump. This is the same for the lower shroud as there will be a pressure profile that increases from inlet pressure at the eye of the shroud to outlet pressure at the periphery of the shroud.

A review of a number of CFD simulations within miniature blood pumps showed that there seemed to be a largely linear pressure development profile across the radius of the shroud (Chua *et al*. 2005; Miyazoe *et al*. 1999; Burgreen *et al*. 2001; Zhang *et al*. 2006). However, the nature of the pressure development with respect to shroud radius was not discussed directly in any of the articles. So an assumption was made by viewing static pressure plots within these articles. It was assumed from the article material that the pressure development is approximately linear. To illustrate the pressure function, again the LVAD is used as an example. The radius dependent pressure function is,

$$p_{LVAD}(r) = p_{37} + \frac{r - r_{inlet}}{r_{outlet} - r_{inlet}}(p_6 - p_{37}),$$

Equation 5-19

where the pressure indexes can be found in Figure 5-21.

A five second trace from a larger simulation is presented in Figure 5-29. The simulation included a hub translation range of y = ±1.5 mm, (therefore a total translational range of 3.0 mm). Note this range was reduced dramatically in later simulations. Left and right ventricular function was decreased by 90% and 50%

respectively and the respective VADs operated at N = 2200 and 1050 RPM respectively.

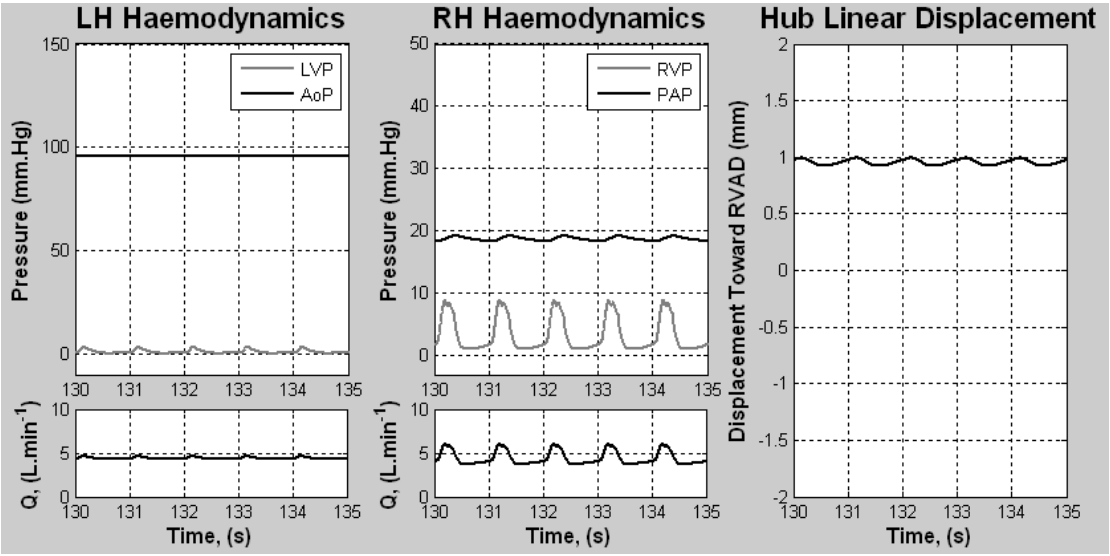

Figure 5-29: Simulation of supported patient with BiVF using the linear performance VADs with a passively responding floating assembly.

The transient hub position is now shown on the right hand side of the figure and the oscillatory inlet condition is causing slight perturbation in the c profile.

Figure 5-30 provides a similar plot to that shown in Figure 5-27 although the VAD performance profiles are shown at c = 0 and 3.0 mm. These are the two extreme positions of the floating assembly.

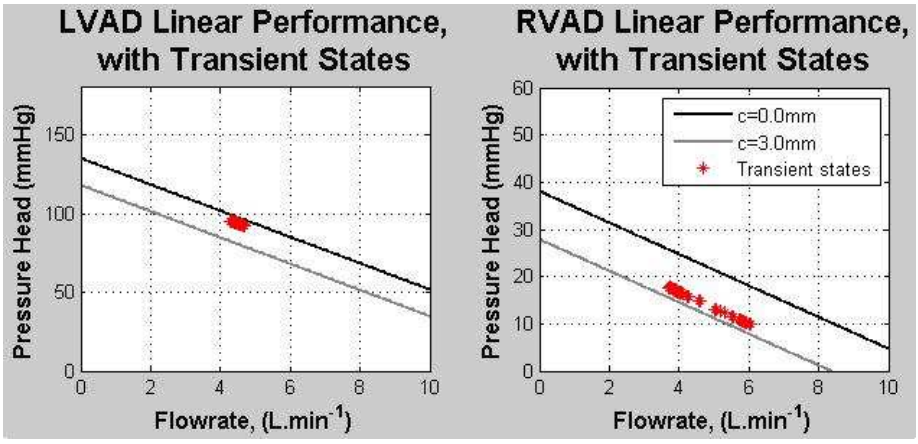

Figure 5-30: Transient VAD states, (H, Q, N, c), where the pump speeds were 2200 and 1050 RPM for the LVAD and RVAD respectively. Included are the linear VAD performance profiles a c = 0.0 mm and $c = 2\times c_{CL}$ = 3.0 mm.

At this point, the dynamics of the passive controller had been successfully assimilated into the program. Progress from this point required the incorporation of the experimentally derived pump performance interpolating functions. Incorporating these functions was the most time consuming part of the development of the program. This is detailed in the next section.

5.5.4 Version 4: Circulation Model Using Experimental VAD Performance Curves

As discussed earlier, experimental testing of the BiVAD rotary pumps highlighted non-linear relationships between pump performance and clearance *c*. Due to the importance of this variable in this study, these non-linear relationships could not be ignored in the construction of the numerical simulation.

Much effort was involved in constructing the solution algorithm so that non-linear pump performance functions could be used. To incorporate these functions into the already linear system saw numerous attempts that were rendered unstable. Because the VAD inlets subjected the pumps to a pulsatile operating environment, the high rates of change of inlet pressure and pump flow rate created a system with little tolerance for solution fragility. All the failed attempts to create a robust linear approximation have been documented in Appendix C provided on the attached compact disk. The Parabolic Performance Vertex Adjustment Method, the most successful method, is documented in this section. It is explained in a number of steps, initially starting with explaining how the clearance decrement functions are incorporated into the performance function then the means of linear approximation of the performance functions.

5.5.4.1 The Incorporation of the Decoupled Decrement Functions, ξ_H and ξ_Q

Ideally the function given in Equation 5-8 would have been used to model the pump performance curves. This function relates the pressure head, *H,* to a product of a second order flow rate polynomial, a second order pump speed polynomial and an exponential clearance function. However, this function incorporates a number of non-

linear features including the Q^2 and exp(c) term and the associated products of flow and clearance terms. This makes its use in the linear $\underline{\mathbf{A}} \times \mathbf{x} = \mathbf{b}$ type solution impossible unless additional functions can be sourced for each of these non-linear terms. So, a robust method for linear approximation of the performance function was needed.

To begin with, the Decrement Functions were decoupled from the performance function. This provided three functions, the performance function $H(Q,N)$ as given in Equation 5-12, and the pressure and flow decrement functions; Equation 5-9 and Equation 5-10.

An explanation of the use of these three functions to arrive at a suitable linear approximation of the performance function will begin with describing the use of the decrement functions. Let us assume the program is being employed to run a BiVS simulation. At some time t^i the operating points for each of the VADs from the previous time step t^{i-1}, (i.e. $\Phi^{i-1}{}_{LVAD}$ and $\Phi^{i-1}{}_{RVAD}$), is known. Thus, for each VAD the pressure head, flow and clearance, $\Phi^{i-1}(H^{i-1},Q^{i-1},c^{i-1})$, (note, the pump speed is constant during an entire simulation). Since the solution progresses through time, the clearance is also known from two time steps ago c^{i-2}. With this in mind, a procedural explanation follows which is carried out every time step to adjust the numerical approximation of the VAD performance curves.

Now consider one VAD only. Figure 5-31 shows a sketch of the VAD performance at c = 0 mm and $c = c^{i-1}$. The operating point at $t = t^{i-1}$ is also shown with the associated hydraulic coordinates.

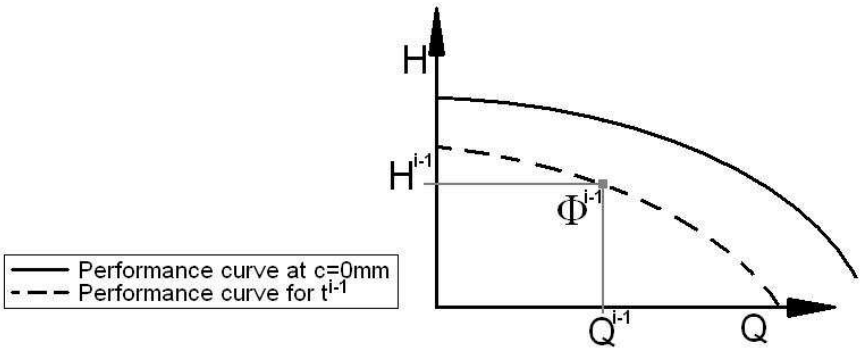

Figure 5-31: Performance description of a VAD showing the performance curves at c = 0 mm and at $c = c^{i-1}$. Also located is the VAD operating point, Φ^{i-1}, at time t^{i-1}.

Note that the performance curve at t^{i-1} is below the performance curve at c = 0 mm. This is because at t^{i-1} the VAD was operating at a clearance c^{i-1} which incorporated a degraded pressure and flow according to the decrement functions Equation 5-9 and Equation 5-10. It is assumed, provided the solution method is reasonably accurate, that the performance curve at t^{i-1} was correctly located and therefore Φ^{i-1} is representative of the VAD's performance at that clearance.

Now 'grounding' pressure and flow coordinates are found, $H^{i-1}{}_G$ and $Q^{i-1}{}_G$ respectively which will prevent the updated position of the performance function from drifting. The locations of these coordinates are shown in Figure 5-32.

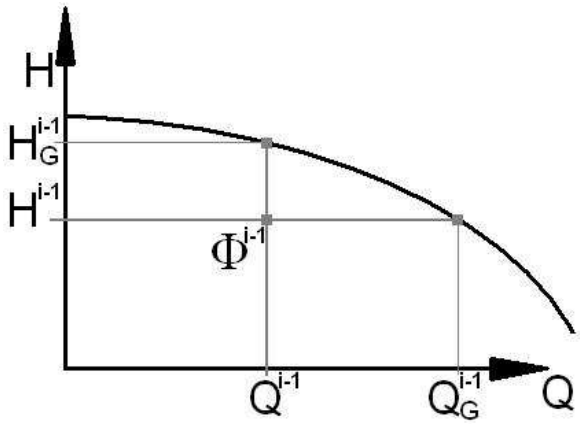

Figure 5-32: Location of the 'grounding' coordinates, $H^{i-1}{}_G$ and $Q^{i-1}{}_G$, with which the updated performance function will be evaluated.

$H^{i-1}{}_G$ is found by simply evaluating the quadratic performance equation, Equation 5-12 at Q^{i-1}. The grounding flow rate, $Q^{i-1}{}_G$, was evaluated by rearranging Equation 5-12 to form the quadratic,

$$\begin{aligned}&\left[Q_G^{i-1}\right]^2\left(D_1N^2+D_2N+D_3\right)+\\&\left[Q_G^{i-1}\right]\left(D_4N^2+D_5N+D_6\right)+\\&\left(D_7N^2+D_8N+D_9-H^{i-1}\right)=0\end{aligned},$$

Equation 5-20

and solving for the roots, from which the maximum root was selected.

Now, the program prepares to solve the linear system for time $t = t^i$. Initially, a linear approximation of c^i is made using c^{i-1} and c^{i-2}. This assumed value of what c^i will be is then used to evaluate the pressure and flow clearance decrement functions, ξ_H and ξ_H for the i'th time step. This provides a guess at what the proportional reduction in pressure and flow will be given a clearance c^i.

Now an approximation for what the degraded pressure and flow will be at $t = t^i$ can be evaluated. Using the new pressure and flow decrements; the magnitude of the degraded pressure and flow are found by multiplying them by the grounded pressure and flow, ${H^{i-1}}_G$ and ${Q^{i-1}}_G$. The evaluation of the degraded pressure head is graphically represented in Figure 5-33.

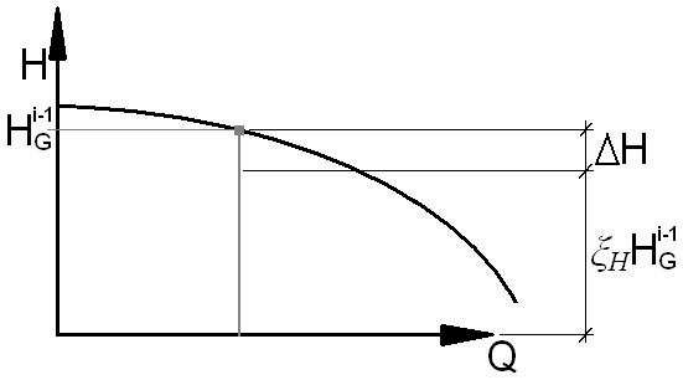

Figure 5-33: Sketch of the assumed degraded pressure head for $t = t^i$ evaluated using the pressure decrement and the grounded pressure head.

The difference between the grounded pressure head and flow and the assumed degraded pressure head and flow are now found, ΔH and ΔQ respectively. By definition, ΔH and ΔQ are the pressure and flow drop due to the associated assumed clearance c^i.

Now that the assumed pressure head and flow drop have been quantified, a new performance curve is found. This performance curve has exactly the same form as the performance curve at c = 0 mm. However, the vertex of the new performance curve has been shifted by -ΔH and -ΔQ as shown in Figure 5-34.

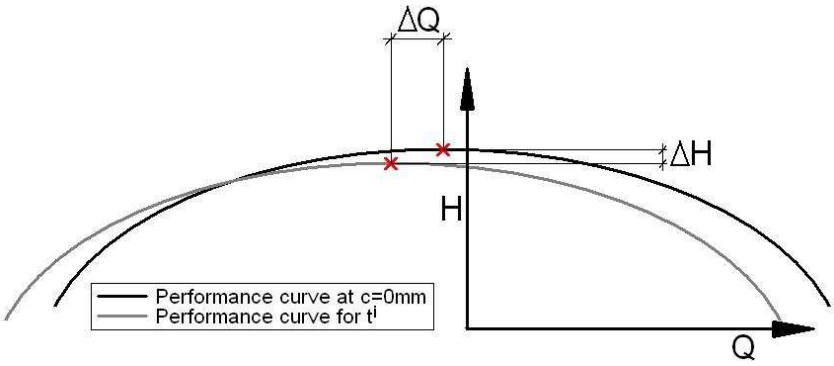

Figure 5-34: Sketch of the vertex adjustment to find the new performance curve given an assumed clearance of c^i.

To evaluate a function that is representative of the new performance function, the form of the parabolic function given in Equation 5-12 is manipulated to accommodate the vertex adjustment. Let us consider a generalised parabolic equation where a variable z has a parabolic relationship with x;

$$z = d(x-e)^2 + f\,.$$

Equation 5-21

This can then be rearranged so that,

$$\begin{aligned} z &= d\left(x^2 - 2xe + e^2\right) + f \\ &= dx^2 - 2dex + \left(de^2 + f\right), \end{aligned}$$

Equation 5-22

where z is a theoretical dependent variable, x is the theoretical variable, d is a constant, e is a constant prescribing the x coordinate of the vertex and f is a constant prescribing the z coordinate of the vertex.

The form of Equation 5-21 allows the parabola vertex to be explicitly positioned by defining *e* and *f*. A small amount of manipulation provides Equation 5-22 which is in the same from as the parabolic performance function as given in Equation 5-12. This allows us to define a new function used to find the approximated performance function at $c = c^i$,

$$H^i(Q^i, N) = dQ^2 - 2deQ + \left(de^2 + f\right).$$

Equation 5-23

In this equation, *d* is equivalent to the Q^2 coefficient as given in Equation 5-12. Note, it is reasonable that this coefficient doesn't change as this describes the second derivative of the function and therefore the function 'form'. Additionally, the position of the vertex of performance function at $c = 0$ mm is known as well as the magnitude of the hydraulic degradation due to $c = c^i$, $-\Delta H$ and $-\Delta Q$. With these it is possible to evaluate *e* and *f*. Therefore, evaluating the new coefficients of Equation 5-23 can be carried out every time step to update the performance function.

Now, a function which explicitly relates the developed pressure head, *H*, to the flow rate *Q* is obtained whilst incorporating the decaying effects of clearance on both the pressure and the flow. However, the function is still non-linear as *H* is proportional to Q^2. Some linear approximation of this function, therefore, needs to be made. This is done by formulating an approximating linear performance function for the VAD performance.

5.5.4.2 **Linear Approximations of the VAD Performance**

In order to determine a linear approximation of the non-linear performance function, both a performance gradient and a 'locating' operating point were needed. It is called a 'locating' operating point because, just like the constant *c* in the generic linear function y = mx + c, it positions the linear profile on a two dimensional axis. Finding the performance gradient was not a difficult task. However, since the vertex of the performance function is relocated every time step, the previous time step's operating point (Φ^{i-1}) was not a valid 'locating' point. So, a dummy location operating point,

Φ_D, was required to be evaluated every time step. The linear approximation of the performance function was then defined using,

$$H(Q)^{i}_{Lin} = H_D + \frac{\partial H}{\partial Q}\left(Q^i - Q_D\right).$$

Equation 5-24

It was important, of course, that the dummy operating point lay on the updated parabolic performance function. This is important to ensure that the integrity of the 'grounding' of the performance function to the performance at c = 0 mm was maintained; otherwise the performance would be able to drift in a similar way to an unearthed electric potential. So, the flow rate from the previous time step, Q^{i-1}, was used, and a new pressure head was evaluated upon the new performance curve as graphically illustrated in Figure 5-35.

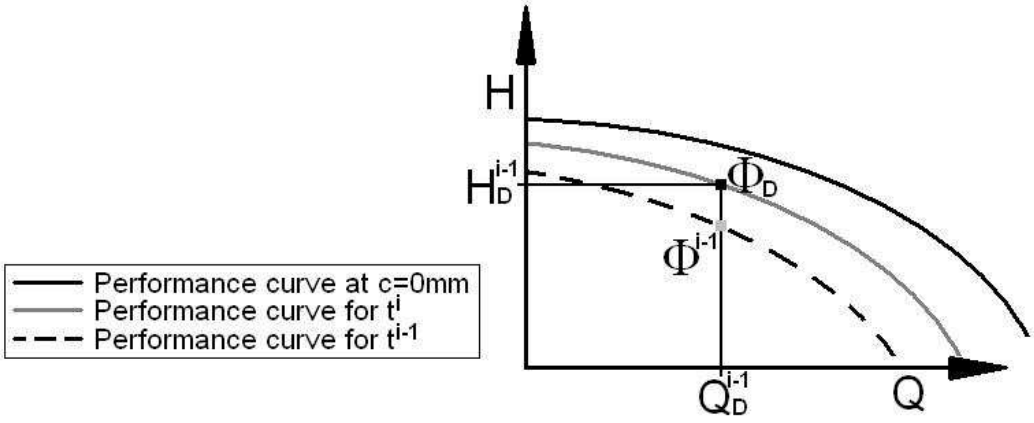

Figure 5-35: Location of the dummy 'locating' operating point used for evaluating the linear performance approximation.

Now the approximated linear performance function, $H(Q)^{i}_{Lin}$, can be made using Equation 5-24. The performance functions are then formulated into the **A** × **x** = **b** type solution and all the system states are solved using the LU decomposition.

5.5.4.3 **Issues with the Solution Method**

There are, of course, a number of issues involved in the solution method. Aside from the linear approximations in time, these issues arise through the potential errors in the linearization of the VAD performance functions and the decoupled functions.

As discussed, in creating linear approximations of the VAD performance curves a dummy pressure head and approximated clearance are required. These two approximations certainly have the highest potential to cause instability in the solution particularly if the transient pressure head or clearance profile becomes highly unsteady. Fortunately, in the case of the clearance approximations, high damping of the floating assembly motion is considered advantageous to filter pulsatile pressure signals. Given this damped motion, provided the time step is sufficiently small, it is likely that a linear prediction of the clearance will be sufficiently robust. As for the pressure head error, an analysis of this error will be carried out in a 'worst case scenario' simulation. This will be done later in this chapter once an appropriate time step has been selected.

Another issue is the use of the decrement functions in their present form to simulate the effect of clearance on the developed pressure head and flow rate. Recall that for each VAD, the decrement functions were based on experimental data taken at one speed, N, and a set circuit resistance, R. In order to remove the effect of pump speed on the pressure and flow drop, the decrements were normalised. However, this linear scaling will not completely remove the effect of pump speed; after all, it was considered that the pressure and flow have a slightly parabolic relationship with pump speed.

The effect of circuit resistance was not so easy to minimise. Consider Figure 5-36 where a pump is operating at some pump speed N at a clearance $c = c_a$. Depending on the vascular resistance, e.g. R_1 or R_2, the pump will operate at the corresponding operating point; Φ = A or B respectively.

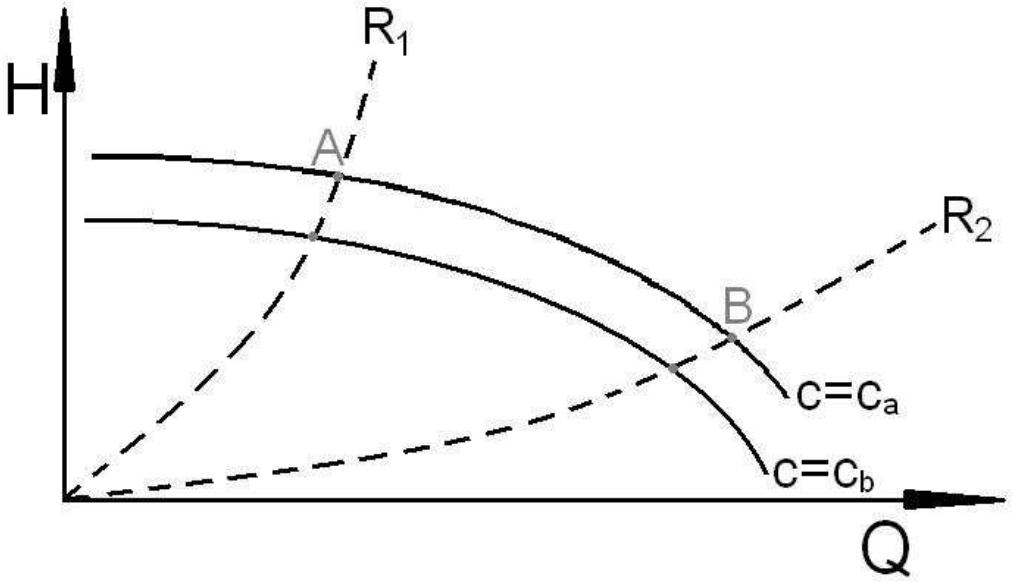

Figure 5-36: Sketch of a pump performance curve at two different clearances, $c = c_a$ and $c = c_b$.

Now let the clearance be increased from $c = c_a$ to c_b. In doing so, the operating point will follow down the profile of constant resistance until it lies upon the new decayed performance curve at $c = c_b$. As can be seen from the figure, the change in flow rate and pressure head depends on the circuit resistance. If the resistance is high, e.g. R_1, then there will be a comparatively high pressure head drop and low flow drop. If the resistance is low, e.g. R_2, the decay will affect the flow more than the pressure.

Despite this discrepancy, the clearance decrement functions were kept in the solution method. It is understood that this will make the modelled VAD performances less representative. However, they allow an effective means of incorporating the effect of clearance on both the pressure head and flow rate into in the performance models within the linear solution.

5.6 Convergence

It is, of course, important to realise the required time step length to ensure that the solution has converged. Using a time step too large will induce errors incurred by the linear approximation made in time using the pressure flow relationship through vessels, (Equation 5-5 and Equation 5-7) and the ODE for the floating assembly's equation of motion, (Equation 5-17). So an analysis of the time step length and its effect on the result was carried out.

To do this, a 120 second BiVS simulation was set up. Left and right heart failure was simulated by scaling the inverse contractility during systole, (1/*C*), of each ventricle by 90%. Then the LVAD and RVAD pump speeds were set to *N* = 4020 and 940 RPM respectively and the ventricular cannulation sites were opened.

The simulation was then run using a range of time step lengths. A coarse time step length of Δt = 0.64 seconds was used to begin with, then the time step was halved successively so that,

$$\Delta t = \frac{0.64}{2^n},$$

Equation 5-25

where n = 0, 1, 2….12, (therefore 13 simulations were run). This provided a minimum assessed time step of $\Delta t = 1.5625\times10^{-4}$ seconds when n = 12.

The solution state vector for each successive simulation was compared at T = 120 seconds. This allowed sufficient time for initial condition induced perturbations to settle. Recall that 47 system states are evaluated every time step which includes pressures, flow rates and the floating assembly hub position. A normalised Euclidian norm, $\|x\|$, was chosen to compare the state vectors from successive simulations so as to include the error from all 47 states. A Euclidian norm effectively evaluated the length of a vector. In general then, if a vector x is defined as,

$$x = [x_1, x_2, x_3, \ldots\ldots\ x_{47}],$$

Equation 5-26

then the $\|x\|$ would be evaluated as,

$$\|x\| = \sqrt[2]{\sum_{k=1}^{47} x_k^2}\ .$$

Equation 5-27

For some value of n, let $j = \Delta t$ and $j + 1 = \Delta t/2$. From the simulations with time steps j and j+1, the solution vectors at T = 120s were extracted for comparison. The normalised error, E^j, was then evaluated according to Equation 5-28.

$$E^j = \frac{\left\| x^j - x^{j+1} \right\|}{\left\| x^{j+1} \right\|}$$

Equation 5-28

Thus, E^j provides a scalar representation of the error between subsequent refinements of time step length. A plot of the scalar error E^j, vs. number of time steps per second is shown in Figure 5-37.

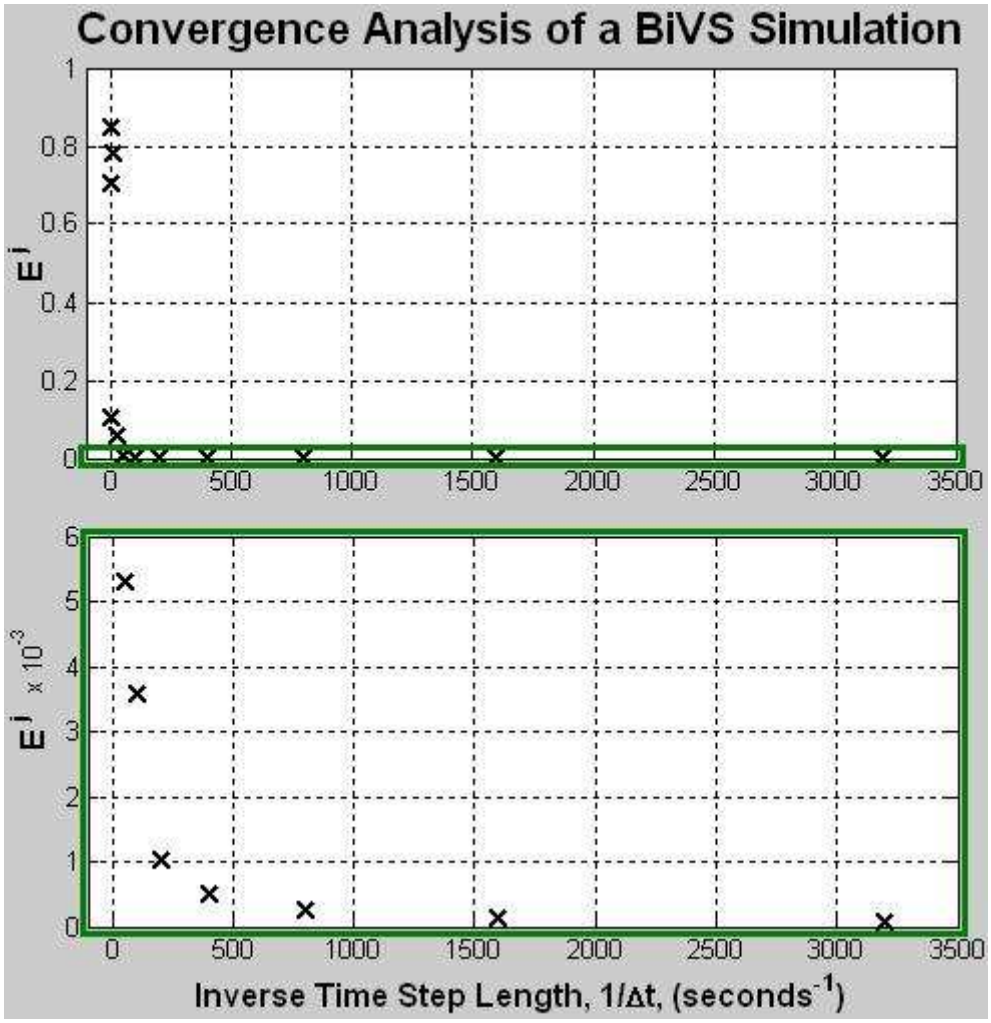

Figure 5-37: Normalised error vs. number of time steps per second for a 90% BiVS simulation, (above), with a reduced 1/Δt scale (below).

The above plot in the figure shows the resulting error for all the compared simulations. Note, since n = 0 to 12 (i.e. 13 simulations), and comparisons were made between simulations, there were 12 comparisons made and therefore 12 data points plotted. For clarity, the below plot has been included with a reduced scale showing the last seven comparisons of state vectors. It is apparent that the difference between solutions does not vary much after 200 time steps per second, (Δt = 0.005s, or n = 7). However, it is difficult to see using the absolute error and inverse time step lengths as axis. Figure 5-38 compares the $\log_{10} E^{j}$ and the time step exponent, n, see Equation 5-25.

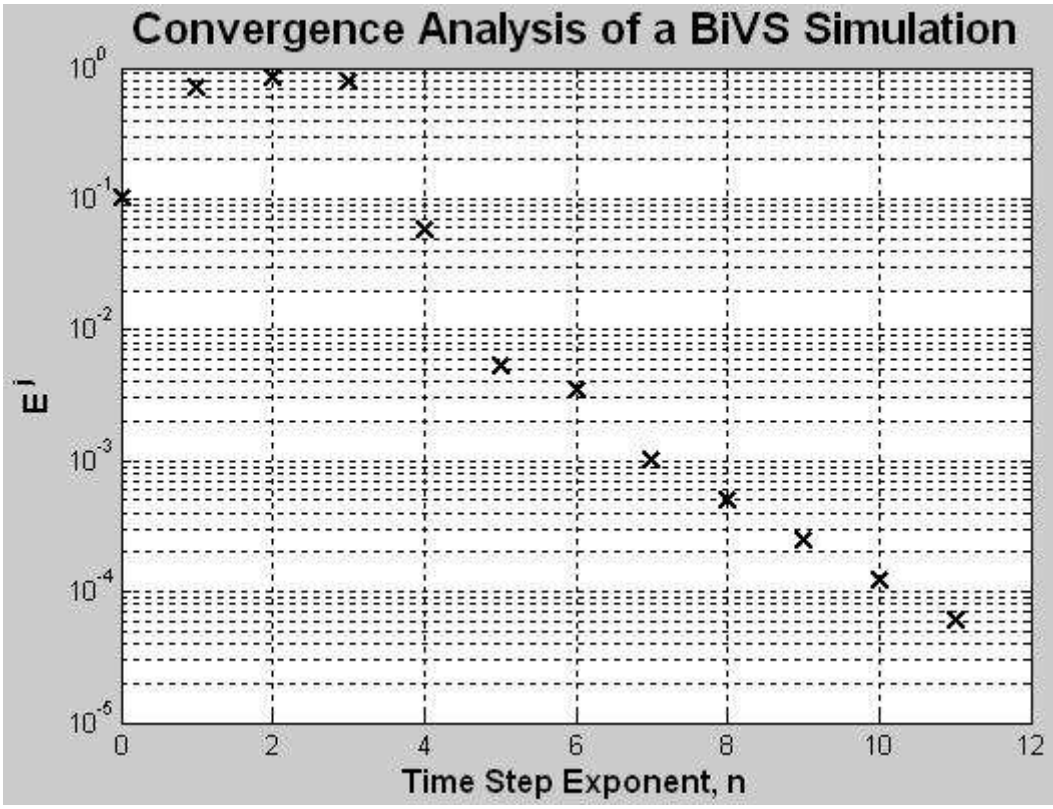

Figure 5-38: Normalised error (log scale), vs. time exponent, *n*.

The profile becomes approximately linear after n = 7. For future simulations it will be considered that the solution will have converged provided that $n > 7$. A time step of Δt = 0.0025s, or n = 8, will be used from this point forward. This time step incorporated an error of less than 5×10^{-4}, or 5×10^{-2} %.

5.7 Examination of the Linear Performance Approximation Method with Clearance Decrements

Convergence criteria can now be met by setting the time step. This allows certainty that successively smaller time steps will have no detectable effect on the result. So, now the program is tested to make sure the errors are small from the linear performance approximations using the Vertex Adjustment Method.

5.7.1 Method

To test the hydraulic solution method, two support simulations were carried out for analysis. The first simulation was a 'worst case senario' with respect to solution stability. This lack of flow continuity was used to observe how the VAD performance equations would handle numerical discontinuities such as the arterial valves suddenly opening. For this simulation the level of heart failure and BiVAD support was adjusted such that there was fluid ejection through the cannulation sites and heart valves. The left heart was modelled with a 40% reduction in systolic inverse compliance and the right heart with a 30% reduction. The LVAD and RVAD pump speeds were set to N = 3490 and 820 RPM respectively.

A second simulation was run using the same 90% heart failure simulation used in the convergence study earlier. This will be used to see what the induced errors would be for the type of simulation which will most commonly be presented later in this thesis.

Both simulations aimed to restore the arterial pressure and flow rates to healthy levels. An air spring was included in the 'worst case scenario' simulation to ensure that the hub did not reach the y = 0.15 mm limit. This was to stop any error from the program's forcing of the clearance position to stay within the hub translational limits, (y = ±0.15 mm).

For simulation, three transient error profiles were measured. These were the LVAD and RVAD pressure errors due to the use of the dummy pressures, H_D^{i-1}, for each VAD and the clearance error due to the linear approximation of the clearance for the evaluation of the decrements. The error was evaluated by taking the difference

between the estimated values, (the dummy pressures or approximated clearance), and the resulting VAD pressure heads and clearance from the LU decomposition. The errors were then normalised. Choosing the quantity with which to normalise the errors was an issue. Initially, the formulations given in Equation 5-29 and Equation 5-30 were used to find the normalised errors. To render a percentage error, the order of the error was increase by two so that,

$$Error_H^i = \frac{H_D^{i-1} - H^i}{H^i} \times 100,$$

Equation 5-29

and,

$$Error_c^i = \frac{c_{approx}^i - c^i}{c^i} \times 100.$$

Equation 5-30

However, when the simulation saw solution VAD pressure heads and clearances near nil, the errors became excessively large. These large errors were not representative of the solution strategy, but were a product of the numerical scale on the denominator. So, standard pressures, (MAP), and clearances, (y_{max}), were used on the denominators of both error functions so that,

$$Error_{H,LVAD}^i = \frac{H_D^{i-1} - H^i}{100} \times 100,$$

Equation 5-31

$$Error_{H,RVAD}^i = \frac{H_D^{i-1} - H^i}{20} \times 100,$$

Equation 5-32

and,

$$Error_y^i = \frac{c_{approx}^i - c^i}{y_{\max}} \times 100 = \frac{c_{approx}^i - c^i}{0.15} \times 100 .$$

Equation 5-33

5.7.2 Results

The transient haemodynamics over one second for the first simulation are shown in Figure 5-39. Also included are vertical black lines to indicate the opening and closing of the mitral, aortic, tricuspid and pulmonary valves, (e.g. MC indicates the Mitral valve Closing, PO indicates the Pulmonary valve Opening, etc.). The plots show the absolute ventricular and arterial pressures as well as absolute arterial and VAD flow rates. The VAD pressure head has been left as a mean pressure so as to provide some indication of the level of work done by the VADs. Recall, the absolute VAD pressure is the difference between the absolute arterial and ventricular pressures.

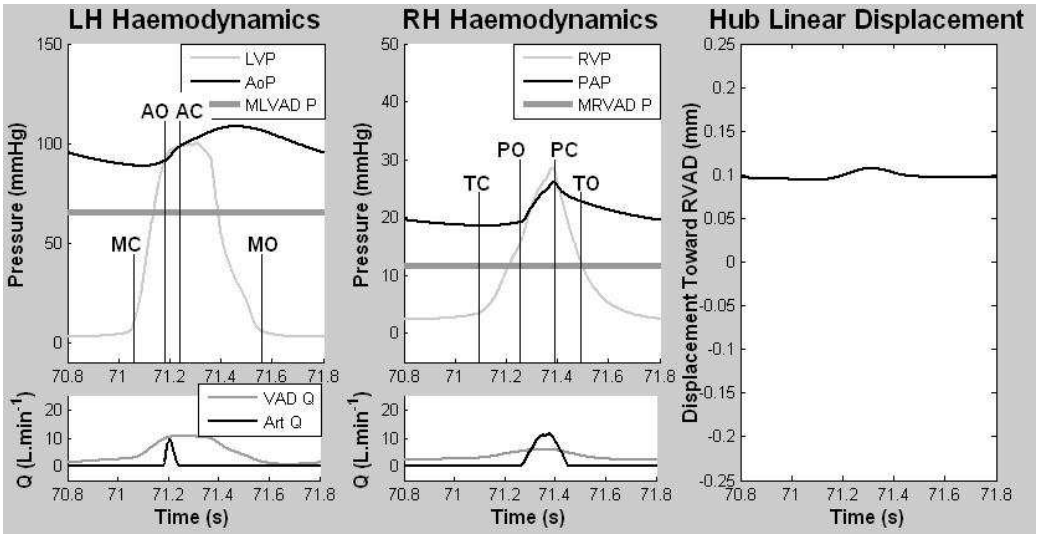

Figure 5-39: Modelled haemodynamics for the first linear performance examination simulation with annotated valve actions, (the 'worst case scenario' simulation).

The transient errors over the same time range has been plotted for the LVAD dummy pressure, the RVAD dummy pressure and the clearance as shown in Figure 5-40. The valve has also been included.

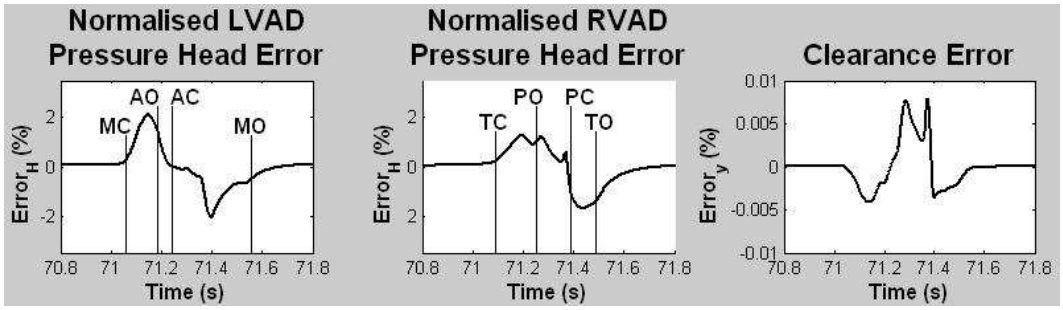

Figure 5-40: Transient errors for the first linear performance examination simulation with annotated valve actions, (the 'worst case scenario' simulation).

The haemodynamic and error results for the second simulation are shown in Figure 5-41 and Figure 5-42.

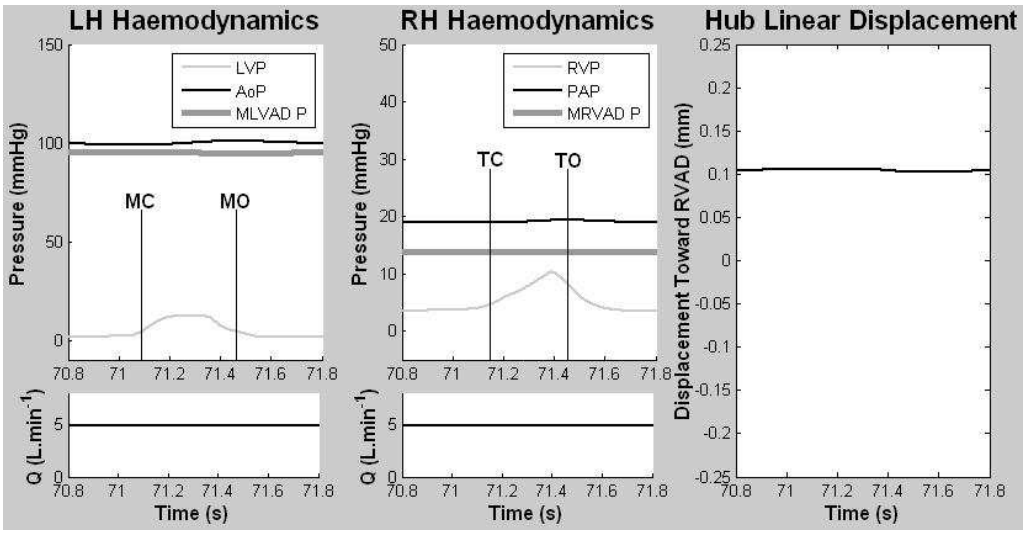

Figure 5-41: Modelled haemodynamics for the second linear performance examination simulation.

Note the different error scales used in Figure 5-42 and Figure 5-40.

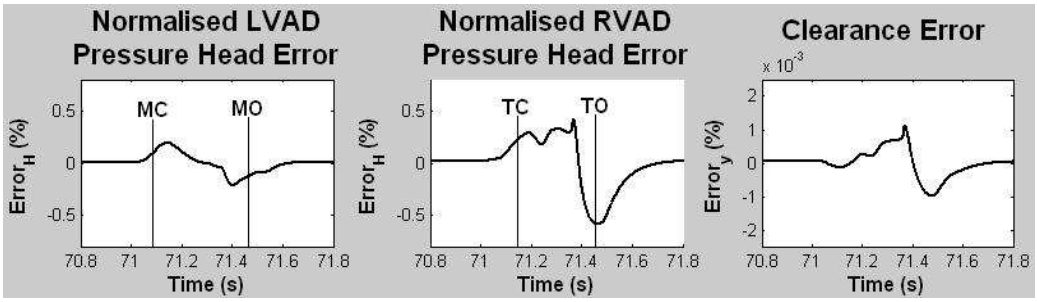

Figure 5-42: Transient errors for the second linear performance examination simulation.

5.7.3 Discussion

The most obvious observation from these results is that the worst case scenario did incur significantly higher errors through the linear approximations associated with the VAD performance functions. The next observation is that the errors associated with the dummy pressure estimates, $Error_H$, were significantly higher than the hub position errors, $Error_y$. This is probably because some damping was used for the hub's motion.

The arterial valves do not open in the second simulation. This is because the severity of the heart failure, (and therefore reduction in the inverse systolic compliance), is high enough so that the ventricular pressure doesn't become high enough to drive fluid through the arterial valves.

It is interesting to see that the opening and closing of the valves did not identify with sudden increases in error magnitude. It seems that the magnitude of the error was probably more dependent on the magnitude of the second derivative of transient pressure head and hub position profiles. For instance, a high value of $\partial^2 c/\partial t^2$ would increase the local error associated with making a linear approximation for c^i.

A low level support simulation, therefore, provides the most precarious hydraulic environment for the linear approximations associated with the Vertex Adjustment method. Given that the first simulation is a 'worst case senario' it can assume that the maximum associated error will not exceed 2%. This is a moderately large error. However, in terms of providing representative simulations of a passively controlled BiVAD, the solution method is still very effective.

5.8 Method of In Vitro *Simulation; the MCL*

Just like any model for simulation, the simulated results are only reliable if the model has been compared to either 'real life' results or another validated model. Since the passive controller BiVAD was tested in the Mock Circulation Loop (MCL) the numerical model was validated against MCL *in vitro* data. This aided in the

development of the device, particularly in the spring, mass, damper design, without time-consuming redesign and machining of new device parts.

5.8.1 Creating the Reduced MCL Circuit Structure

To simulate the MCL circuit structure in Figure 5-7 certain vascular sub-units were made redundant so as to create an exclusive flow path. The associated resistances within the redundant systemic branches were set to be very high, thus preventing flow. Similarly, fluid was restricted from residing in these redundant branches by allocating very low associated compliances. It was a concern that the redundant systemic branch *R* and *C* parameters would induce instability through poor scaling of the **A** matrix. However, this was not the case, and MATLAB handled the solution well. Figure 5-43 shows a number of flow rate plots overlayed over Figure 5-5 during a healthy MCL simulation.

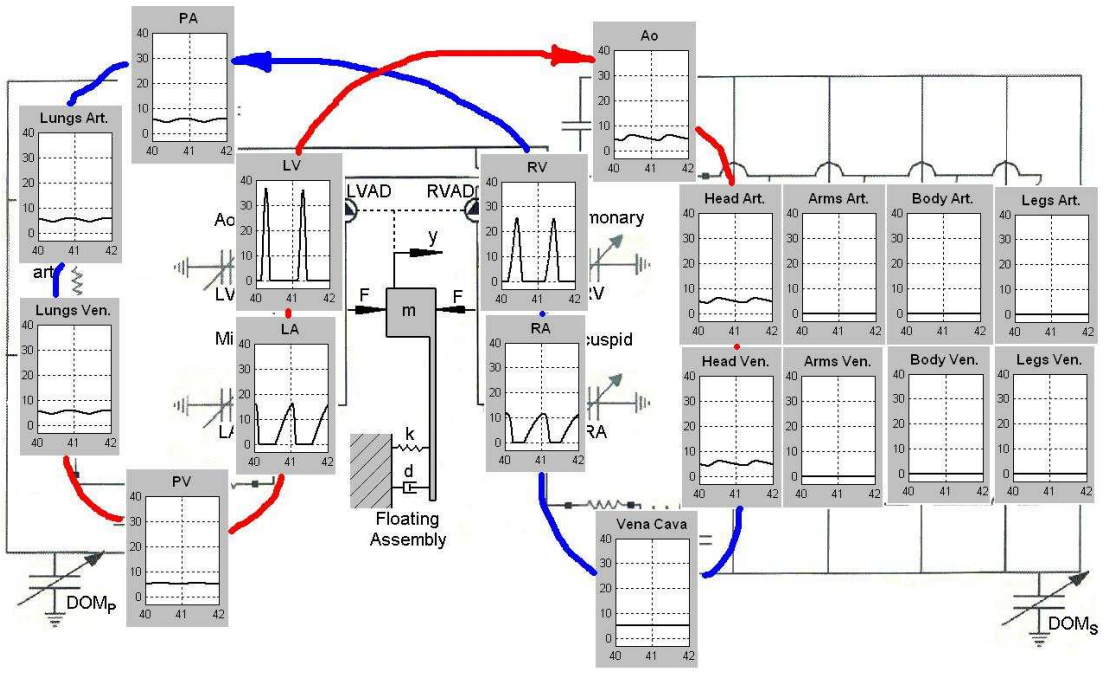

Figure 5-43: Overlayed transient vessel flow rate plots [*Q*, (L.min^{-1}) vs. Time (s)] for a Mock Circulation *in vitro* simulation of healthy unsupported haemodynamics.

Flow around the circuit has been indicated using red and blue lines. The red line, indicating oxygenated blood, originates from the lungs venous vessels and runs through the LH, into the aorta, and into the body. Then the deoxygenated blue flow path takes the fluid back to the RH and into the PA and lungs.

The figure shows pulsing flow through the head vessels which are used as the MCL 'body' branch. Additionally, the remaining three redundant branches display zero flow due to the imposed high resistances. The units for the plot have been omitted for clarity. They are [Q] = L.min^{-1} on the vertical axis and [Time] = seconds on the horizontal axis. A formal validation of the MCL simulation will be carried out in the following chapter. However, for now observe that the flow is isolated to one systemic branch.

5.8.2 Issues Associated with Simulation of the MCL

The primary intended function of the numerical model as an investigation tool is to simulate the Passive Controller BiVAD in a comprehensive and flexible human circulation model. This will allow a more comprehensive analysis of the device performance, when compared to the experimental study. So, the vascular sub-unit is specifically designed to model a flexible blood vessel. However, the MCL does not incorporate flexible tubes to model the resistive and compliant chambers. Instead, resistance is applied through inherent viscous drag through the plumbing and active solenoid valves, (SR and PR), and compliance is achieved using parallel upright cylinders as shown in Figure 5-44. Note that the direction of flow is different to that shown in the circuit structure in Figure 5-43.

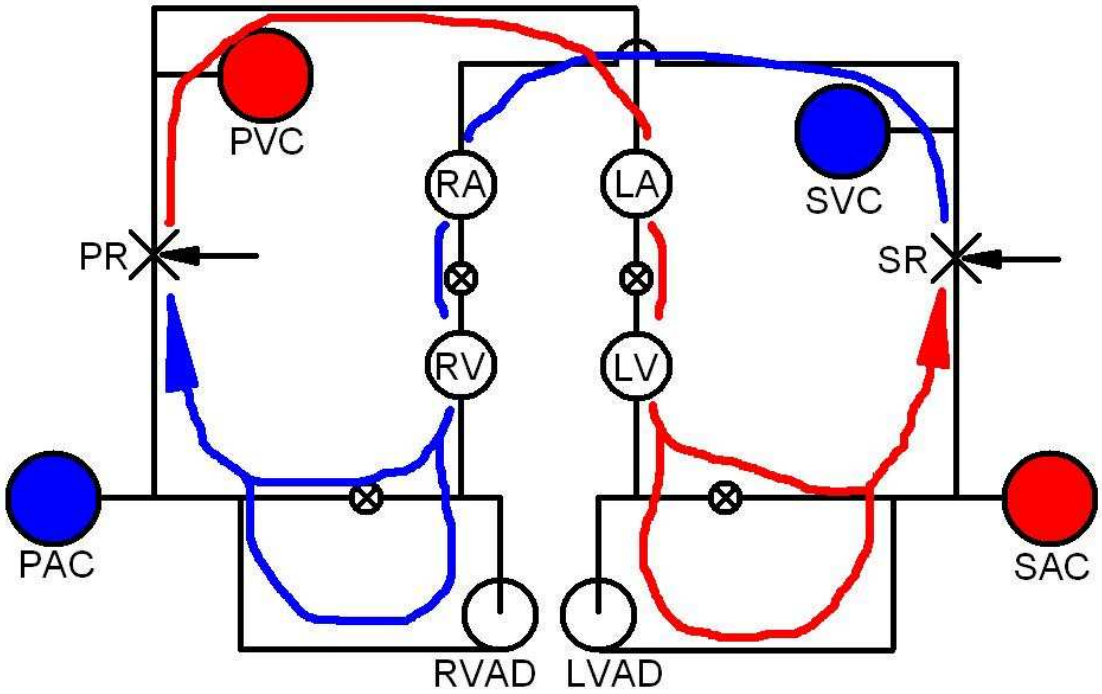

Figure 5-44: Schematic plan view of the MCL indicating parallel compliance chambers and bification locations. Note that the compliant vessel, indicated as red and blue circles are upright cylinders plumbed in parallel.

The global series circuit indicated by the red and blue arrows can be adequately modelled using the vascular structure in Figure 5-21. However, the parallel compliance chambers and their associated inertiances and resistances are not correctly characterised using the vascular sub-unit shown in Figure 5-8.

Calculation of fluid inertiance in the MCL simulation did not use the volume dependent equation used in the human simulations as given in Equation 5-3. Since the plumbing is rigid, both the vessel lengths and diameters stay constant. So, the relationship given in Equation 5-1 was used. However, this can only model the inertiance of the fluid moving through the horizontal plumbing sections, (i.e. along the paths indicated by the red and blue arrows in Figure 5-44). However, the inertiance of the fluid moving up and down the vertical compliance chamber and heart chambers is not negligible. In fact, it will be shown that the vessel inertiance could be increased by around 400% when considering the vertical movements of the fluid within these chambers. In the next chapter the validation step was used to approximate the combined vessel inertiances of the horizontal and vertical MCL plumbing.

5.9 Discussion of Numerical Program

The construction of the flexible model and numerical algorithm included a large body of work which, when including the large number of failed attempts, consumed a considerable portion of the candidature. The three major components of note were the development of the circuit structures, construction of the pump performance functions and the solution algorithm.

Encompassed within the entire human CV model there are 22 sub-units, 22 inertiance parameters, 22 compliance parameters (4 of these time varying), 26 resistance parameters (8 of these binary valves of cannulation sites), 18 vessel diameters and 18 vessel lengths. This provides a large amount of control upon the simulated cardiovascular response. It also allows for large errors to be made in parametric allocation.

This provided an issue for the program as there is very little literature providing comprehensive dynamic human circulation parameters. However, vascular parameters vary substantially between people of varying sizes, shapes and states of health. So, like other numerical models the parametric allocation will be based on a trial and error based method in the validation process. These will be documented in the next chapter.

The inclusion of a global inertiance was a novel feature of the circuit models. Calculation of the vessel fluid inertiance was achieved using a volume dependent function which has not been used in circulation simulation. Numerical stability was compromised when the inertiance was proportional to the inverse volume – this was the constant vessel length assumption. However, a constant vessel diameter assumption allowed stable calculations of the inertiance, even when the resident vessel volume was low.

Table 5-2 and Table 5-3 indicate that previous models have included no more than aortic and/or pulmonary artery inertiance parameters. It was found that global haemodynamics is most sensitive to the nominated inertiance parameters in the atria

and ventricles. After all, Equation 5-4 indicates that the pressure drop due to fluid inertiance is proportional to the rate of change of flow rate. The atria and ventricles experience the highest rates of change of flow as they are in close proximity to the heart valves. It was found that increasing the defined left ventricular diameter, (thus decreasing LV inertiance), decreased the difference between the peak LVP and peak AoP. This was because more fluid was able to pass through the Aortic valve. Similarly, increasing the diameter of the left atrium increased the end diastolic volume in the ventricle thus increasing the peak systolic ventricle pressure. These results are intuitive when considering a simplified scenario. It takes a smaller pressure differential to push a volume of fluid through a wider pipe.

Upon completion of the vascular circuit designs, the VAD interpolating performance functions and the solution algorithm were developed. These two tasks amounted to 95% of the workload sharing approximately equal portions. Due to the large amount of overlap between these tasks' development, some of the discussion too will overlap.

Attempts were made to build a completely non-linear solution algorithm using a Newton-Krylov decent method. This would have been useful as all non-linear relationships would have been fully coupled within the solution reducing the need for state approximation and convergence analysis. However, the inherently stiff system refused to cooperate with the non-linear solver within the time-frame available for this study. So, a linear $\underline{\mathbf{A}} \times \mathbf{x} = \mathbf{b}$ type solution was used and solved using an LU Decomposition of the $\underline{\mathbf{A}}$ matrix to minimise computational time. Given that a linear solution method was incorporated, all non-linear relationships were either decoupled or approximated using updated linear performance approximations.

Just like any numerical simulation, its quality is reflected in the representative nature of the numerical relationships. The VADs themselves needed to be included into the model and so the performance functions needed to be both representative and stable within the solution environment.

Pressure head H, flow rate Q, pump speed N and also blade clearance c needed to be included in these performance functions as experimental tests suggested that these

were performance sensitive parameters. However, the pump speed was to be maintained constant throughout the simulation. Experimentation also indicated that the H vs. Q and H vs. N both needed to be parabolic relationships and H vs. c and Q vs. c needed to be exponential. These non-linear relationships demanded development of the performance functions so that they could be incorporated into the linear solution algorithm.

Due to the desired performance function in Equation 5-8 incorporating numerous non-linear components, it was decided to decouple the effect of blade clearance completely from the linear solution. So the performance function now looked like $H(Q,N)$. The remaining non-linear variable component in the function, a Q^2 term, was included in the solution using a linear performance approximation updated every time step. The linear performance approximations each required a partial derivative $\partial H/\partial Q$ and a 'locating' operating point. Both of these employed the decoupled clearance decrement functions as well as the reduced performance function $H(Q,N)$.

An interesting effect was the 'two flows one pressure' problem when the interpolation functions were first used. The inverted parabola form of the H vs. Q relationship saw a global maximum at some flow near zero. When the VAD operating point moved from positive flow rates to this maximum, it was prone to 'slide' down the left side of the inverted parabola and induce high negative flow rates through the VAD. In practise, it is very difficult to induce negative flow through a pump so this region of the performance range was not tested.

To solve this issue, a piecewise performance function was used. The interpolating performance function was used for flow rates greater than the function maximum, and a steep linear function was used for flows lower than this. This was a binary decision made by the program, like the heart valves, using a linear interpolation to predict what Q^i would be before the LU decomposition solver was run. Since the VAD modelling in these flow ranges is not interpolated, simulations that employ the linear, low flow performance function will be subject to qualitative analysis only.

Development of the solution algorithm started with simulations of the unsupported vascular system just through the resistance, inertiance and compliance equations given in Equation 5-5 and Equation 5-7. The transient compliance profiles specified for the atria and ventricles provided the pulse input to the system and a healthy circulation simulation was achieved. This program was relatively simple to put together as the linearised vascular equations in time were stable and induced a low error.

When the BiVAD was incorporated into the solution, the associated non-linearities attributed to much instability in the program. Development was then focused on ways of including the non-linear VAD equations but solving them in a linear environment.

Excluding the attempts to construct a fully non-linear solution algorithm, a number of approximation techniques were used to predict the Q^2 term in the VAD performance functions. These included a quadratic state approximation, prediction-correction-observing functions, state preconditioning for initial stability and decoupling the Q^2 term into a $Q^i \times (Q^{i-1} + Qdiff)$ product. The methods either failed to settle the initial system or lacked stability during worst case scenario simulations of low level support. The Vertex Adjustment Method, however, showed high stability and accuracy and so was selected as the method to proceed through the validation step.

The Vertex Adjustment Method allowed the effect of blade clearance on the developed pressure head and flow to be modelled despite the coupled performance function being independent of clearance. This method first evaluated the pressure and flow decrements using a linear approximation of the clearance to determine the corresponding degradation of the pumps' outputs. Then the vertex of the parabolic performance curve was shifted to account for this degradation. The result was a parabolic function located such that it represented the pump's output given its respective clearance. A linear approximation of the parabolic function was then made based on the evaluated partial derivate $\partial H/\partial Q$ and a dummy operating point with which to provide the function 'location'.

Associated with the linear approximation of each VAD's performance are a number of issues which have the potential to cause errors in the solution. These are the linear

approximation of the clearance, the evaluation of the dummy operating point and the use of the decrement functions to model the effect of clearance on the VAD outputs. It was shown that in a worst case scenario simulation, the errors associated with the clearance and dummy operating point did not exceed 0.008% and 2% respectively. Errors incurred through the use of the decrement functions stem from their derivation from empirical performance data run at a single speed and a single resistance. Efforts were made to reduce errors from simulating different pump speeds by normalising the decrement losses. However, simulation error incurred through using difference vascular resistances could not be reduced. It is considered however, not so important as the BiVAD model will still incorporate a passive action and so aid in the understanding of this control strategy. What is most important is that the effect of clearance on both the pressure and flow rate can be modelled by the program. As shown in Appendix C, (see attached compact disk), including the degrading effect on both parameters was something very difficult to simulate using the linear model.

Convergence of the solution was analysed in a 90% BiVS simulation using a time step that was halved successively until the simulation time exceeded 2 hours. Successive solutions were compared by subtracting state solutions and a Euclidian norm was used to normalise the error. An analysis of the normalised errors showed the characteristic exponential decay which began to settle on a solution at time steps less than Δt = 0.005s. So, a time step of Δt = 0.0025s which had an associated error of less than 5×10^{-4}, or 5×10^{-2} %, was chosen for future simulations.

5.10 Conclusion

A flexible numerical model of the circulation was designed as a parallel investigation into passive control of cardiac support devices. A program written in MATLAB employs the model in a time-stepped linear solution algorithm. The program is useful for hydraulic simulations of healthy as well as diseased circulation. Most importantly, however, is the program's ability to simulate support devices augmenting circulation in the form of a VAD, BiVAD or total support device. This chapter introduced the model structure, program solution algorithm and means of employing experimental pump performance data to simulate the heart pump(s) performance.

The model structure was designed so that it could be used to simulate a complex human cardiovascular system as well as more simplified *in vitro* testing rigs. The model incorporates contracting atria and ventricles as well as the four main arteries and veins. Up to four systemic branches can be included in circulation simulations so as to model perfusion through different parts of the body.

The atrial kick and inertial parameters in the atria and ventricles were found to strongly dictate the global haemodynamics. Unfortunately, neither feature can be validated using the *in vitro* testing rig.

Simulation of the BiVAD prototype's operation used a combination of piecewise performance functions derived from experiments, clearance decrement functions and an ODE to model the floating assembly's motion. The performance functions were created from a product of polynomials and modelled each VAD's hydraulic performance with a blade clearance of $c = 0.0$ mm. Experimental results were used as boundary conditions (BCs) to construct the LVAD and RVAD interpolating performance functions. Forced, or engineered, BCs were also used in the construction of the RVAD performance function to 'tame' the function form to ensure it was representative.

Finally, the solution algorithm itself was a linear $\underline{\mathbf{A}} \times \mathbf{x} = \mathbf{b}$ type solution solved using an LU decomposition of the $\underline{\mathbf{A}}$ matrix to increase solution time. A number of non-linear relationships were included into the solution method through either decoupling from the solution step or linear approximation. The effect of decoupling on the solution error was analysed with a worst case scenario showing a maximum error of 0.25%. It was found that the solution result converged at time steps $\Delta t \leq 0.0025$s.

An excellent means of numerical circulation simulation has been developed to validate against *in vitro* results. The inclusion of cardiac support devices modelled with geometry specific performance functions means that the results are representative of the prototype's pump geometry. Furthermore, the program can be used to compare individual support devices. Once validated, the program will be used to investigate the BiVAD prototype's operation in a more complex circulation model, i.e. human circulation.

6 Numerical Program Validation and Results

6.1 Introduction

This chapter introduces the numerical model as a validated investigation tool in order to predict the behaviour of the BiVAD device within the human circulation. To expand the study of passive control beyond the experimental work in Chapter 4, a more representative human vascular circuit is employed within the numerical model. Furthermore, since the BiVAD prototype was characterised numerically, a number of changes were made to increase the performance of the passive controller such as dynamics components, lower shroud radii and clearance decrement functions. This chapter adds to the understanding gained from Chapter 4 by offering a more comprehensive analysis of the passive control of cardiac support devices in humans.

The validation step employed a simplified vascular circuit in order to represent the plumbing structure of the Mock Circulation Loop, MCL. The numerical model simulated steady and unsteady MCL haemodynamics for comparison to experimental results. Vascular resistances and compliances were modified, as well as the VAD speeds and dynamic PC parameters to achieve similarity between the numerical and experimental simulations.

The validated MCL simulation is then extended to a complex human vascular circuit model and compared to human circulation data from the literature. Following this three supported circulation studies are presented. The first simulates steady support and the implications of the removal of the native pulsatile environment, and replacing it with a constant flow supported environment with a modified passively controlled BIVAD. Then the effect of periodic vasoconstriction from outside the arteries, such as breathing or exercise, during BiVAD support is examined. Finally a close analysis of the BiVAD's passive response to reduced venous return is simulated. The latter study was prompted by the occurrence of ventricular suckdown during hypertension simulations from the experimental testing. The three studies extend the understanding of passively controlled support beyond what was observable from the physical experiments.

6.2 Validation of the Numerical Program

As explained in Chapter 4 seven real time experimental data sets were recorded per simulation when testing the BiVAD prototype using the MCL data acquisition hardware. These were the two ventricular pressures, the aortic and pulmonary artery pressures, the systemic and pulmonary flow rates and the hub's linear displacement measurement. However, in order to validate the numerical model more data were needed to analyse the simulation performance. So, additional steady simulation tests were used for comparison which included atrial pressure measurements without the LVDT displacement. Atrial pressure traces allowed the CVP to be monitored as it is indicative of the right atrial pressure (RAP).

The ventricular Ejection Fractions, (*EF*), and Pressure Volume loop plots, (PV loops), were also derived from the numerical results and are presented as part of the validation. Since these relationships were not quantified experimentally they were compared with textbook data or checked that they were 'representative'.

Steady simulations include healthy and chronic heart failure (unsupported) simulations. As discussed in the literature review, the kidneys retain fluid when the heart fails to increase the Central Venous Pressure, CVP. This increases end diastolic ventricle volume in an attempt to increase the *EF*. A chronic heart failure simulation was chosen for the verification process so that the effect of circuit fluid volume could be tested more thoroughly.

Initially, these two simulations provided a means of checking that the solution algorithm was functioning correctly. Furthermore a number of simulation parameters were quantified by analysing pressures, flow rates, *EF* and pressure-volume (PV) loops. It is difficult to strictly define the analysis as the model required many parameters and the interdependence between them all upon the hydraulics of the system was very complex. However, an effort to explain this analysis has been made in the steady simulation discussion.

6.2.1 Quasi-Steady Simulation

The quasi-steady simulations included the healthy and unsupported chronic heart failure simulations.

Both simulation methods were allowed to settle from the initial static conditions into a quasi-steady operational state. The numerical model, for example simulated 80 seconds of circulation from start up. For clarity of the results however, only five cardiac cycles are shown from the last 10 seconds of the simulated circulation. This introduced a time scale along the x axis that provides sufficient resolution for comparison. Once again, it should be noted that the experimental results are set on a white background and the numerical model results have a grey background.

6.2.1.1 **Method**

Experimental Method

Additional experimental tests were run recording the atrial, ventricular and arterial pressures as well as systemic and pulmonary flow rates, (eight real time data traces). The tests simulated healthy and unsupported chronic heart failure.

Recall from the General MCL Operation Procedure, documented in Section 4.2.2, that the collective displacement of the compliance chambers, including the ventricles and atria, is around 1-2 litres. Addition of this volume, once all the horizontal plumbing has been filled and the pressure sensors set to zero, creates the physiological CVP of around 5mmHg. Due to error and drift in the pressure sensors as well as fluctuations in the mains compressed air reservoir, the pressure readings would vary during the test. An error of ±3 mmHg was assumed for the pressure readings. This is particularly important when referring to the RAP as an indication of the CVP as the error, 2 mmHg, is around 40% of the CVP.

Once the vascular compliances had been set, the healthy simulation was achieved through active manipulation of the ventricular contractility and vascular resistance. Chronic heart failure was then simulated by throttling the compressed air line to the ventricle chambers and increasing the fluid volume.

Numerical Set Up

The cannulation sites were closed by setting the VAD inlet resistances to a very high value, (900 mmHg.s.ml^{-1}). The simulation was started and allowed to settle. Once the solution was complete data was plotted for comparison with the experimental results. Plotted data included transient atrial, ventricular and arterial pressures as well as the systemic and pulmonary flow rates.

Tuning of the numerical model vascular parameters to achieve similarity involved incremental parameter adjustment. No formal tuning process was following due to the large number of parameters. Instead tuning the model consisted of a 'trial and educated adjustment' process. The vascular resistances, compliances and inertiances were varied along with the fluid volume and upper and lower limits of the transient ventricular compliance profiles. Sensitivity of parameters to particular haemodynamic characteristics will be commented on in the following discussion. Like the experimental tests, an air spring was not used and so the only proportional response was the inherent clearance spring driven by changes in VAD pressure head.

6.2.1.2 **Healthy Heart Function**

Figure 6-1 shows the results of a healthy simulation from the additional testing set. The layout and scaling of the plots have been kept similar between the experimental and numerical results for clarity and comparison.

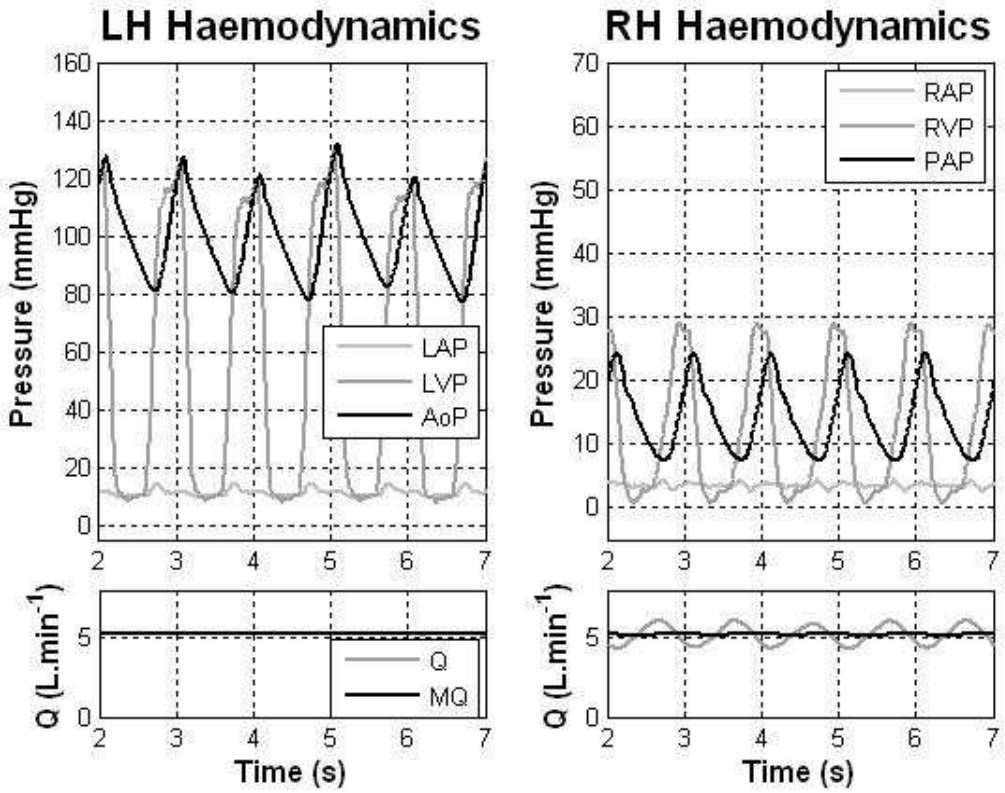

Figure 6-1: Simulated healthy haemodynamics using the Mock Circulation Loop.

This result was mimicked in Figure 6-2. The main discrepancies between the two simulations are the RAP and the pulsatility in the systemic flow profile. Note the difference in the figure colour schemes indicating an experimental result in Figure 6-1 and a numerical simulation result in Figure 6-2.

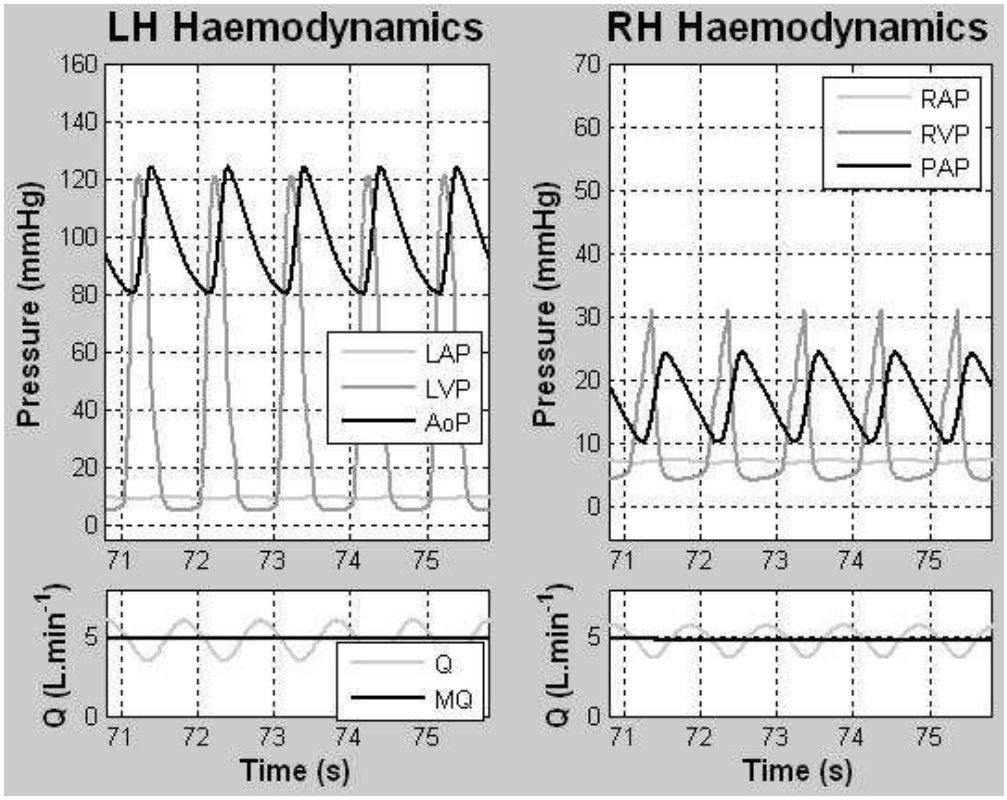

Figure 6-2: Simulated healthy haemodynamics using the Numerical Program.

The *EF* for the left and right ventricles per cardiac cycle are given in Figure 6-3. As discussed in the literature review, a healthy LV *EF* is around 50%.

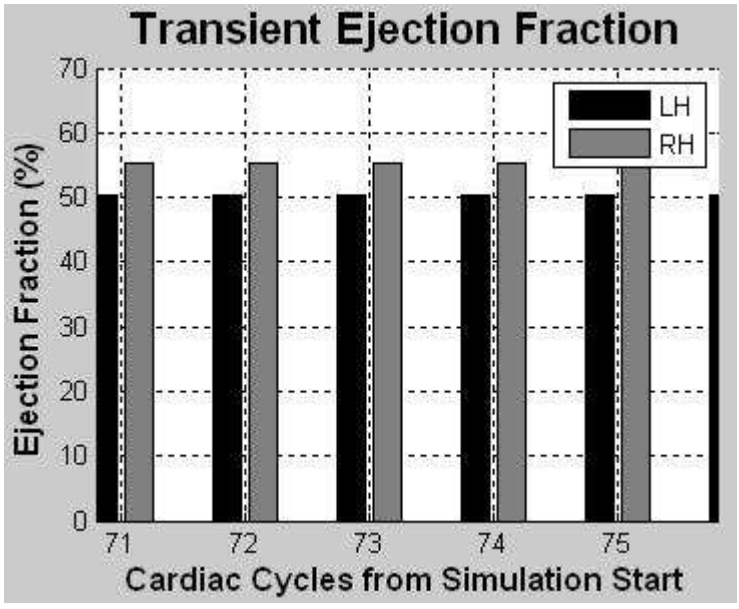

Figure 6-3: *EF* per cardiac cycle from the healthy numerical model simulation.

Figure 6-4 shows that the LV volumes for the healthy numerical model simulation remain within the limits of 80 and 150 ml. The literature review sourced textbook data which documents that this volume range is indicative of healthy adult LV function (Guyton 2005).

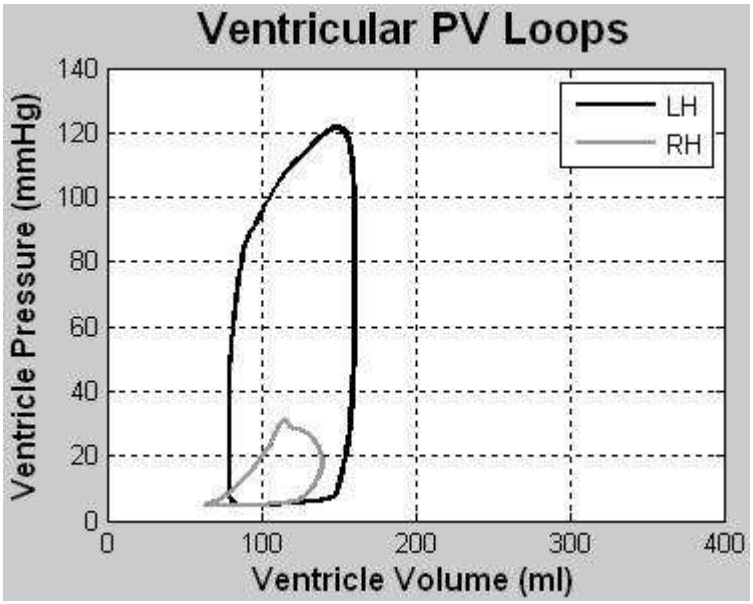

Figure 6-4: PV loops for the LV and RV during a healthy simulation.

To achieve the numerical results shown in the previous three figures, the circuit volume was set at 1340 ml and the vascular parameters were defined as given in Appendix 10.2, Table 10-2.

Note that resistive components are made redundant by making them very low, i.e. equal to $0.1e^{-3}$ mmHg.s.ml^{-1}, the compliant components are made redundant by making them very stiff, i.e. 0.1 ml.mmHg^{-1} and the redundant inertial components are set to an inertiance of 0 mmHg.s^2.ml^{-1}.

The resistive components of the PA and PV account for the pulmonary pipe flow losses just as the Higher Aorta and Vena Cava resistances account for systemic pipe flow losses. These arterial and venous pipe loss resistances were set at a ratio of 1:1.8 respectively due to approximate ratios of pipe length. They were then scaled to provide appropriate haemodynamics. Note also that the simulated pulmonary resistance applied by the pinch valve (the arterial vessels in the lungs) is zero. The MCL too applies a minimal pulmonary resistance with the pinch valve as the pipe

losses are approximately sufficient. The systemic pinch valve resistance was applied at the arterial vessel in the head.

6.2.1.3 **Chronic Heart Failure**

The experimental chronic heart failure simulation is shown in Figure 6-5. The increased CVP is indicated by the elevated RAP.

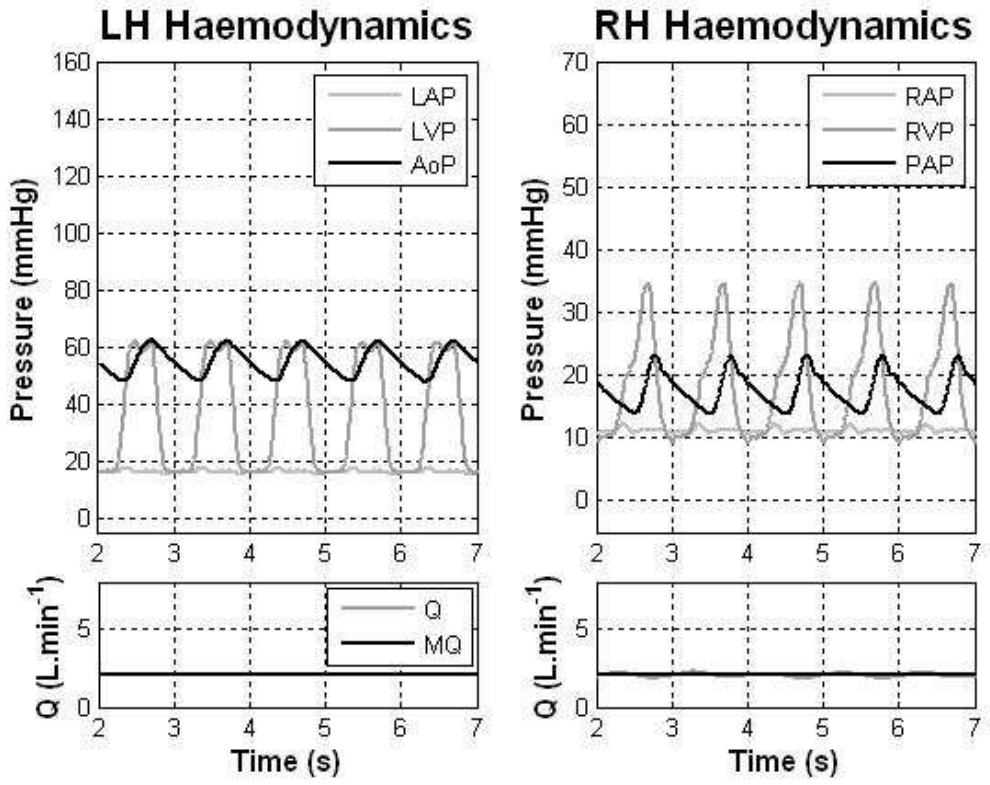

Figure 6-5: Simulated heart failure haemodynamics using the Mock Circulation Loop.

To simulate chronic heart failure in the numerical program, the inverse compliance profiles for both ventricles during systole were scaled down to reduce contractility. Therefore, the reduction saw increases in the peak systolic compliances for the left and right ventricles from 1.08 and 4.07 ml.mmHg^{-1} to 12.04 and 18.45 ml.mmHg^{-1} respectively. These reductions corresponded to a 91% and 78% decrease in the peak inverse compliances respectively. Furthermore, the renal response to increase CVP was simulated by increasing the fluid volume. The fluid volume was increased by 250% from 1340 to 2300 ml. The resulting haemodynamics from the numerical simulation are shown in Figure 6-6.

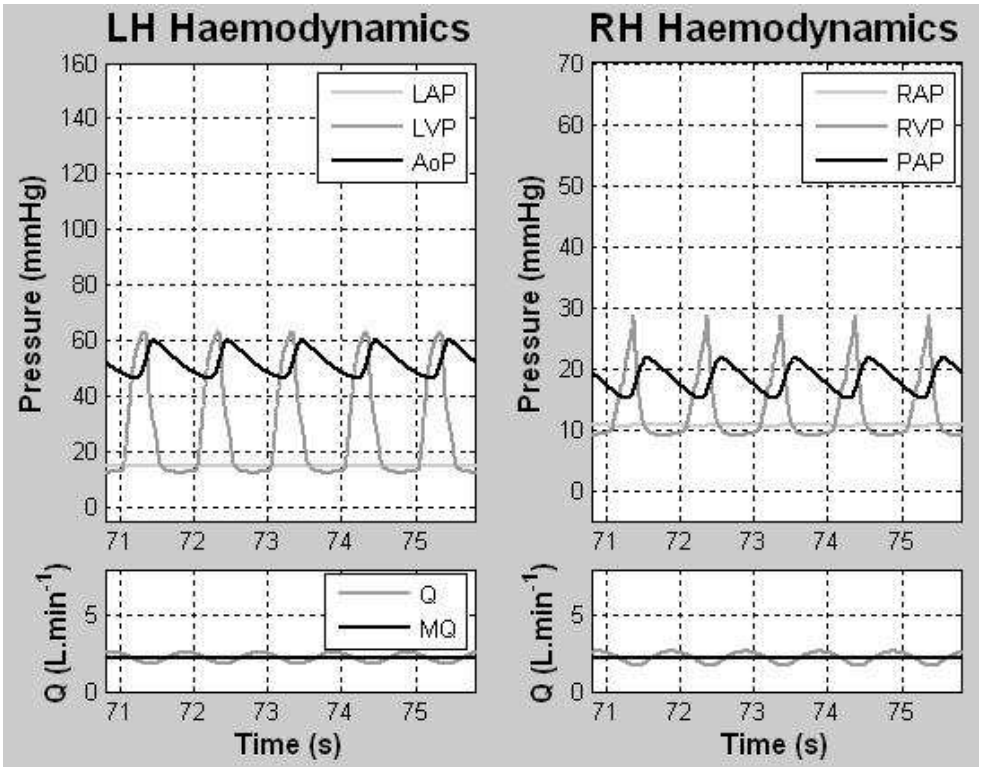

Figure 6-6: Simulated heart failure haemodynamics using the Numerical Program.

Figure 6-7 shows a dramatic drop in EF for both ventricles and Figure 6-8 shows that the increased CVP has caused the LV, and to a lesser extent the RV, to become highly distended.

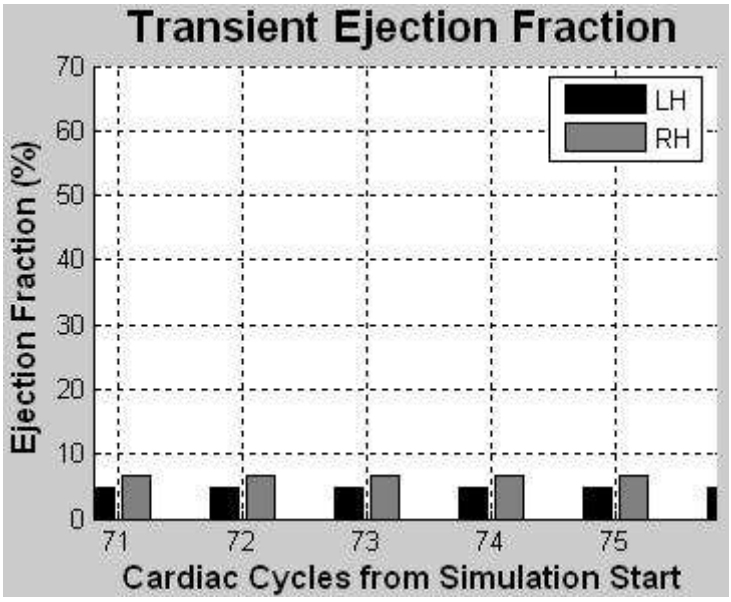

Figure 6-7: EF per cardiac cycle from the heart failure numerical model simulation.

Note the difference in volume and pressure scales in Figure 6-8 when compared to Figure 6-4.

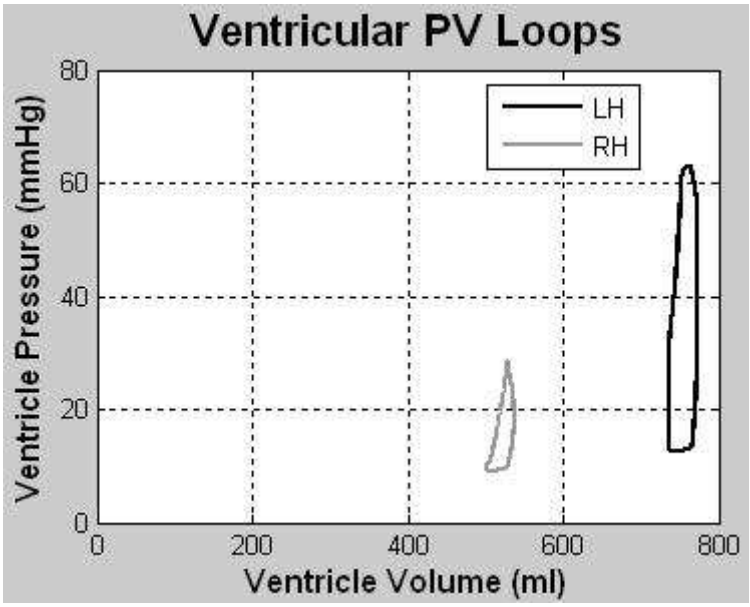

Figure 6-8: PV loops for the LV and RV during a heart failure simulation.

6.2.2 Unsteady Simulation

At the very least a comprehensive verification process requires testing both the steady state response and the response to some unsteady disturbance. A classic example of an unsteady disturbance is a singular step input to the system. The numerical program will therefore be compared to a sudden resistance change as seen in the sudden hypertension tests in Chapter 4.

The resulting haemodynamics from a sudden pulmonary hypertension simulation is shown in Figure 6-9. A total clearance of $y = \pm 0.17$ mm was used and the VAD speeds were $N_{LVAD} = 3870$ RPM and $N_{RVAD} = 920$ RPM. Note, that with the inclusion of the LVDT displacement data, the atrial pressures could not be read. However, since the simulation is a total support simulation the atrial pressures and ventricle pressure will be very similar.

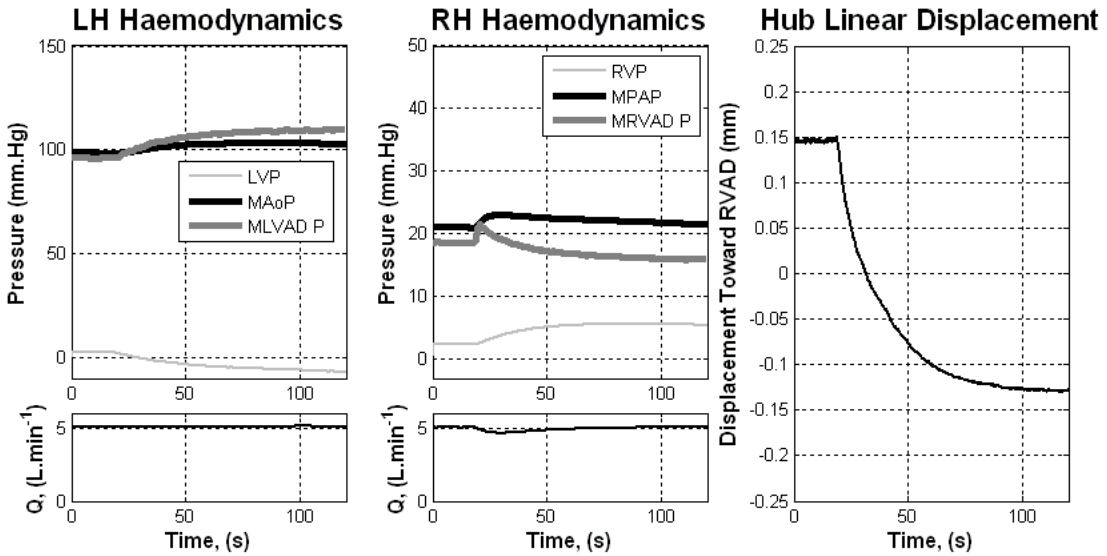

Figure 6-9: Unsteady pulmonary hypertension simulation from the experimental MCL tests.

Numerical simulation of the sudden pulmonary hypertension was applied simply by increasing the arterial resistance of the lungs, (used to simulate the pulmonary circuit proportional pinch valve in the MCL), from 0 to $120e^{-3}$ mmHg.s.ml^{-1}.

The experimental result in Figure 6-10 shows good agreement between the two simulations. Considerably higher pump speeds were required as N_{LVAD} = 4080 RPM and N_{RVAD} = 1000 RPM.

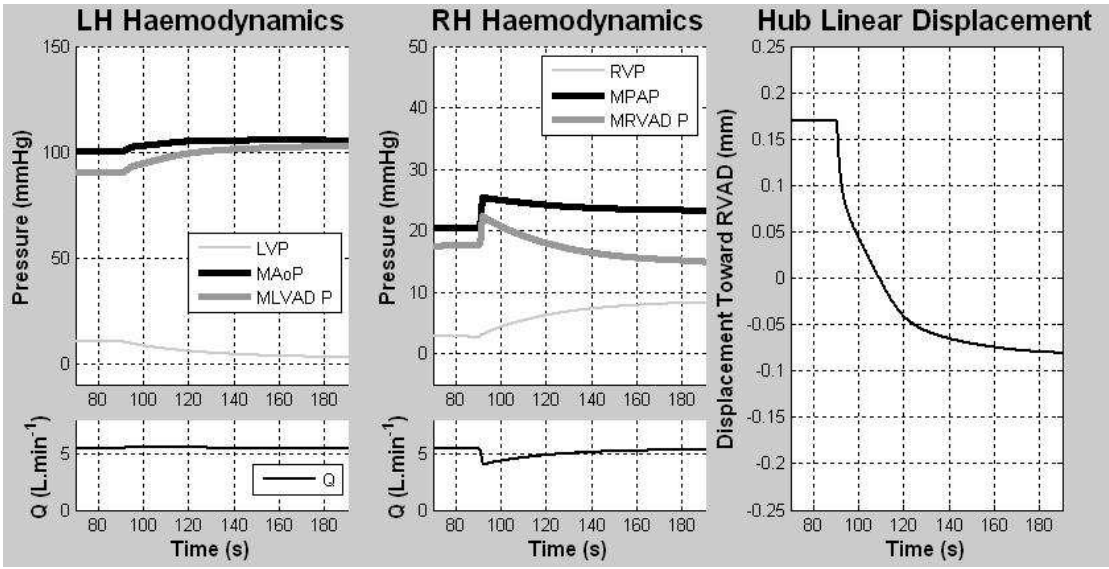

Figure 6-10: Unsteady pulmonary hypertension simulation using the numerical program.

The damping coefficient was approximated as 50 $N.s.mm^{-1}$. This provides an approximate figure with which to continue simulation. The mass of the floating assembly was approximately m = 160 g. This was used as the mass term in the dynamic equations.

6.2.3 Discussion

In order to quantify the vascular parameters given in Appendix 10.2, Table 10-2, a gradual tuning process was carried out in which parameters were adjusted so that similarity was observed between the experimental and numerical tests. A number of bullet points have been compiled to provide a broad indication of haemodynamic states which are highly sensitive to particular parameters. The bullet points are intended to indicate some of the tuning processes, as well as outline the interdependence of the parameter selection.

Tuning process bullet points:

- The Central Venous Pressure, CVP, or Right Atrial Pressure, RAP, was dependent on the fluid volume and the global compliance values.
- The peak systolic pressure was heavily dependent on the minimum transient ventricular compliance and the arterial resistance.
- Decreasing the peak systolic ventricular compliance decreases the End Systolic Volume (ESV), (i.e. increases the Stroke Volume, SV)
- Increasing the diastolic ventricular compliance increases the End Distolic Volume (EDV).
- The arterial pulse pressure was heavily dependent on the arterial compliance as well as the ventricular inertiance.
- The end diastolic ventricular volume depended on the diastolic ventricular compliance, the atrial inertiance, the open/closed criteria of the atrial/ventricular valve and the atrial pressure.
- The peak systolic pressure phase difference between the ventricle and artery depended heavily on the ventricular inertiance and to a lesser extent the arterial inertiance.

- Mean vascular flow was dependent on the difference between the Mean Arterial Pressure (MAP) and the venous pressure, (or downstream atrial pressure), and the vascular resistance.
- The pulsatility of the vascular flow was affected by arterial compliance as well as ventricular, arterial and, to a lesser extent, venous inertiance.

It is important to note that there are also haemodynamic states which are weakly sensitive to other parameters, (e.g. arterial pressure to venous resistances). The interdependent nature of all the haemodynamic states and the defined global vascular parameter meant that the tuning process was a time consuming and repetitive process.

A good agreement was seen between the experimental and numerical simulations of healthy haemodynamics. Replicating the ratio and phase difference of peak ventricle pressures to arterial pressures was a time consuming exercise. It required careful selection of the atrial, ventricular and arterial inertiances along with peak ventricular systolic compliances, total fluid volume and arterial resistances. Maintaining an LV $EF \approx 50\%$ and an EDV ≈ 150 ml aided in this tuning as, although experimental volume data were not gathered, the MCL had been designed to simulate healthy haemodynamics at these volumes.

The renal response to decreased arterial pressure, (i.e. heart failure), is to increase total blood volume and therefore CVP. The increased pre-load increased EDV, (as shown in Figure 6-8), and the strain dependent contractility of the native heart responds by increasing EF. Neither the MCL nor the numerical model incorporates the volume dependent heart chamber compliance. This means that comparisons between the two will be unaffected. However, it should be realised that the *in silico* human simulations will be without this feature.

Simulated renal function in chronic heart failure increased the fluid volume by 250% which raised the atrial pressures in both simulations. A good agreement was seen between the experimental and numerical simulations, however, the numerical model displayed a slightly higher flow pulsatility and a lower peak systolic RVP.

High similarity between the unsteady simulations indicated the modelling of the passive action was representative of that of the prototype. An approximate damping coefficient of d = 50 N.s.mm^{-1} was found. This may be varied in the *in vivo* simulations but the order of magnitude, at least, was established.

Perhaps the most encouraging result from the unsteady simulation was that the numerical simulation of the RVAD pressure head adjusted to counter the elevated PAP. Similarly, the LVAD head increased due to the negative translation of the hub indicating that the linear solution using the parabolic performance vertex adjustment method provides a representative response of the Passive Controller BiVAD.

The LVAD and RVAD running speeds were both around 6% higher in the numerical simulations when compared to the experimental simulations when running the device in total support mode. Attempts were made to vary the vascular parameters to decrease the numerical simulation pump speeds, (i.e. increase blood volume and decrease vascular resistances). However, the increased blood volume increased the CVP beyond 20mmHg thus creating a non-representative simulation. It was assumed that the reason for this discrepancy was in the choice of the locations of the experimental BCs used to define the interpolating polynomials. So as to increase the interpolating range of the polynomials the defining BCs were selected from the maximum and minimum flow rates from each test. This can be seen by locating the employed BCs in Figure 5-13 and Figure 5-16. The lack of resolution in the mid flow ranges may have decreased the function's accuracy. However, for the purpose of investigating the implications of passive control this is not a serious issue.

6.2.4 Validation Comments

Excellent agreement was seen between the experimental MCL results and the numerical simulations. Both the simulated vascular responses and BiVAD prototype responses were very similar. The MCL circuit model and numerical simulation method was considered representative and therefore validated.

The validation process, however, outlined a number of parameters that are particularly sensitive to global haemodynamics. These are fluid volume, the ventricular

contractility, arterial resistance and compliance and the inertiance of the atria, ventricles and arteries. It was found that analysis of the *EF* and PV loops was just as important as an analysis of the haemodynamics in and around the heart and VADs.

For the *in vivo* simulations, healthy haemodynamics will be simulated reflecting those described as healthy in the literature review. Similarly the *EF* and PV loops will imitate those described in the literature review. This way, heart failure and supported circulation can be simulated simply by adjusting ventricular contractility and VAD pump speeds.

6.3 Numerical Simulation in the Human Circuit Model

So far, the experimental and numerical simulations have employed a simplified dual circuit circulation model defined as the MCL circuit. These studies have complemented each other through comparison of the simulated hydraulics and dynamics of the floating hub. *In silico* simulations using a circuit model more representative of a human's are now presented to extend the understanding of the interactions between the circulation and the prototype.

The experimental data demonstrated the passive controlling action of the BiVAD prototype. It was shown that the floating assembly encouraged the stabilisation of arterial pressures during sudden haemodynamic events which have been shown in literature to compromise the safety of cardiac assistance. Numerical simulations of the MCL were then used as a validation tool for the solution algorithm, the vascular sub-unit and the user-defined parameterisation procedure. Now the validated MCL model will be extended to the human circulation model. To be confident that this extension of the model is still verified; healthy human circulation will first be compared to text book haemodynamics. Furthermore, a brief analysis of the *EF* and PV loops will be employed to increase confidence in the changes made to the model.

Following this, the BiVAD's operation will be observed during steady support. The implications of continuous flow dual support will be examined with reference to published clinical BiVS data.

Finally, an analysis of ventricular suckdown during BiVAD support will be carried out using the numerical model. This is because the experimental testing outlined this as an issue with the employed means of providing passive control.

6.3.1 Simulated Healthy Human Circulation

To extend the validated model's vascular circuit model from the MCL circuit to the human circuit, a comparison to representative human data was needed. Detailed clinical data for healthy circulation was not readily available without ethics approval. So, textbook data was used as a means of comparison.

A multiplot of the haemodynamics within the heart was presented in Figure 2-4 however; this was not used for comparison as it didn't include flow data. A more comprehensive multiplot of healthy adult human circulation is shown in Figure 6-11 from text (Milnor 1982). Although the figure does not detail clinical experimental data, it illustrates the 'diagram of events in (the) cardiac cycle of a man' and was therefore assumed to be sufficiently representative.

The figure includes atrial, ventricular and arterial pressure traces as well as flow through the Aortic and Pulmonic valves. Additionally, the time of opening and closing of the Mitral Valve, (MO and MC), Aortic Valve, (AO and AC), Tricuspid Valve, (TO and TC) and Pulmonic Valve, (PO and PC) are shown.

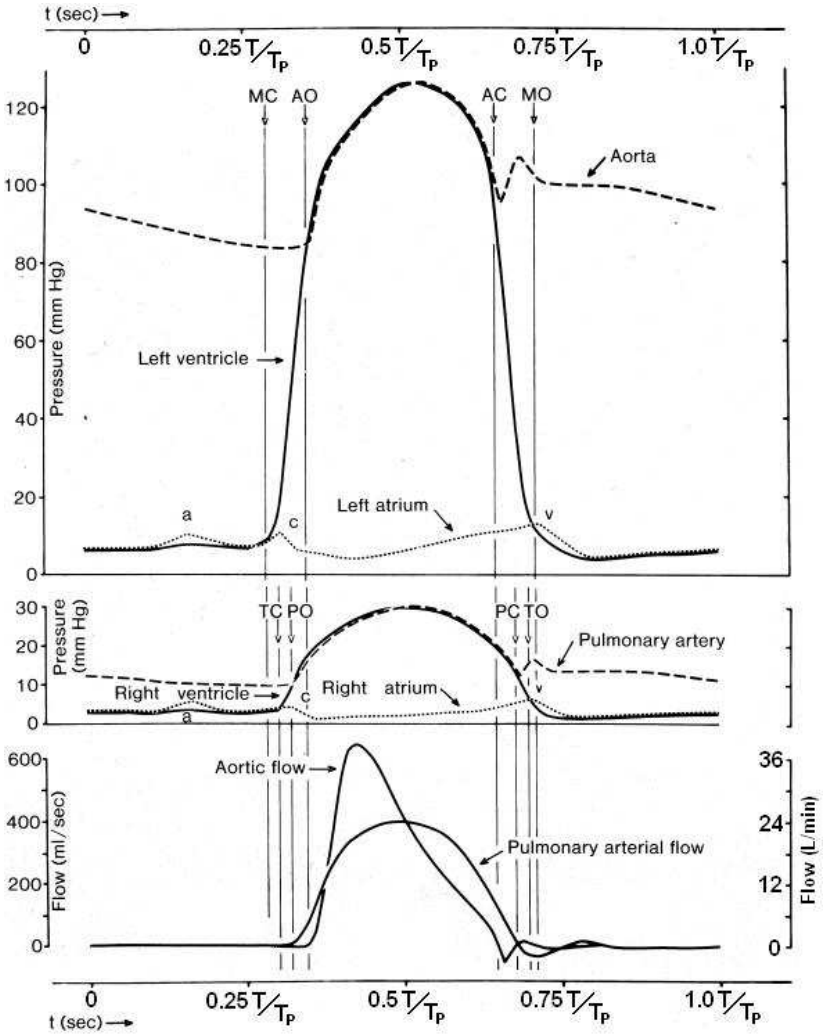

Figure 6-11: Textbook cardiac haemodynamics, [modified from source (Milnor 1982)].

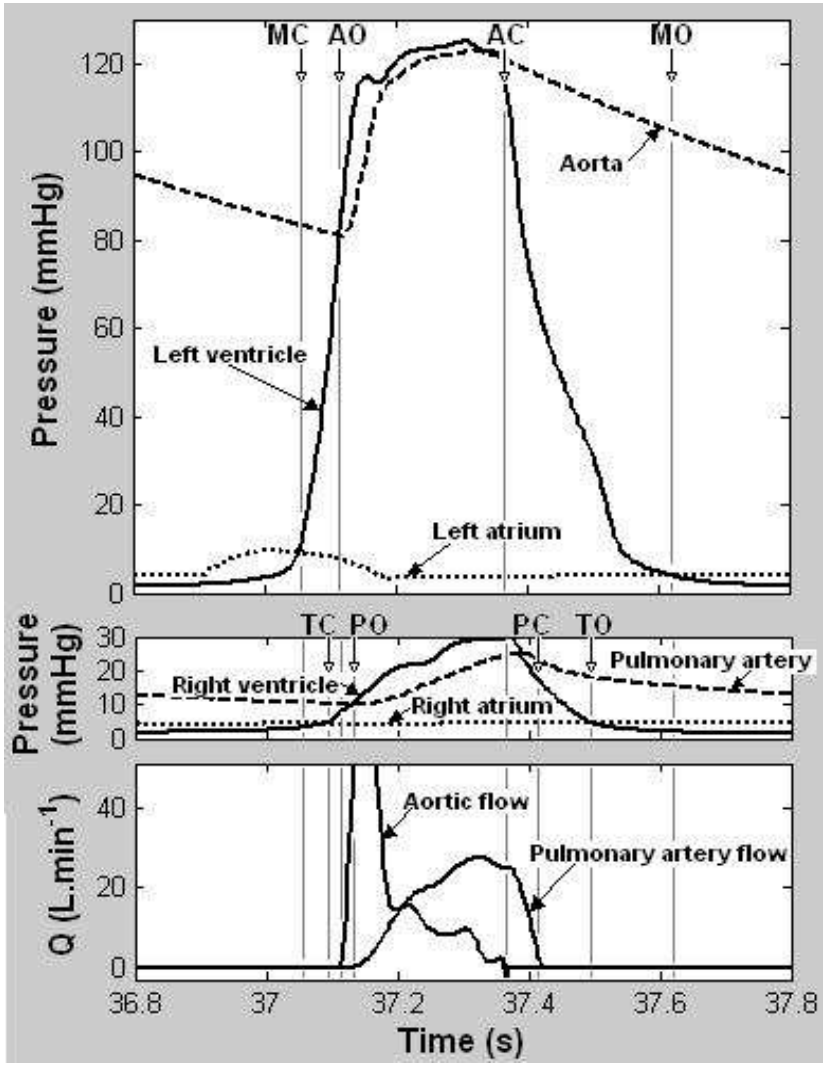

Figure 6-12: Numerical model of human cardiac haemodynamics.

Figure 6-12 shows a numerical simulation of healthy human circulation. The simulation was run for 40seconds to allow settling with a time step resolution of $\Delta t = 2.5E^{-3}$. The DOM pressure for both the pulmonary and systemic systems were prescribed as the mean subcutaneous pleural pressure p_d = -3 mmHg, (Guyton 2005). The density of blood was taken as ρ_{blood} = 1050 kg.m^3 and this was used in the updated calculations of each vascular sub-unit's inertiance Equation 5-3. Recall that the inertiance for the human circulation was updated every time step as a function of nominated vessel diameter and the resident vessel volume. The vascular parameters are given in Appendix 10.2, Table 10-3. To give an idea of the resulting inertiances updated every time step for the human model, a set of vascular parameters are given in Appendix 10.2, Table 10-4. The inertiance parameters are for the healthy simulation in Figure 6-12 at the end of systole.

Note that the format and layout of the plots differ from other presented simulations. This has been done for ease of comparison. Note also the difference in magnitude of flow scales, (a L.min^{-1} scale was added to the right hand side of the clinical data for ease of comparison). The time scale for the text data was also changed as it documented a cardiac cycle of time period T_P = 0.8 seconds.

It is true that there are differences in the dynamic detail between the modelled haemodynamics and the text data. In particular there are notable differences in the peak flow through the aortic valve, the form of the PAP wave, the absence of the dicrotic notch and the delay between the arterial valves closing (AC and PC), and the atrial ventricular valves opening (MO and TO).

Besides the fact the text data is a 'diagram of events' only (Milnor 1982), it is important to discuss reasons for the differences in comparison. The discrepancies were attributed to two main factors. The first is that the form of the pressure and atrial and ventricular transient compliance profiles are indicative of the resulting pressure and flow wave forms. Figure 5-22 shows that the form of the employed RV compliance profile is quite triangular with a notable apex every cycle. So too is the RVP in Figure 6-12. This also offers an explanation for the differences in valve actions as the rate of change of ventricular pressure at the beginning and end of systole is partially governed by the ventricular compliance profile.

The second attributed factor causing differences is the lack of modelling detail paid to the heart valves themselves. Without accurate modelling of the fluid-structure interaction around the compliant valves, as well as the elastic nature of the downstream vasculature the dicrotic notch cannot be effectively emulated.

No serious concern was raised by the discrepancies highlighted from the comparison. The text data is representative but not experimental clinical data and the numerical model simulation showed that it provides a good physiological likeness. Furthermore, texts readily admit the high variability in haemodynamics between people depending on body size, lifestyle, health, vascular geometry, activity etc (Milnor 1982; Guyton 2005). However, to be sure that the model is, in fact, providing a good physiological likeness, the simulation was compared to quantified textbook data such as defined in the Chapter 1. These are displayed as *EF* and PV loops in Figure 6-13. The figure shows that the LV *EF* is approximately the nominated 47% and the EDV and EVS are around 150 and 80 mls respectively.

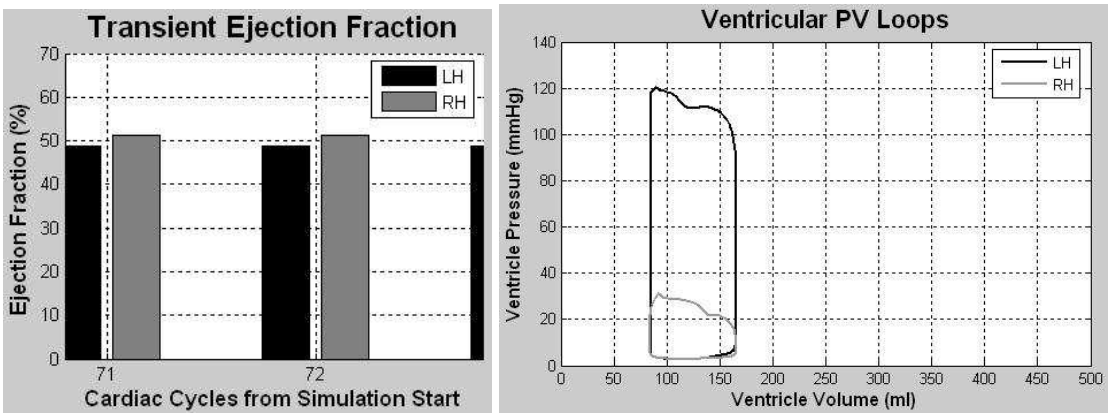

Figure 6-13: Healthy human circulation simulation, LH and RH ejection fraction (left), PV loop for one cardiac cycle at T = 79-80 seconds (right).

Following the presented human circulation results, the model is considered to be validated for the human model. The replication of the text data saw a MAoP of 100 mmHg, a MPAP of 16 mmHg, (note, these mean pressures were not added to Figure 6-12 for clarity in comparison), and mean flow rates of 5 $L.min^{-1}$. They are essentially identical to those outlined in Section 2.3.1. From this point on, these will be the target healthy pressures and flow rates for BiVS.

6.3.2 Steady BiVAD Support with Modified RVAD Characteristics

Until this point, all experimental simulation has been restricted to the physical limits of the MCL and the Passive Controller BiVAD prototype. Still, this has provided a clear insight into the ability of the rotary prototype to provide steady support and cope with sudden changes to CV haemodynamics. Also, until this point, all numerical simulation has been to replicate experimental or textbook circulation data with the aim to validate the solution algorithm and modelling of the vasculature and assist devices. In this section, the concept of passive control of a BiVAD is simulated *in silico* in what the candidate considers to be the most representative human heart failure model available to this project.

Running a numerical investigation alongside an experimental study allows changes to the experimental rig to be simulated that would otherwise be costly and time consuming. In this section, adjustments to the LVAD passive response and the RVAD hydraulic response were made in an attempt to improve the performance of the passive controller. This was achieved by simply adjusting the user input parameters which describe the BiVAD performance and response in the numerical program.

Without comprehensive data from chronic clinical trails, it is difficult to identify the pressing issues associated with rotary Bi-Ventricular Support, BiVS. However, it is known that poor flow balancing between the VADs has affected the success of chronic trials and that pulmonary hypertension seems to be an associated vice, (Nonaka *et al*. 2002). Additionally, the results shown in this section will show that there is a notable change in ventricle volumes due to the differing flow dynamics between the native pulsatile circulation and the constant flow support circulation. It will be argued that this may also be attributed to the poorly balanced circuits.

6.3.2.1 **Method**

Up until now, the RVAD to LVAD impeller radii ratio has been 2:1 as described in Chapter 3. This caused a lower shroud area ration of 4:1. However, the MAoP to MPAP ratio for steady state circulation of an adult human is 1:5. For this reason, experimental and numerical results of supported simulation, (without employing an

air spring, i.e. k_{air} = 0), have had a steady state hub position on the RVAD side of the central hub location, (typically around y = +0.15 mm). To centrally locate the floating assembly during steady state support, the radius of the LVAD was reduced from 25 to 20.90 mm. The resulting reduction in area of the LVAD lower shroud decreased the pressure force from the LVAD side, F_{LVAD}.

Additionally the RVAD decrement functions, ξ_H and ξ_Q, were redefined so as to reduce the high negative gradient at low clearances. The reason for this was to make the numerical simulation of the RVAD performance more sensitive to clearance over the whole translational range. As seen in Chapter 5, the existing RVAD decrement functions saw 83% and 79% of the pressure and flow drop respectively, over the first 0.02 mm of clearance from the RVAD impeller, (y = +0.17 to +0.15 mm). So, the LVAD decrement functions were used for both RVAD as well as the LVAD.

Healthy, Bi-Ventricular Failure (BiVF), and BiVS simulations were then run using a time step of Δt = 2.5E^{-3} s for 80 seconds to allow settling. BiVF was simulated by scaling the transient ventricular and atrial compliance profiles down by 90%. The vascular parameters were maintained from the previous section, including the heart rate of 1 Hz.

Numerically applying BiVS involved reducing the high resistances at the cannulation sites of the ventricles to allow flow through to the VADs. Then the VADs' speeds were increased until the mean arterial pressures and circuit flow rates were restored. The LVAD and RVAD speeds for the BiVS simulations were N = 3760 and 2060 RPM respectively. The dynamic damping and mass of the hub were set to d = 50 N.s.mm^{-1} and m = 160 g respectively. No air spring was employed so the proportional response was given by the inherent clearance spring only. The cardiac and VAD haemodynamics were observed as well as the PV diagrams.

6.3.2.2 **Results**

As has been shown bi-ventricular heart failure reduces the EF of both ventricles. This in turn distends both ventricles and reduces the CO. Figure 6-14 shows simulations of the shift in the PV loops, (once allowed to settle), before and after BiVF.

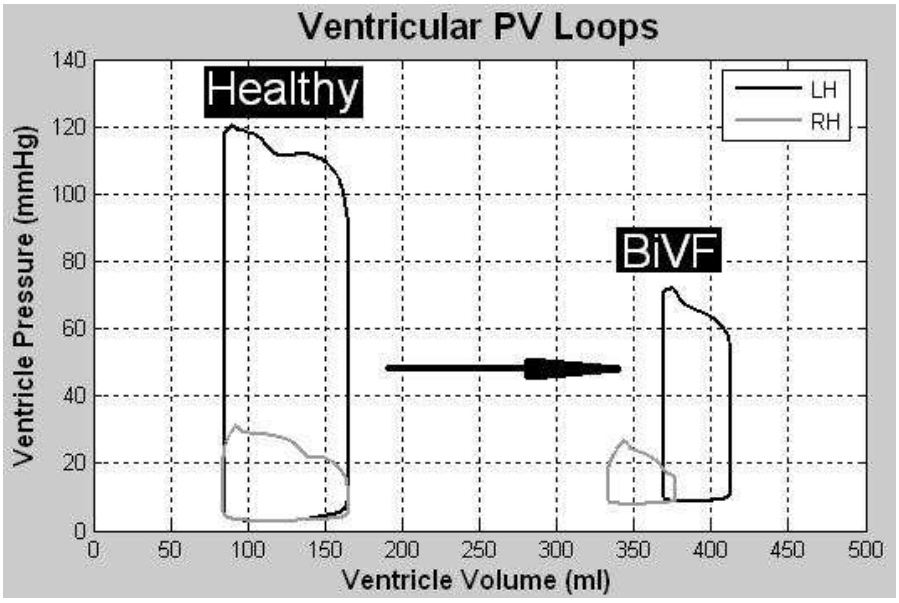

Figure 6-14: PV loops from human simulations of healthy circulation and BiVF.

The healthy EDV and ESV are around the levels prescribed in the literature as representative of healthy for an adult, approximately 150 and 80 ml respectively. Then, acute bi-ventricular failure sees severe distension of the heart due to the reduced CO and continued diastolic filling. The shift of the PV loops from BiVF haemodynamics to BiVS are shown in Figure 6-15.

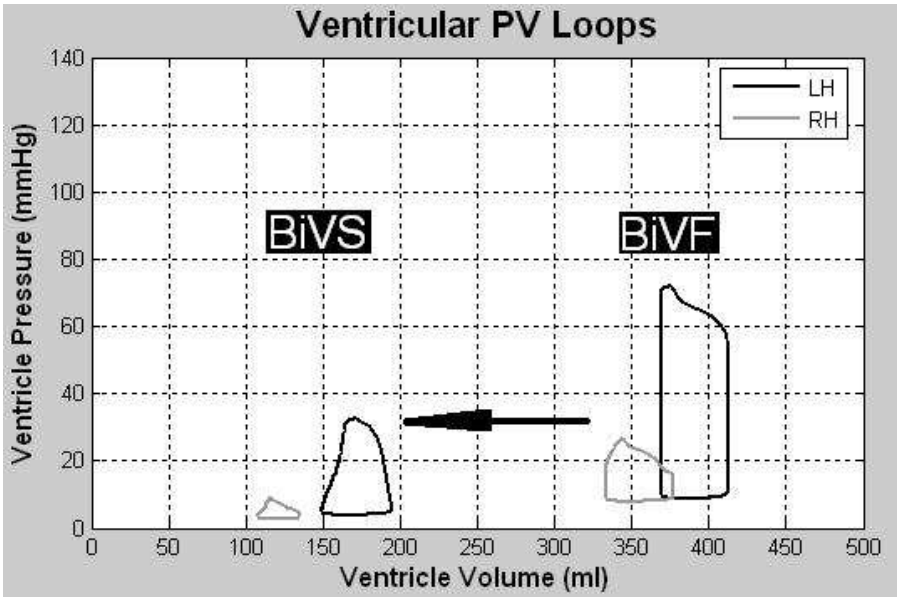

Figure 6-15: PV loops from human simulations of BiVF and BiVS.

The haemodynamics of the supported system have been restored to the new target pressures of MAoP = 100 mmHg, MPAP = 16 mmHg and mean flows

MQ = 5 L.min^{-1} as shown in Figure 6-16. The modified LVAD lower shroud radius of the floating assembly has allowed the hub to occupy the central position during stable support, (i.e. $y \approx 0.0$ mm). Observe that the modified numerical model of the BiVAD prototype provides adequate BiVS with a centrally located hub.

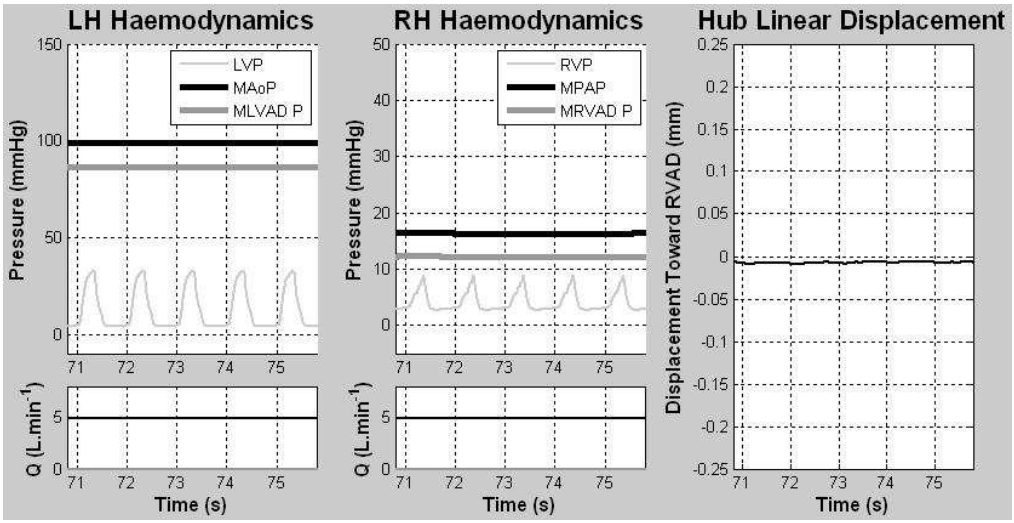

Figure 6-16: BiVS for human simulation with a modified RVAD and LVAD radius.

6.3.2.3 **Discussion**

The new LVAD radius and selected VAD speeds have positioned the floating assembly in the central position. Use of the numerical model has allowed design adjustments to the BiVAD without the costly and time consuming task of changing the experimental setup.

An interesting result was the volume staggering of the BiVS and the healthy simulation PV plots. It could be assumed that provided there was no change to the vascular parameters, the mean volumes should be approximately the same. The result therefore, is due to reduced vascular impedance in the BiVS simulation from the lack of pulsatility. With a zero rate of change of flow the inertiance of the vessels cannot contribute any pressure loss. Therefore, with different inertial parameters in either circuit, the lack of pulsatility induces a different effective resistance thus slightly unbalancing the circuits. The result is a slightly distended LV.

This effect is dependent on the relative impedance attributed to each circuit, and therefore the associated diameters and resident volumes (the latter is a function of the associated compliances). Since the validation step was compared to text data only, it is unfounded to conclude outright that LV congestion will result from continuous flow BiVS. Perhaps if the model were compared to clinical data allowing higher confidence in the resulting inertiance parameter, the RV would be distended and the LV nearing suckdown. Either way it is important to realise that this effect may very likely cause an imbalance in ventricle volumes. This could increase the likelihood of chronic distension of the ventricle or even suckdown.

Considering clinical reports of *in vivo* BiVS, where pulmonary hypertension was common accounted, it may be concluded that the simulated volumes were correctly modelled. Perhaps a nervous response via the Vagi senses the low right atrial volume and high left atrial volume and consequently constricts the pulmonary vessels. In doing do, the PAP will rise and the RV volume will increase. Similarly, the venous return to the LH will decrease unloading the LV. This hypertension of the pulmonary circuit would satisfy the claims from clinical reports. This study cannot prove such a claim; however, it offers a theory and could be the subject of future work.

6.3.3 Periodic Vascular Constriction, i.e. Deep Breathing

The circulation cannot be treated as an isolated system with one energy input at its heart. It is affected by numerous systems of the body in a complex interdependent network. For example, exercise causes the muscles around the arteries and veins to contract. This causes immediate increased venous return. Furthermore, increased oxygen take-up by the muscles promotes localised secretion of Bradykinins to dilate capillary networks to decrease vascular resistance and increase flow. Another example is the effect of breathing on the vasculature around the heart. Depending on the depth of the breath, the induced pressure inside the upper torso can drive blood out of the low pressure venous system into their respective atria affecting the haemodynamics. The effect of deep breathing will be examined in this section.

Pleural pressure is the static potential of the fluid between the outer lung wall, (lung pleura), and the chest wall. During respiration, the ribs and diaphragm move to

increase and decrease the pleural pressure which in turn moves the lung pleura. This induces a pressure gradient from the tracheal airway all the way to the lung alveolar where gas exchange takes place.

Normal, or resting, respiration sees the pleural pressure oscillating between DOM_P = -5 to -7.5 mmH_20 with a time period of around 5 seconds, (mean values). Deep breathing can extend these limits by a large margin during a sigh, yawn or exercise. In fact, a resting breath has amplitude of approximately 250 ml in an adult lung with a maximum capacity of around 6 L, (Guyton 2005).

The added effects of deep breathing were simulated to observe respiration's affect upon the device's operation.

6.3.3.1 **Method**

A sinusoidal resting pleural pressure function was used so that,

$$DOM_P(t) = P_{pleural} \sin\left(\frac{2\pi t}{T_{breath}}\right) - 6.25,$$

Equation 6-1

where $P_{pleural}$ is the pleural pressure amplitude and T_{breath} is the time period of breath. For resting breaths, the amplitude and the mean pleural pressure was set to 1.25 and -6.25 mmH_20 respectively. This recreated the textbook pleural pressure limits as given above. When a deep breath was simulated, the amplitude was increased tenfold to $P_{pleural}$ = 12.5 mmH_20. This amplitude was an arbitrary choice in order to create a noticeable increase in pressure. The time periods for both the resting and deep breaths were kept constant at 5 seconds. The pleural pressure waveform, including two deeps breaths, is shown in Figure 6-17.

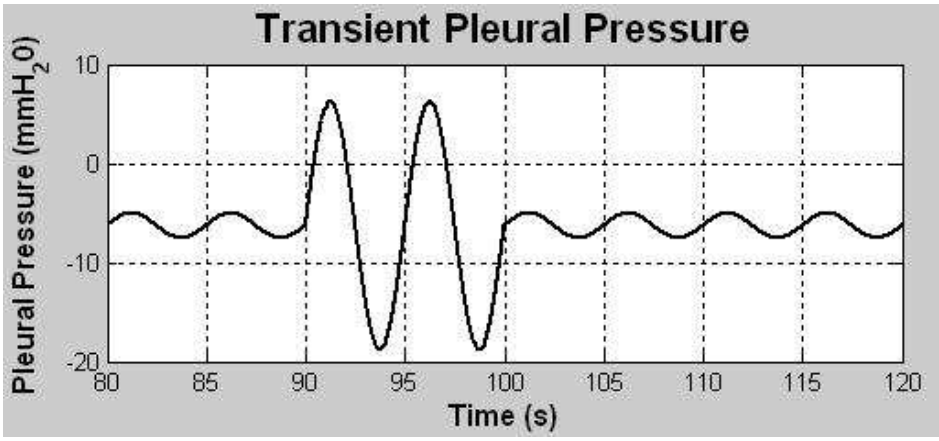

Figure 6-17: Pleural pressure waveform for human BiVS simulation.

Note, 1 mmH_20 is equivalent to $7.35E^{-2}$ mmHg. So, amplitudes of $P_{pleural}$ = 1.25 and 12.5 mmH_20 correspond to pressures of $9.319E^{-2}$ and $9.319E^{-1}$ mmHg.

The vascular, BiVAD, passive controller and time parameters were kept as those used in the steady BiVS simulations.

6.3.3.2 **Results**

The resulting supported haemodynamics are shown in Figure 6-18. Note that the arterial pressure traces have not been given as mean values in the figure. This is to show the simulated effect of breathing on arterial pressure. Boxes have been drawn around some of the transient data in the top plot. These are the sections of the plot which have been magnified in the lower plot.

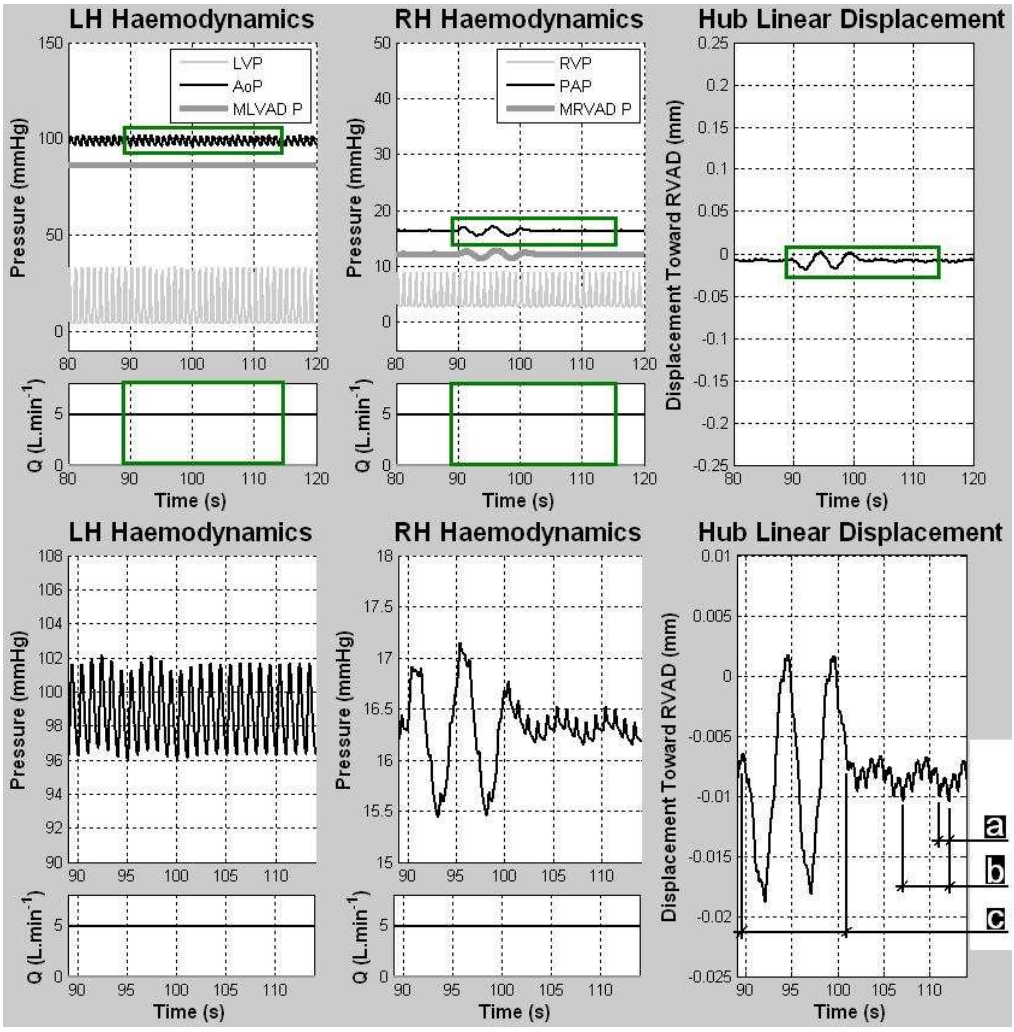

Figure 6-18: Supported human haemodynamics with simulated resting and deep breathing, (above), and with reduced time and hydraulic scales (below).

The reduced time and hydraulic scale plot in the figure has three time lengths dimensioned on the hub displacement plot. These indicate (a), the residual ventricular function time period, (b), the resting breath time period and (c), the two deep breaths.

6.3.3.3 **Discussion**

Deep breaths have some impact on the passive response of the BiVAD. The deflections for breaths of this size are minimal and so it can be concluded that the spring stiffness and damping are sufficient to reduce the deflection and damp the disturbances.

6.3.4 Venous Return and Ventricular Suckdown during BiVS

Ventricular suckdown is an issue exclusive to cardiac support using devices with suction at the inlet(s). This damaging event is of particular concern for designers of rotary devices and has received a lot of attention. In essence, suckdown occurs when venous return is insufficient to supply the required flow at the VAD's operating point. There are a number of reasons why venous return may be too low including pulmonary embolism and hypertension as described in Chapter 1.

The BiVAD prototype was designed to respond to the pressure fluctuations between the pulmonary and systemic circuits. The design of the controller is such that it responds to a decrease in blood pressure around the VAD with an increase in output down stream of the VAD. This is advantageous in maintaining arterial pressure at a set systemic to pulmonary ratio. These advantages were demonstrated in a number of experimental simulations in Chapter 4. However, both pulmonary embolism and hypertension induce a decreasing LVAD inlet pressure due to the decreased venous return.

In theory, ventricular suckdown is surely the passive controller concept's greatest challenge. Sensing the decrease in pressure due to low ventricular volume, the floating assembly will translate toward the VAD draining that ventricle in an attempt to increase flow. From this viewpoint, therefore, the passive controller is actually encouraging the collapse of the ventricle.

This idea was hinted at in the discussion of the experimental testing. Ventricle collapse was observed in the form of all fluid having been sucked out of the ventricle by the VAD in simulations where venous return was reduced. These were the hypertension simulations. An increased vascular resistance reduced circuit flow rate and thus decreased venous return as shown in Figure 4-13. Experimental results were not shown as no volume data was collected. The experimental ventricle pressure data, however, could indicate collapse in the form of suddenly unstable pressure readings. So, the numerical model was used to investigate the passive controller's response to reduced venous return and the incidence of ventricular collapse.

6.3.4.1 **Method**

Solution and vascular parameters were maintained as those defined in the steady BiVS and deep breathing simulations. Then the solution was allowed to settle. At t = 86.5 seconds the user defined Pulmonary Vein resistance was increased from R = 15 to 135 mmHg.s.ml^{-1}. This resistance change was selected as it was the smallest resistance increase in the PV that would induce a left ventricular suckdown. It should be noted, however, that this is a very large resistance increase. Data in Appendix 10.2, Table 10-3, shows that the total pulmonary circuit resistance was 120 mmHg.s.ml^{-1}, thus, this increase doubles the pulmonary resistance. This simulated a sudden hypertension in the pulmonary circuit and therefore decreased venous return into the left heart.

In order to assess whether the passive response encourages ventricular collapse two separate simulations were run. These compared the response of a BiVAD with and without the passive response. To do this, the second simulation incorporated a near infinite air spring, i.e. $k_{air} \approx \infty$. This ensured that the hub remains in the central position.

Haemodynamic data as well as PV loops were used to assess when the ventricles had collapsed. Then the VAD performance curves were analysed with transient operating points plotted on them. From this the range of operating point could be viewed before and after the application of the sudden hypertension.

6.3.4.2 **Results**

The haemodynamics of the sudden pulmonary hypertension simulation actuating a passive response are shown in Figure 6-19. Note that the mean and absolute flow rates have been included. It is important to take note of both these flow traces as they will be referred to closely later.

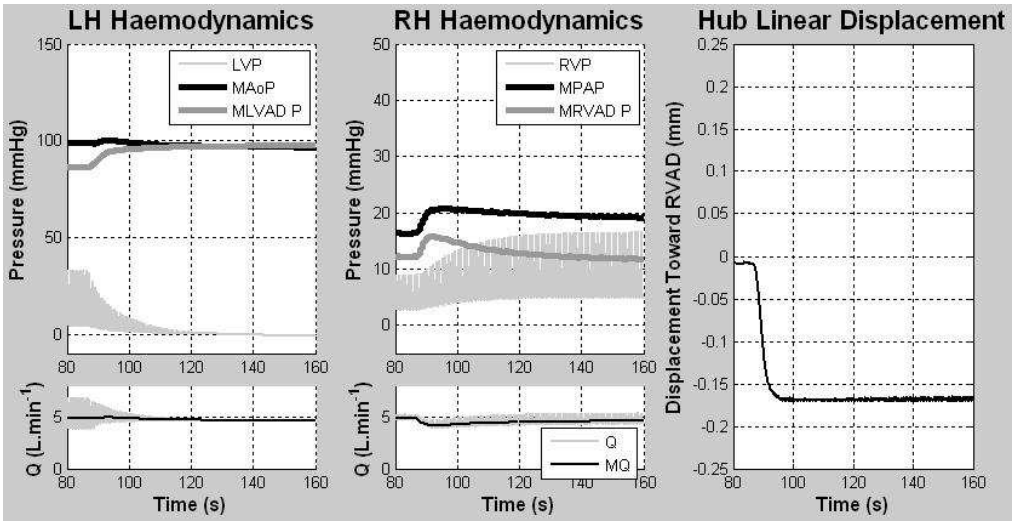

Figure 6-19: Simulation of sudden hypertension in the pulmonary vein with an incorporated passive response from the BiVAD.

Figure 6-20 shows a small plot of VAD performance curves at their associated pump speeds as well as the transient operating points. Then, the main body of the figure is a reduced scale plot of the transient states of the LVAD. The plotted transient states were down-sampled before they were plotted, every fifth time step's operating point was used. Note the black profiles are the performance profiles at a clearance of zero.

The annotations on the main body of the plot show the range of flows, and the mean flow at t = 80 seconds, (before the resistance increase), and t = 160 seconds, (after the resistance increase and after the system has settled). These should be compared by eye to the Q and MQ data in the systemic flow plot in Figure 6-19. Furthermore, the direction of the change in mean flow is given with a grey arrow.

During the steady BiVS, (a), the flow is oscillating between Q = 3.78 and 6.83 L.min^{-1} with a mean flow, (a_{mean}), of MQ = 4.86 L.min^{-1}. Then after the sudden hypertension, (b), the flow oscillation is reduced to Q = 4.62 to 4.65 L.min^{-1} with a mean flow, (b_{mean}), of MQ = 4.64 L.min^{-1}. When considering just the mean flows, there was a decrease in flow of 0.22 L.min^{-1}.

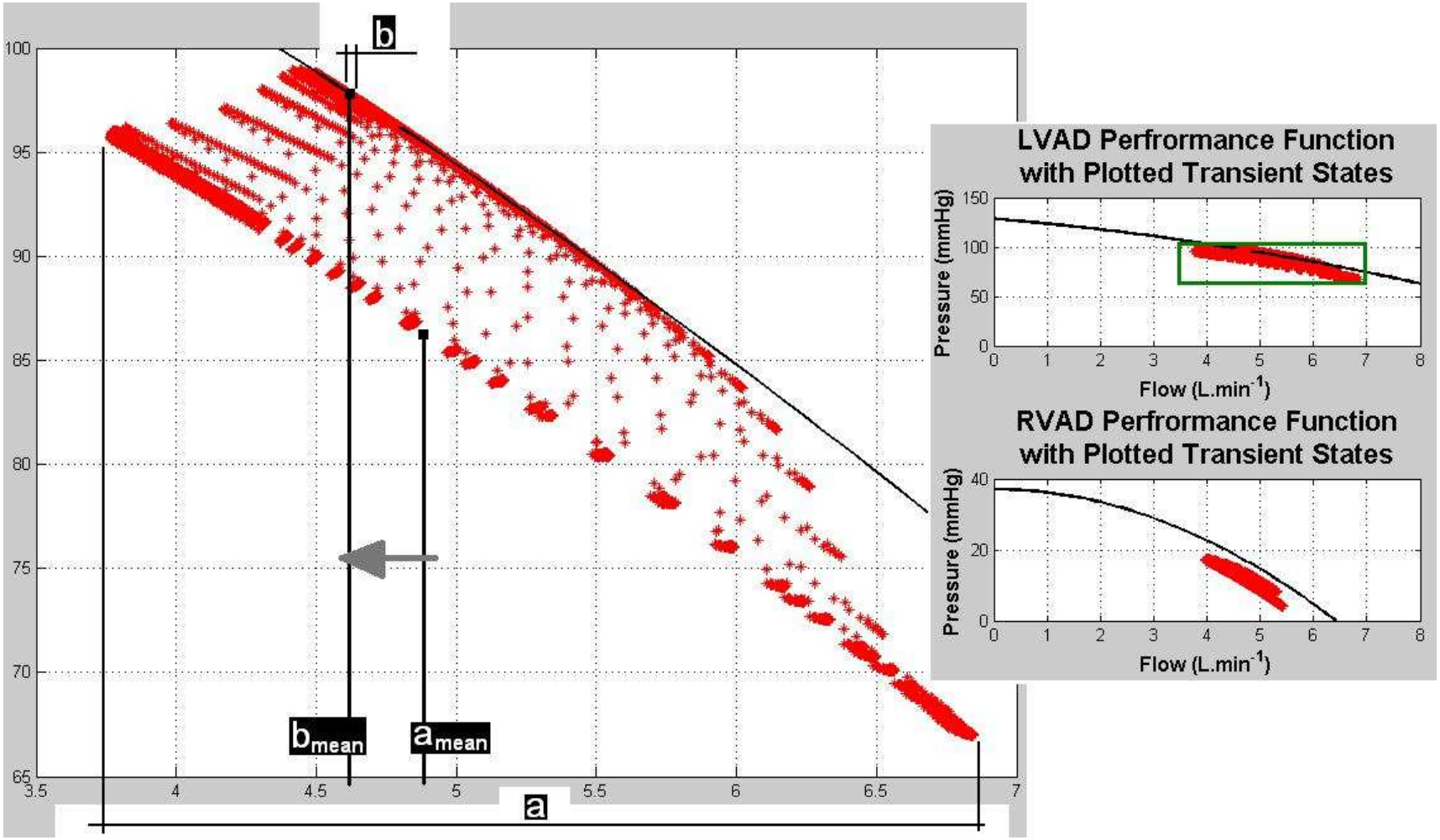

Figure 6-20: Transient LVAD and RVAD operating points with a passive response, (right), reduced scale plot of the transient LVAD states leading to the subsequent LV suckdown, (left). Note, for clarity, only every fifth transient operating point was plotted.

The PV loops in Figure 6-21 show the transient volumes of both ventricles before and after the simulated sudden pulmonary hypertension. As has been seen in the previous sections, the LV PV loop is centred on V = 170 ml and the RV PV loops on V = 120 ml. Arrows have been added to indicate the change in ESV from steady BiVS to after the sudden hypertension.

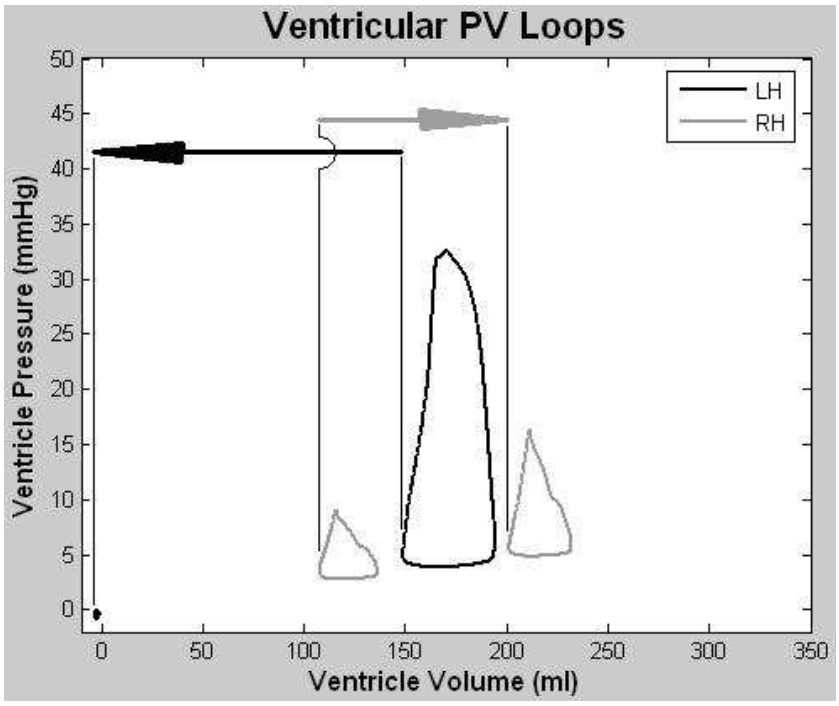

Figure 6-21: The PV loops before and after the sudden hypertension from the simulation with the passive response showing the reduction in LV volume and subsequent suckdown.

As would be expected, the LV volume decreases after the resistance increase. This is confirmed by the dropping LV pressure seen in Figure 6-19. The simulation shows ventricular collapse as the small black dot in the bottom left of the figure show that the simulated LV volume is slightly negative. The increased pulmonary resistance decreases flow out of the RV for a time which causes it to distend.

The haemodynamics of the simulation without a passive response are shown in Figure 6-22. As required for this simulation, the floating assembly starts, and remains in the central position.

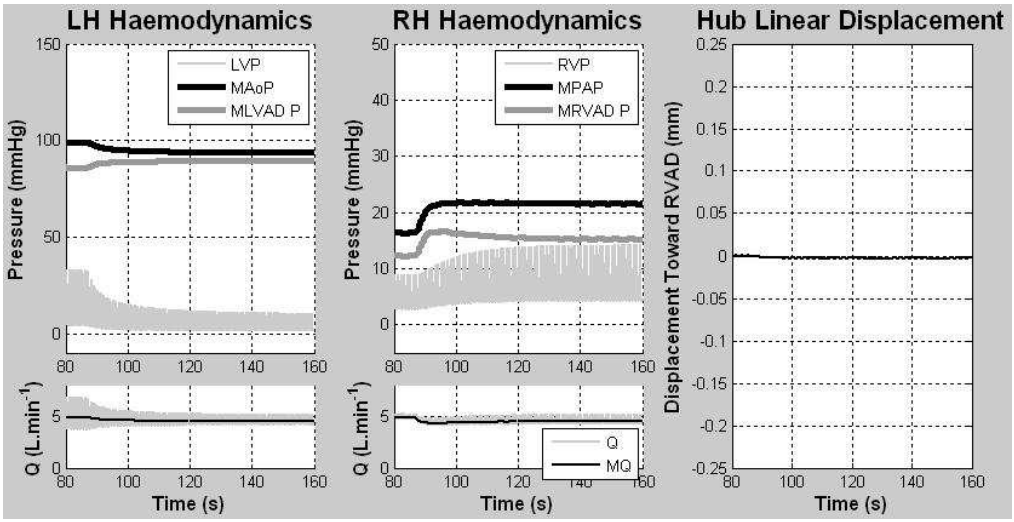

Figure 6-22: Simulation of sudden hypertension in the pulmonary vein with no passive response from the BiVAD.

The mean flow rates without a passive response went from MQ = 4.85 to 4.36 L.min^{-1}. This is a total reduction in flow of 0.49 L.min^{-1}.

The associated PV loops are shown in Figure 6-23. Note that there is a smaller reduction in the LV volume and no subsequent ventricular collapse for this resistance change.

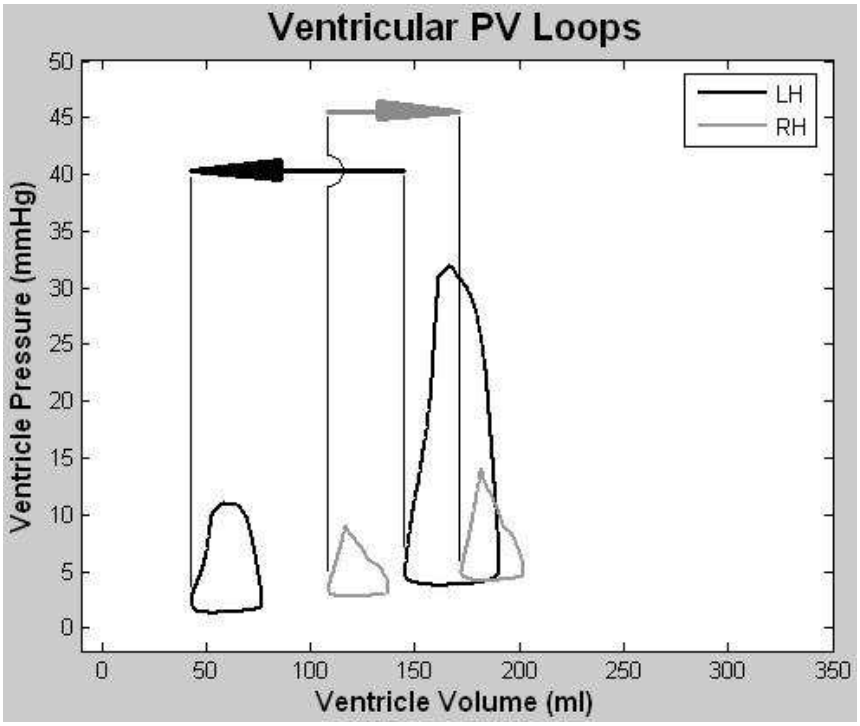

Figure 6-23: The PV loops before and after the sudden hypertension from the simulation with no passive response.

6.3.4.3 **Discussion**

This was a comparative study, not to see if the passively controlled BiVAD could induce ventricular suckdown, but whether the passive action accelerated the onset of collapse. The two simulations were successful in illustrating the effect of the passive controller.

The PV was selected for the resistance increase because it is very hard to induce suckdown in the ventricle by increased arterial resistance. The reason for this is that arterial compliance is low and so only a small volume of fluid is required to congest this part of the vasculature. Increased venous resistance allows fluid to congest throughout the whole pulmonary circuit and therefore allow sufficient time of low venous return to exhaust the ventricle volume.

The reduced venous return into the LV is immediately apparent as the LVP quickly drops below 0mmHg at around 145 seconds signalling a negative ventricle volume and therefore collapse. The collapsed ventricle is confirmed in the PV loops with sub-zero pressures and volumes in the LV. The numerical model has furthered the

understanding of the prototype's response to a hypertensive vascular circuit. This was permitted through increased observabilty in the model as ventricle volumes could be observed in a repeatable testing regeime.

The results show that the action of the passive controller increases the flow rate out of a ventricle suffering from decreased venous return. This effect can be quantified through comparing the decrease in mean LVAD flow rate between the two simulations. The passively controlled BiVAD saw a decrease of 0.22 $L.min^{-1}$, where no passive response saw a decrease of 0.49 $L.min^{-1}$. It is worth reiterating that the increase in pulmonary resistance of 120 $mmHg.s.ml^{-1}$ doubles the total circuit resistance. According to the numerical simulation, then, the resistance change imitates a supported patient with severe hypertension. Additional simulations were run to find out what resistance increase would be required to make the BiVAD simulation **without** the passive response cause ventricular collapse. It was found that the resistance increase needed to be 210 $mmHg.s.ml^{-1}$ which is 163% of the resistance increase required to suckdown the LV supported by the passively controlled BiVAD.

However, as has been pointed out from the experimental simulations, the passive controller is able to reduce arterial pressure caused by hypertension. The numerical simulation showed that a translation of the floating assembly away from the RVAD impeller meant that the PAP increased by only around 3 mmHg by t = 160 s. The simulated BiVAD without the passive action, however, saw an increase in PAP of around 6 mmHg. The passive controlling action of the BiVAD, therefore, imitates the native baroreceptor response.

Numerical simulation in this study provided a more observable investigation of the haemodynamics of hypertension. Using the program to simulate hypertension while supported by the BiVAD has extended the understanding of the use of the passive action as a control strategy. It illustrated how the device can reduce pathological pulmonary vascular pressures. However, it also showed how the passive action increases suction out of, and decreases flow into, the left atrium encouraging the onset of suckdown. It is clear therefore that hypertension, particularly pulmonary hypertension due to low venous fluid reserve, is a dangerous condition for any rotary BiVAD control strategy.

6.4 Numerical Simulation Discussion

The validation processes for both the MCL and human model were very successful. Good agreement was observed between the comparisons particularly between the MCL simulations. The validation process was actually carried out a number of times as it brought up a number of issues that required reworking the algorithm before the validation could be attempted again. However, this is, of course, why a validation is done.

The most notable reworking of the program was modifying the Planar Functions with Pressure and Flow Decrements method to model the VAD performance, (detailed in Appendix C in the attached compact disk), to formulate the Parabolic Performance Vertex Adjustment method as described in Chapter 5. On top of this, the gradual adjustment of the 58 vascular parameters given in Appendix 10.2, Table 10-2 and Appendix 10.2, Table 10-3 was a slow procedure.

Parametric adjustment of the vascular parameters, (as well as the BiVAD parameters), was an invaluable task in the development of the candidate's understanding of the circulation. Tuning such a comprehensive dynamic system provided insight into the interaction of integral, proportional and derivative controllers. Furthermore, it was interesting to identify parameters that have global effects and others which only really induce localised effects.

The inclusion of global inertiance was a novel feature of the model. As mentioned in the previous chapter regions of high rates of change of flow, such as the atria, ventricle and arteries are particularly sensitive to this parameter. For example the validation process revealed that a variation in arterial vessel diameter of only 1mm would heavily impact the ratio and delay of the peak pressures between the ventricle and the corresponding artery.

The unsteady MCL simulation showed that the Parabolic Performance Vertex Adjustment method was representative of the passively controlled BiVAD's operation. This was very encouraging as six methods were tried in total, (therefore

five failed attempts), in order to model the non-linear VAD performance along with the effect of clearance.

Despite the success of the Vertex Adjustment method, the numerical model overestimated the required VAD speeds for BiVS by 6% for both VADs. This was an issue with the construction of the interpolating functions generated in Chapter 5. This is not a serious concern for the purpose of this study as the important feature which is being assessed is the response of the passive controller.

Unfortunately, the comparison for the human simulation was made to 'diagrammatic' textbook data. Steady healthy data could not be obtained because of its scarcity, (there would rarely be a reason to place pressure, flow and imaging sensors throughout a healthy human heart), and required ethics approval. Furthermore, the model was not compared to an unsteady haemodynamic event, (such as sudden hypertension), to validate the dynamic response to sudden changes in vascular parameters. For this reason, the human simulations were assessed with a heavier weight on qualitative analysis.

Further simulations were then carried out using the numerical model to extend the understanding gained from the experimental study presented in Chapter 4. This began with steady simulations comparing the ventricle volumes before and after heart failure and subsequent BiVS. Simulation of healthy circulation saw virtually identical EDV and EVS for both ventricles. Then once the pulse was removed and the diseased ventricles were supported with BiVS, poor volume balancing was observed once arterial pressures and flows had been restored. The RV was sufficiently unloaded but the LV remained moderately distended. This was attributed to the difference in inertial components in each circuit's total impedance. However, due to the lack of certainty in the dynamic parameters in the human model, this result should be viewed as a potential threat to the stability of the LV or the RV during BiVS.

On the other hand, assuming the inertial parameters were indicative of the human vasculature, the result may provide an explanation of clinical observations. Clinical tests have observed subsequent pulmonary hypertension during rotary BiVS. The low

blood pressure in the right heart and the high pressure in the left heart, caused by deflated and distended ventricles respectively, may be sensed by the Vagi via the S-A and the A-V nodes. In an attempt to balance the circuits, a sympathetic nervous response could induce a narrowing of the pulmonary vessels thus increasing pulmonary resistance. The resulting pulmonary hypertension would increase the resident volume in the RH by increasing the RV afterload. Furthermore, the LV volume would decrease due to a decreased venous return. As mentioned earlier, this theory is not proven by these tests; however, it provides a hypothesis for subsequent pulmonary hypertension during rotary BiVS.

The numerical representation of the VADs was then changed so as to make them more responsive to changes in haemodynamics. The first change involved removing the RVAD pressure and flow decrement functions and replacing them with the LVAD decrement functions. It was thought that because the LVAD decrement functions were not as steep at low clearances, the performance's high sensitivity to clearance could be maintained over the whole simulated clearance range, c = 0 to 0.34 mm, (y = ±0.17 mm). It should be noted that the form of the RVAD decrement functions might be a function of the 50 mm diameter impeller. If this is the case, then the decrement functions may not be representative of the impeller geometry. Unfortunately further investigations into ways of manipulating the H vs. c and Q vs. c profiles through changes in geometry were not carried out. The second change was to the lower shroud radius on the LVAD side of the floating assembly. It was reduced from 25.00 to 20.90 mm. This allowed the floating assembly to be positioned approximately central during stable BiVS. It was thought that this would be beneficial as from the central position it can cope with the widest range of vascular pressure variations. It could be that possible future clinical testing sees the need for the hub to be positioned off-centre to cope with more likely CV events such as pulmonary hypertension etc.

Breathing was simulated as an example of an external energy input to the CV system haemodynamics. Its effect on the passive controller was assessed to determine if it has the potential to destabilise the passive action. A transient sinusoidal pleural pressure function was employed to affect the compliant response of the pulmonary vasculature. It was shown that an oscillatory pleural pressure amplitude of around

12.5 mmH_20, (ten times that of resting tidal breaths), caused minimal deflection of the hub. Obviously this would be magnified if the breaths were much higher. The result added to the confidence in the device's ability to provide inherently stable operation in the human CV system.

Results form the experimental testing in Chapter 4 alluded to difficulties experienced when simulating pulmonary hypertension. It was common for the simulation to result in ventricle suckdown depending on how much fluid had been put in the MCL prior to calibrating the pressure sensors, (and therefore referencing a zero pressure level). Gathering effective experimental data to document this was difficult. For this reason, this part of the investigation was left to the numerical simulations. The venous return and ventricular suckdown study compared BiVS simulations subjected to sudden pulmonary hypertension with and without a passive response.

Pulmonary hypertension was induced by increasing the pulmonary vein resistance by 120 $mmHg.s.ml^{-1}$. This doubled the vascular resistance in the complete pulmonary circuit. The induced hypertension increased PA blood pressure and decreased venous return to the left heart for both simulations. This causes a drop in LVP as the LV volume drops.

Without the passive response the LV did not suckdown as venous return was sufficient at the resistance to keep fluid in the LV. In the passively controlled BiVAD simulation, however, the increased PAP caused the floating assembly to translate away from the RVAD impeller decreasing RVAD output into the pulmonary circuit. At the same time the LVAD output increased as the hub moved towards its impeller. The decreased venous return to the left heart and the increased LVAD output rapidly decreased the LV volume until the ventricle collapsed.

When the two simulations were compared it was found that the LVAD flow for the simulation without a passive response decreased by 0.49 $L.min^{-1}$ as the operating point moved to the left of the performance curve due to increased global vascular resistance. The LVAD flow for the simulation with the passive response however, only decreased by 0.22 $L.min^{-1}$. A pathogenic response to hypertension was observed

from the passive action in the form of reduced venous return encouraging ventricular suckdown.

However, at the same time, the passive action reduced the elevated PAP caused by the hypertensive pulmonary circuit. This was the observation also seen in the experimental studies. Therefore, the passive action also provides a positive therapeutic response to hypertension in the form of maintained arterial pressure.

The numerical investigation has shown that the passively controlled BiVAD increased as well as decreased the safety of the support. Regardless of the apparent positive and negative aspects of this response, this study showed that decreased venous return, for whatever physiological reason, is a major vice for the prototype. Ventricular collapse is associated with serious complications such as thrombus formation, damage to the cannulation site and damage to the myocardium itself. In order to continue the development of the passive controller this problem will need to be addressed either through a design alteration or in the incorporation of active speed control to decrease LVAD output.

6.5 Conclusion

This chapter has seen the validation of two circuit models, and from these two sets of vascular parameter data have been defined. The models have been useful in gaining a deeper understanding into the mechanism of BiVAD control both with and without a passive controller. BiVAD support is a new science with a number of very serious concerns. The numerical model has provided a second tool for this project with which to examine a way to overcome these concerns.

A new concept was identified which may be part of the reason rotary BiVS has been identified as a treatment fraught with so many complications. When the circulation is weened away from a pulsatile environment to one of constant flow, there are potentially dramatic changes to the effective resistance. This is due to different levels of inertiance in the pulmonary and systemic circuits. It is very possible that nervous responses soon after BiVF or even cardiac and vascular remodelling in the following weeks to month will have some impact on this effect also. As to whether they will

help or hinder the balance in ventricular volume once BiVS has been provided remains uncertain.

Concern raised earlier in this thesis over the passive controller BiVAD's ability to stabilise and respond safely to a decreasing venous return was studied in this chapter. It was found that the passive response was not sympathetic to ventricular collapse. The passive response actually advances the onset of suckdown by increasing flow out of the endangered ventricle and at the same time reducing flow into it. This is an unfortunate effect of the passive response in its present physical form in the BiVAD prototype. Still, the controller does act to restore pathogenic arterial pressures during hypertension. It outlines how hypertension is a two edged sword when considering rotary support. Output needs to be decreased into a hypertensive circuit to drop the arterial pressure, but it must also be increased so as to maintain adequate venous return through the increased resistance. The result indicates that active control of the VAD impeller speeds will be important in treating this condition.

The ability of the passive controller to sense and manage a number of hydraulic CV events has been outlined in this chapter as well as Chapter 4. The results have seen the assessment of the prototype designed to be inherently stable in its operation to respond passively to the dynamic CV system. Favourable experimental and numerical results have provided an encouraging starting point from which to investigate passively controlled cardiac support devices.

7 Discussion

Left ventricular support using rotary Ventricular Assist Devices, VADs, is complicated by a range of issues including blood damage, miniaturisation and control. Rotary Bi-Ventricular Support is affected by these same issues too; however, recent clinical studies report that poor balancing of circuit volumes is a particular concern. Like the native heart, the Passive Controller BiVAD was designed to take pressure signals from the circulation and passively adjust its output in order to provide volume balance. Two comprehensive studies provided an investigation into the interaction between the Passive Controller BiVAD and the supported circulation to assess the viability of such a device.

In the preceding chapters, experimental and numerical studies have been presented. Individual discussions provided commentaries specific to the works of each chapter. This section offers a broader discussion of the entire project as an investigation into passive control of artificial hearts. To begin with, the implications of providing passive control in a BiVS are discussed before the specific aims of the project are examined in light of the prototype's viability as a safe treatment for heart failure. Following this a number of findings from the project are highlighted which are not specifically involved in the project aims. A discussion documenting issues and problems encountered throughout the project concludes the chapter. Shortcomings in the investigation methodology are included along with their assumed repercussions on the results from this study.

7.1 Implications and Benefits of a Passive Response in BiVS

A BiVAD that is exclusively passively responding must take its control signals from its environment to maintain safe cardiac support without intervening active signalling. In order for this to be possible, the operating environment needs to be able to communicate its hydraulic requirements. The circulation is quite capable of communicating these signals as they are naturally provided to the native heart, and in turn the body's haemodynamics are regulated. So prior to reflection on the findings from this study, it is important to discuss what can be gained from a passively controlled BiVS system and what would be required to make such a system viable.

Rotary VADs are available to the commercial market however, there have been few efforts to try and make these devices passively stable. So what benefits are there in a BiVAD emulating this device-vascular interdependence?

To begin with, it is reasonable to assume that BiVS has additional control issues when compared to single VAD control. After all, a CV system supported by a single rotary VAD still enjoys the stability offered by the remaining functional ventricle providing a Frank Starling (Starling and Visscher 1926) relationship between preload and CO. This will inherently allow some balancing of vascular circuit volumes. If both vascular circuit pumps do not passively fill, such as a rotary BiVAD, there will not be any contributed Frank Starling balancing. Perhaps it is imperative, therefore, to incorporate some inherent stability into the support system to prevent inevitable volume imbalance. At this point in the development of rotary BiVADs, there is not enough evidence to say. However, from the few clinical reports available, it can be said that flow balancing and suckdown management are difficult issues for rotary BiVADs.

Maintaining adequate circulation is crucial. Clearly, the repercussion of device failure is likely to be fatal. If a circulation support device incorporates inherent stability in its operation then it relies less on active maintenance. Another benefit in the passive communication between the circulation and the device, therefore, is that the device relies less on active control systems which are subject to sensor, computer or actuator failure.

Finally, the human circulation operates over a range of pressures and flow rates as well as vascular properties. It is difficult to instruct active systems how to sense and then provide support for exercise, rest, physical movement, hypo- and hypertension etc. An artificial heart which can sense haemodynamic requirements from the circulation and passively respond appropriately need not rely on pre-programmed responses.

Given the benefits in a passive responding system, what would make a BiVAD viable? The circulation can adequately signal haemodynamic imbalance, however if the mechanical support device isn’t sensitive to these signals then it cannot regulate

effectively. A viable device needs to be sufficiently sensitive to these circulation signals such that imbalance is not ignored. Furthermore a viable device needs to be tuned such that the mechanical response to circulation imbalance doesn't over, or under compensate. Provided the device, therefore, is both sensitive and stable in its ability to respond and control then it is potentially viable as a cardiac support device.

7.2 Is the Passively Controlled Rotary BiVAD Prototype Viable?

Although both studies were initiated at the same time, the numerical investigation was very much a progression from the findings observed in the experimental works. This resulted in a progressive analysis rather than identical tests through two testing mediums. Detailed discussion of both the individual experimental and numerical results can be found at the end of Chapters 4 and 6. However, the results of both studies will be summarised specifically in light of the thesis aim which was to assess the viability of the rotary BiVAD prototype.

First of all, it was important to establish whether the floating assembly configuration actuated an output change during *in vitro* simulation. This was confirmed in the first presented experimental result of a supported simulation where severe systemic hypertension was simulated. Two simulations were carried out, one with and the other without, a passive movement of the floating assembly. This result showed that the passive controller was effective at responding to pressure signals from the vascular system.

Following this, a number of experimental simulations showed that the passive controller responded constructively to restore pathogenic arterial pressures. On top of this, the magnitude of the passively adjusted VAD outputs was approximately equivalent to the level of pressure destabilisation. This response emulated the native baroreceptor response in which the sympathetic and parasympathetic nerves regulate arterial pressure by affecting the heart's contractility and heart rate. It was concluded, therefore, that the passive controller action imitated the native barorecpetor response.

Once the experimentation was complete, the numerical model set about simulating the interaction between the supported circulation haemodynamics and the ventricular volumes. This study was encouraged by observed suckdown during *in vitro* hypertension simulations which were unquantified due to the lack of observability in the MCL. The last presented numerical simulation, therefore, was sudden pulmonary hypertension during supported circulation. Two tests were carried out; the first with and the second without a passive response. The latter test provided a control data set for comparison.

As seen in the experimental tests, the increased resistance induced by the pulmonary hypertension increased the PAP and decreased the flow rate through the lungs. The passive action, as also seen in the experimental tests, saw the hub translate away from the RVAD impeller toward the LVAD impeller. This decreased the RVAD output and in doing so reduced the PAP providing the baroreceptor response mentioned earlier. However, what was not quantified in the experimental tests was that the reduced flow through the pulmonary circuit together with the pooling of blood in the pulmonary venous system decreased the venous return to the LV. This response endangered the LV as the LVAD's suction inlet will collapse the LV when the ventricular volume is exhausted. To add to this precarious supported state, the translation of the hub toward the LVAD impeller increased the LVAD output. This reduces the safety of the LV further as the LVAD was attempting to increase the rate of fluid evacuation from the ventricle. It was found that an increase in the Pulmonary Vein resistance from R = 15 to 135 mmHg.s.ml^{-1} was the minimum resistance increase to induce LV suckdown when supported by the passively controlled BiVAD.

The second test without passive control was subjected to the same resistance increase and, although the LV volume was reduced, suckdown did not occur. In fact, simulated LV collapse was not achieved until the pulmonary vein resistance was increased from R = 15 to 210 mmHg.s.ml^{-1}. This is 163% of the threshold resistance for the passively controlled BiVAD. A closer inspection of this result showed that the passively controlled BiVAD saw an LVAD flow decrease of 0.22 L.min^{-1} after the induced hypertension. The simulated BiVAD with no passive response, however, saw an LVAD flow decrease of 0.49 L.min^{-1}. The difference between flow reductions can be wholly accounted for by the passive control action. It can therefore be concluded

that the passively controlled BiVAD accelerates the onset of ventricular collapse when venous return is reduced.

So, is the rotary BiVAD passively controlled by vascular pressure a viable means of bi-ventricular support? Viability, in this sense, was defined earlier as being both sensitive to input signals from the circulation and able to respond constructively. Its performance during simulated hypertension shows that the passive controller response accelerates the onset of ventricular collapse. This is reason enough to conclude that the control system, as it stands, is **not** viable.

The Passive Controller BiVAD prototype, however, provides the design basis for an inherently stable support device. The safety of this device could be vastly improved by incorporating a means of increasing its sensitivity to venous return. This could be as simple as incorporating collapsible inlet cannulae which suckdown before the ventricle. Alternatively an active suckdown prevention control system, such as observations of the current waveform, could be incorporated like many commercially available LVADs. From this point of view further development of the device could render a BiVS system which is not only viable but safer than other fully active cardiac support systems. With a suitable suckdown prevention system, the self balancing nature of the Passive Controller BiVAD prototype offers the potential to overcome the issues seen in early clinical trials.

7.3 Additional Research Findings

There were a number of additional findings from the research that were not exclusively assessing the passive controller's viability. They are however, important outcomes from the research. This section has been added to the discussion in order to highlight these additional findings. These include the effect of steady state BiVS on ventricle volumes, the importance of modelling the inertiance of the atria and ventricles and the performance of the mechanical damper.

7.3.1 Complications in Steady State Rotary BiVS

Clinical reports documenting attempts to provide rotary BiVS have highlighted poor flow balancing, pulmonary hypertension and ventricular collapse as common complications. The numerical model showed that when vascular parameters are kept constant, the mean ventricular volumes during healthy circulation and then supported diseased circulation are not the same. This indicates that in weaning the vascular system away from a pulsatile environment into a constant flow environment each circuit experiences a non-proportional change in the effective resistance. The result is not such a surprise, without a pulse, the pressure drop associated with accelerating the fluid, (inertial response), will be nil. Furthermore, the contributions from the fluid inertia to the impedance of either circuit will not be the same due to differences in vascular volume and length. This implies that when there is no pulse, the resistance of each circuit becomes imbalanced, and in order to maintain the same mean pressures and flow rates, circuit volumes will change. Therefore, by default, non-pulsatile BiVS will be operating in a poorly balanced environment.

The numerical result showed that during healthy circulation, both ventricles maintained a mean volume of around 125 ml. After BiVF and then the application of BiVS restoring healthy haemodynamics, the mean volumes of the RV and LV were around 115 ml and 170 ml respectively. This agrees with the clinical reports of poor flow balancing. Perhaps then, the sympathetic nervous system senses the imbalance and constricts the pulmonary vessels. This pulmonary hypertension will increase RV afterload and decrease venous return into the LV correcting the respective ventricular volumes. This too agrees with the clinical report observing subsequent pulmonary hypertension. Then, as seen in the numerical simulations, the decreased venous return along with a low pulmonary fluid reserve can make the LV susceptible to suckdown. This includes the final observation made by clinical studies into rotary BiVS. Note, this theory was not proved by the numerical study. Without the necessary nervous response to restrict vessels along with representative inertial parameters this idea cannot be tested. However, it provides a hypothesis for future clinical experimentation.

7.3.2 Inertiance Modelling in the Heart Chambers

Many of the reviewed articles documenting circulation models seemed to be hesitant to include inertial parameters. Many of them excluded the effect of fluid inertia completely; others included it exclusively in the main arteries. One recent article included global vascular inertial parameters but excluded those for the atria and ventricles. The candidate found this surprising. The inertial effects of the blood flow are greatest in long blood vessels and/or vessels with high rates of change of flow, (i.e. main arteries and heart chambers). Why then have previous studies been so reluctant to include the ventricular and atria inertiance?

Both the human and the MCL models included global inertial parameters. Defining the inertiance in the validation step, especially in the ventricles and main arteries, was a particularly difficult task. Small changes in their inertiance could completely destabilise the solution. Undoubtedly, this was because the fluid acceleration in the vessels either side of the heart valves was very high. Perhaps, then, ventricular and atrial inertiance has not traditionally been included in these models because of the induced instability and therefore high demand on the computational algorithm. Or perhaps it is because the flow rate through the ventricles and atria is very hard to physically measure. As it is very hard to experimentally approximate the inertiance, research employing experimental vascular data may exclude this. For whatever reason, the numerical model showed that modelling of these parameters was very important in order to obtain representative haemodynamics. The characteristic systolic pressure peak delay between the ventricular pressure and the arterial pressure cannot be modelled without ventricular and arterial inertiance terms. It is also thought by the candidate that a representative dichrotic notch cannot be effectively emulated without modelling the fluid inertia around the aortic or pulmonary valves.

7.3.3 Mechanical Damper

It was required for the functionality of the prototype that the floating assembly should be unaffected by residual ventricular function. The mechanical damper was a custom designed feature of the prototype to restrict the velocity of the floating assembly. Its job was to provide a means of mechanical damping to filter out the higher frequency pulses from the ventricles. This was a very successful design feature of the device.

The damping was not quantified, however, the hub oscillation Amplitude Ratio, *AR*, was decreased by up 94% when the damping was increased from a 'low' to a 'high' level. Hub motion damping was particularly appropriate for this prototype's geometry as the resonant frequency was found to occur around 30 BMP. This beat frequency should be expected as quite possible in a heart failure patient as it is a frequency between approximately normal and fibrillating.

7.4 Issues with the Investigation and Comparison

Although the two studies were initiated together, the completion and testing of the numerical program followed the completion of the experimental study. This was necessary to ensure that the numerical BiVAD model was representative of the experimental device. Furthermore, it provided for a comprehensive validation process which proved to be a valuable step in refining the characterisation of the non-linear performance functions into the linear solution. This sequence of events made for a progressional study where the numerical program extended upon the simulations carried out in the experimental work.

There were a number of issues during the research. In most cases, these issues have been highlighted in the discussion sections thus far. Some were simply a case of problems which were resolved in time, and others remained shortcomings in the project methodology. Fortunately, none of these issues compromised the assessment of the viability of the prototype as a BiVAD, and therefore the primary aim of this investigation. Since the experimental and numerical studies formed a progressional study, the issues raised in this project are presented in their separate studies.

7.4.1 Experimental Device Construction and Testing

After conceptualising the aims for this thesis the initial task was to design a device which incorporated some kind of passively actuated controller. This was a time consuming problem as not only was the prototype required to be sensitive to pressure signals from the CV system, but it needed to respond constructively to these signals. Additionally the magnitude and dynamics of the response needed to be such that the system could be as inherently stable as possible. As shown in Chapter 3, the concept

of the floating assembly was taken on early in the development of the device. In fact, this concept was conceived concurrently with the project aims. The candidate recognises, however, that there are other ways to achieve a passive response. Future research into this concept could investigate different mechanical configurations to achieve passive control.

The primary concern in the experimental setup was that the physical prototype was responsive to pressure signals. The candidate was convinced the device was functional on paper, however, it was recognised that the complex design left many possibilities for unforseen complications. For this reason, it was important that the prototype be manufactured with high geometric accuracy.

The overall translational range used in most of the testing was 0.34 mm, (y = ±0.17 mm). Considering that this range is determined by the axial length between the VAD impeller shafts this was a difficult manufacturing problem. This length is defined by the length of the floating assembly and the combined height of the stacked BiVAD components. The eight stacked BiVAD components include the VAD casings, the passive controller body components and the gaskets (see Appendix 10.1, drawing 1.7). To achieve this clearance the machinist manufactured the floating assembly shaft last. This meant that the tolerance of the stacked components was relaxed and the shaft could be customised during final assembly.

Another fine tolerance was the location and concentricity of the impellers. With such small clearance adjustments providing the passive response the impellers were required to be concentric with the floating assembly, and therefore the corresponding lower shroud. Much credit must be given to the machinist who exceeded expectation in the precision in the manufacture of this complicated prototype. As the experimental results show, with very small hub deflections the device was responsive. The manufactured prototype was an appropriate device to test the project aims.

A requirement for the functionality of the prototype was that it should be unaffected by residual ventricular function. A quasi-steady flow regime may never be reached if the floating assembly was subjected to periodic high amplitude deflections. For this reason, manually adjustable mechanical damping of the floating assembly's motion

was applied. This was a difficult design problem, especially including a means of manual adjustment. The final design of the dual chambered passive controller body with the adjustable occluder worked very well. Regardless of the fact that the damping was unquantified, the micrometer head allowed repeatability through fine adjustment of the protruding spindle length and therefore fluid gap, see Figure 3-29.

Two resources were made available for this project from its outset which proved to be invaluable. These were the Mock Circulation Loop (MCL) and the 3D prototyping machine. The MCL's ability to simulate a pulsatile environment which is representative of human circulation allowed a comprehensive analysis of the physical device. Not having to procure an *in vitro* testing rig not only allowed time for the device development, but it permitted an entire numerical study to be carried out in addition to the experimental study. Similarly, the complicated forms of the mixed flow impellers as well as the casing volutes were not manufacturing complications using the 3D prototyping machine. The VAD components were able to be manufactured quickly and at a low cost.

The largest issue met taking the prototype from the workshop and getting it running in the MCL was fluid leakage. Early testing saw high leakage from the LVAD, into the controller body and then into the RVAD. This began an iterative search for a means of isolating fluid between either VAD and the controller body while still enabling relatively free translation of the hub.

A custom cut out butyl rubber gasket was made for each VAD. This was used in conjunction with a thin latex sheet commercially available for dental surgery called Dental Dam. The combined sealing arrangement allowed adequate sealing once the stacked components were drawn together as well as providing very little axial deflection stiffness to restrict the hub motion.

On top of this water leakage issue, was the problem of air leaks. O rings and O ring grease were used to seal the passive controller body parts; however, these were used with limited success. Air would leak in or out of the controller body when sufficiently substantial negative or positive static pressures were experienced inside the controller body respectively. This made it very difficult to maintain a constant air

spring. Hence, many of the tests were carried out only employing the inherent clearance spring and with the controller cavities open to air, i.e. $k_{air} = 0$. The main consequence of the air leakage problem was that the steady support position of the hub could not be altered using an air spring. Consequently the experimental tests had a steady support hub position of around $y = +0.15$ mm dictated by the resultant pressure force across the floating assembly.

The use of the latex Dental Dam sheets as flexible membranes within the prototype were able to maintain the seal between VADs and the controller body while still allowing hub translation. Flexible material inside a blood pump however is not ideal. Even though pulsatile devices commonly employ polyurethane diaphragms with which to create a variable volume reservoir, the risk of fatigue failure of flexing components reduces their expected life. However, the range and frequency of flexure of the prototype diaphragms are comparatively low as the hub translates a maximum of 0.17 mm and only when the local haemodynamics change. In terms of the reliability of the prototype the use of twin diaphragms is still a cause for concern as they provide potential modes of failure for the BiVAD.

In the candidate's opinion, the poorest result from the whole study was the characterising of the inherent clearance spring. There are a number of reasons for this poor characterisation. The first was that the existence of this inherent spring effect was not foreseen during testing and therefore not directly tested. The second was a consequence of the first, as spring rates were found using a number of hypertension simulations which were carried out on different days. These hypertension simulations often translated over a large clearance range and then were used to characterise the spring rate at the mean translation position. This was a very crude approximation method. Furthermore, the selected parabolic function was not representative of the clearance spring response especially at the translational extremities, (i.e. $y = +0.17$ mm and $y = -0.17$ mm). The final reason for a poor characterisation of this parameter was a lack of time. In hind-sight, the continuous clearance vs. pressure head tests would have been far more suitable experimental data sets to characterise the clearance spring. However, this test was done late in the research and the numerical model development held more pressing issues. It should be noted that this poor result did not carry any bearing on meeting the aims of this project. The

intention of characterising this spring response was only to indicate the magnitude of this response. The numerical relationship was not employed in the numerical model as the inherent clearance spring was applied in the relationship between clearance and pressure head; the Clearance Decrement Functions.

It was unfortunate that the mechanical damping was not quantified. This would have been a difficult undertaking with the configuration of the prototype. Methods for a basic quantification of this parameter have been formulated although require work and experimentation. For the purpose of this study, it was found that the inclusion of the mechanical damping was important if the device is to be used as a support device as opposed to a total support device. Comparative quantities were used to conclude that a 'high' level of damping reduced much of the hub oscillation observed when 'low' damping was used.

Due to the nature of the prototype, restraining the floating assembly from its passive response was very difficult. This was a particular concern when trying to obtain individual pump performance profiles. It was important that these were each tested at a constant speed and a constant clearance. Maintaining the pump speed was a relatively simple task. A constant voltage was provided to the DC motor and the pump speed was observed from the motor encoder reading. Restraining the floating assembly however, was very difficult.

Initially tests were run with both passive controller cavities filled with water and no air bubble. Due to the incompressibility of water, it was hoped that there would be no deflection, (i.e. $k_{air} \approx \infty$). The linear displacement transducer was used to detect any deflection. It was found that deflections in the flexible Dental Dam around the periphery of the lower shrouds caused sufficient compliance within the passive controller body for the hub to deflect during each test. The next attempt saw the removal of the VAD **not** participating in the test from the prototype. This revealed the corresponding lower shroud protruding from the partially exposed floating assembly. The protruding end of the floating assembly was then physically restrained during each performance test. Physical restraint still allowed a slight deflection. This is not surprising considering the range of pressure forces on the hub over an entire performance test. However, the deflections were sufficiently small to be neglected.

7.4.2 Numerical Model Construction and Simulation

The numerical study was a cheap, but time consuming activity. The bulk of this time was spent in the characterisation of the non-linear pump responses and their incorporation into the solution method. Two attempts at rewriting the program using a non-linear Newton-Decent algorithm failed mainly due to a lack of time in which to implement a robust solution. However creating the final linear model, as well as attempting the non-linear models, was a valuable learning experience for the candidate.

Perhaps the most important interaction within the whole numerical program is the effect of varying the clearance, c, on the pump performance. This is, after all, the passive mechanism through which passive control was hoped to be achieved. However, integrating the VADs' performance functions into the linear model was a difficult task. Experimental testing of the effect of a clearance increase showed two important characteristics. The first is that a clearance adjustment impacted on both the pressure head and flow rate significantly enough that neither can be ignored. This meant that within the performance function, the clearance term needed to be coupled to both the pressure and flow terms. The second was that the pressure and flow decay could only be representative if modelled as exponentially related to clearance. This encouraged the complete decoupling of the clearance term from the performance functions themselves. Appendix C, (see the attached compact disk), documents a number of numerical methods used to try and create suitable linear approximations of non-linear performance functions.

Finally, satisfactory solution convergence was obtained through a method which redefined the parabolic performance functions, $H(Q)$, every time step. The redefinition first considered the effect of the expected clearance on the pressure and flow rate. This effect was then quantified using the Clearance Decrement Functions. Then the parabolic vertex was shifted according to the considered decay in pressure and flow. This was the Vertex Adjustment Method. The new shifted performance function was then approximated with an updated linear performance function for application into the linear equation set for solution. Most importantly, this method

incorporates the effect of clearance changes on both pressure and flow despite the linear solution environment. More detail on this method can be found in Chapter 5.

The presented validation study provided confidence in the model's simulation accuracy. A number of numerical simulations imitated the MCL results to ensure that the modelling of both the vascular circuits and the BiVAD were representative. Initially unsupported simulations of healthy and chronic heart failure were presented. This provided the candidate with experience in setting the vascular parameters, and then making changes to the CVP through fluid volume changes respectively.

It was considered important to also validate non-steady numerical simulations. A numerical simulation of sudden pulmonary hypertension was therefore compared to the unsteady experimental result. It provided an opportunity to approximate the spring, mass, damper parameters for the model by comparing the hub motion induced by the sudden pressure rise in the PA. The mechanical damping was approximately quantified as 50 $N.s.mm^{-1}$ through comparison of the experimental and numerical hub response. A validation of the air spring formulation was not carried out due to the inconsistencies caused by the air leakage during experimentation. Only the inherent clearance spring response provided a proportional response to clearance changes in both investigations. The measured floating assembly mass of m = 160g was maintained for this test.

It was unfortunate that the numerical model was not validated against clinical human data. This was primarily because the device has not been physically tested in a human or animal model for comparison. Even obtaining unsupported human clinical data required communications and approval from ethics committees which the candidate did not have. Regardless of the lack of clinical data, the model still needed to be compared to something beyond the MCL data before human simulations could be initiated. Characteristic circulation diagrams were sourced from literature and used as comparative human circulation data. At the very least this provided a basis from which to approximate the vascular parameters as well as the total circuit blood volume.

Once the solution algorithm was validated and the human circuit parameters had been defined, two changes were made to the passive response. It was thought that these changes would optimise the operation of the BiVAD although due to time restraints the effects of these changes could only be qualified. The first change was to decrease the radius of the LVAD lower shroud from 25.00 to 20.90 mm. This reduced the pressure force from the LVAD and allowed the floating assembly to be centrally located during steady support. The second change was to redefine the RVAD Clearance Decrement Functions. The original functions, derived from experiments, saw 83% and 79% of the pressure and flow drop respectively over the first 0.02 mm of blade clearance, (y = +0.17 to +0.15 mm). The RVAD, therefore, was only responsive to clearance when the hub was very close to its impeller blades, (as it was for most of the experimental testing with a LVAD lower shroud radius of 25.00 mm). In order to make the RVAD performance responsive over the whole hub translational range, the LVAD decrement functions were used for both VADs.

The numerical simulation overestimated the required pump speeds to support the failed heart by 14% for both VADs. Careful revision of the pump characterisation found that this was very likely due to an oversight of the clearance parameter used to obtain the experimental pump performance curves. Recall that in obtaining the individual VAD performance curves one end of the floating assembly was physically restrained in order to keep an approximately constant clearance. In order to prevent the lower shroud from coming in contact with the impeller blades during the test, a very small clearance was introduced during the test. However, within the Vertex Adjustment Method, this performance curve was used to reference the performance at a clearance of c = 0.0 mm. In actual fact, it was very likely that this clearance was around c = 0.05 mm at least. Let us consider the performance curves in Section 4.3.2. The running speeds for the VADs in the H vs. c and Q vs. c tests were N_{LVAD} = 3400 RPM and N_{RVAD} = 1100 RPM. Comparing these plots to the performance curve at that speed, one can determine the clearance at which the continuous clearance tests were carried out. These were approximately $c_{LVAD} \approx$ 1.0 mm $c_{RVAD} \approx$ 0.25 mm. For both VADs the output at these clearances has already seen a large decay. It is unsurprising then that the program has to overestimate the pump speed since the output it assumes is at zero clearance is actually already substantially decayed.

This could have been accounted for using the decrement functions. The decrement functions should have been normalised using the pressure and flow at the clearance used in the continuous clearance test rather than the maximum pressure and flow. In this case, the decrements would be greater than unity at low clearances in order to magnify the pump output. This was an oversight in the development of the numerical model of the performance curves. Although a misrepresentation of the pump speed did not hinder the aims of this project, future work involving the program shouldn't be carried out before the decrement functions are redefined.

In an attempt to increase the representative nature of simulation, models such as the MCL and the numerical simulation are often under constant development. The candidate found it difficult to cease the development of the numerical model and begin the validation process as there was a list of improvements still to be implemented. Eventually time restrictions signalled the end of the development to begin validation and the BiVAD simulations. Aside from redefining the clearance decrement functions the next development was planned to be implementing the volume dependent compliances of the ventricles and atria. This would model the non-linear stress-strain relationship as well as the elastic limit of the ventricle. It was decided it was not a necessary feature for this study because the ventricle volumes during supported simulation did not approach the elastic limits of the myocardium. However, the PV loop for the bi-ventricular failure simulation in Figure 6-14 and Figure 6-15 is probably not representative of severe BiVF PV loops as the diastolic pressures are too low.

It should be noted that even when using the numerical model to simulate steady BiVS, ventricular suckdown was very sensitive to the pump speeds. Consider a set of vascular parameters. Given the described system, there is a narrow range of safe LVAD and RVAD speeds where no vessel volumes will become negative within the model, (hence suckdown). The candidate found that the program would have to be run numerous times gradually tuning the VAD speeds in order to simulate steady support without suckdown. This alone indicates the precarious nature of rotary BiVS. The candidate believes that single rotary VAD support may be less dangerous as there is still one functional passively filling ventricle to balance circuit volumes. A

comparison of the stability of single and bi-ventricular rotary support could be carried out as an indication of the relative difficulty in the two forms of cardiac assistance.

It was envisioned at the outset of the program development that the inclusion of multiple parallel branches in the human circuit model would be useful. It was hoped that a vascular baroreceptor response would be included in the final model in order to regulate cerebral blood flow. This was not implemented due to time restraints as well as lack of access to clinical data with which to characterise human vessel properties.

The validated numerical program is a valuable resource that can be used beyond this study. It is particularly useful for supported circulation simulation. The novel method of characterising pump performance could be applied to a range of devices. *In silico* simulations such as these are especially valuable when modelling patients with serious illness such as heart failure. Testing, which would otherwise see euthanasia or device failure in a clinical setting, can be carried out and repeated on the computer.

8 Conclusions and Future Research

8.1 Conclusion

A rotary Bi-Ventricular Assist Device (BiVAD) prototype was developed and tested to assess its viability as a completely self regulating artificial heart. Two methods of assessment were used. The first, an experimental study saw the construction and then testing of the prototype in mock circulation. The second was a numerical simulation where the human circulation, BiVAD pumps and passive controller were characterised *in silico*. Passively controlled through blood pressure signals only, the BiVAD regulated VAD flow rates to passively balance circuit volumes through a baroreceptor-like response. However, in its present form the device's lack of sensitivity to venous return makes it unable to stabilise imminent ventricular suckdown.

The use of both tests was advantageous for the study because each of them offered insight into the device's operation. The experimental tests, although less observable due to sensing limitations, provided a means with which to validate the numerical model and characterising the BiVAD and controller. On top of this, testing the physical prototype provided an initial indication of the interaction between the CV system and the device passive controller. These results were valuable as they didn't have the associated error through numerical characterisation of the physical BiVAD parameters such as the dynamic mechanical components of the controller.

Once validated, the numerical model was used to study the interaction between ventricle volume and the supported circulation haemodynamics. Initially, the baroreceptor-like response of the controller was confirmed in the numerical simulations. However, the device accelerated the onset of left ventricular collapse during simulated pulmonary hypertension. This was because on top of reduced pulmonary venous return, the resulting passive action increased LVAD output encouraging further evacuation of fluid from the LV. Without the numerical model, the incidence of ventricular suckdown could not have been quantified.

Throughout the study there were a number of additional findings. Perhaps the most significant was in an investigation into steady state rotary BiVAD support. Simulating the reduction in flow pulsatility as the healthy circulation was affected by heart failure and then received subsequent BiVS, the ventricle volumes became unbalanced. It was thought that the difference in contributions of fluid inertia to each vascular circuit's impedance unbalanced the circuit resistances during constant flow support. The consequences of this inherent volume imbalance could not be simulated as it would depend on the native circulation's auto regulatory response. However, in light of the few documented *in vivo* studies of rotary BiVS, volume imbalance could explain clinically observed poor flow balancing, pulmonary hypertension and LV collapse.

The result encourages further development of the passive control system. In its present form it provides an inherently stable support system provided venous return is maintained. It is suggested that the use of collapsible inlet cannulae as sacrificial hardware be investigated to complete the completely passively controlled system. Otherwise the incorporation of an active system to observe the transient current supply, similar to existing VAD control protocol, should be employed to prevent ventricular suckdown.

8.2 Future Research

Throughout this thesis, there have been numerous mentioned opportunities for further research. Below are briefly documented areas of investigation which could add further understanding to the study of providing rotary BiVS through a passively controlled mechanical device:

8.2.1 The Passively Controlled BiVAD

- Clinical testing of the device to observe the interaction of the auto regulating vascular system with the dynamic passive controller. However, this will require:
    - Miniaturisation of the device

    - Redesign of the blood contacting areas to remove regions of potential stagnation
    - Adequate material selection to reduce platelet activation
    - Quantifying the effect of clinically induced vascular pressure fluctuations and what the desired performance adjustment should be. This study will essentially allow a relationship between lower shroud areas, passive controller spring stiffness and rate of pressure and flow decay with blade clearance.
- Development of a magnetically coupled impeller drive and suspension system. This will allow the removal of the impeller drive shaft, lip seals and impeller mounting bearings so as to minimise blood damage as a clinical device.
- Development of suitable cannulae. Cannulation development could include the incorporation of collapsible inlet cannulae to provide a BiVS sensitive to low inlet pressures caused by decreased venous return.
- Experimental testing into the effect of impeller radius on the blade clearance vs. pressure head and flow rate profiles. This may explain the difference in the decay rate of the pressure and flow with clearance between the LVAD and the RVAD.
- Development of a robust means of providing a steady state bias force of the floating assembly. This will allow the ratio of lower shroud areas to be selected based on assumed pressure fluctuations in each vascular circuit rather than the ratio of static pressure within each VAD.
- An investigation into the development of a fully active magnetic levitation system to locate the floating assembly. A PID type response to blood pressure could then implemented, similar to the spring, mass, damper configuration. Although being reliant on an active control system, it would allow the BiVS system to enjoy the flexibility to override the PID response if needed.
- Investigate different ways of providing a passive response. This would ideally reveal a controller configuration that is sensitive to pressure and ventricle volume.
- Redesign of both VADs to increase hydraulic efficiency. Following this, a CFD and/or flow visualisation study of pulsing flow through both VADs to isolate any areas of low flow. This may be particularly necessary for the

region between the upper shroud and the pump casing. Perhaps this study will recommend the removal of the upper shroud so that the impeller becomes fully open.

8.2.2 Clinical Testing of the Vascular System

It is understood that many of the investigations in this section are complicated by ethical issues. Since the modelling attempted to be representative of the human circulation, accurate models will need clinical human data. Obtaining such data would require highly intrusive and probably fatal experimentation. Regardless of this, future work has been listed in this section as an indication of the lack of knowledge available regarding cardiac support – particularly rotary BiVS.

- Observations of mean ventricle volumes during healthy circulation and then after heart failure and subsequent rotary BiVS. This will provide a clinical study to repeat the numerical findings that inherent volume imbalance is associated with the reduction in pulse.
- Quantification of likely vascular pressure fluctuations during hypertension, oedema, further failing of the left and right ventricles, standing up and lying down as well as breathing and the Valsalva manoeuvre.
- Quantification of the vascular resistance, compliance and geometry of the human vasculature in both circuits. It is important that testing be carried out on a subject with heart failure as opposed to one with a healthy circulation system as this will be representative of an appropriate patient.
- Selection of the inlet cannulation sites. This is of particular concern for the right heart as there are significant dangers in both right ventricular and right atrial cannulation. The distance between the RV outer wall and the septum is small leaving little room for the cannula tip to draw blood increasing the risk of suction events. However, cannulation of the right atrium also poses a problem as device failure will result in the RVAD providing a shunt between the arterial system and the venous system.

8.2.3 The Numerical Simulation

- Development of the linear system
    - Redefine the Clearance Decrement Functions so that they reference the clearance used during the experimental pump performance tests
    - Employ the experimental LVAD and RVAD clearance vs. pressure head relationships to redefine the clearance spring function.
    - Integrate the volume dependent ventricular and atrial compliance profiles into the system. This will simulate the non-linear stress-strain relationship as well as the elastic limit of the myocardium.
    - Integrate the volume dependent compliance of arterial and venous vessels into the model.
    - Remodelling of the heart valves to include their dynamic opening and closing actions. This should allow the dicrotic notch to be more accurately modelled in the healthy simulation.
- Development of a robust non-linear solution algorithm. This will allow the non-linear pump performance curves and the effect of clearance on performance to be fully coupled into the solution algorithm.
- The incorporation of a discretised heart model so as to simulate the movement of fluid through the ventricles and atria more accurately. This will allow a more accurate representation of the inertiance in the heart as well as allowing simulations of the cannulation sites to be carried out.
- Carry out a comparative study of single VAD support and BiVAD support using rotary pumps to quantify the relative susceptibility of suction events. Due to the lack of data in the field of rotary BiVS this study will be useful as a warning for groups beginning to develop such systems.

9 References

ABS. 2005. ABS National Health Survey 2004-2005: Australian Bureau of Statistics.

Ahlers, M O, A Abdullah, and U Platzer. 2003. Physical Properties of Latex and Non-latex Dental Dam Materials. Paper read at 81st General Session of the International Association for Dental Research, at Goteborg, Sweden.

AIHW. 2004. Heart, Stroke and Vascular Diseases - Australian Facts 2004, edited by A. I. o. H. a. Welfare and N. H. F. o. Australia.

AIHW, (Australian Institute of Health and Welfare). *Latest Mortality Data* 2006 [cited. Available from www.aihw.gov.au.

Araki, K., and Y. Taenake. 1995. Hemolysis and heat generation in six different types of centrifugal blood pumps. *Artificial Organs* 19 (9):928-932.

ASTM_F1841-97. 1998. Standard Practice for Assessment of Hemolysis in Continuous Flow Blood Pumps. *Annual Book of ASTM Standards* 13 (1):1-5.

Ayre, P J, S S Vidakovic, G D Tansley, P A Watterson, and N H Lovell. 2000. Sensorless flow and head estimation in the VentrAssist rotary blood pump. *Artificial Organs* 24 (8):585-588.

Berger, R., E. Gruber, P. Mares, H. Schima, R. Seitelberger, and M. Hiesmayr. 1998. Biomedicus BIVAD as a successful bridging to recovery strategy in fulfilment myocardial failure. *Artificial Organs* 22 (2):152-171.

Bhunia, S.K., and R.T.V. Kung. 2004. Indirect Bronchial Shunt Flow Measurements in AbioCor Implantable Replacement Heart Recipients. *ASAIO Journal* 50 (3):211-214.

Bourque, K, D B Gernes, H M Loree, 2nd, J S Richardson, V L Poirier, N Barletta, A Fleischli, G Foiera, T. Gempp, R. Schoeb, K. Litwak, T. Akimoto, M. Watach, and P. Litwak. 2001. HeartMate III: pump design for a centrifugal LVAD with a magnetically levitated rotor. *ASAIO Journal* 47 (4):401-405.

Burgreen, G W, J Antaki, Z J Wu, and A J Holmes. 2001. Computational Fluid Dynamics as a Development Tool for Rotary Blood Pumps. *Artificial Organs* 25 (5):336-340.

Choi, Seongjin, J. Robert Boston, and James F. Antaki. 2007. Hemodynamic Controller for Left Ventricular Assist Device Based on Pulsatility Ratio. *Artificial Organs* 31 (2):114-125.

Chou, Nai-Kuan, Shoei-Shen Wang, Yuan-Hsiang Lin, Jeou-Jong Shyu, Kuo-Huang Hsieh, Gwo-Jen Jan, and Shu-Hsun Chu. 2001. Development of a Totally Implantable Pulsatile Centrifugal Pump as a Ventricular Assist Device. *Artificial Organs* 25 (8):603-606.

Christiansen, Stefan, Alberto Perez-Bouza, Helmut Reul, and Rudiger Autschbach. 2006. In Vivo Experimental Testing of a Microaxial Blood Pump for Right Ventricular Support. *Artificial Organs* 30 (2):94-100.

Chua, L. P., G. Song, S. C. M. Yu, and T. M. Lim. 2005. Computational Fluid Dynamics of Gap Flow in a Biocentrifugal Blood Pump. *Artificial Organs* 29 (8):620-628.

Dargie, H. J., J. J. V. McMurray, and T. A. McDonagh. 1996. Heart failure - implications of the true size of the problem. *Journal of Internal Medicine* 239 (4):309-315.

Debakey, M E. 2000. The odyssey of the artificial heart. *Artificial Organs* 24 (6):405-411.

Dolgin, Martin. 1994. *Nomenclature and Criteria for Diagnosis of Diseases of the Heart and Great Vessels*: Little Brown and Company.

Drews, T, M Loebe, E Hennig, F Kaufmann, J Muller, and R Hetzer. 2000. The 'Berlin Heart' assist device. *Perfusion* 15 (4):387-396.

El-Banayosy, Aly, Latif Arusoglu, Michel Morshuis, Lukasz Kizner, Gero Tenderich, Peter Sarnowski, Hendrik Milting, and Reiner Koerfer. 2005. CardioWest Total Artificial Heart: Bad Oeynhausen Experience. *The Annals of Thoracic Surgery* 80 (2):548-552.

Endo, George, Kenji Araki, Kazushi Kojima, Kunihide Nakamura, Yasunori Matsuzaki, and Toshio Onitsuka. 2001. The Index of Motor Current Amplitude Has Feasibility in Control for Continuous Flow Pumps and Evaluation of Left Ventricular Function. *Artificial Organs* 25 (9):697-702.

Endo, George, Kenji Araki, Mitsuo Oshikawa, Kazushi Kojima, Tomokazu Saitoh, Kunihide Nakamura, and Toshio Onitsuka. 2000. Control Strategy for Biventricular Assistance with Mixed-Flow Pumps. *Artificial Organs* 24 (8):594-599.

Engineers Edge - Pump Impeller Types [cited. Available from http://www.engineersedge.com/pumps/impellar_classification.htm.

Fukamachi, K, DJ Horvath, AL Massiello, Y Ootaki, K Kamohara, M Akiyama, F Zahr, MW Kopcak, Jr., R Dessoffy, Ji-F Chen, S. Benefit, and L. Golding. 2005. Development of a small, implantable right ventricular assist device. *Asaio Journal* 51:730–5.

Fukamachi, K, P M McCarthy, N G Smedira, R L Vargo, R C Starling, and J B Young. 1999. Preoperative risk factors for right ventricular failure after implantable left ventricular assist device insertion. *The Annals Of Thoracic Surgery* 68 (6):2181-2184.

Furukawa, Kojiro, Tadashi Motomura, and Yukihiko Nose. 2005. Right Ventricular Failure After Left Ventricular Assist Device Implantation: The Need for an Implantable Right Ventricular Assist Device. *Artificial Organs* 29 (5):369-377.

Gaddum, N., D Timms, and CC Tann. 2006. Mixed Flow Impeller Design to Improve RVAD Performance for BiVAD Application. Paper read at 14th Congress of the International Society for Rotary Blood Pumps, at Leuven, Belgium.

Goldowsky, Michael. 2004. Magnevad - The World's Smallest Magnetic-bearing Turbo Pump. *Artificial Organs* 28 (10):945-952.

Goldowsky, Michael, Rocco Lafaro, and George Reed. 2005. Magnevad Status of Design Improvements Human Blood Results and Preliminary Sheep Trial. *Artificial Organs* 29 (10):855-857.

Goldstein, D.J., and M.C. Oz. 2000. *Cardiac Assist Devices*: Futura Publishing Company, Inc.

Guyton, A. C. 2005. *Textbook of Medical Physiology*. 11 ed: W.B. Saunders Company.

Hanson, B M, M C Levesley, K Watterson, and P G Walker. 2005. Simulation of the Human Cardiovascular System for Real-Time Physical Interaction with an Assist Device. Paper read at Engineering in Medicine and Biology 27th Annual Conference, September 1-4, 2005, at Shanghai, China.

James, Natalie L., Carmel M. Wilkinson, Nicole L. Lingard, Anita L. van der Meer, and John C. Woodard. 2003. Evaluation of Hemolysis in the VentrAssist Implantable Rotary Blood Pump. *Artificial Organs* 27 (1):108-113.

Japikse, D., WD Marscher, and RB Furst. 1997. *Centrifugal pump design and performance*: Wilder, VT: Concepts ETI.

Kameneva, Marina V, Greg W Burgreen, Kunisha Kono, Brandon Repko, James F Antaki, and Mitsuo Umezu. 1992. Effects of turbulent stresses upon mechanical hemolysis: experimental and computational analysis. *ASAIO Journal (American Society For Artificial Internal Organs: 1992)* 50 (5):418-423.

Kohrt, Kevin. *PHYSBE* 1999 [cited. Available from http://www.mathworks.com/matlabcentral/fileexchange/loadAuthor.do?objectType=author&objectId=804600.

Korakianitis, T, and YB Shi. 2006. Numerical simulation of cardiovascular dynamics with healthy and diseased heart valves. *MEDICAL ENGINEERING & PHYSICS* 28 (8):762-779.

Larnard, L.D. 1986. Simulation of cardiac arrhythmia haemodynamics with a real-time computer model. *Med. & Biol. Eng. & Comput.* 24:456-470.

Leverett, LB, JD Hellums, CP Alfrey, and EC Lynch. 1972. Red blood cell damage by shear stress. *Biophysical journal* 12:257-72.

Mackay, Judith, and George Mensah. 2004. *The Atlas of Heart Disease and Stroke*: World Health Organization.

Mandarino, WA, RL Kormos, A Kawai, TA Gasior, MR Pinsky, and BP. Griffith. 1994. Dynamic biventricular response to alterations in preload in patients undergoing left ventricular device implantation. *Asaio Journal* 40 (3):M295-8.

Masuzawa, Toru, Tomonori Tsukiya, Seiko Endo, Eisuke Tatsumi, Yoshiyuki Taenaka, Hisateru Takano, Takashi Yamane, Masahiro Nishida, Balazs Asztalos, Yuki Miyazoe, Kazuyuki Ito, Toshio Sawairi, and Yoshiaki Konishi. 1999. Development of Design Methods for a Centrifugal Blood Pump with a Fluid Dynamic Approach: Results in Hemolysis Tests. *Artificial Organs* 23 (8):757-761.

McLeod, J. 1968. PHYSBE...a year later. *Simulation* vol.10 (no.1):27-45.

McLeod, John. 1966. PHYSBE...a physiological simulation benchmark experient. *SIMULATION* 7 (6):324-329.

McNeil, K. 2008. Hypertension, Discussions of Haemodynamic Complications. Brisbane.

Mesana, Thierry G. 2004. Rotary Blood Pumps for Cardiac Assistance: A "Must"? *Artificial Organs* 28 (2):218-225.

Meyns, B. 2005. Right Ventricular Support After Left Ventricular Assist Device Implantation - Pro Left Ventricular Support. Paper read at Proceedings of the 4th Berlin Symposium on Mechanical Circulatory Support, at Deutsches Herzzentrum Berlin, Germany.

Milnor, William. R. 1982. *Hemodynamics*: Williams & Wilkins.

Misgeld, B J E, J Werner, and M Hexamer. 2005. Robust and self-tuning blood flow control during extracorporeal circulation in the presence of system parameter uncertainties. *Medical and Biological Engineering and Computing* 43 (5):589-598.

Mitsui, N, S Fukunaga, Y Koura, S Morita, H Hotei, M Sueshiro, T Sueda, and Y Matsuura. 1996. Numerical simulation of nonpulsatile left ventricular bypass. *Artificial Organs* 20 (6):632-636.

Mitsui, Norimasa, Shintaro Fukunaga, Taijiro Sueda, Yuichiro Matsuura, Patrick Havlik, Jean Trinkl, Jean-Luc Demunck, Thierry Mesana, and Jean-Raoul Monties. 1998. Study of Left Ventricular Bypass Using Wankel Type Semipulsatile Blood Pump. *Artificial Organs* 22 (5):419-425.

Miyazoe, Yuki, Toshio Sawairi, Kazuyuki Ito, Yoshiaki Konishi, Takashi Yamane, Masahiro Nishida, Balazs Asztalos, Toru Masuzawa, Tomonori Tsukiya, Seiko Endo, and Yoshiyuki Taenaka. 1999. Computational Fluid Dynamics Analysis to Establish the Design Process of a Centrifugal Blood Pump: Second Report. *Artificial Organs* 23 (8):762-768.

Neil, Eric. 1979. *Human Circulation*: Carolina Biological Supply Co.

Nonaka, Kenji, Joerg Linneweber, Seiji Ichikawa, Shinji Kawahito, Tadashi Motomura, Hiroshi Ishitoya, Daniel Oestmann, Julia Glueck, and Yukihiko Nose. 2002. Assessing the Calf Pulmonary Function During a Long-Term Biventricular Assist Device Study with a Centrifugal Blood Pump. *Artificial Organs* 26 (11):924-926.

Nose, Y, and K Kawahito. 1997. Development of a non-pulsatile permanent rotary blood pump. *Eur J Cardiothorac Surg* 11:S32-S38.

Olegario, Paul S., Makoto Yoshizawa, Akira Tanaka, Ken-ichi Abe, Hiroshi Takeda, Tomoyuki Yambe, and Shin-ichi Nitta. 2003. Outflow Control for Avoiding Atrial Suction in a Continuous Flow Total Artificial Heart. *Artificial Organs* 27 (1):92-98.

Oshikawa, M., K. Araki, G. Endo, H. Anai, and M. Sato. 2000. Sensorless Controlling Method for a Continuous Flow Left Ventricular Assist Device. *Artificial Organs* 24 (8):600-605.

Park, Chan Young, Jun Woo Park, Jung Joo Lee, Wook Eun Kim, Chang Mo Hwang, Kyong-Sik Om, Jaesoon Choi, Jongwon Kim, Eun Bo Shim, and al. Jo et. 2003. Development of totally implantable pulsatile biventricular assist device. *Artificial Organs* 27 (1):119-123.

Paul, Reinhard, Jorn Apel, Sebastian Klaus, Frank Schugner, Peter Schwindke, and Helmut Reul. 2003. Shear Stress Related Blood Damage in Laminar Couette Flow. *Artificial Organs* 27 (6):517-529.

Pinsky, Michael R., Stefano Perlini, Pier Luigi Solda, Paolo Pantaleo, Alessandro Calciati, and Luciano Bernardi. 1996. Dynamic right and left ventricular interactions in the rabbit: Simultaneous measurement of ventricular pressure-volume loops. *Journal of Critical Care* 11 (2):65-76.

Song, Xinwei, Amy L. Throckmorton, Alexandrina Untaroiu, Sonna Patel, Paul E. Allaire, Houston G. Wood, and Don B. Olsen. 2003. Axial Flow Blood Pumps. *ASAIO Journal* 49 (4):355-364.

Starling, E.H., and M.B. Visscher. 1926. The Regulation of the Energy Output of the Heart. *J Physiol* 62:243-261.

Stepanoff, A.J. 1957. *Centrifugal and Axial Flow Pumps*: John Wiley and Sons, Inc.

Takami, Yoshiyuki, Goro Otsuka, Jurgen Mueller, Yohichi Sugita, Kin Ichi Nakata, Eiki Tayama, Yukio Ohashi, Heinrich Schima, Helmut Schmallegger, Ernst Wolner, and Yukihiko Nose. 1998. In Vivo Evaluation of the Miniaturized Gyro Centrifugal Pump as an Implantable Ventricular Assist Device. *Artificial Organs* 22 (8):713-720.

Takatani, Setsuo. 2006. Progress of Rotary Blood Pumps. *Artificial Organs* 30 (5):317-321.

Tansley, G., S. Vidakovic, and J. Reizes. 2000. Fluid Dynamic Characteristics of the VentrAssist Rotary Blood Pump. *Artificial Organs* 24 (6):483-487.

Tayama, Eiki, Don B. Olsen, Yukio Ohashi, Robert Benkowski, Deborah Morley, George P. Noon, Yukihiko Nose, and Michael E. DeBakey. 1999. The DeBakey Ventricular Assist Device: Current Status in 1997. *Artificial Organs* 23 (12):1113-1116.

Teixeira, P. B. D., P. B. Goncalves, I. A. Cestari, A. A. Leirner, and D. Pamplona. 2001. Mechanical behaviour and stability of the internal membrane of the InCor ventricular assist device. *Artificial Organs* 25 (11):912-921.

Timms, D. 2006. Design, Development and Evaluation of Centrifugal Ventricular Assist Devices. PhD, School of Built Environment and Engineering,, Queensland University of Technology, Brisbane.

Timms, D, K. McNeil, J. Dunning, A. Galbraith, M. Hayne, and M. Pearcy. 2006. Left/Right Flow Balancing with a Rotary BiVentricular Assist Device. Paper read at 14th Congress of the International Society for Rotary Blood Pumps, at Leuven, Belgium.

Timms, Daniel. 2007. Acute Animal Experience with the Bivacor Rotary BIVAD/TAH. Paper read at International Society for Rotary Blood Pumps, at Sydney.

Timms, Daniel , John Fraser, Mark Hayne, John Dunning, Keith McNeil, and Mark Pearcy. 2008. The BiVACOR Rotary Biventricular Assist Device: Concept and In Vitro Investigation. *Artificial Organs* 32 (10):816-819.

Timms, Daniel, Mark Hayne, Keith McNeil, and Andrew Galbraith. 2005. A Complete Mock Circulation Loop for the Evaluation of Left, Right, and Biventricular Assist Devices. *Artificial Organs* 29 (7):564-572.

Transplant Australia. Transplant Australia Ltd [cited. Available from http://www.transplant.org.au.

Tuzson, J. 2000. *Centrifugal Pump Design*. Evanston, Illinois: John Wiley & Sons, Inc.

UNOS. 2005. United Network for Organ Sharing - Number of Transplants Perfromed.

UNOS, United Network for Organi Sharing. 2006. OPTN/SRTR 2006 Annual Report.

Ventracor. 2008 [cited. Available from http://www.ventracor.com/.

Vollkron, Michael, Heinrich Schima, Leopold Huber, and Georg Wieselthaler. 2002. Interaction of the Cardiovascular System with an Implanted Rotary Assist Device: Simulation Study with a Refined Computer Model. *Artificial Organs* 26 (4):349-359.

Wada, Hideichi, Shintaro Fukunaga, Masanobu Watari, Hiroshi Sakai, Yuji Sugawara, Hiroyuki Ochikubo, Katsuhiko Imai, Hidenori Shibamura, Kazumasa Orihashi, Taijiro Sueda, and Yuichiro Matsuura. 1999. Flow Balance Between the Left and Right Cardiac Output of an Eccentric Roller Type Total Artificial Heart. *Artificial Organs* 23 (8):741-746.

Watanabe, Kuniyoshi, Seiji Ichikawa, Toshimasa Asai, Tadashi Motomura, Atsushi Hata, Seiichi Ito, Toshiyuki Shinohara, Shinichi Tsujimura, Julia A. Glueck, Daniel J. Oestmann, and Yukihiko Nose. 2004. Centrifugal Blood Pump with a Hydraulically-levitated Impeller for a Permanently Implantable Biventricular Assist Device. *Artificial Organs* 28 (6):556-563.

Wilhelm, Markus J., Dieter Hammel, Christof Schmid, Andreas Rhode, Timo Kaan, Markus Rothenburger, Jorg Stypmann, Michael Schafers, Christoph Schmidt, Hideo A. Baba, and Hans H. Scheld. 2005. Long-term support of 9 patients with the DeBakey VAD for more than 200 days. *Journal of Thoracic and Cardiovascular Surgery* 130 (4):1122-1129.

Wood, Houston, Amy Throckmorton, Alexandrina Untaroiu, and Xinwei Song. 2005. The medical physics of ventricular assist devices. *Reports on Progress in Physics* 68 (3):545-576.

Wu, Yi, Paul E. Allaire, Gang Tao, Milton Adams, Yingjie Liu, Houston Wood, and Don B. Olsen. 2004. A Bridge from Short-term to Long-term Left Ventricular Assist Device : Experimental Verification of a Physiological Controller. *Artificial Organs* 28 (10):927-932.

Yozu, R., L. Golding, I. Yada, H. Harasaki, S. Takatani, S. Kawada, and Y. Nose. 1994. Do we really need pulse? Chronic nonpulsatile and pulsatile blood flow: From the exercise response viewpoints. *Artificial Organs* 18 (9):638-642.

Yuhki, Hatoh, Nogawa, Miura, Shimazaki, and Takatani. 1999. Detection of Suction and Regurgitation of the Implantable Centrifugal Pump Based on the Motor Current Waveform Analysis and Its Application to Optimization of Pump Flow. *Artificial Organs* 23 (6):532-537.

Zhang, Juntao, Barry Gellman, Andrew Koert, Kurt A. Dasse, Richard J. Gilbert, Bartley P. Griffith, and Zhongjun J. Wu. 2006. Computational and Experimental Evaluation of the Fluid Dynamics and Hemocompatibility of the CentriMag Blood Pump. *Artificial Organs* 30 (3):168-177.

10 Appendix

10.1 Prototype Assembly, Component List and Assembly Detail

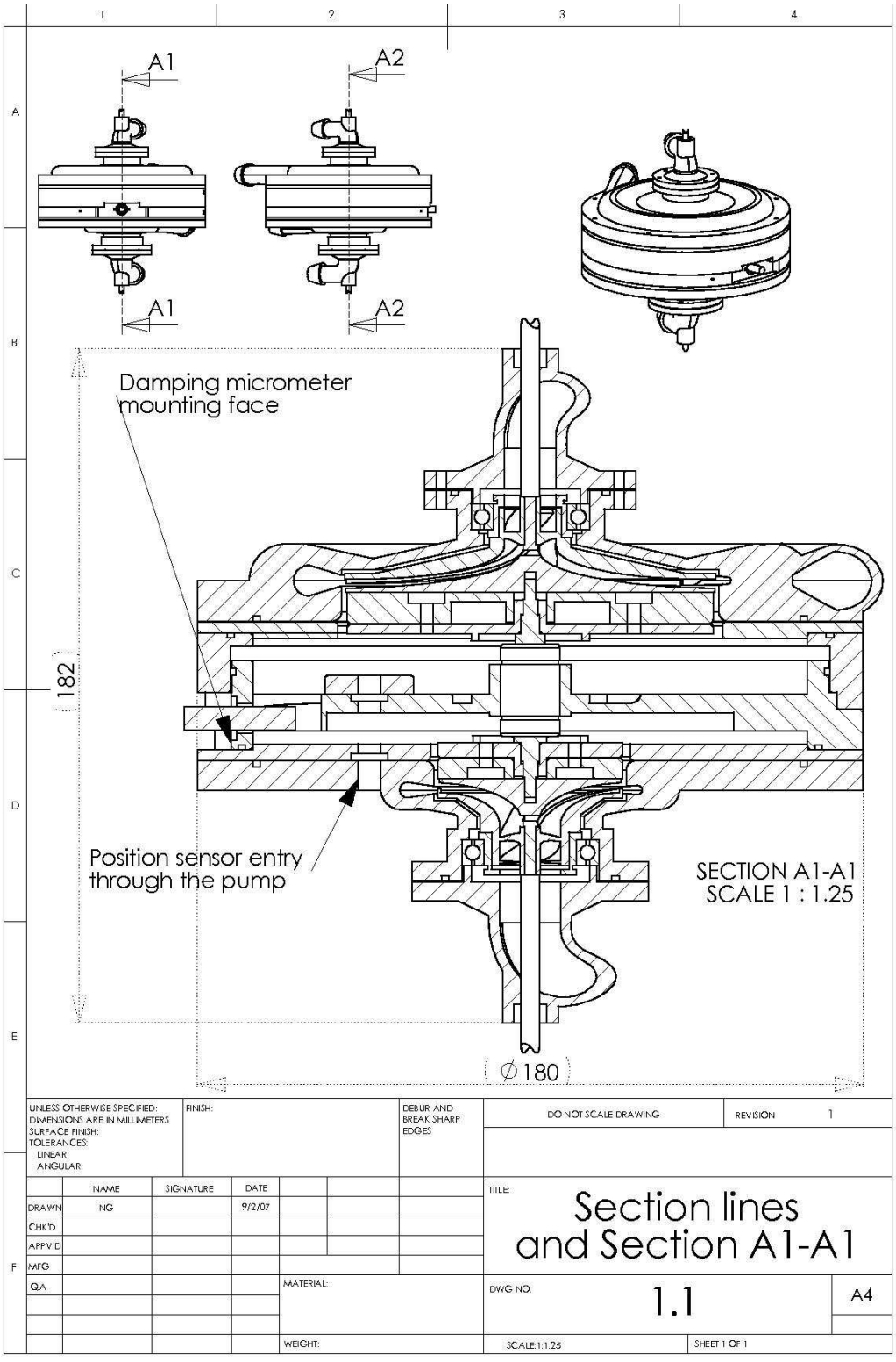

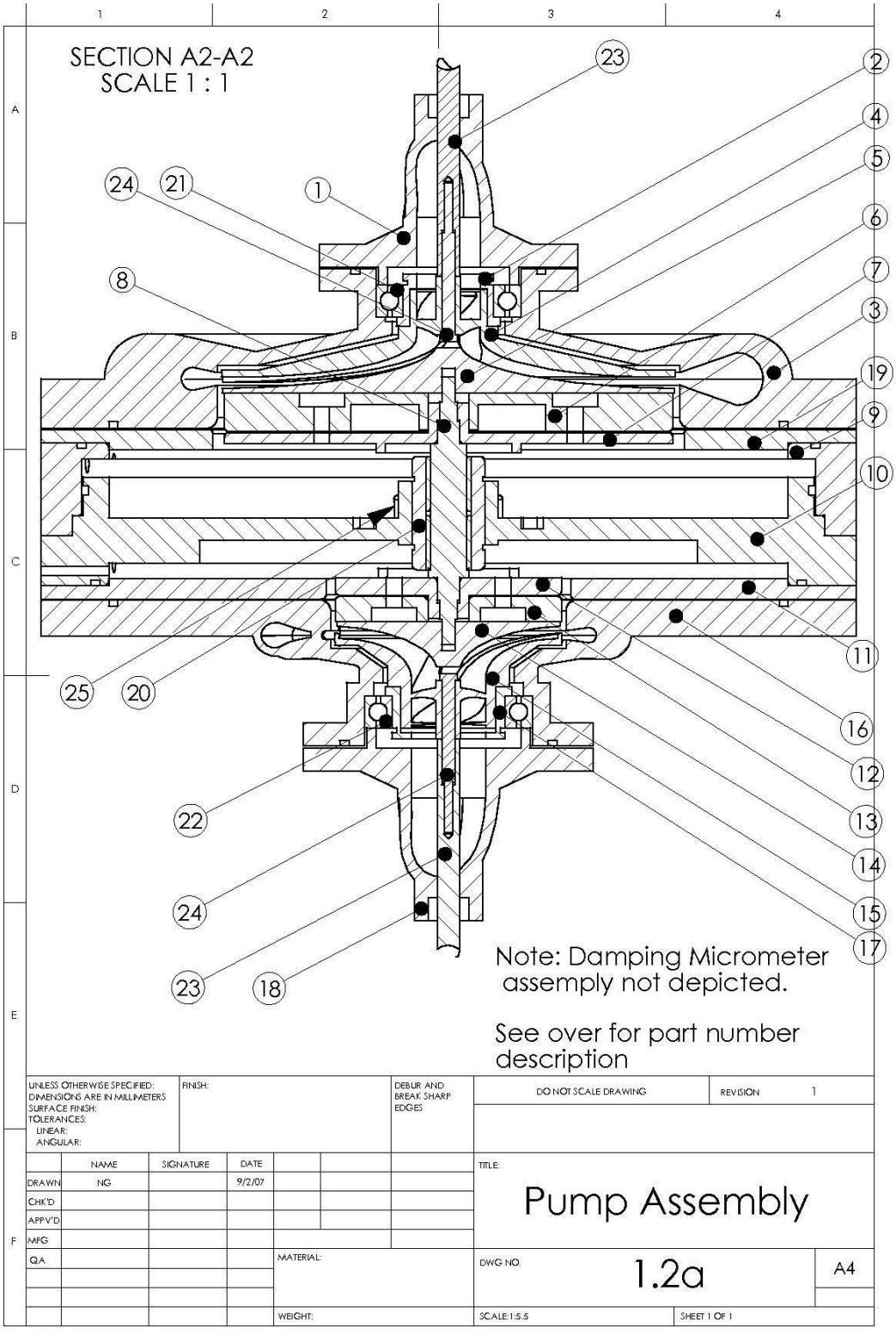

UNLESS OTHERWISE SPECIFIED: DIMENSIONS ARE IN MILLIMETERS SURFACE FINISH: TOLERANCES: LINEAR: ANGULAR:		FINISH:		DEBUR AND BREAK SHARP EDGES		DO NOT SCALE DRAWING	REVISION 1	
	NAME	SIGNATURE	DATE			TITLE: Pump Assembly		
DRAWN	NG		9/2/07					
CHK'D								
APPV'D								
MFG								
Q.A				MATERIAL:		DWG NO. 1.2a		A4
				WEIGHT:		SCALE:1:5.5	SHEET 1 OF 1	

Bill of Parts

1 RVAD inlet *^*
2 RVAD bearing housing
3 RVAD pump casing *^*
4 RVAD impeller *^*
5 RVAD lower shroud *^*
6 RVAD membrane mount A
7 RVAD membrane mount B
8 Passive controller shaft (con rod)
9 Pasive controller body 2
10 Passive controller body 1
11 Pump casing mount 2
12 LVAD membrane mount B
13 LVAD membrane mount A
14 LVAD lower shroud *^*
15 LVAD impeller *^*
16 LVAD pump casing *^*
17 LVAD bearing housing
18 LVAD inlet *^*
19 Pump casing mount 1
20 Passive controller linear beaing
21 RVAD Impeller bearing
22 LVAD Impeller bearing
23 Impeller shaft female
24 Impeller shaft male
25 Position sensor location

^
Manufactured with Rapid Prototyper

Note1: See drawing 1.2a for numbered part direction

UNLESS OTHERWISE SPECIFIED: DIMENSIONS ARE IN MILLIMETERS SURFACE FINISH: TOLERANCES: LINEAR: ANGULAR:			FINISH:			DEBUR AND BREAK SHARP EDGES	DO NOT SCALE DRAWING	REVISION 1
	NAME	SIGNATURE	DATE				TITLE: Bill of Parts	
DRAWN	NG		8/3/07					
CHK'D								
APP'V'D								
MFG								
Q.A				MATERIAL:			DWG NO. 1.2b	A4
				WEIGHT:			SCALE:1:5.5	SHEET 1 OF 1

The Fluid Damper comprises of a modified micrometer with a non-rotating spindle. The Micrometer is mounted to face, (*), machined on the side of part 10, (see Drawing 1.2, or part drawing P 10). The spindle then provides a means of occluding a triangular section slot machined near the peripheral of the major circular face of part 10

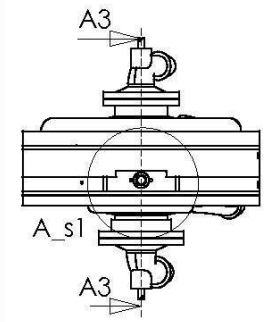

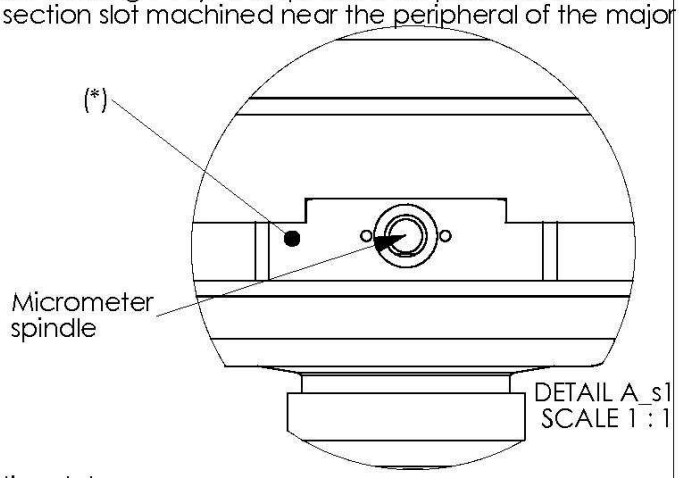

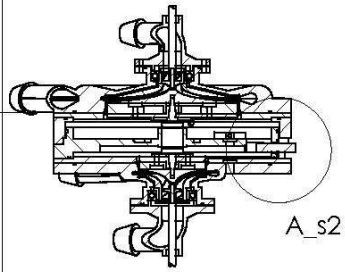

SECTION A3-A3

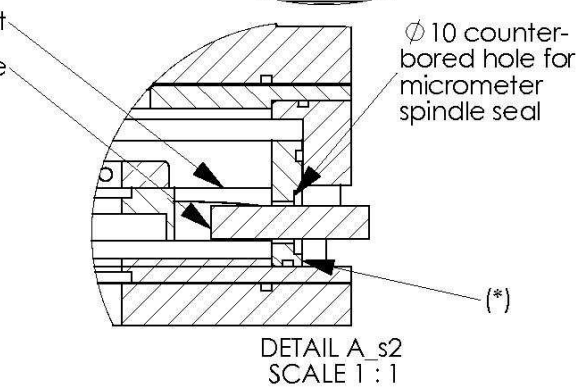

Note1: The micrometer spindle provides an adjustable occlusion to regulate fluid flow through the triangular section 'Damper' hole. Spindle occluder is shown in the partially open position

Note2: The micrometer will need to be located, (and sealed), so that the flat face of the machined spindle prevents water leakage around its sides

Note3: A locating sleve to be manufactured to fix the micrometer to the (*) face and to hold the seal in place and

UNLESS OTHERWISE SPECIFIED: DIMENSIONS ARE IN MILLIMETERS SURFACE FINISH: TOLERANCES: LINEAR: ANGULAR:		FINISH:		DEBUR AND BREAK SHARP EDGES			DO NOT SCALE DRAWING	REVISION 1
	NAME	SIGNATURE	DATE				TITLE: Damper Assembly	
DRAWN	NG		23/2/07					
CHK'D								
APPV'D								
MFG								
Q.A				MATERIAL:			DWG NO. 1.3	A4
				WEIGHT:			SCALE:1:4	SHEET 1 OF 1

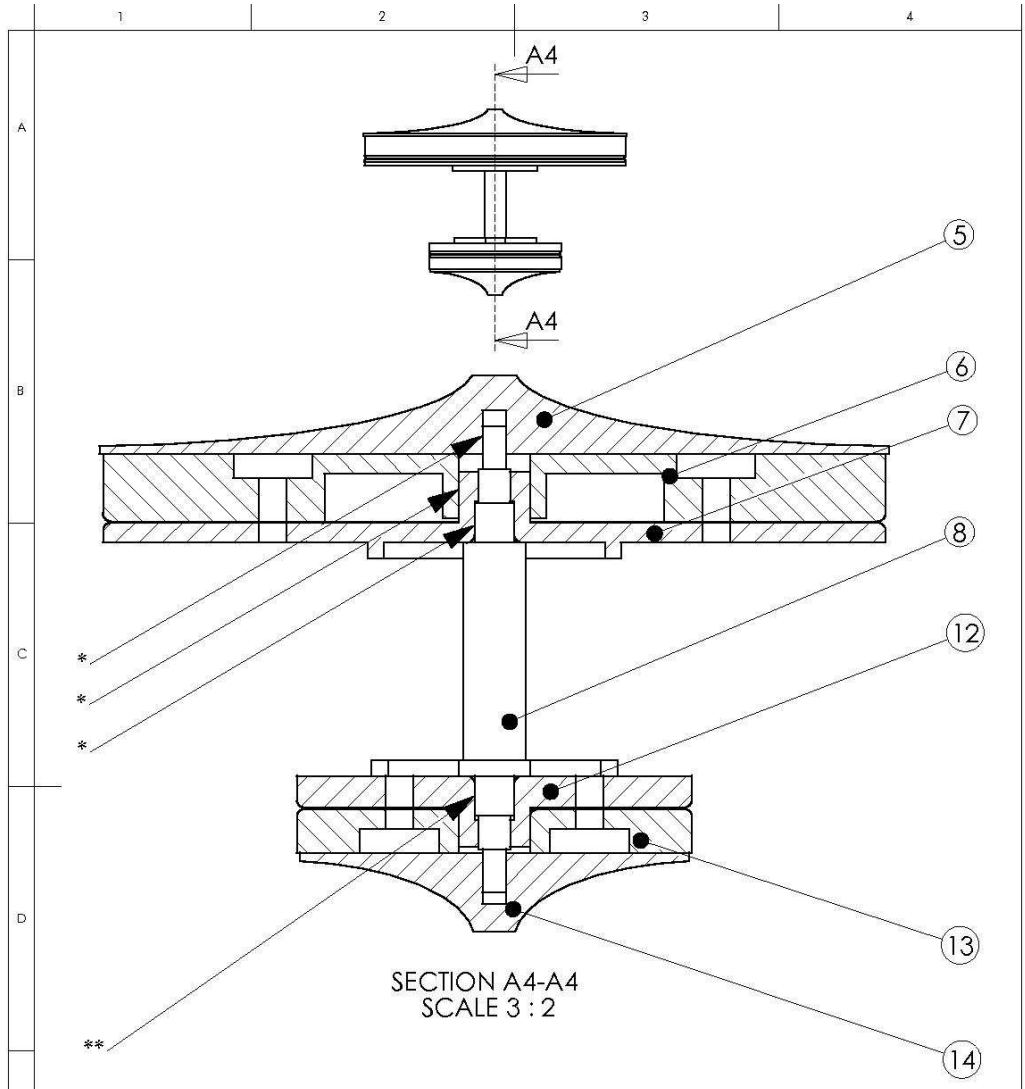

Note1: * indicates TYP position of radial location

Note1: ** indicates TYP position of threaded axial location

UNLESS OTHERWISE SPECIFIED: DIMENSIONS ARE IN MILLIMETERS SURFACE FINISH: TOLERANCES: LINEAR: ANGULAR:			FINISH:			DEBUR AND BREAK SHARP EDGES	DO NOT SCALE DRAWING	REVISION 1
	NAME	SIGNATURE	DATE				TITLE: Floating Hub Assembly	
DRAWN	NG		23/2/07					
CHK'D								
APPV'D								
MFG								
Q.A				MATERIAL:			DWG NO. 1.4	A4
				WEIGHT:			SCALE:1:2	SHEET 1 OF 1

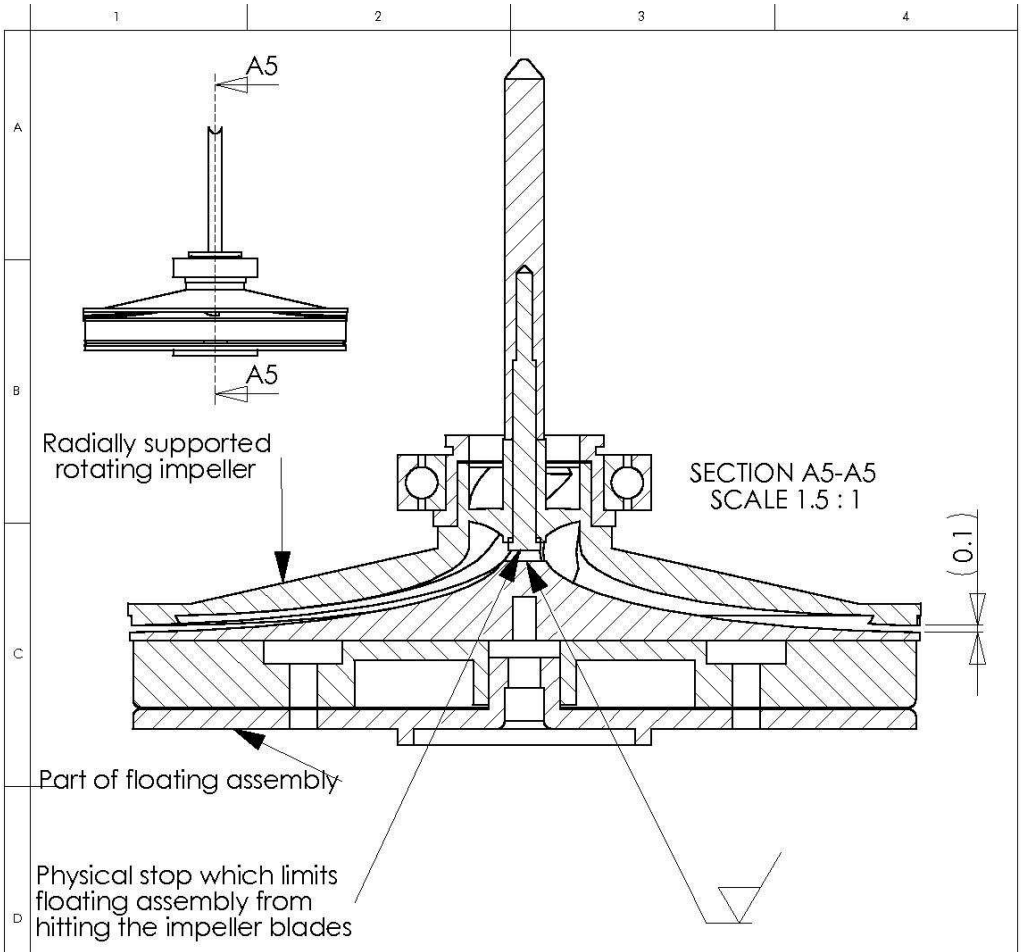

Note1: Much of the floating assembly depicted in drawing 1.4 has been omitted for clarity

Note2: The machining of the lower shroud to obtain this clearance between the lower shroud and the impeller blade is the same for both VADs. This detail shows only one VAD for simplicity

Note3: Impellers are driven by the shaft by way of a torque transmitting washer between part 24 and the impeller. The washer is grips the plastic impeller hub as the impeller shaft pieces are screwed together

UNLESS OTHERWISE SPECIFIED: DIMENSIONS ARE IN MILLIMETERS SURFACE FINISH: TOLERANCES: LINEAR: ANGULAR:	FINISH:			DEBUR AND BREAK SHARP EDGES	DO NOT SCALE DRAWING	REVISION 1
	NAME	SIGNATURE	DATE		TITLE: Floating and fixed assembly clearances	
DRAWN	NG		27/2/07			
CHK'D						
APP'V'D						
MFG						
Q.A				MATERIAL:	DWG NO. 1.5	A4
				WEIGHT:	SCALE:1:2	SHEET 1 OF 1

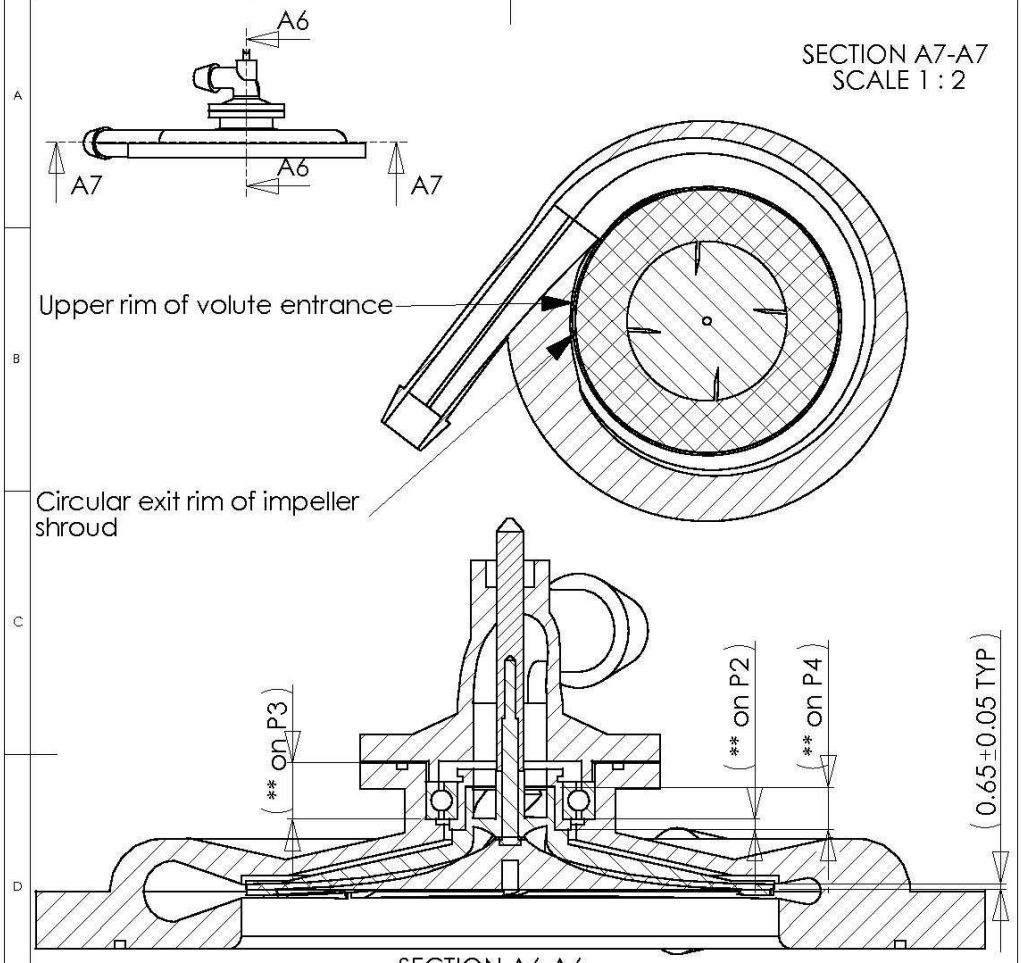

SECTION A6-A6
SCALE 1 : 1

Note1: Either of the dimension marked with a (**) maybe adjusted to allow for the clearance indicated. The clearance is between the upper rim of the volute entrance of part P3 (RVAD), or P16 (LVAD), and the circular exit rim of the impeller shroud, see detail (A7-A7),(not to be confused with the protruding exit edge of the impeller blade).

Note2: This clearance specification is the same for pumps

UNLESS OTHERWISE SPECIFIED: DIMENSIONS ARE IN MILLIMETERS SURFACE FINISH: TOLERANCES: LINEAR: ANGULAR:	FINISH:	DEBUR AND BREAK SHARP EDGES	DO NOT SCALE DRAWING / REVISION 1

	NAME	SIGNATURE	DATE
DRAWN	NG		12/3/07
CHK'D			
APPV'D			
MFG			
Q.A			

TITLE: Impeller and Casing clearance

MATERIAL:

DWG NO. 1.6

A4

WEIGHT:

SCALE:1:4

SHEET 1 OF 1

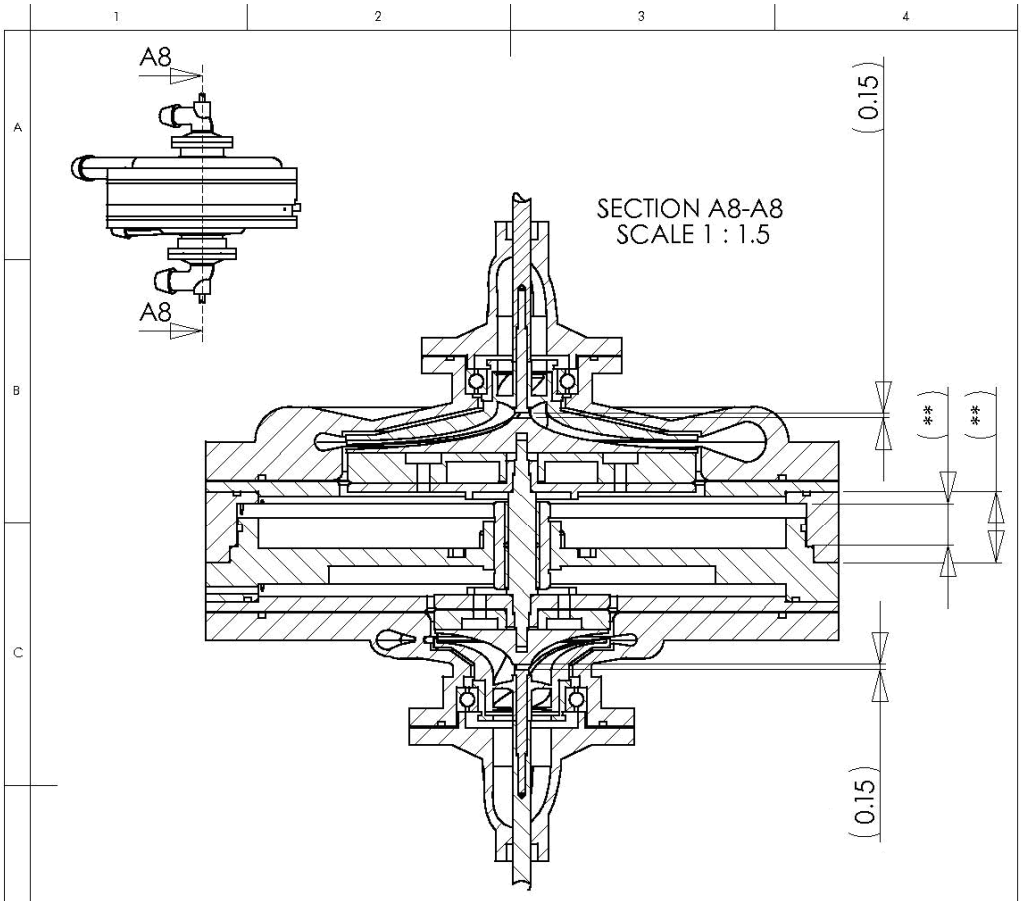

Note1: DImensions (**) are to be adjusted by the machinists from that given in drawing P9 so as to all for the given clearances between the heads of the impeller shaft male parts, (see P24), and the machined flats of the lower shrouds, (see P5 and P14). Drawings P24, P5 and P14 give reference to this note. To be carried out once all the parts have been made and assembled once the detail on drawings 1.5 and 1.6 is added

Note2: Once this is achieved, 0.5 or 1.0mm shims can be used to space the passive controller body components apart (parts 9 and 10) so as to increase the clearances on either side from 0.5mm to 0.75mm or 1.0mm

UNLESS OTHERWISE SPECIFIED: DIMENSIONS ARE IN MILLIMETERS SURFACE FINISH: TOLERANCES: LINEAR: ANGULAR:		FINISH:		DEBUR AND BREAK SHARP EDGES	DO NOT SCALE DRAWING	REVISION 1	
	NAME	SIGNATURE	DATE		TITLE:		
DRAWN	NG		12/2/07		Final dimension detail		
CHK'D							
APP'V'D							
MFG							
Q.A				MATERIAL:	DWG NO. 1.7		A4
				WEIGHT:	SCALE:1:5	SHEET 1 OF 1	

10.2 Tables of Vascular Parameters

Table 10-1: Early Vascular Parameters from General Circulation Model.

		Numerical Program Vascular Parameters Prior to Validation													
		Cardiovascular Sub-unit													
		RA	RV	PA	Lungs	PV	LA	LV	H. Aorta	L. Aorta	Head	Arms	Body	Legs	Vena Cava
Resistance ÷1000 (mm.Hg.s/ml)	Arterial	12.8	11.1	15	40	60	12.8	11.1	280		750	980	975	975	250
	Venous				80						2300	2000	1950	1950	
Compliance (ml/mm.Hg)	Arterial	75-50	75-2.4	5.6	3.2	30	80-11.1	80-1.6	1.45		1.5	1.8	1.8	1.8	100
	Venous				5						4.2	3.5	5.5	6.5	
Inductance (mm.Hg.s^2/ml)	Arterial	UpDtd	UpDtd	UpDtd	UpDtd	UpDtd	UpDtd	UpDtd	UpDtd		UpDtd	UpDtd	UpDtd	UpDtd	UpDtd
	Venous				UpDtd						UpDtd	UpDtd	UpDtd	UpDtd	
Diameter ÷1000 (m)	Arterial	45	55	35	150	15	40	40	35		80	40	40	50	20
	Venous				150						80	40	40	50	

Key:		Vascular sub-unit not recognised
	UpDtd	Updated every time step

Table 10-2: Employed Vascular Parameters for the MCL Simulations.

		Numerical Program Vascular Parameters for MCL Simulation															
		Cardiovascular Sub-unit															
		RA	RV	PA	Lungs	PV	LA	LV	H. Aorta	L. Aorta	Head	Arms	Body	Legs	Vena Cava	LVAD and Cannulae	RVAD and Cannulae
Resistance ×1000 (mm.Hg.s/ml)	Arterial	6.8	5.1	35	0	63	6.8	5.1	35		890	9.0E+05	9.0E+05	9.0E+05	63	0.1-9.0E5	0.1-9.0E5
	Venous				0.1						0.1	9.0E+05	9.0E+05	9.0E+05			
Compliance (ml/mm.Hg)	Arterial	56.25	4.07-56.25	4	0.1	5	60	1.08-60.00	1.6		0.1	0.1	0.1	0.1	20	0.1	0.1
	Venous				0.1						0.1	0.1	0.1	0.1			
Inductance ×1000 (mm.Hg.s^2/ml)	Arterial	5.9	6.6	67.5	0	27.2	5.9	7.1	97		0	0	0	0	25.3	44.4	44.4
	Venous				0						0	0	0	0			

Key:		Vascular sub-unit not recognised

Table 10-3: Employed Vascular Parameters for the Human Simulations.

		Numerical Program Vascular Parameters for Human Simulation															
		Cardiovascular Sub-unit															
		RA	RV	PA	Lungs	PV	LA	LV	H. Aorta	L. Aorta	Head	Arms	Body	Legs	Vena Cava	LVAD and Cannulae	RVAD and Cannulae
Resistance ×1000 (mm.Hg.s/ml)	Arterial	15	15	25	40	15	15	15	780		315	270	158	173	150	0.1-9.0E5	0.1-9.0E5
	Venous				40						750	450	525	525			
Compliance (ml/mm.Hg)	Arterial	50-57.60	3.00-72.00	1.8	5	4	20-57.60	0.73-72.00	1.5		7.2	7.8	7.8	7.8	18	0.1	0.1
	Venous				12						13.2	18.5	21.5	23.5			
D (mm)	Arterial	60	60	55	100	25	60	60	22		80	40	40	50	25	10	10
	Venous				180						80	40	40	50			

Key: Vascular sub-unit not recognised

Table 10-4: Employed Vascular Parameters for Healthy Human Simulations Including the Example Inertiance Calculated at the End of Systole.

		Numerical Program Vascular Parameters for Human Circulation													
		Cardiovascular Sub-unit													
		RA	RV	PA	Lungs	PV	LA	LV	H. Aorta	L. Aorta	Head	Arms	Body	Legs	Vena Cava
Resistance ×1000 (mm.Hg.s/ml)	Arterial	12.8	11.1	15	40	60	12.8	11.1	280		750	980	975	975	250
	Venous				80						2300	2000	1950	1950	
Compliance (ml/mm.Hg)	Arterial	75-50	75-2.4	5.6	3.2	30	80-11.1	80-1.6	1.45		1.5	1.8	1.8	1.8	100
	Venous				5						4.2	3.5	5.5	6.5	
Inductance (mm.Hg.s^2/ml)	Arterial	0.0002	0.0002	4E-05	9.22E-06	0.0013	0.0002	0.0001	0.0069		0.0001	0.0014	0.0014	0.0006	0.012
	Venous				1.79E-06						0.0001	0.0028	0.0034	0.0015	
Diameter ÷1000 (m)	Arterial	45	55	35	150	15	40	40	35		80	40	40	50	20
	Venous				150						80	40	40	50	

Key: Vascular sub-unit not recognised